

**REMARKS**Interview Summary

Applicants would like to thank the Examiner for her time discussing this case over the phone. During the phone interview, Applicants' representative and the Examiner discussed providing published references to support enablement of the claimed invention.

Status of the Claims

Claims 1-3, and 32-63 are pending before the Examiner for examination. Claims 4-31 have been cancelled without prejudice or disclaimer of the subject matter claimed therein. Claims 3, 41-50, and 53-57 have been amended to clarify the claimed invention. Support for the amendment to claims 41-45 can be found in claim 1.

New claims 58-63 have been added. Support for the new claims are summarized below.

Support for new claim 58 is found in original claim 50.

Support for new claim 59 is found in original claim 3.

Support for new claims 60-62 is found in original claim 53.

Support for new claim 63 is found on page 22 paragraph 0081.

Rejection Under 35 U.S.C. § 112 First Paragraph

Claims 1-3, 32- 57 are rejected under 35 U.S.C. § 112, first paragraph, as being enabling only for a method of removing amyloid deposits from mice comprising administering synthetic fibrils composed of immunoglobulin light chain variable region domains and for a pharmaceutical composition comprising the synthetic fibrils.

The present invention is based in part on the finding that immunization with amyloid fibrils can result in the induction of an immune response that promotes removal of amyloid deposits, including deposits comprising fibrils whose precursor proteins are distinct from those of the immunogen. Although amyloid fibrils from various diseases differ from each other in their primary sequence, these fibrils are structurally homologous molecules, as discussed in detail below. Accordingly, based on the structural homology of amyloid fibrils (paragraph 0132), the

present invention provides a method of removing amyloid deposits from a subject using any amyloid fibril as an immunogen and administered as a vaccine.

The Office Action asserts that the specification only discloses cursory conclusions without data supporting the findings. Applicants respectfully point out that Example D on page 35 discloses data supporting the removal of amyloid deposits from mice. First, the mice were immunized with synthetic fibrils and were shown to have anti-fibril antibodies. Subsequently, the mice were subcutaneously injected with human AL amyloid extract to produce a huge AL amyloidoma. Since the mice were immunized with synthetic fibrils prior to injection with the human AL amyloid extract, the amyloidoma disappeared in 5 days as compared to more than 15 days in non-vaccinated control mice. Thus the specification provides data to support the findings.

The Office Action also asserts that the specification does not enable the full scope of the claims and cites the Wands factor for determining whether undue experimentation is required.

#### 1. The Breadth of the Claims

The Office Action alleges that the claims are broad in scope and encompass unspecified variants of amyloid fibrils and subjects which are not adequately described or demonstrated in the specification. Applicants respectfully point out that the claimed method of removing amyloid deposits from a subject can be accomplished with any amyloid fibrils because amyloid fibrils, irrespective of the precursor protein that they are made from, are structurally homologous molecules and thereby elicit a generic anti-fibril immune response. Below, Applicants discuss data from different research groups showing amyloid fibrils are structurally homologous molecule. Moreover, Applicants submit that the murine model used in the present application is a well known model for studying human systemic amyloidosis. Further, the specification enables vaccines comprising amyloid fibrils.

##### a. Amyloid fibrils are structurally homologous molecules.

First, there is immunological evidence from various research groups showing the structural identity of amyloid fibrils. The data of O'Nuallain *et al.* (Proc. Natl. Acad. Sci. 2002,

99(3): 1485-90, attached to the response of July 14, 2004) confirm that disease related amyloid fibrils share a common structure. (See reference attached to the response dated July 14, 2004). O'Nuallain show that WO1 and WO2, monoclonal antibodies generated using A $\beta$ (1-40) fibrils as an immunogen, bind not only A $\beta$  fibrils, but also other disease related amyloid fibrils and amyloid-like aggregates composed of transthyretin, islet amyloid polypeptide,  $\beta_2$ -microglobulin, and polyglutamine (see abstract and page 1488, left column, second full paragraph). Although WO1 and WO2 are able to bind various amyloid fibrils, they exhibit little or no binding to the precursor proteins for each of these fibrils. These data establish that the conformation of disease related amyloid fibrils is similar, and that this generic fibril-associated conformation can be recognized by the immune system and that furthermore, this conformation is absent from the native precursor proteins.

Likewise, the data of Hrnčić *et al.* substantiate that the conformation shared by different amyloid fibrils is recognized by the monoclonal antibody (mAb) 11-1F4 (Hrnčić *et al.*, 2000, Am. J. Path. 157(4): 1239, attached to the response of July 14, 2003). Hrnčić *et al.* shows that mAb 11-1F4 expedited the resolution of implanted human immunoglobulin light chain (AL), amyloidomas in mice by binding to the amyloid fibrils thereby opsonizing them, and inducing a targeted, cell-mediated dissolution. Mab 11-1F4 was generated using, as an immunogen, the heat aggregated fibrillar form of a human V<sub>L</sub> fragment obtained from proteolytic cleavage of the human  $\kappa$ 4 immunoglobulin light chain protein LEN. Hrnčić *et al.* shows that the therapeutic efficacy of the mAb 11-1F4 was independent of the V<sub>L</sub> isotype of the AL amyloids tested (*Id.* at 1242 (left column, third full paragraph)). The binding of the 11-1F4 mAb to the implanted human AL amyloidomas and its ability to accelerate their removal was independent of the V <sub>$\kappa$</sub>  or V <sub>$\lambda$</sub>  subgroup from which the fibrils were composed. The data of Hrnčić *et al.* indicate that the mAb 11-F4 was interacting with a conformational (structural) epitope shared by different amyloid fibrils composed of immunoglobulin light chains and that this demonstrated a shared homologous structural epitope is present on amyloid fibrils.

In an extension of the work of Hrnčić *et al.*, Wall *et al.* shows that the mAb 11-1F4 expedited the removal of systemic AA amyloid deposits, composed of serum amyloid protein A in a murine model of inflammation-associated amyloidosis (Wall *et al.*, 2001, Amyloid and

Amyloidosis: Proceedings of the IXth International Symposium on Amyloidosis, Budapest, Hungary, David Apathy, Attached to the response of July 14, 2003). This evidence confirms that the structure of *in vivo* amyloid fibrils associated with different diseases are similar.

In addition, the phenomenon of cross-seeding further establishes a fundamental structural homology between amyloid fibrils composed of different precursor proteins. Cross-seeding involves the use of one type of amyloid fibril to act as a template to support the growth of a different type of protein. For example, fibrils composed of transthyretin, when injected into mice can initiate (or seed) the growth of amyloid fibrils composed of the protein serum apolipoprotein A (sAA). (Johan *et al.* Proc Natl Acad Sci U S A. 1998 Mar 3;95(5):2558-63, see attached, especially page 2561, right column, second full paragraph). Similarly, fibrils composed of spider silk can seed sAA amyloid growth. (Kisilevsky *et al.*, Amyloid. 1999 Jun;6(2):98-106, see attached). Other examples of the cross seeding phenomenon include the ability of islet amyloid polypeptide fibrils (associated with type 2 diabetes) to seed A $\beta$ (1-40) fibril growth (O'Nuallain *et al.*, J Biol Chem. 2004 Apr 23;279(17):17490-9, see attached). In each of these references, the fibrils used to seed the amyloid deposits are composed of different proteins from the fibrils that they form *in vivo*. The phenomenon of cross-seeding demonstrates that amyloid fibrils and amyloid deposits composed of various precursor proteins are structurally homologous macromolecules.

Other evidence from structural studies of amyloid fibrils performed using x-ray diffraction and electron microscopy suggests that all amyloid fibrils are structurally homologous. These studies establish that amyloid fibrils, irrespective of the precursor protein that they are made from, have identical x-ray diffraction patterns. Sunde *et al.* (Journal of Molecular Biology, 1997, 273:729-739, see attached) investigated the structure of six different amyloid fibrils and two synthetic fibril preparations using intense synchrotron sources. They observed that all these fibrils gave similar high-resolution X-ray fiber diffraction patterns, consistent with a helical array of  $\beta$ -sheets parallel to the fibril long axis, with strands perpendicular to this axis (*Id.* abstract and page 735). Other data showing that all amyloid fibrils have a similarly ordered structure include the work of Makin *et al.* (Biochem Soc Trans. 2002 Aug;30 (4):521-5, see attached) and Serpell *et al.* (Methods in Enzymology, 1999, 309:526-36, see attached). Accordingly, data collected



from structural analysis of different amyloid fibrils confirm that amyloid fibrils are structurally homologous molecules.

The binding of all amyloid fibrils to two specific dyes, Congo red and thioflavin (ThT), also indicates that amyloid fibrils made from different precursor proteins share structural features (homologies). Congo red binding and subsequent birefringence, and ThT fluorescence emission remain the most common techniques to identify the presence of amyloid fibrils in patient tissue samples and laboratory preparations of synthetic fibrils (Nilsson *et al.*, Methods 2004, 34: 151-160, especially 153, see attached; Hazenburger *et al.*, The Journal of Medicine, 2004, 62(4): 121-128, see attached). In fact, the first step in the diagnosis of systemic (non cerebral) amyloidosis is the detection of Congo red stained positive amyloid deposits in patient tissue samples (Hazenburger *et al.*, at 122). Any amyloid disease can be diagnosed using Congo red staining.

Congo red was developed as a cotton dye and was found to bind specifically to amyloid fibrils when applied to tissues in an alkaline solution. When viewed under a microscope using cross-polarized illumination, Congo red binding to amyloid fibrils in tissue sections emits a blue-green birefringence. Birefringence is a property of light that arises from the illumination of molecules that are aligned in a very organized manner. It is believed that the Congo red molecules intercalate into grooves along the amyloid fibrils to give highly-ordered arrays of dye molecules that when illuminated produce birefringence. Because all amyloid fibrils produce birefringence when stained with Congo red this implies that they all possess a binding site for Congo red irrespective of the precursor protein that the fibrils are comprised of (*e.g.*, A $\beta$ (1-40), transthyretin, cystatin C, light chains, apolipoprotein A, islet amyloid polypeptide, insulin, calcitonin, fibrinogen).

The same reasoning applies to ThT binding to amyloids. ThT is a benzothiazole dye that emits a novel fluorescence light when bound to amyloid fibrils. The binding of ThT to amyloid deposits and the production of novel fluorescent light is diagnostic of amyloid disease. The ubiquitous presence of ThT binding sites on amyloid fibrils also supports the contention that there is considerable homology in the structure of all amyloid fibrils.

In summary, there is a body of evidence that supports the thesis that amyloid fibrils are structurally homologous at a number of levels. Accordingly, given the teachings of the present

specification, one would expect that any amyloid fibril, whether synthetic or natural, would be able to induce an immune response to this generic structure, an immune response that would recognize the entire range of amyloid fibrils and promote removal of amyloid deposits in a patient.

b. The murine model used by Applicants is a well known model for the study of human amyloidosis.

Applicants used two art accepted murine models of amyloidosis in developing the present invention. This first murine model of human AL amyloidosis is described on page 5, paragraph 0018, and in Example D (page 35) of the specification. In this murine model, the mouse is injected with human AL amyloid extract to produce a palpable subcutaneous AL-amyloidoma Hrnčić *et al.* (Am. J. of Pathology 2000, 157: 1239, attached to response of July 14, 2003) who developed and used this same murine model of AL amyloidosis confirms on page 1241 and figure 1 that the murine model is an accepted model for studying human disease. Similarly, Solomon *et al.* (Clinical Cancer Research 2003, 9: 3831, see attached) on pages 3833 and 3837 (final paragraph) substantiates that the murine AL amyloidosis model used by Applicant is a useful model for the human disease, because based on the data with the murine model, the research can proceed to clinical trials.

The second murine model of systemic AA amyloidosis is also described on page 5, paragraph 0018, and in Example D (page 35) of the specification. This murine model has depended upon the injection of an inflammatory chemical or biological agent such as casein, silver nitrate, or lipopolysaccharide to develop AA amyloid deposits. To accelerate the deposition of AA amyloid, the mouse is also injected with amyloid enhancing factor (AEF). As evidenced in the cited references, both the AL and AA mice are widely used to study human amyloidosis (Hrnčić *et al.* Am. J. of Pathology 2000, 157: 1239, attached to response of July 14, 2003); also, see attached references: Solomon *et al.*, Clinical Cancer Research 2003, 9: 3831; Cohen *et al.* Am. J. Pathol. 1972, 68: 441; Skinner *et al.* Lab. Invest. 1977, 36(4): 420; and Axelrad *et al.*, Lab. Invest. 47(2): 139).

Cohen *et al.*, Skinner *et al.* and Axelrad *et al.* are an additional three representative examples of references that have concluded that the AA amyloidosis murine model used by Applicant can be employed to study human amyloidosis. In each of these references, the mice were subcutaneously injected with casein or silver nitrate. In Axelrad, AEF is administered either immediately prior to or a day after the casein or silver nitrate administration. Cohen *et al.* concludes,

Since the model is quite comparable to human disease, it has been and can be used for studies of the course, pathogenesis and treatment of amyloid. (Cohen *et al.* 443).

Skinner *et al.* asserts,

Murine amyloidosis induced by the chronic administration of casein, endotoxin, and other agents has been used as a model for the study of human systemic amyloidosis for many years. (Skinner *et al.*, 420).

Axelrad *et al.* states,

Amyloid-enhancing factor (AEF) is a transferable activity that in CBA/J mice reduces the induction time of splenic amyloid deposition to 48 hours. Azocasein, or AgNO<sub>3</sub>, can induce AEF in the spleen and liver. (Axelrad *et al.* abstract).

These references show that this murine model developed decades ago, is the archetypal model that has been used to evaluate novel anti-amyloid therapeutics and to study potential methods to prevent amyloid disease in humans. As shown by the references, the disease in mice, efficiently recapitulates the mechanism by which amyloid forms in humans. This murine model is recognized as an invaluable tool for researchers to validate the potential therapeutic efficacy of novel molecules in a mammalian system. Kisilevsky *et al.* routinely uses this murine model to test potential anti-amyloid agents for use in humans (Kisilevsky *et al.* J. Mol. Neuroscience 2004, 24: 167; Kisilevsky *et al.* J. Mol. Neuroscience 2003, 20: 291; Kisilevsky *et al.* J. Mol. Neuroscience 2002, 19: 45).

In summary, the cited references suggest that the AA-amyloidosis murine model used by Applicants is an accepted animal model for studying amyloidosis in human. The disease in the AA-amyloidosis mice is representative of the disease in humans.

c. The specification enables vaccines.

The specification enables the vaccine compositions comprising amyloid fibrils. Vaccine is generally defined as a preparation comprising an agent that is administered to a subject to stimulate an immune response that provide clinical benefit. A vaccine can be administered prior to the subject developing an illness. Likewise, the vaccine can be administered after the subject has been in contact with the agent. An example of this is the rabies vaccine. The specification on pages 22-25 provides guidance for making and using vaccines comprising amyloid fibrils. The specification in Example D specifically teaches administering amyloid fibrils to a subject. In the absence of a reasonable basis to question the enablement of disclosed vaccines, the specification enables the breadth of the claims. As stated by the Federal Circuit, the Examiner has the initial burden to establish a reasonable basis to question the enablement provided for the claimed invention. *In re Wright*, 999 F.2d 1557, 1562, 27 USPQ2d 1510, 1513 (Fed. Cir. 1993). Respectfully, in this case, no such reasonable basis has been established by the Examiner.

In summary, since amyloid fibrils are structurally homologous and the murine model used by Applicants is an accepted animal model for studying amyloidosis in human and since there is no reason to doubt the enablement of the disclosed vaccines, Applicants have enabled the breadth of the claims.

## 2. The Absence of Working Examples

The Office Action alleges that there are no working examples using various amyloid fibrils to generate an immune response and to reduce amyloid deposits in mice and that there is insufficient guidance to enable the scope of the claims. As discussed above, Example D shows that synthetic amyloid fibrils administered as a vaccine to mice in an art accepted murine model resulted in the removal of the amyloidoma. The Example also teaches the removal of AA amyloid from mice induced to develop systemic AA amyloidosis. Also as discussed above, these murine models are well known and accepted as animal models for studying human amyloidosis. Moreover, the specification in paragraph 0018 discusses in detail animal models for amyloidosis.

Additionally, as discussed above and in the specification in paragraphs 0005 and 0132, it is well known that amyloid fibrils are structurally homologous molecules that can be used to induce a cross-reactive immune response. Accordingly, the example provided in the specification is adequate to enable the scope of the claims.

3. The State of the Prior Art ; The Relative Skill of Those in the Art and The Predictability or Unpredictability of the Art

The Office Action alleges that the general knowledge and skill of those in the art is not sufficient to enable the scope of the claimed invention. Applicants respectfully submit that given the general knowledge of the murine mouse models for amyloidosis and the structural properties and similarities of amyloid fibrils and given the guidance in the specification for administering amyloid fibrils to subjects (pages 22-25) and for methods of treating amyloidosis (pages 6 and 7), there is sufficient guidance to enable the scope of the claims.

The Office Action alleges that specific guidance on the identities of the proteins or variants thereof in amyloid fibrils and the effects of the amyloid fibrils are necessary. The Office Action also alleges that the invention is highly unpredictable because the specification does not demonstrate the effects of amyloid fibrils comprising various proteins or variants. Applicants respectfully point out that as taught in the specification, a specific amyloid fibril need not be administered to a subject to remove a specific type of deposit, because as discussed above, amyloid fibrils, irrespective of the precursor proteins from which they are made, are structurally related molecules. As shown in Example D, Applicants unexpectedly discovered that a synthetic amyloid fibril comprising immunoglobulin light chain variable region domain was capable of inducing an immune response sufficient to remove an *in vivo* murine amyloidoma generated by injecting human AL amyloid extract into a mouse. As discussed above and taught in the specification, since amyloid fibrils are structurally homologous molecules, the immune response induced by the synthetic amyloid fibril was sufficient to remove the murine amyloidoma generated from human AL amyloid extract by virtue of its reactivity with the generic, shared amyloid fibril epitopes. Moreover, the claimed invention can be performed with any amyloid

fibril whether synthetic or naturally occurring as a consequence of the structural identity of amyloid fibrils.

Given the guidance provided by the specification and given the state of the prior art disclosing amyloidosis and the structural properties of amyloid fibrils, the present invention is neither unpredictable nor lacks enablement for the scope of the claims.

4. The Amount of Direction or Guidance Presented and the Quantity of Experimentation Necessary

The Office Action alleges that there are no working examples demonstrating the effects of amyloid fibrils containing various amyloid proteins or variants thereof in subjects other than mice. As discussed above, the specification teaches that amyloid fibrils are structurally homologous molecules and that immunization of mice with an amyloid fibril generates an immune response that promotes the removal of amyloid deposits, including deposits comprising fibrils whose precursor molecules are distinct from those of the amyloid fibrils used to immunize the mice. As discussed above, the guidance provided by the specification, including Example D, and the state of the prior art are sufficient to enable the scope of the claimed invention.

The Office Action also alleges that the specification has not identified any variants or allelic variants thereof. Applicants respectfully submit that the claimed invention is not directed to a protein, but to a method of using an amyloid fibril comprising a protein. In fact, these proteins are well known in the art. Moreover, proteins that are associated with amyloidosis are known in the art to contain mutations. For example, the cystatin C variant associated with amyloidosis is the Leu68Q variant form of cystatin C. (Grubb *et al.*, [http://www.research.swegene.org/project\\_details.php?Proj=194](http://www.research.swegene.org/project_details.php?Proj=194), attached to the response dated July 14, 2003, attached to response of July 14, 2003). Transthyretin associated with amyloidosis also has various amino acid mutations (paragraph 0012). Ghiso *et al.* (Journal of Alzheimer's Disease 2001, 3, 65-73, see attached) discloses the amyloidogenic variants of several proteins, such as A $\beta$ , cystatin C, transthyretin, gelsolin, and prion. Booth *et al.* (Nature 1997, 385:127-787, see attached) discusses the amyloidogenic variants of lysozyme.

In view of the discussion above, the specification enables the claimed invention. Applicants respectfully request withdrawal of the rejection.

Rejection Under 35 U.S.C. § 112, Second Paragraph

Claims 37, 38, and 41-45 have been rejected under 35 U.S.C. § 112, second paragraph as being indefinite for failing to particularly point out and distinctly claim the subject matter which applicant regards as the invention.

Claim 37 and 38 have been rejected as being indefinite because the use of the term “cystatin C variant” or “the one or more proteins is a variant or allelic variant thereof.” As discussed in the last response, dated July 14, 2003, it is well known that the cystatin C variant associated with amyloidosis causes Hereditary Cystatin C Amyloid Angiopathy (HCCAA) and that HCCAA is caused by a mutation in the gene encoding the peptidase inhibitor cystatin C. Thus, it is known that the term “cystatin C variant” refers to the Leu68Q variant form of cystatin C. (Grubb *et al.*, [http://www.research.swegene.org/project\\_details.php?Proj=194](http://www.research.swegene.org/project_details.php?Proj=194), attached to the response dated July 14, 2003).

Additionally, all the proteins listed in claim 37 are well known. These proteins are routinely used by the skilled artisan and have been characterized by the skilled artisan to be associated with amyloidosis. Applicants respectfully point out that claim 37 is not directed to novel proteins. Rather, claims 37 and 38 are directed to a method of using these known proteins and their variants to remove amyloid from patients. Accordingly, claims 37 and 38 are definite as they stand.

Claims 41-45 are rejected because there is insufficient antecedent basis for the recitation of “amyloid fibrils.” Claims 41-45 have been amended to recite “the amyloid deposits are removed” to overcome this rejection. Moreover, Applicants respectfully point out that claim 1 includes the limitation that the amyloid fibrils are administered to the subject. Accordingly, there is antecedent basis for claims 41-45 in claim 1.

**CONCLUSION**

In view of the foregoing claim amendments and accompanying remarks, Applicants respectfully request reconsideration and timely allowance of the pending claims. Should the Examiner feel that there are any issues outstanding after consideration of this response, the Examiner is invited to contact Applicants' undersigned representative to expedite prosecution.

If there are any additional fees due in connection with the filing of this response, please charge the fees to our Deposit Account No. 50-0310. If a fee is required for an extension of time under 37 C.F.R. § 1.136 not accounted for above, such an extension is requested and the fee should also be charged to our Deposit Account.

Respectfully submitted,

**MORGAN, LEWIS & BOCKIUS LLP**

Dated: February 22, 2005

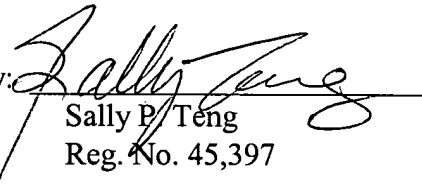
**CUSTOMER NO. 09629**

**MORGAN, LEWIS & BOCKIUS LLP**

1111 Pennsylvania Ave., N.W.

Washington, D.C. 20004

(202) 739-3000

By:   
Sally P. Teng  
Reg. No. 45,397



# Cerebral amyloidosis, amyloid angiopathy, and their relationship to stroke and dementia

Jorge Ghiso\* and Blas Frangione

Department of Pathology, New York University School of Medicine, New York, NY, USA

Cerebral amyloid angiopathy (CAA) is the common term used to define the deposition of amyloid in the walls of medium- and small-size leptomeningeal and cortical arteries, arterioles and, less frequently, capillaries and veins. CAA is an important cause of cerebral hemorrhages although it may also lead to ischemic infarction and dementia. It is a feature commonly associated with normal aging, Alzheimer disease (AD), Down syndrome (DS), and Sporadic Cerebral Amyloid Angiopathy. Familial conditions in which amyloid is chiefly deposited as CAA include hereditary cerebral hemorrhage with amyloidosis of Icelandic type (HCHWA-I), familial CAA related to A $\beta$  variants, including hereditary cerebral hemorrhage with amyloidosis of Dutch origin (HCHWA-D), the transthyretin-related meningocerebrovascular amyloidosis of Hungarian and Ohio kindreds, the gelsolin-related spinal and cerebral amyloid angiopathy, familial PrP-CAA, and the recently described chromosome 13 familial dementia in British and Danish kindreds. This review focuses on the various molecules and genetic variants that target the cerebral vessel walls producing clinical features related to stroke and/or dementia, and discusses the potential role of amyloid in the mechanism of neurodegeneration.

## 1. Introduction

Amyloidosis is a disorder of protein conformation leading to aggregation and fibrillization. A diverse group of proteins normally present in body fluids as soluble precursors can self-assemble into amyloid fibrils and produce insoluble deposits in different tissues which may lead to cell damage, organ dysfunction and death. These fibrils, composed of low molecular weight mass peptides (~ 4 to 30 kDa), adopt a predominant

$\beta$ -pleated sheet structure, the conformation responsible for their physicochemical properties and tinctoreal characteristics. So far, 20 different proteins have been identified as subunits of amyloid fibrils [56,57,60 (for review and nomenclature)]. Although collectively they are products of normal genes, several amyloid precursors contain abnormal amino acid substitutions that can impose an unusual potential for self-aggregation. Increased levels of amyloid precursors, either in the circulation or locally at sites of deposition, are usually the result of overexpression, defective clearance, or both. Of all the amyloid proteins identified, less than half are known to cause amyloid deposition in the central nervous system (CNS), which in turn results in cognitive decline, dementia, stroke, cerebellar and extrapyramidal signs, or a combination of them.

## 2. A $\beta$ - related cerebral amyloidosis

Alzheimer's disease (AD) is an age-dependent neurodegenerative disorder that causes a chronically progressive decline in cognitive functions. The brains of patients suffering from AD are characterized by the extracellular deposition of amyloid A $\beta$  (A $\beta$ ) protein in plaques and cerebral blood vessels, the presence of intraneuronal neurofibrillary tangles (NFT) and reactive gliosis, and the loss of presynaptic terminals and neuronal subpopulations in well defined brain areas. At autopsy, senile plaques and NFT chiefly define the disease whereas other pathological features are often ignored or regarded as coincidental findings. It is now becoming clear that a large majority of the patients diagnosed with AD when examined at autopsy bear stroke-like lesions or infarctions, ranging from CAA, degenerative microangiopathy compromising both the endothelium and smooth muscle cells, cerebral infarcts, microinfarction, white matter changes related to small vessel disease and even hemorrhages [20,22,58]. Although it is accepted that the presence of cerebrovascular disease or strokes may cause rapid cognitive decline and worsen the outcome in AD, it remains debat-

\*Correspondence to: Jorge Ghiso, Ph.D., Department of Pathology, New York University School of Medicine, 550 First Avenue, room TH-432, New York, NY 10016, USA. Tel.: +1 212 263 5775; Fax: +1 212 263 6751.

able whether the vascular lesions are coincidental or causal to the pathological processes. In sporadic AD, wild type A $\beta$  species, 39 to 43 residues in length, are the main constituents of the parenchymal and vascular amyloid lesions and the inheritance of the apolipoprotein E (apoE, chromosome 19) 4 allele is a prevailing risk factor [31,40,49,61].

Mutations in the amyloid precursor protein (A $\beta$ PP) on chromosome 21 or presenilins (PS) 1 (chromosome 14) and 2 (chromosome 1) genes have been linked to autosomal dominant forms of familial AD (FAD) (reviewed in [48]). As indicated in Fig. 1, multiple mutation sites either within or immediately outside the A $\beta$  segment have been identified in the A $\beta$ PP gene. Surprisingly, A $\beta$ PP mutations found outside the A $\beta$  peptide are mainly associated with dementia whereas those found inside the A $\beta$  sequence result in stroke as the main clinical phenotype. These genetic variants are concentrated in the middle of the A $\beta$  sequence (positions 21–22, corresponding to codons 692–693 of A $\beta$ PP) and are invariably associated with extensive cerebrovascular pathology. The Flemish mutation A to G at codon 692, is the only variant so far described at position 21, resulting in an Ala to Gly substitution and a clinical phenotype of presenile dementia and cerebral hemorrhage [19]. At position 22 of A $\beta$ , three variants have been described: i) the Arctic mutation (A to G at codon 693, resulting in the replacement of Glu for Gly), presenting as an early onset AD with prominent vascular symptomatology [23], ii) the Dutch mutation (G to C at codon 693, with the subsequent replacement of Glu for Gln), showing a phenotype predominantly associated to cerebral hemorrhage (see below) [26], and iii) the Italian mutation (G to A at codon 693, bearing Lys for Glu), presenting as a presenile dementia with cerebral hemorrhage [51]. The deposition of these vasculotropic mutants in the cerebral vessel walls suggest alteration of the clearance-uptake mechanisms at the blood-brain barrier.

Of interest is the first mutation described in the A $\beta$ PP gene linked to hereditary cerebral hemorrhage with amyloidosis, Dutch type (HCHWA-D), an autosomal dominant disease clinically defined by recurrent strokes, vascular dementia and fatal cerebral bleeding in the fifth to sixth decades of life [30]. Pedigrees from the villages of Katwijk and Scheveningen have been described in The Netherlands [29]. Around two-thirds of the patients will die as a result of the first acute cerebral hemorrhage, while the rest will have several minor stroke episodes leading to cognitive decline and dementia [18,59]. Histologically, there is a mas-

sive amyloid deposition in the walls of leptomeningeal and cortical arteries and arterioles as well as in vessels in the brainstem and cerebellum. In addition to the vascular involvement, there is a moderate number of parenchymal amyloid deposits resembling the diffuse plaques seen in Alzheimer disease. Dense plaque cores and neurofibrillary tangles are absent; cortical and hippocampal neurons outside the infarcts appear to be well preserved. Cerebral and cerebellar white matter show varying degrees of edema and myelin loss. The amyloid subunit in HCHWA-D is homologous to A $\beta$ ; amyloid deposits are composed of a mixture of wild-type A $\beta$  peptide and the A $\beta$ -Q22 variant [41,54]. A single nucleotide change (G for C) at codon 693 of A $\beta$ PP [26] results in a single amino acid substitution (glutamine for glutamic acid) at position 22 of the A $\beta$  peptide. This was the first of a large series of mutations in the A $\beta$ PP gene described in several kindreds with early onset familial Alzheimer disease [48] (Fig. 1). Although the mechanism of fibril formation is not known, *in vitro* studies [3,5,62] have shown that the A $\beta$ -Q22 variant forms fibrils at a more accelerated rate than wild-type A $\beta$ . This increased amyloidogenic tendency is probably due to a higher content of  $\beta$ -pleated sheet structure and a conformational change in the middle part of the molecule induced by the disappearance of the negatively charged Glu side-chain in the mutant peptide [9,45]. The presence of both allele products in the amyloid deposits suggest that the mutant peptide may induce a conformational change in the structure of the normal A $\beta$  peptide. Treatments to inhibit amyloidogenesis have been proposed [44,46].

### 3. Cystatin C – related cerebral amyloid angiopathy

Hereditary cerebral hemorrhage with amyloidosis, Icelandic type (HCHWA-I) is an autosomal dominant disorder characterized by massive amyloid deposition within small arteries and arterioles of leptomeninges, cerebral cortex, basal ganglia, brainstem and cerebellum [16]. Although brain involvement is the main clinicopathological feature, silent amyloid deposits are also present in peripheral tissues such as skin, lymph nodes, spleen, salivary glands, and seminal vesicles [2].

Including information on progenitors born up to 200 years ago, seven pedigrees have been described in small rural communities of West Iceland [21]. The main clinical hallmark of the disease is cerebral hemorrhage with fatal outcome in the third to fourth decade of life in

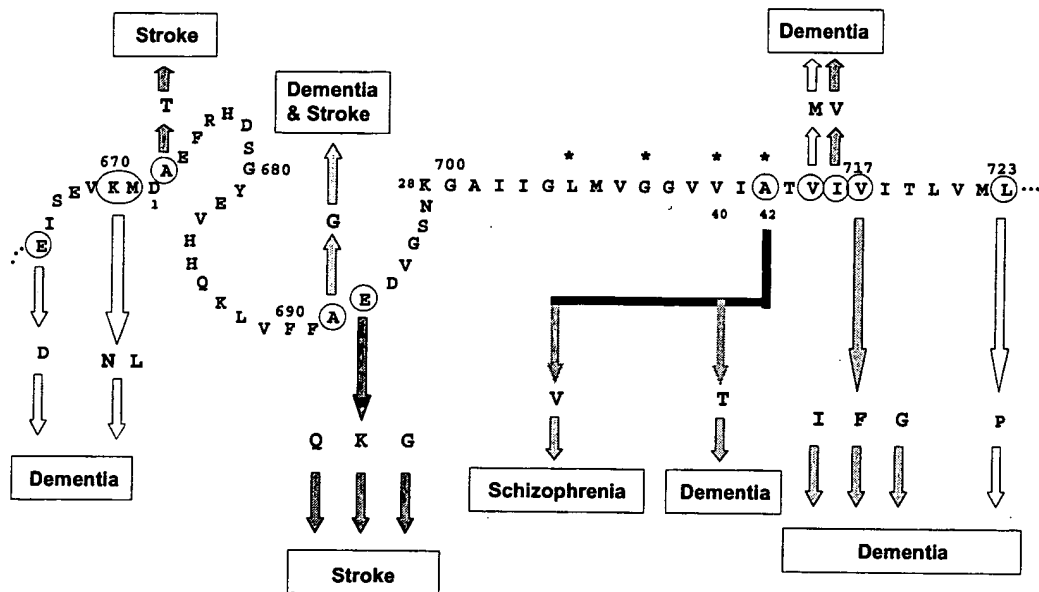


Fig. 1. A $\beta$ PP mutants associated to different phenotypes in familial AD.

approximately 50% of the cases. Strokes are rare after the age of 50, and cognitive decline followed by dementia may occur in those cases that survive the hemorrhagic episodes. In addition to the amyloid deposition, patients have low levels of cystatin C in their cerebrospinal fluid.

The constituent protein of the amyloid deposits in HCHWA-I was the first amyloid purified and characterized from the CNS (1983) [6]. It is a genetic variant of cystatin C (ACys-Q68), a ubiquitously expressed inhibitor of cysteine-proteases codified by a single gene located on chromosome 20 and normally present in biological fluids [1]. The 110-residues-long ACys-Q68 amyloid subunit is degraded at the N-terminus, starting at position 11 of the normal cystatin C and bearing an amino acid substitution (glutamine for leucine) [13] as a result of a single nucleotide change, A for T at codon 68 [28] (Fig. 2).

#### 4. Transthyretin – related cerebral amyloid angiopathy

Familial transthyretin (TTR) amyloidosis is usually associated with peripheral neuropathy and involvement of visceral organs, whereas signs of central nervous system involvement are exceptional. Meningocerebrovascular and oculoleptomeningeal amyloid deposits con-

sisting of TTR variants ATTR-G18 [55] and ATTR-G30 [37] have been reported in two families carrying different point mutations in the *TTR* gene mapped to chromosome 18. A kindred of Hungarian origin containing 56 members spanning 4 generations was recently described. The major clinical symptoms include short-term memory decline, hearing loss, a cerebellar dysfunction with ataxia and bilateral pyramidal dysfunction with progressive spasticity. The onset of symptoms varied from ages 36 to 53, with death occurring between ages 51 and 60. Extensive amyloid deposition is present in meningeal vessels and subpial areas; although not associated to the clinical symptoms, small systemic deposits are present in kidney, skin, ovaries and peripheral nerves. All amyloid lesions are immunoreactive with antibodies against TTR. A single nucleotide change (A for G) at codon 18 results in the presence of glycine instead of aspartic acid (Fig. 2). A second kindred comprising 59 members spanning 4 generations has been described in a large Ohio family of German ancestry. It is clinically characterized by the presence of slowly progressive dementia, seizures, ataxia, hemiparesis, decreased vision and mutism. The age of onset is 46–56 years and the duration of the disease varies between 3 and 26 years. Amyloid deposits are present in the arachnoid and arachnoid blood vessels in the brain and spinal cord, with small and medium size vessels being the most severely affected.

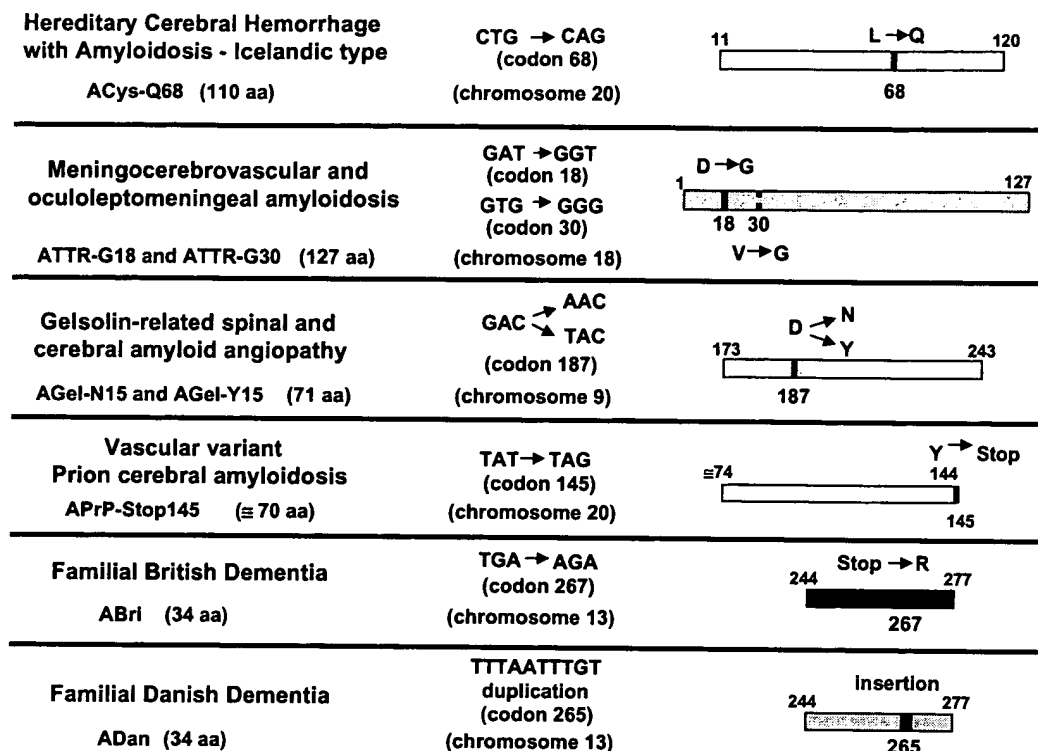


Fig. 2. Diagram summarizing the amyloid diseases and the corresponding amyloid subunits associated with familial cerebral amyloid angiopathies related to dementia.

All these lesions are Congo red positive and immunoreactive with anti-TTR antibodies. Interestingly, vascular amyloid is not longer detectable after the vessels penetrate into the brain parenchyma. Amyloid deposits are also detectable in choroid plexus, ventricular regions and, although infrequently, in vessels of virtually all visceral organs, skin, and skeletal muscle. In this family, a T for G substitution at codon 30 results in the substitution of valine for glycine in the TTR molecule.

### 5. Gelsolin – related spinal and cerebral amyloid angiopathy

Familial amyloidosis, Finnish type (FAF), is an autosomal dominant systemic form of amyloidosis characterized by slowly progressing cranial and peripheral neuropathy, dry and itchy skin, intermittent proteinuria and cardiac abnormalities [34]. The patients gradually develop a typical facies with droopy eyelids and protruding lips. Corneal lattice dystrophy, lace-like deposition of amyloid within the stroma, is the earliest

clinical finding of the syndrome. It is more common in southeastern Finland, but it is encountered elsewhere in Europe, the United States and Japan [24]. The genetic defect underlying FAF has been revealed and the amyloid subunit (AGel) identified. The amyloid fibrils correspond to a 7 kDa internal degradation product of human gelsolin, a widely abundant regulatory protein involved in actin severing and gel – sol transformation [12,32]. AGel spans from position 173 up to residue 243 of the gelsolin protein and bears an amino acid substitution at position 187 (aspartic acid for asparagine) due to a single G to A transition at position 654, the first nucleotide at codon 187 [27] (Fig. 2). FAF cosegregates with the mutation, and the disease is particularly severe in those homozygously affected. The mutation has been detected in Finnish, Dutch, American and Japanese families. A different amino acid substitution at the same codon 187 has been described in patients of Danish and Czech origin suffering the same disorder. In these cases, a transition of G to T at the same codon results in the presence of a tyrosine instead of the normally occurring aspartic acid [8]

(Fig. 2). Although facial palsy, mild peripheral neuropathy and corneal lattice dystrophy are characteristic of both gelsolin-related amyloidoses, atrophic bulbar palsy, ataxia of gait and minor cognitive impairment also occur. Recent immunohistochemical studies in Finnish cases carrying the 187 Asn for Asp mutation have demonstrated a widespread spinal, cerebral and meningeal amyloid angiopathy [25]. The study showed that deposition of A $\beta$  in the spinal and cerebral blood vessel walls, meninges as well as spinal nerve roots and sensory ganglia is an essential feature of this form of systemic amyloidosis that contribute to the CNS symptoms. In addition, anti-FAF antibodies stained Lewy bodies in the cytoplasm of nigral neurons and occasionally in other brainstem nuclei, including locus ceruleus and substantia innominata [10]. The relationship between intracellular gelsolin deposits and synuclein, the main component of Lewy bodies [47], remains to be determined.

#### 6. Prion – related cerebral amyloidosis

A unique category in the conformational disorders are the prion – related diseases (or prionoses), where the etiology is thought to be related to the conversion of the normal prion protein PrP<sup>C</sup> into an infectious and pathogenic form PrP<sup>SC</sup>. Prionoses include Creutzfeldt-Jakob disease (CJD), kuru, Gerstmann-Sträussler-Scheinker disease (GSS) and fatal familial insomnia in humans as well as scrapie and bovine spongiform encephalopathy in animals. Extensive cortical spongiform change, gliosis and neuronal loss are common although not invariable features of prionoses. The parenchymal amyloid load, characteristic of the autosomal dominant GSS, is only present in about 10% of the CJD cases, whereas amyloid angiopathy is virtually absent in all of them. Interestingly, an early onset form of dementia characterized by the deposition of PrP amyloid in leptomeningeal and parenchymal blood vessels in conjunction with neurofibrillary lesions in the cerebral gray matter has been recently described. Although a single case of the so-called PrP cerebral amyloid angiopathy (PrP-CAA) has been reported, it constitutes the first example of PrP amyloid angiopathy in humans [11]. The patient, with clinical diagnosis of AD, presented with memory disturbance and disorientation at age 38, developing a progressive severe dementia. Neuroimaging at the terminal stage (age 58) indicated a severe atrophy of the cerebrum with dilation of the lateral ventricles.

Neuropathologically, extensive amyloid deposition was observed in parenchymal and leptomeningeal vessels as well as in the perivascular neuropil. Cerebral and cerebellar gray matter were the most affected areas whereas amyloid was absent in the white matter. In addition, classical neurofibrillary tangles, neuropil threads and dystrophic neurites were abundant in the cerebral gray matter, particularly in the hippocampus.

The amyloid subunit composing the vascular deposits was identified as a 7.5 kDa fragment of PrP. In this patient, a point mutation TAT to TAG was found at codon 145 of the *PRNP* gene, replacing the normally occurring tyrosine for a newly created stop codon. Based on molecular size, immunoreactivity and molecular genetic analysis, it was deduced that the PrP amyloid subunit in the Y145Stop variant comprises around 70 amino acids and is an N- and C-terminal truncated form of the normal PrP (Fig. 2). In PrP-CAA, the association of amyloid and neurofibrillary lesions does not appear to be casual, since abnormal neurites immunolabeled with anti-phosphorylated tau antibodies co-localize with the PrP amyloid in the neuropil surrounding blood vessels, suggesting that the dyschoric angiopathy may affect the neuronal cytoskeleton [11].

#### 7. ABri – related cerebral amyloidosis

Familial British dementia (FBD), is an autosomal dominant form of CAA clinically characterized by progressive dementia, spastic tetraparesis and cerebellar ataxia, with an age of onset in the fourth to fifth decade. A single extensive pedigree with the disease occurring in multiple generations has been reported [33,39]. Neuropathologically, there is severe and widespread amyloid angiopathy of the brain and spinal cord with perivascular amyloid plaque formation, periventricular white matter changes resembling Binswanger's leukoencephalopathy, neuritic and non-neuritic amyloid plaques affecting cerebellum, hippocampus, amygdala and occasionally cerebral cortex, and neurofibrillary degeneration of hippocampal neurons. In spite of the extensive amyloid deposition of the CNS vasculature, large intracerebral hemorrhage is a rare feature of the disease. The disease was originally described as a familial presenile dementia with spastic paralysis [63]; however, due to the extensive cerebrovascular involvement, the disorder was later on designated familial cerebral amyloid angiopathy, British type [39] and cerebrovascular amyloidosis, British type [42].

The biochemical nature of the amyloid fibrils extracted from leptomeningeal deposits in FBD was recently uncovered [56]. The amyloid subunit, named ABri, is composed of 34 amino acids (EASNC-FAIRHFENKFAVETLICSRVTKNIIEEN) with certain degree of N- and C-terminal heterogeneity and no sequence identity to any known amyloid protein. ABri is devoid of glycine, methionine, proline, aspartic acid, tryptophane, tyrosine and glutamine, featuring pyroglutamate at its N-terminus. The post-translational modification observed at position 1 (pyroglutamate) has been previously found in other brain amyloids, i.e. peptides derived from Alzheimer A $\beta$  [35,43,52]. The N-terminal pyroglutamate may offer protection against *in vivo* proteolysis as well as increase the  $\beta$ -sheet content of the ABri peptide and its tendency to aggregate and polymerize. The two cysteine residues at positions 5 and 22 may be of importance for polymerization and fibrillization, and the predicted isoelectric point (7.0) suggests low solubility at physiologic pH, a property mimicked by synthetic peptides homologous to the full length ABri that spontaneously polymerize and aggregate in solution. This new amyloid protein is a degradation product of a 277 amino acids precursor molecule with a primary structure that resembles a type II single-spanning transmembrane protein. The precursor protein is codified by a single gene *BRI* (also known as *ITM2B* [38]) located on the long arm of chromosome 13. In patients with FBD, a single nucleotide substitution (TGA to AGA at codon 267) results in the presence of an arginine residue in place of the stop codon normally occurring in the wild type precursor molecule and a longer open-reading frame of 277 amino acids instead of 266. The ABri amyloid peptide is formed by the 34 C-terminal amino acids of the mutated precursor protein (Fig. 2).

#### 8. ADan – related cerebral amyloidosis

Familial Danish dementia, also known as hereditary ophthalmic-oto-encephalica, is an early-onset autosomal dominant disorder originating in the Djursland peninsula, Denmark. The disease, identified in nine cases spanning three generations of a single family, is clinically characterized by the development of cataracts, deafness, progressive ataxia and dementia [50]. Cataracts seem to be the early manifestation of the disease, starting before the age of 30, whereas impaired hearing usually develops 10–20 years later. Cerebellar ataxia occurs shortly after the age of 40,

followed by paranoid psychosis and dementia 10 years later. Most patients die in their fifth to sixth decade of life. Neuropathologically, the disease is characterized by diffuse atrophy of all parts of all parts of the brain with a particularly severe involvement of the cerebellum, cerebral cortex and white matter, as well as very thin and almost demyelinated cranial nerves. There is a widespread amyloid angiopathy in the blood vessels of the cerebrum, choroid plexus, cerebellum, spinal cord, and retina. The presence of parenchymal plaques and neurofibrillary tangles is the major histological finding in the hippocampus, whereas the cerebral white matter also shows some ischemic lesions.

Biochemical analysis of the vascular lesions unveiled a 34 amino acids amyloid subunit, ADan (EASNC-FAIRHFENKFAVETLICFNLFLNSQEKHY), with N-terminal homology to the ABri, the peptide originated by a point mutation at the stop codon of gene *BRI* in familial British dementia. The ADan molecule has an isoelectric point of 6.1 and is devoid of glycine, proline, aspartic acid, methionine and tryptophane residues. As in ABri, the isolated ADan amyloid features N-terminus pyroglutamate and two cysteine residues which may be important for the formation and perpetuation of fibrillar deposits. Molecular genetic analysis of the *BRI* gene in the Danish kindred showed a different defect, namely the presence of a 10 nucleotides duplication (795–796insTTTAATTGT) between codons 265 and 266, one codon before the normal stop codon 267. The decamer duplication mutation produces a frame-shift in the *BRI* sequence generating a larger-than-normal precursor protein, of which the amyloid subunit ADan comprises the last 34 C-terminal amino acids [57] (Fig. 2).

#### 9. Conclusion

There is now extensive data indicating that the neuropathology of AD extends beyond amyloid plaques and neurofibrillary tangles. A wide range of vascular lesions (CAA, microvascular degeneration and periventricular white matter lesions) are evident in almost all cases of AD. Single lobar hemorrhages due to amyloid angiopathy, usually associated with focal neurological symptoms, are not a common clinical feature of AD; however, multiple micro-hemorrhages can cause (or contribute to) cognitive decline and dementia. Whether these vascular lesions are coincidental or causal in the pathogenetic processes of AD constitutes an issue of interest to investigate in the next coming years. The poor

correlation between the severity of amyloid angiopathy and the magnitude of parenchymal changes together with the failure to reproduce neuronal loss in transgenic animal models of AD suggest that other still undiscovered factors may modulate the generation of amyloid and neurofibrillary tangles. New clues regarding the relationship between amyloid and neuronal dysfunction may well arise from future research involving other mutant peptides different from A $\beta$ . Particularly interesting will be the study of the novel molecules ABri and ADan, originated from different defects in a gene not previously known to be related to human neurological disorders. Immunohistochemical and electron microscopical studies have demonstrated that the cytoskeletal pathology in FBD and FDD patients is identical to that seen in patients with other neurodegenerative conditions, including Alzheimer disease, Prion disorders, brain trauma, or mutations in chromosome 17 [4,7,14,42,53]. Therefore, different amyloid peptides at distinct cerebral areas could trigger similar neuropathological changes leading to the same scenario: neuronal loss and dementia, supporting the notion that amyloid peptides may be of primary importance in the initiation of neurodegeneration.

### Acknowledgments

This work was supported by NIH grants AG05891 (Merit Award) and AG08721 (to BF). JG is the recipient of the N.I.D.A. from the American Heart Association, New York City affiliate.

### References

- [1] M. Abrahamson, A. Barret, G. Salversen and A. Grubb, Isolation of six cysteine proteinase inhibitors from human urine. Their physiological and enzyme kinetic properties and concentrations in biological fluids, *J. Biol. Chem.* **261** (1986), 11281–11289.
- [2] E. Benedikz, H. Blondal and G. Gudmunsson, Skin deposits in hereditary cystatin C amyloidosis, *Virchows Arch. A* **417** (1990), 325–331.
- [3] E. Castaño, F. Prelli, T. Wisniewski, A. Golabek, A. Kumar, C. Soto and B. Frangione, Fibrillogenesis of Alzheimer's amyloid-peptides and apolipoprotein E, *Biochem. J.* **306** (1995), 599–604.
- [4] L. Clark, P. Poorkaj, Z. Wszolek, D. Geschwind, Z. Nasreddine, B. Miller, D. Li, H. Payami, F. Awert, K. Markopoulou, A. Andreadis, I. D'souza, V. Lee, J. Trojanowski, V. Zhukareva, T. Bird, G. Schellenberg and K. Wilhelmsen, Pathogenic implications of mutations in the tau gene in pallidoponto-nigral degeneration and related neurodegenerative disorders linked to chromosome 17, *Proc. Natl. Acad. Sci. USA* **95** (1998), 13103–13107.
- [5] A. Clements, D. Walsh, C. Williams and D. Allsop, Effects of the mutations Glu22 to Gln and Ala21 to Gly on the aggregation of a synthetic fragment of the Alzheimer's amyloid  $\beta$ /A4 peptide, *Neurosc. Lett.* **161** (1993), 17–20.
- [6] D.H. Cohen, H. Feiner, O. Jensson and B. Frangione, Amyloid fibril in hereditary cerebral hemorrhage with amyloidosis (HCHWA) is related to the gastroenteropancreatic neuroendocrine protein, gamma trace, *J. Exp. Med.* **158** (1983), 623–628.
- [7] D. Dickson, Neurodegenerative diseases with cytoskeletal pathology: a biochemical classification, *Ann. Neurol.* **42** (1997), 541–544.
- [8] A. de la Chapelle, J. Kere, G.H. Sack Jr., R. Tolvanen and C.P. Maury, Familial amyloidosis, Finnish type: G654 – a mutation of the gelsolin gene in Finnish families and an unrelated American family, *Genomics* **13** (1992), 898–901.
- [9] H. Fabian, G. Szendrei, H. Mantsch and L. Otvos, Comparative analysis of human and Dutch-type Alzheimer's -amyloid peptides by infrared spectroscopy and circular dichroism, *Biochem. Biophys. Res. Commun.* **191** (1993), 232–239.
- [10] B. Frangione, M. Haltia, E. Levy, J. Ghiso, S. Kiuru and F. Prelli, Co-occurrence of two amyloid proteins in a patient with familial amyloidosis, Finnish type, in: *Alzheimer's disease: basic mechanisms, diagnosis and therapeutic strategies*, K. Iqbal, D. McLachlan, B. Winblad and H. Wisniewski, eds., John Wiley & Sons Ltd, New York, 1991, pp. 255–264.
- [11] B. Ghetti, P. Piccardo, M.G. Spillantini, Y. Ichimiya, M. Porro, F. Perini, T. Kitamoto, J. Tateishi, C. Seiler, B. Frangione, O. Bugiani, G. Giaccone, F. Prelli, M. Goedert, S.R. Dlouhy and F. Tagliavini, Vascular variant of prion protein cerebral amyloidosis with tau-positive neurofibrillary tangles: the phenotype of the stop codon 145 mutation in PRNP, *Proc. Natl. Acad. Sci. USA* **93** (1996), 744–748.
- [12] J. Ghiso, M. Haltia, F. Prelli, J. Novello and B. Frangione, Gelsolin variant (Asn-187) in familial amyloidosis Finnish type, *Biochem. J.* **272** (1990), 827–830.
- [13] J. Ghiso, O. Jensson and B. Frangione, Amyloid fibrils in hereditary cerebral hemorrhage with amyloidosis of Icelandic type is a variant of  $\gamma$ -trace basic protein (cystatin-C), *Proc. Natl. Acad. Sci. USA* **83** (1986), 2974–2978.
- [14] G. Giaccone, F. Tagliavini, L. Verga, B. Frangione, M. Farlow, O. Bugiani and B. Ghetti, Neurofibrillary tangles in the Indiana kindred of Gerstmann-Sträussler-Scheinker disease share antigenic determinants with those of Alzheimer's disease, *Brain Res.* **530** (1990), 325–329.
- [15] G.G. Glenner and C. Wong, Alzheimer's disease: initial report of the purification and characterization of a novel cerebrovascular amyloid protein, *Biochem. Biophys. Res. Commun.* **120** (1984), 885–890.
- [16] A. Grubb, O. Jensson, G. Gudmunsson, A. Arnason, H. Lofberg and J. Malm, Abnormal metabolism of  $\gamma$ -trace alkaline microprotein, *New Engl. J. Med.* **311** (1984), 1547–1549.
- [17] G. Gudmundsson, J. Hallgrímsson, T. Jonasson and O. Bjarnason, Hereditary cerebral hemorrhage with amyloidosis, *Brain* **95** (1972), 387–404.
- [18] J. Haan, R. Roos, P. Briet, M. Herpers, W. Lujendijk and G. Bots, Hereditary cerebral hemorrhage with amyloidosis-Dutch type: clinical characteristics, *Clin. Neurol. Neurosurg.* **91** (1989), 285–290.
- [19] L. Hendriks, C.M. van Duijn, P. Cras, M. Cruts, W. Van Huij, F. van Harskamp, A. Warren, M. McInnis, S.E. Antonarakis, J.J. Martin, A. Hofman and C. Van Broeckhoven, Presenile dementia and cerebral hemorrhage linked to a mutation at

- codon 692 of the  $\beta$ -amyloid precursor protein gene, *Nature Genet.* 1 (1992), 218–221.
- [20] A. Heyman, G.G. Fillenbaum, K.A. Welsh-Bohmer, M. Gearing, S.S. Mirra, R.C. Mohs, B.L. Peterson and C.F. Pieper, Cerebral infarcts in patients with autopsy-proven Alzheimer's disease: CERAD, part XVIII. Consortium to establish a registry for Alzheimer's disease, *Neurology* 51 (1998), 159–162.
  - [21] O. Jensson, A. Palsdottir, L. Thorsteinsson and A. Arnason, The saga of cystatin C gene mutation causing amyloid angiopathy and brain hemorrhage-clinical genetics in Iceland, *Clin. Genet.* 36 (1989), 368–377.
  - [22] R.N. Kalaria, D.R. Premkumar, A.B. Pax, D.L. Cohen and I. Lieberburg, Production and increased detection of amyloid beta protein and amyloidogenic fragments in brain microvessels, meningeal vessels and choroid plexus in Alzheimer's disease, *Brain Res. Mol. Brain Res.* 35 (1996), 58–68.
  - [23] K. Kamino, H.T. Orr, H. Payami, E.M. Wijsman, M.A. Alonso, S.M. Pulst, L. Anderson, S. O'Dahl, E. Nemens, J.A. White, A.D. Sadovnick, M.J. Ball, J. Kelly, A. Warren, M. McInnis, S.A. Antonarakis, J.R. Korenberg, V. Sharma, W. Kukull, E. Larson, L.L. Heston, G.M. Martin, T. Bird and G. Schellemborg, Linkage and mutational analysis of familial Alzheimer disease kindreds for the APP gene region, *Am. J. Hum. Genet.* 51 (1992), 998–1014.
  - [24] S. Kiuru, Gelsolin-related familial amyloidosis, Finnish type (FAF) and its variants found worldwide. A review, *Amyloid, Int. J. Exp. Clin. Invest.* 3 (1998), 55–66.
  - [25] S. Kiuru, O. Salonen and M. Haltia, Gelsolin-related spinal and cerebral amyloid angiopathy, *Ann. Neurol.* 45 (1999), 305–311.
  - [26] E. Levy, M. Carman, I. Fernandez-Madrid, M. Power, I. Lieberburg, S. van Duinen, G. Bots, W. Luyendijk and B. Frangione, Mutation of the Alzheimer's disease amyloid gene in hereditary cerebral hemorrhage, Dutch type, *Science* 248 (1990), 1124–1126.
  - [27] E. Levy, M. Haltia, I. Fernandez-Madrid, O. Kouvainen, J. Ghiso, F. Prelli and B. Frangione, Mutation in gelsolin gene in Finnish hereditary amyloidosis, *J. Exp. Med.* 172 (1990), 1865–1867.
  - [28] E. Levy, C. Lopez-Otin, J. Ghiso, D. Geltner and B. Frangione, Stroke in Icelandic patients with hereditary amyloid angiopathy is related to a mutation in the cystatin-C gene, an inhibitor of cysteine proteases, *J. Exp. Med.* 169 (1989), 1771–1778.
  - [29] W. Luyendijk and J. Schoen, Intracerebral haematomas. A clinical study of 40 surgical cases, *Psychiat. Neurol. Neurochir.* 67 (1964), 445–468.
  - [30] W. Luyendijk, G. Bots, M. van der Vlis, L. Went and B. Frangione, Hereditary cerebral hemorrhage caused by cortical amyloid angiopathy, *J. Neurol. Sci.* 85 (1988), 267–280.
  - [31] C.L. Masters, G. Simms, N.A. Weinman, G. Multhaup, B.L. McDonald and K. Beyreuther, Amyloid plaque core protein in Alzheimer disease and Down syndrome, *Proc. Natl. Acad. Sci. USA* 82 (1985), 4245–4249.
  - [32] C. Maury and M. Baumann, Isolation and characterization of cardiac amyloid in familial amyloid polyneuropathy type IV (Finnish): relation of the amyloid protein to variant gelsolin, *Biochem. Biophys. Acta* 1096 (1990), 84–86.
  - [33] S. Mead, M. James-Galton, T. Révész, R.B. Doshi, G. Harwood, E.L. Pan, J. Ghiso, B. Frangione and G. Plant, Familial British dementia with amyloid angiopathy: Early clinical, neuropsychological and imaging findings, *Brain* 123 (2000), 975–986.
  - [34] J. Meretoja, Familial systemic paramyloidosis with lattice dystrophy of the cornea, progressive cranial neuropathy, skin changes and various internal symptoms, *Ann. Clin. Res.* 1 (1969), 314–324.
  - [35] H. Mori, K. Takio, M. Ogawara and D. Selkoe, Mass spectrometry of purified amyloid beta protein in Alzheimer's disease, *J. Biol. Chem.* 267 (1992), 17082–17086.
  - [36] C. Nilsberth, C. Forsell, K. Axelman, C. Gustafson, J. Luthman, J. Naslund and L. Lannfelt, A novel APP mutation (E693G) – the Arctic mutation – causing Alzheimer's disease with vascular symptoms, *Soc. Neurosci.* 25 (1999), 120.4S.
  - [37] R. Petersen, H. Goren, M. Cohen, S. Richardson, N. Tresser, A. Lynn, M. Gali, M. Estes and P. Gambetti, Transthyretin amyloidosis: A new mutation associated with dementia, *Ann. Neurol.* 41 (1997), 307–313.
  - [38] K. Pittois, W. Deleersnijder and J. Merregaert, cDNA sequence analysis, chromosomal assignment and expression pattern of the gene coding for integral membrane protein 2B, *Gene* 217 (1998), 141–149.
  - [39] G. Plant, T. Révész, R. Barnard, A. Harding and P. Gautier-Smith, Familial cerebral amyloid angiopathy with nonneuritic plaque formation, *Brain* 113 (1990), 721–747.
  - [40] F. Prelli, E.M. Castaño, G.G. Glenner and B. Frangione, Differences between vascular and plaque core amyloid in Alzheimer's disease, *J. Neurochem.* 51 (1989), 648–651.
  - [41] F. Prelli, E. Levy, S. van Duinen, G. Bots, W. Luyendijk and B. Frangione, Expression of a normal and variant Alzheimer's  $\beta$ -protein gene in amyloid of hereditary cerebral hemorrhage, Dutch type: DNA and protein diagnostic assays, *Biochem. Biophys. Res. Commun.* 170 (1990), 301–307.
  - [42] T. Révész, J. Holton, B. Doshi, B. Anderton, F. Scaravilli and G. Plant, Cytoskeletal pathology in familial cerebral amyloid angiopathy (British type) with non-neuritic plaque formation, *Acta Neuropath.* 97 (1999), 170–176.
  - [43] T. Saido, W. Yamao-Harigaya, T. Iwatsubo and S. Kawashima, Amino- and carboxyl-terminal heterogeneity of beta-amyloid peptides deposited in human brain, *Neurosci. Lett.* 13 (1996), 173–176.
  - [44] D. Schenk, R. Barbour, W. Dunn, G. Gordon, H. Grajeda, T. Guido, K. Hu, J. Huang, K. Johnson-Wood, K. Khan, D. Kholodenko, M. Lee, Z. Liao, I. Lieberburg, R. Motter, L. Mutter, F. Soriano, G. Shopp, N. Vasquez, C. Vandevert, S. Walker, M. Wogulis, T. Yednock, D. Games and P. Seubert, Immunization with amyloid-beta attenuates Alzheimer-disease-like pathology in the PDAPP mouse, *Nature* 400 (1999), 173–177.
  - [45] K. Sorimachi and D. Craik, Structure determination of extracellular fragments of amyloid proteins involved in Alzheimer's disease and Dutch-type hereditary cerebral hemorrhage with amyloidosis, *Eur. J. Biochem.* 219 (1994), 237–239.
  - [46] C. Soto, E. Sigurdsson, L. Morelli, A. Kumar, E. Castaño and B. Frangione,  $\beta$ -sheet breaker peptides inhibit fibrillogenesis in a rat brain model of amyloidosis: implications for Alzheimer's disease, *Nature Med.* 4 (1998), 822–826.
  - [47] M.G. Spillantini, M.L. Schmidt, V.M. Lee, J.Q. Trojanowski, R. Jakes and M. Goedert, Alpha-synuclein in Lewy bodies, *Nature* 388 (1997), 839–840.
  - [48] P.H. St George-Hyslop, Molecular genetics of Alzheimer disease, *Biol. Psychiatry* 47 (2000), 183–199.
  - [49] W.J. Strittmatter, A.M. Saunders, D. Schmechel, M. Pericak-Vance, J. Enghild, G.S. Salversen and A.D. Roses, Apolipoprotein E: High avidity binding to  $\beta$ -amyloid and increased frequency of type 4 allele in late-onset familial Alzheimer disease, *Proc. Natl. Acad. Sci. USA* 90 (1993), 1977–1981.



- [50] H. Stromgren, Heredopathia ophthalmoto-encephalica, in: *Handbook of Clinical Neurology*, (Vol. 42), P.J. Vinken and G.W. Bruyn, eds., North Holland Publishing Co., Amsterdam, 1981, pp. 150–152.
- [51] F. Tagliavini, G. Rossi, A. Padovani, M. Magoni, G. Andora, M. Sgarzi, A. Bizzi, M. Savoiardo, F. Carella, M. Morbin, G. Giaccone and O. Bugiani, A new APP mutation related to hereditary cerebral hemorrhage, *Alzh. Reports* 2 (1999), S28.
- [52] T. Tekirian, T. Saido, W. Markesbery, M. Russell, D. Wekstein, E. Patel and J. Geddes, N-terminal heterogeneity of parenchymal and cerebrovascular A $\beta$  deposits, *J. Neuropathol. Exp. Neurol.* 57 (1998), 76–94.
- [53] T. Tokuda, S. Ikeda, N. Yanagisawa, Y. Ihara and G. Glenner, Re-examination of ex-boxers' brains using immunohistochemistry with antibodies to amyloid beta-protein and tau protein, *Acta Neuropath.* 82 (1991), 280–285.
- [54] S. van Duinen, E. Castaño, F. Prelli, G. Bots, W. Luyendijk and B. Frangione, Hereditary cerebral hemorrhage with amyloidosis in patients of Dutch origin is related to Alzheimer's disease, *Proc. Natl. Acad. Sci. USA* 84 (1987), 5991–5994.
- [55] R. Vidal, F. Garzuly, H. Budka, M. Lalowski, R. Linke, F. Brittig, B. Frangione and T. Wisniewski, Meningocerebrovascular amyloidosis associated with a novel Transthyretin mis-sense mutation at codon 18 (TTRD18G), *Am. J. Pathol.* 148 (1996), 361–366.
- [56] R. Vidal, B. Frangione, A. Rostagno, S. Mead, T. Révész, G. Plant and J. Ghiso, A stop-codon mutation in the BRI gene associated with familial British dementia, *Nature* 399 (1999), 776–781.
- [57] R. Vidal, T. Révész, A. Rostagno, E. Kim, J. Holton, T. Bek, M. Bojsen-Møller, H. Braendgaard, G. Plant, J. Ghiso and B. Frangione, A decamer duplication in the 3' region of the BRI gene originates a new amyloid peptide that is associated with dementia in a Danish kindred, *Proc. Natl. Acad. Sci. USA* 97 (2000), 4920–4925.
- [58] H. Vinters, Cerebral amyloid angiopathy: a critical review, *Stroke* 18 (1987), 311–324.
- [59] A. Wattendorff, G. Bots, L. Went and L. Endtz, Familial cerebral amyloid angiopathy presenting as recurrent cerebral hemorrhage, *J. Neurol. Sci.* 55 (1982), 121–135.
- [60] P. Westermark, S. Araki, M. Benson, A. Cohen, B. Frangione, C. Masters, M. Saraiva, J. Sipe, G. Husby, R. Kyle and D. Selkoe, Nomenclature of amyloid fibril proteins, *Amyloid, Int. J. Exp. Clin. Invest.* 6 (1999), 62–66.
- [61] T. Wisniewski and B. Frangione, Apolipoprotein E: A pathological chaperone protein in patients with cerebral and systemic amyloid, *Neurosc. Lett.* 135 (1992), 235–238.
- [62] T. Wisniewski, J. Ghiso and B. Frangione, Peptides homologous to the amyloid  $\beta$ -protein of Alzheimer's disease containing a glutamine for glutamic acid substitution have accelerated amyloid fibril formation, *Biochem. Biophys. Res. Commun.* 173 (1991), 1247–1254.
- [63] C. Worster-Drought, T.R. Hill and W.H. McMenemey, Familial presenile dementia with spastic paralysis, *J. Neurol. Psychopathol.* 14 (1933), 27–34.

# Instability, unfolding and aggregation of human lysozyme variants underlying amyloid fibrillogenesis

David R. Booth\*<sup>1</sup>, Margaret Sundet<sup>1</sup>, Vittorio Bellotti\*<sup>2</sup>, Carol V. Robinson<sup>3</sup>, Winston L. Hutchinson\*, Paul E. Fraser<sup>4</sup>, Philip N. Hawkins\*, Christopher M. Dobson\*, Sheena E. Radford<sup>5</sup>, Colin C. F. Blaket & Mark B. Pepys\*

\* Immunological Medicine Unit, Royal Postgraduate Medical School, Hammersmith Hospital, London W12 0NN, UK

<sup>1</sup> Laboratory of Molecular Biophysics and <sup>2</sup> New Chemistry Laboratory, Oxford Centre for Molecular Sciences, University of Oxford, Oxford OX1 3QT, UK

<sup>3</sup> Centre for Research in Neurodegenerative Diseases, University of Toronto, Toronto M5S 3112, Canada

<sup>4</sup> These authors contributed equally to this work.

**Tissue deposition of soluble proteins as amyloid fibrils underlies a range of fatal diseases. The two naturally occurring human lysozyme variants are both amyloidogenic, and are shown here to be unstable. They aggregate to form amyloid fibrils with transformation of the mainly helical native fold, observed in crystal structures, to the amyloid fibril cross- $\beta$  fold. Biophysical studies suggest that partly folded intermediates are involved in fibrillogenesis, and this may be relevant to amyloidosis generally.**

Tissue deposition of soluble autologous proteins as insoluble amyloid fibrils is associated with serious diseases including systemic amyloidosis, Alzheimer's disease, and transmissible spongiform encephalopathy, but the mechanisms of amyloid fibrillogenesis are poorly understood. Although the diverse human proteins that can form amyloid fibrils in vivo have unrelated sequences and tertiary folds, they can all polymerize into fibrils with similar ultrastructural appearance and identical tinctorial properties. Furthermore, the core structure of all amyloid fibrils consists of  $\beta$ -sheets with the strands perpendicular to the long axis of the fibre<sup>1,2</sup>. Knowing which conformational rearrangements converge on the same final fold is important for understanding the determinants of protein structure, and may enable the development of rational approaches to the treatment of amyloid diseases. However, although a lot is known about the mutations and substitutions responsible for hereditary and acquired amyloidosis (see, for example, refs 5-14), there is little detailed information about the relationship between structure and folding in amyloid proteins.

The two known natural mutations in the human lysozyme gene both cause autosomal dominant hereditary amyloidosis. Affected individuals are heterozygous for single base changes which encode non-conservative amino-acid substitutions, Ile56Thr and Asp67His, respectively, and the amyloid fibrils consist exclusively of the variant protein<sup>15</sup> (see below). The structure, dynamics and folding of c-type lysozymes and the related (x-lactalbumins have been studied comprehensively<sup>16-21</sup>. The identification of lysozyme as an amyloidogenic protein was therefore of particular interest.

Here we present a detailed analysis of the structure, stability, conformational dynamics and fibrillogenic properties of the amyloidogenic lysozyme variants which links the formation of amyloid with the folding behaviour of proteins.

## Amyloidogenic variants have native folds

Wild-type lysozyme and the amyloidogenic variants<sup>15</sup>, which have

**Table 1 Molecular masses and enzyme characteristics of wild-type and variant lysozymes**

Protein	Electrospray ionization mass spectrometry		Enzyme properties	
	Observed $M_i$	Predicted $M_i$	$K_M$ ( $\mu M$ )	$k_{cat}$ ( $M s^{-1}$ )
Natural wild type	14,691 <sup>1</sup>	14,693	not done <sup>1</sup>	not done <sup>1</sup>
Recombinant wild type	14,696	14,693	16.5(4)	14.5 (0.5)
Recombinant Ile56Thr	14,681 <sup>1</sup>	14,680 <sup>2</sup>	18.5 (3)	15.0 (0.5)
Recombinant Asp67His	14,719	14,715	38.0 (9)	9.5 (0.5)

<sup>1</sup>  $k_M$  and  $k_{cat}$  are given as mean (s.d.)

not previously been isolated, were produced in the baculovirus expression system, and the correct mass of each purified, recombinant protein was demonstrated by electrospray ionization mass spectrometry<sup>22</sup> (ESI-MS) (Table 1). They were all enzymatically active, although the Asp67His variant had a higher  $K_M$  and lower  $k_{cat}$  than the wild type and the Ile56Thr variant (Table 1).

The native folds of the two amyloidogenic variants determined by X-ray crystallography both resemble that of the wild-type protein<sup>23</sup> (Fig. 1a), and all have the four correct, intact disulphide bonds. However, substitution of Asp 67 by histidine destroys the network of hydrogen bonds that stabilizes the (3-domain, resulting in a large, concerted movement of the (3-sheet and the long loop within the (3-domain away from each other, distortion of the active site, and an overall displacement of backbone atoms in the vicinity of residues 48 and 70 by as much as 11 Å (Fig. 1a). The crystal structure of the Ile56Thr variant does not show such changes, indicating that the movements in the  $\beta$ -domain are not the direct cause of amyloidogenicity. However, closer inspection of the two structures demonstrates that subtle, but structurally significant, changes at the interface region between the  $\alpha$ - and (3-domains occur in both variants (Fig. 1b, c). Ile 56 is a pivotal residue for the structural integrity of the lysozyme fold in that it links the two domains; its importance is emphasized by its high conservation in the lysozyme sequences. An increased B-factor (11.7 Å<sup>2</sup>) was found for the Cot

<sup>1</sup> Present addresses: Dipartimento di Biochimica, Università di Pavia, Via Taramelli 3B, 27100 Pavia, Italy (V.B.); Department of Biochemistry and Molecular Biology, University of Leeds, Leeds LS2 9JT, UK (S.E.R.).

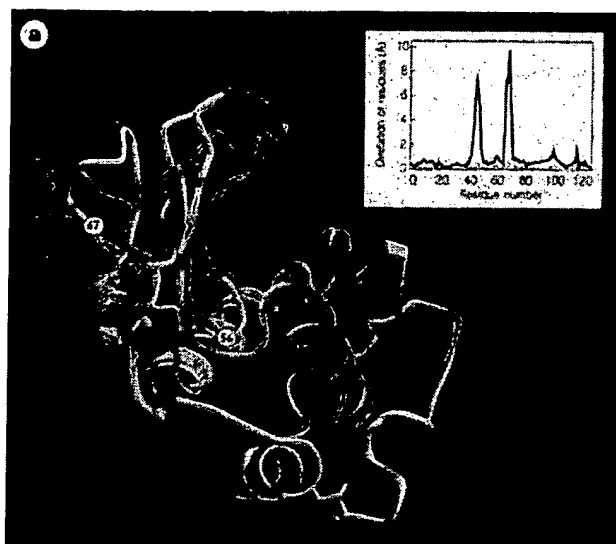
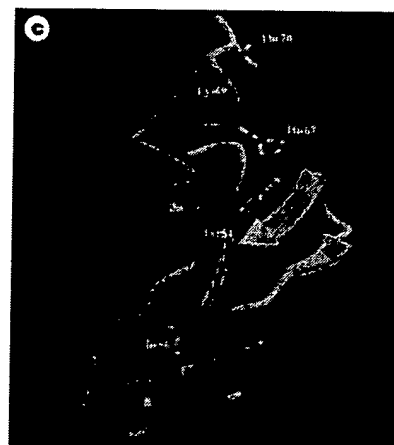


**Figure 1** a, Overlay of ribbon diagrams representing the structures of wild-type human lysozyme (grey) and the soluble form of Asp67His lysozyme (coloured from blue at the N terminus to red at the C terminus). Red arrows indicate the relative movement in the positions of residues 45-54 and 67-75 in the Asp67His variant compared with those in the wild-type protein. The four native disulphide bonds in the wild-type protein and both variant structures are shown in yellow. Inset, plot showing the displacement of the residues of the Asp67His (solid line) and Ile56Thr (broken line) variants from their positions in the wild-type protein. b, Ribbon diagram of the p-domain of the wild-type protein, showing the critical role of Asp 67 in the network of hydrogen bonds that stabilizes this domain. c, Ribbon diagram illustrating the same region in the Asp67His variant and the disruption of the domain that occurs when the aspartate at position 67 is replaced by histidine and the hydrogen-bonding network is destroyed.



atom of residue 56 in the Ile56Thr variant, relative to that of Ile 56 in the wild-type protein (6.4 Å). This is presumably due to the now hydrophilic side chain being in an unfavourable hydrophobic environment, even though its hydrogen-bonding potential seems to be at least partly satisfied by a hydrogen bond (length 3.3 Å) to one of the water molecules found in both the wild-type and the variant structures. In the Asp67His variant, the changes in the conformations of the (3-sheet and long loop are transmitted down to residue 56, resulting in a new orientation for the side chain and an increase in the B-factor of the C $\alpha$  atom of the latter (9.7 Å<sup>2</sup>). This suggests that the crucial interface region between the  $\alpha$ - and (3-domains is less constrained in both variants than in the wild-type protein. This common feature of both structures implies that it could be an important factor in their amyloidogenic properties. Substitution of Ile 55 in hen lysozyme (the corresponding residue to Ile 56 in human lysozyme) by threonine also reduces the stability of the protein and generates a tendency to aggregate<sup>15</sup>, further supporting the view that this residue is essential for the maintenance of the lysozyme fold.

#### Fibril formation occurs in vitro

In contrast to the reversible thermal denaturation of wild-type lysozyme from both natural and recombinant sources, the amyloidogenic variants were inactivated by heating (Fig. 2). The variants were also less stable than wild-type lysozyme, with unfolding transition midpoints reproducibly 10 °C or more below that of

the wild-type protein. Furthermore, both variants eventually lost all activity when incubated at pH 7.4 at the physiological temperature of 37 °C, whereas the wild-type protein retained full activity under these conditions (data not shown).

The amyloidogenic lysozyme variants also aggregated on heating, unlike the wild-type protein. The rate and extent of aggregation varied with protein concentration and the expression batch, and although the aggregates stained with Congo red, they generally did not give the green-red birefringence in polarized light that is pathognomonic of amyloid. Nevertheless, negatively stained electron micrographs revealed rigid, non-branching fibres of indeterminate length and approximately 8-10 nm diameter, with the typical appearance of amyloid fibrils. Fibrils were also seen in electron micrographs of the sediment that formed spontaneously at 4 °C in concentrated solutions of both Ile56Thr and Asp67His variants (Fig. 3). Strikingly, one preparation of heated Asp67His lysozyme contained fibres that stained with Congo red and did display the diagnostic green birefringence, confirming the capacity of the variant to form the classical amyloid structure in vitro independently of any other component.

Fourier-transform infrared spectroscopy (FTIR) of recombinant Asp67His lysozyme heated under conditions in which fibrils form demonstrated a predominance of (3-structure and a loss of helical structure relative to the wild-type protein (Fig. 4). The FTIR spectrum also indicated the persistence of some helical structure in the heated sample. This could arise from residual soluble forms of

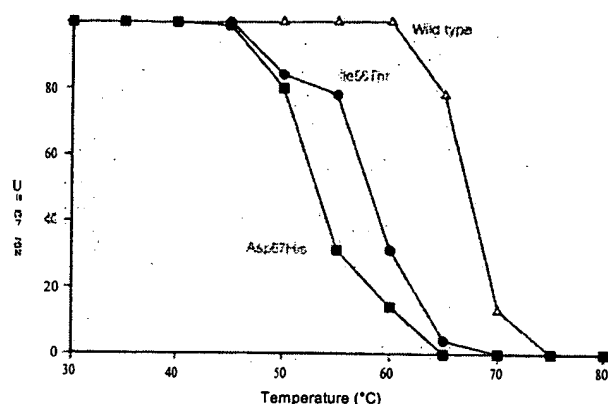


Figure 2 Melting temperatures of wild-type and amyloidogenic variant lysozymes.



Figure 3 Electron micrograph of sediment from the Ile56Thr lysozyme, after standing at 1 mg ml<sup>-1</sup> for 14 days at 4°C in 10 mM HEPES, 1M LiCl, pH 8.0. Scale bar, 100 nm.

Table 2 Recovery of enzymatically active lysozyme from *ex vivo* Asp67His lysozyme amyloid fibrils

	$V_o$ on gel filtration (ml)	Lysozyme recovered ( $\mu$ g)		Electrospray ionization mass spectrometry	
		Protein by A <sub>280</sub>	Active enzyme	Observed $M_r$	Predicted $M_r$
<i>Ex vivo</i> Asp67His lysozyme fibrils solubilized in 6 M guanidinium-HCl, pH 6.7	13.20 (0.13)	100	80	14,716.0 14,733.8	14,715 for Asp67His lysozyme 14,729 for Asp67His lysozyme with MetSO
<i>Ex vivo</i> Asp67His lysozyme fibrils solubilized in 6M guanidinium-HCl, pH 6.7, 0.1 % 2-mercaptoethanol	12.57 (0.06)	113	0	No signal obtained	

<sup>a</sup> given as mean (s.d.) from 3 experiments.

the lysozyme variant, from persistence of helical structure in the fibril, or both.

### Fibrillogenesis is reversible

Our identification of a second Asp67His family<sup>27</sup>, apparently unrelated to the original kindred<sup>15</sup>, provided the opportunity to study Asp67His lysozyme amyloid fibrils. The X-ray fibre diffraction pattern (not shown) contains distinctive reflections at 4.6–4.8 Å on the meridian and at 8–14 Å on the equator of the image, indicating that the underlying ordered structure is a (3-sheet in which the constituent  $\beta$ -strands are at right angles to the fibre axis<sup>4</sup>. Such cross- $\beta$  structures are characteristic of amyloid and have also been described in the glutamine repeats that are associated with several neurodegenerative diseases, including Huntington's disease, and which cause oligomerization of proteins<sup>28</sup>. The fibre diffraction pattern of *ex vivo* Asp67His lysozyme fibrils contains no reflections attributable to helical structure, suggesting that, if helices persist after transformation of the soluble protein to the fibrillar form, they are not regularly ordered.

As previously reported for Ile56Thr fibrils<sup>15</sup>, 85% of the total protein in water-extracted *ex vivo* Asp67His fibrils ran in reduced SDS-PAGE in the same position as intact monomeric lysozyme; the remainder consisted of oligomeric lysozyme aggregates and traces of uncharacterized high-molecular-weight material that is seen in all *ex vivo* amyloid fibrils. However, like the fibrils from the Ile56Thr case<sup>15</sup>, the Asp67His lysozyme fibrils could not be dissociated to a form detectable by ESI-MS using either acetonitrile/acetic acid mixtures or up to 100% formic acid. We therefore solubilized some of the *ex vivo* Asp67His fibrils by denaturation in 6 M guanidine HCl, isolated the lysozyme by gel filtration in the same denaturing conditions, and attempted to refold it by dialysis into water at pH

3.8, a solvent in which natural wild-type lysozyme is stable. Although some reaggregation occurred during dialysis, the recovered lysozyme was detectable by ESI-MS with a mass corresponding to intact, monomeric, Asp67His variant (Table 2). The exclusive presence of variant lysozyme in either Asp67His or Ile56Thr (ref. 15) *ex vivo* amyloid fibrils indicates that their pathological aggregation does not engage wild-type lysozyme *in vivo*, presumably because the wild type has greater stability than the variants.

Remarkably, the refolded Asp67His variant lysozyme was enzymatically active, in contrast to the absence of any activity in the original fibril preparation, using soluble penta-*N*-acetyl- $\beta$ -chitopentaoside substrate. Although the variant protein must have undergone major conformational change *in vivo* to form characteristic cross- $\beta$  amyloid fibrils, it remained able, after unfolding, to renature spontaneously into the active enzyme. However, when the disulphide bonds within the chain were reduced with 2-mercaptoethanol during solubilization and unfolding, no lysozyme activity was observed and the protein could not be detected by ESI-MS (Table 2).

### Stabilized molten globule intermediate

We have used circular dichroism to monitor the unfolding behaviour of the two lysozyme variants under conditions in which they form fibrils *in vitro*. The results (Fig. 5a–d) showed that both variants were less thermostable than the wild-type protein, with midpoints of denaturation approximately 12°C lower than that of the wild-type protein at pH 5.0. More importantly, however, the unfolding transition of the two amyloidogenic variants, although reversible under conditions in which fibril formation did not occur, was not cooperative. This resulted in a partly folded state being significantly populated near the midpoint of unfolding. This state

Table 3 Crystallographic data statistics

Parameters	Recombinant wild type	Asp67His variant	Ile56Thr variant
Structure determination			
Resolution (Å)	30–1.8 Å	30–1.75 Å	30–1.8 Å
Data completeness (%)	89.9	90.9	92.8
<i>I/a</i> for all <i>hkl</i>	12.1	8.5	11.2
<i>I/a</i> at high-resolution limit	3.7	3.1	3.6
Observations	51,285	41,333	49,524
Unique reflections	10,221	11,071	10,578
Space group	P2 <sub>1</sub> 2 <sub>1</sub> 2 <sub>1</sub>	P2 <sub>1</sub>	P2 <sub>1</sub> 2 <sub>1</sub> 2 <sub>1</sub>
Unit cell (Å)	56.62 × 60.88 × 33.79	37.34 × 31.86 × 51.50	56.80 × 60.89 × 33.70
$\beta$ -angle		102.56°	
R sym [%]	8.3	10.3	9.2
Structure refinement			
Resolution (Å)	8–1.8 Å	848 Å	8–1.8 Å
Non-H atoms	1,029	1,031	1,028
Water molecules	38	115	43
R-factor (reflections)	21.3 (10,216)	22.8 (10,216)	21.1 (10,513)
Average B-value	13.11	13.54	16.76
R.m.s.d. bond lengths (Å)	0.013	0.015	0.013
R.m.s.d. bond angles (°)	1.674	1.814	1.643
R.m.s.d. dihedral angles (°)	24.132	23.076	24.501
R.m.s.d. improper angles (°)	1.463	1.666	1.391

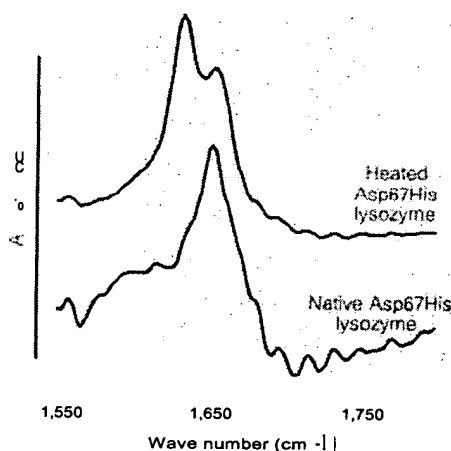


Figure 4 FTIR spectra, offset for comparison, of soluble Asp67His lysozyme, and after heating to induce fibril formation. The dominant absorption band centred at 1,655  $\text{cm}^{-1}$  in the untreated sample reflects the large  $\alpha$ -helical component in the soluble, native protein. The shift to absorption at about 1,630  $\text{cm}^{-1}$  after heating indicates an increase in  $\beta$ -sheet content. The shoulder at 1,655  $\text{cm}^{-1}$  in the heated sample demonstrates the persistence of some helix.

had substantial helical secondary structure but lacked persistent tertiary interactions (Fig. 5b, d). Such behaviour is quite different from the cooperative unfolding displayed by the wild-type protein under these conditions (Fig. 5a, c), but is similar to the thermal unfolding of wild-type human lysozyme under conditions of extremely low pH, where the protein unfolds through a partially structured intermediate with circular-dichroism properties similar to those identified here for the variants at pH 5.0 (ref. 30). Moreover, species with similar properties have been identified on the kinetic or equilibrium folding pathways of other lysozymes and  $\alpha$ -lactalbumins<sup>31,32</sup>. At the midpoint of thermal denaturation, the partly folded amyloidogenic intermediates bound the hydrophobic dye 1-anilino-naphthalenesulphonic acid (ANS) (Fig. 5f); this is one of the major characteristics of the previously characterized lysozyme and  $\alpha$ -lactalbumin molten globules<sup>21,33</sup>. The Ile56Thr variant also bound ANS at 20°C, although it generated weaker

fluorescence than at its midpoint of unfolding, indicating the presence of exposed hydrophobic regions even at this temperature.

#### Transient unfolding

The conformational dynamics of the wild-type and variant proteins in solution at 37°C were investigated by using ESI-MS to monitor the exchange of the labile amide and side-chain hydrogens with solvent deuterons (Fig. 6). The hydrogen exchange kinetics of the two amyloidogenic variants were remarkable in that there was very little protection from exchange (Fig. 6); in contrast, about 55 hydrogens were strongly protected from exchange in the wild-type protein under these conditions (Fig. 6). The lack of protection of the variants cannot be explained simply by their thermal destabilization relative to the wild-type protein; a chemically modified hen lysozyme, which lacks a single disulphide bridge, has a midpoint of unfolding 24°C lower than the wild-type protein, but still shows significant protection against hydrogen exchange. Rather, these results suggest that the alterations in the domain interface of the Ile56Thr and Asp67His variants reduce the stability and cooperativity of the native fold such that both the amplitude and frequency of the native-state fluctuations are increased, even at 37°C, to an extent that allows solvent water access to the interior of the protein. The degree of protection of the variants is similar to that previously observed by ESI-MS in the well-characterized, partly folded, molten globule state of  $\alpha$ -lactalbumin<sup>34</sup>. We suggest, therefore, that the aggregation-prone, partly folded forms are present in dynamic equilibrium with the native protein at significant concentrations, even under conditions where the native state is thermodynamically stable, and could be important determinants of the amyloidogenic properties of the variants and the slow deposition of fibrils observed at 4°C.

The previously characterized kinetic and equilibrium partly folded intermediates of lysozymes and the  $\alpha$ -lactalbumins all have persistent structure in the  $\alpha$ -domain but lack stable, native-like structure in the  $\beta$ -domain<sup>35,36</sup>. Based on the present results, we propose a model for lysozyme fibrillogenesis in which association of the partly folded forms of the variants occurs through the unstable (3-domain (Fig. 7). In support of this, a peptide corresponding to the (3-sheet region of hen lysozyme has been shown to form extensive intermolecular  $\beta$ -structure<sup>34</sup>. The development of stable (3-structure through such intermolecular association could then act as a template for the progressive recruitment of polypeptide chain into the nascent fibril, with the growth of hydrogen-bonded  $\beta$ -structure providing the context<sup>35</sup> for the deposition of poly-

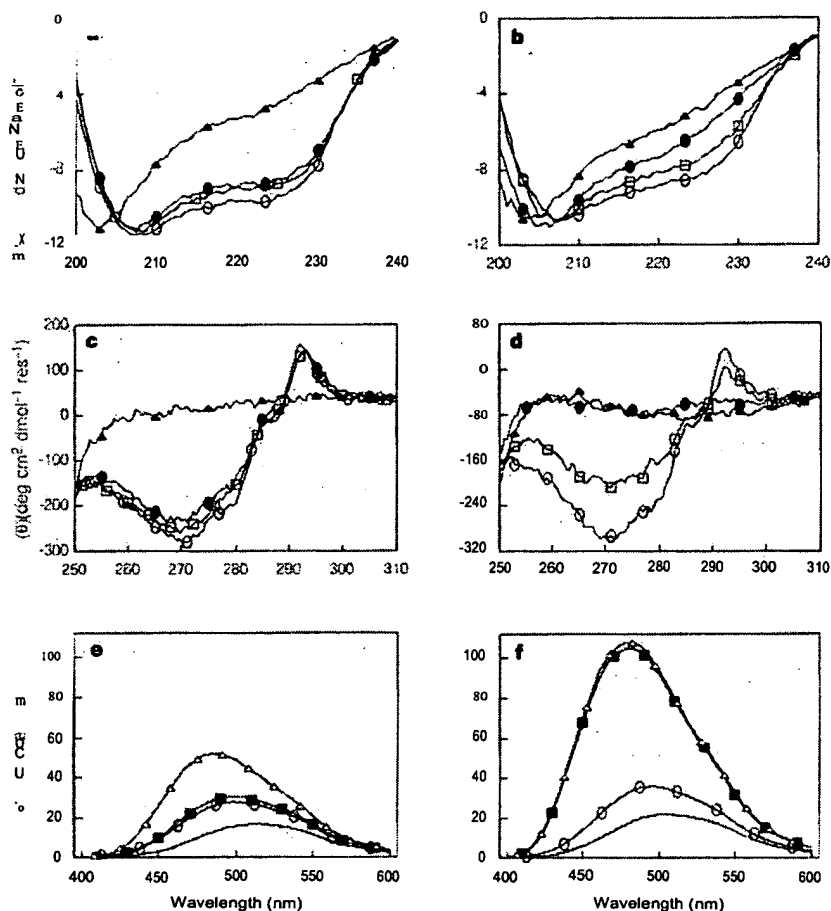


**Figure 5** Thermal denaturation of wild-type and Asp67His human lysozymes. Far-UV (a) and near-UV (c) CD spectra for wild-type human lysozyme and far-UV (b) and near-UV (d) CD spectra for the Asp67His variant lysozyme, all obtained in water at pH 5.0 and collected at 20 (○), 60 (□), 70 (•) and 95°C (•). Binding of 1-anilino-naphthalenesulphonic acid (ANS) to the proteins at 20°C (e) and at the

midpoint of thermal denaturation,  $T_m$  (f). The midpoint of thermal denaturation was 74°C for wild-type human lysozyme and 62°C for the Asp67His and Ile56Thr variants. Fluorescence intensity (arbitrary units) is shown for ANS-containing buffer solution (solid line), wild-type lysozyme (○), Asp67His lysozyme (•) and Ile56Thr lysozyme (Δ). (○), molar ellipticity.

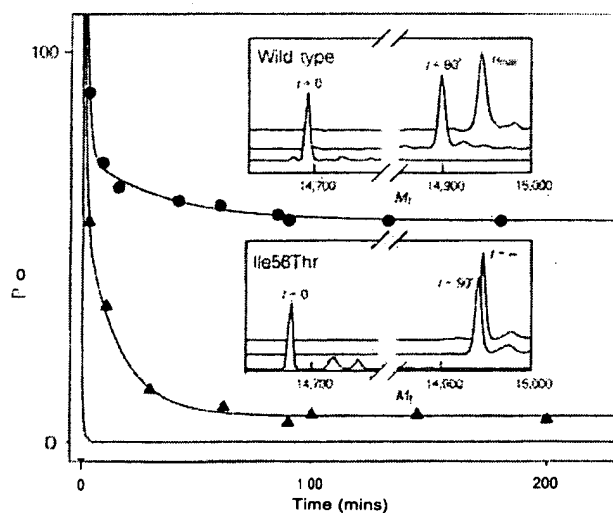


**Figure 6** Kinetic profiles of hydrogen exchange at pH 5.0, 37°C, for wild-type human lysozyme (circles) and Ile56Thr variant (triangles) monitored by ESI-MS. The exchange profile for the Asp67His variant is very similar to that shown here for the Ile56Thr variant. The plain black line is the simulated curve predicted<sup>42</sup> for a completely unstructured peptide with the sequence of human lysozyme at pH 5.0 and 37°C. The two inserts represent mass spectra obtained for the wild-type and variant protein before exposure to D<sub>2</sub>O ( $t=0$ ), 90 min after the initiation of exchange ( $t=90$ ), and after heating to 70°C for 15 min to facilitate complete exchange ( $t_{total}$ ). Data were corrected for the residual 10% H<sub>2</sub>O.

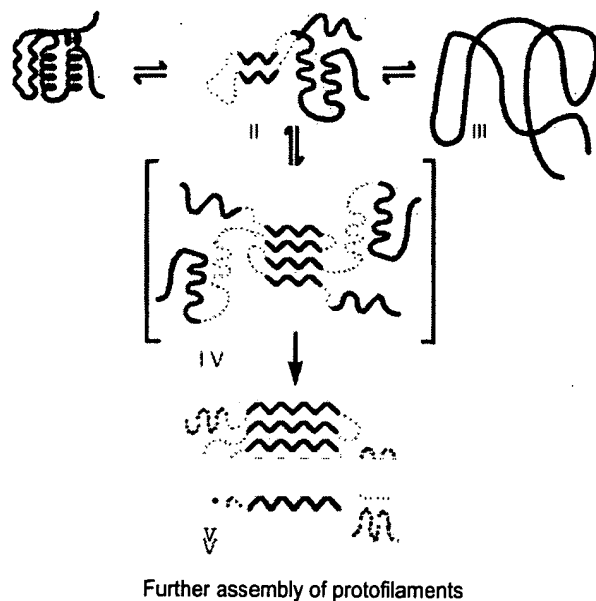


**Figure 7** Proposed mechanism for lysozyme amyloid fibril formation. Blue,  $\beta$ -sheet structure; red, helical structure; dotted lines, undefined structure. A partly folded, molten globule-like form of the protein (II), distinct from the native (I) and denatured (III) states, self-associates through the  $\beta$ -domain (IV) to initiate fibril formation. This provides the template for further deposition of protein and for the development of the stable, mainly  $\beta$ -sheet, core structure of the fibril (V). The undefined regions in V represent the possibility that not all of the polypeptide sequence is involved in the cross- $\beta$  structure. The nature of this residual structure in V is not known, and the figure is not intended to represent any defined secondary structural type (see text).

peptide chain in the stable cross- $\beta$  fold. The FTIR data indicate that fibrillogenesis involves an increase in  $\beta$ -sheet structure; conversion of  $\alpha$ - to  $\beta$ -structure will be easier in the molten globule state than the native state because of the much lower cooperativity of the unfolding process<sup>23</sup>.

### Mechanism of amyloid fibril formation

All amyloid fibrils have similar morphological and tinctorial characteristics and are predominantly (3-sheet structures, indicating that a conformational change, involving a helix-to-sheet transition in some proteins, occurs during fibril formation". As in lysozyme amyloidosis, amino-acid substitutions responsible for amyloid formation in immunoglobulin light chain<sup>24</sup> and transthyretin variants<sup>25</sup> affect the stability of the proteins and their tendency to aggregate. It has been suggested that molten globule states are critical in protein folding and related structural transitions<sup>26</sup>. We propose that transient population of the amyloidogenic proteins in a molten globule-like state that lacks global cooperativity is an important feature of the conversion from the soluble to the fibrillar form. The structure of a domain of the prion protein PrP(121-231)<sup>28</sup> also demonstrates that residues for which mutations are associated with prion disease are involved in maintenance of the hydrophobic core. It has also been suggested that the conversion of the cellular form to the infectious form, which involves helix-to-sheet conversion, may be initiated by the (3-sheet elements of the native structure<sup>31</sup>. There is no evidence for infectivity of other types of amyloidosis or for conversion of non-amyloidogenic wild-type proteins by exposure to amyloidogenic variants. Nevertheless, the mechanism we have described for lysozyme amyloidosis (Fig. 7), proceeding from the soluble forms of amyloidogenic precursor

proteins through a transient population of intermediates with the structural characteristics of molten globules, and on to intermolecular  $\beta$ -sheet association, may occur generally in the amyloidoses. *Note added in proof.* After submission of this manuscript Funahashi *et al.*<sup>32</sup> reported that the crystal structure of Ile56Thr variant lysozyme is similar to that of wild-type human lysozyme, as shown here. Their physicochemical studies also demonstrate reduced protein stability and altered folding kinetics, strongly supporting the idea that partly folded intermediates play an important role in lysozyme fibril formation. □

### Methods

**Lysozyme expression.** Human wild-type and Asp67His variant lysozyme cDNAs were amplified from macrophage RNA of the Asp67His proband. The 5' primer, CTTGGATCCCTAGGCACTCTGACCTAGCAGT contained a *Bam*HI site and targeted sequence in the untranslated region of the cDNA. The 3' primer, NNNNNNTCTAGATTACACTCCACAACCTTG, contained an XbaI site and 6 random nucleotides at its 5' end to facilitate cleavage<sup>33</sup>. The Ile56Thr variant sequence was obtained by in vitro mutagenesis of wild-type cDNA (pAlter system, Promega). The three cDNAs were cloned into the *Bam*HI/XbaI sites of pBacPAK8, transfected into SO cells, and recombinant baculoviruses were selected and amplified (Clontech). Lysozyme was detected in medium from infected cells; spinner cultures of H15 and Sf9 cells, infected at multiplicity of infections from 1 to 15, yielded 2–20 mg l<sup>-1</sup>.

**Isolation and characterization of recombinant lysozymes.** Lysozymes were isolated by cation-exchange chromatography (Macrorep S, BioRad) and FPLC gel filtration (Superose 12, Pharmacia), and gave single bands on reduced SDS 8–18% gradient PAGE (Pharmacia ExcelGel) stained with silver. Lysozyme enzyme kinetics were determined with penta-N-acetyl- $\beta$ -chitopentaoside<sup>34</sup>. For electron microscopy, protein diluted in water was placed on a formvar-coated grid and negatively stained with 2% sodium phosphotungstate.

**Crystal-structure determination.** All crystals were grown by vapour diffusion at 20°C; wild-type lysozyme from 30 mM sodium phosphate, 2.5 M NaCl, pH 4.9, Asp67His from 0.1 M ammonium sulphate, 30% PEG 8000 and Ile56Thr from 0.16 M ammonium sulphate, 24% PEG 8000. Drops initially contained equal volumes of protein (10 mg ml<sup>-1</sup> in 10 mM HEPES, 0.4–0.5 M LiCl, pH 7.1–8.0) and reservoir buffer. X-ray data were collected at 15 °C using a MAR RESEARCH image plate, mounted on a Rigaku rotating anode X-ray generator. Data processing and reduction were performed with the DENZO and SCALEPACK programs<sup>35</sup>. The CCP4 suite of programs<sup>36</sup> was used for map calculation and coordinate analysis. The structures were refined using cycles of restrained molecular dynamics and positional refinement in X-PLOR 3.1 (ref. 44) and manual fitting with the interactive graphics programme O's. Crystallographic data statistics are given in Table 3. Recombinant wild-type human lysozyme data were collected as a control set. The initial  $2F_o - F_c$  map for the Ile56Thr variant structure was produced with phases calculated from the refined model of recombinant wild-type human lysozyme<sup>37</sup>. The structure of Asp67His lysozyme was solved by molecular replacement using X-PLOR<sup>44</sup>. The solution indicated changes in the conformation of the  $\beta$ -domain (regions 45–54 and 66–75). The structure was rebuilt manually and refined with cycles of molecular dynamics and model building guided by interpretation of electron density maps. Figures were generated with O's and a version of MOLSCRIPT<sup>38</sup> modified by R. Esnouf.

**Thermal stability.** Melting temperatures were determined by placing wild-type and variant lysozymes at 2.5  $\mu$ g ml<sup>-1</sup> in 20 mM HEPES, 100 mM LiCl, pH 7.23, containing 1% (w/v) bovine serum albumin, for 15 min at the temperatures shown, then cooling to 21 °C for 15 min, before enzyme assay<sup>39</sup> at 21 °C.

**Infrared spectroscopy.** Infrared spectra of proteins (5–5 mg ml<sup>-1</sup>) dissolved in D<sub>2</sub>O buffer containing 20 mM Tris-HCl, pH 7.0 (uncorrected for deuterium effects) were collected (Bruker IFS-55 spectrometer, 2 cm<sup>-1</sup> resolution) before and after heating to induce unfolding and fibril formation.

### Recovery of active lysozyme from ex vivo lysozyme amyloid fibrils.

Amyloid fibrils were isolated by water extraction from amyloidotic liver tissue of a patient with the Asp67His lysozyme gene mutation who underwent emergency liver transplantation following spontaneous rupture of the liver. Lyophilized fibrils were incubated for 72 h in 6 M guanidine HCl, pH 6.7, with or without 0.1% (w/v) 2-mercaptoethanol, then centrifuged to remove

insoluble material. The supernatants were fractionated by FPLC gel filtration (Superose 12, Pharmacia) eluted with the corresponding solvent; the main peak in each case, composed of monomeric lysozyme, was pooled and dialysed against H<sub>2</sub>O, pH 3.8. Lysozyme enzyme activity was quantified, and the molecular mass of the solubilised protein was determined by ESI-MS<sup>21</sup>. The elution volume (V) of lysozyme recovered in the presence of mercaptoethanol was significantly lower than that obtained without reduction, corresponding to the expected larger volume of unfolded lysozyme without disulphide bridges, confirming that reduction had occurred. This material did not recover enzyme activity and gave no signal in the mass spectrometer, presumably because of its propensity to aggregate. Natural ex vivo wild-type lysozyme dissolved in 6 M guanidine-HCl, pH 6.7, and run on the same column as a control, eluted with the same V as the Asp67His lysozyme from the amyloid fibrils.

**Circular dichroism.** Spectra were collected at 1-nm intervals using a JASCO J720 spectropolarimeter with 1 mm and 10 mm path-length quartz cuvettes in a temperature-controlled housing, over the wavelength ranges 190–250 nm and 250–360 nm respectively. The protein samples were at 0.22 mg ml<sup>-1</sup> in H<sub>2</sub>O, pH 5.0, based on  $\epsilon_{220}^{25}$  for 1 cm path length = 25.5.

**ANS binding and fluorescence.** Proteins at 0.2 mg ml<sup>-1</sup> in 50 mM sodium acetate, pH 5.0, with final ANS concentration 0.1 mg ml<sup>-1</sup>, were analysed in a Perkin Elmer luminescence spectrometer LS50B with a temperature-controlled cell; excitation wavelength, 385 nm; total fluorescence emission monitored between 400 and 600 nm.

**Deuterium exchange and mass spectrometry.** Proteins were washed extensively in water, pH 3.8, then equilibrated in water, pH 5.0, at 20  $\mu$ M for determination of mass spectra<sup>33</sup>. Hydrogen exchange was initiated by a 10-fold dilution from protein in H<sub>2</sub>O at pH 5.0 and 37°C into D<sub>2</sub>O at pH 5.0 (uncorrected for deuterium effects) and 37°C.

Received 12 September 1996; accepted 27 January 1997.

- Pepys, M. B. in *Immunologic Diseases* (eds Frank, M. M., Austen, K. F., Claman, H. N. & Umanue, E. R.) 637–655 (Little, Brown and Company, Boston, 1994).
- Tan, S. Y. & Pepys, M. B. *Arthritis Rheum.* 37, 403–414 (1994).
- Glenner, G. G. Amyloid deposits and amyloidosis—the (3-fibrilloses). *N. Engl. J. Med.* 302, 1283–1292 (1980).
- Blake, C. C. F. & Serpell, L. C. Synchrotron X-ray studies suggest that the core of the transthyretin amyloid fibril is a continuous (3-sheet helix. *Structure* 4, 989–998 (1996).
- Fraser, P. E. et al. Fibril formation by primate, rodent and Dutch-hemorrhagic analogues of Alzheimer  $\beta$ -protein. *Biochemistry* 31, 10716–10723 (1992).
- Goldfarb, L. G., Brown, P., Haltia, M., Ghiso, J. & Frangione, B. Synthetic peptides corresponding to different mutated regions of the amyloid gene in familial  $\beta$ -microglobulin disease show enhanced in vitro formation of morphologically different amyloid fibrils. *Proc. Natl Acad. Sci. USA* 90, 4451–4454 (1993).
- Abrahamson, M. & Grubb, A. Increased body temperature accelerates aggregation of the Leu66Gln mutant cystatin C, the amyloid-forming protein in hereditary cystatin C amyloid angiopathy. *Proc. Natl Acad. Sci. USA* 91, 1416–1420 (1994).
- Hurle, M. R., Helms, L. R., Li, L., Chan, W. & Wetzel, R. A role for destabilizing amino acid replacements in light-chain amyloidosis. *Proc. Natl Acad. Sci. USA* 91, 5446–5450 (1994).
- Maury, C. P. J., Nurmiaho-Lassila, E.-L. & Rossi, H. Amyloid fibril formation in gelsolin-derived amyloidosis. Definition of the amyloidogenic region and evidence of accelerated amyloid formation of mutant A $\alpha$ -187 and Tyr-187 gelsolin peptides. *Lab. Invest.* 70, 558–564 (1994).
- Yamada, T., Kluge-Beckerman, B., Liepnieks, J. J. & Benson, M. D. Fibril formation from recombinant human serum amyloid A. *Biochem. Biophys. Acta* 1226, 323–329 (1994).
- McCutchen, S. L., Lai, Z., Mirov, G. J., Kelly, J. W. & Colon, W. Comparison of lethal and nonlethal transthyretin variants and their relationship to amyloid disease. *Biochemistry* 34, 13527–13536 (1995).
- Lansbury, P. T. et al. Structural model for the  $\beta$ -amyloid fibril based on interstrand alignment of an antiparallel-sheet comprising a C-terminal peptide. *Nature Struct. Biol.* 2, 990–998 (1995).
- Kelly, J. W. Alternative conformations of amyloidogenic proteins govern their behaviour. *Curr. Opin. Struct. Biol.* 11, 1–17 (1996).
- Booth, D. R. et al. Hereditary hepatic and systemic amyloidosis caused by a new deletion/insertion mutation in the apolipoprotein A1 gene. *J. Clin. Invest.* 98, 2714–2721 (1996).
- Pepys, M. B. et al. Human lysozyme gene mutations cause hereditary systemic amyloidosis. *Nature* 362, 553–557 (1993).
- Blake, C. C. F. et al. Structure of hen egg-white lysozyme. *Nature* 206, 757–761 (1965).
- Blake, C. C., Pulford, W. C. & Artymuk, E. J. X-ray studies of water in crystals of lysozyme. *J. Mol. Biol.* 167, 693–723 (1983).

- Artymuk, P. J. & Blake, C. C. F. Refinement of human lysozyme at 1.5 Å resolution analysis of non-bonded and hydrogen-bond interactions. *J. Mol. Biol.* 152, 737–762 (1981).
- McKenzie, H. A. & White, E. H. Jr. Lysozyme and alpha-lactalbumin: structure, function, and interrelationship. *Adv. Protein Chem.* 41, 173–315 (1991).
- Radford, S. E., Dobson, C. M. & Evans, P. A. The folding of hen lysozyme involves partially structured intermediates and multiple pathways. *Nature* 358, 302–307 (1992).
- Radford, S. E. & Dobson, C. M. Insights into protein folding using physical techniques: studies of lysozyme and  $\alpha$ -lactalbumin. *Phil. Trans. R. Soc. Lond. B* 348, 17–25 (1995).
- Kuwajima, K. The molten globule state as a clue for understanding the folding and cooperativity of globular-protein structure. *Proteins Struct. Funct. Genet.* 6, 87–103 (1989).
- Pitsyn, O. B. Molten globule and protein folding. *Adv. Protein Chem.* 47, 83–229 (1995).
- Fenn, J. B., Mann, M., Meng, C. K., Wong, S. E. & Whitehouse, C. M. Electrospray ionization for mass spectrometry of large biomolecules. *Science* 246, 64–71 (1989).
- Shih, P., Holland, D. R. & Kirsch, J. E. Thermal stability determinants of chicken egg-white lysozyme core mutants: hydrophobicity, packing volume, and conserved buried water molecules. *Protein Sci.* 4, 2050–2062 (1995).
- Puchler, H., Sweat, F. & Levine, M. On the binding of Congo red by amyloid. *J. Histochem. Cytochem.* 10, 355–364 (1995).
- Harrison, R. F. et al. 'Fragile' liver and massive hepatic haemorrhage due to hereditary amyloidosis. *Gut* 38, 151–152 (1996).
- Stott, K., Blackburn, J. M., Butler, P. J. & Perutz, M. Incorporation of glutamine repeats makes protein oligomeric: implications for neurodegenerative diseases. *Proc. Natl Acad. Sci. USA* 92, 6509–6513 (1995).
- Nelson, S. R., Lyon, M., Gallagher, J. T., Johnson, E. A. & Pepys, M. B. Isolation and characterization of the integral glycosaminoglycan constituents of human amyloid A and monoclonal light-chain amyloid fibrils. *Biochem. J.* 275, 67–73 (1991).
- Haezebrouck, P. et al. An equilibrium partially folded state of human lysozyme at low pH. *J. Mol. Biol.* 246, 382–387 (1995).
- Wu, L. C., Peng, Z.-y. & Kim, P. S. Bipartite structure of the  $\alpha$ -lactalbumin molten globule. *Nature Struct. Biol.* 2, 281–286 (1995).
- Eyles, S. J., Radford, S. E., Robinson, C. V. & Dobson, C. M. Kinetic consequences of the removal of a disulfide bridge on the folding of hen lysozyme. *Biochemistry* 33, 13038–13048 (1994).
- Robinson, C. V. et al. Conformation of GroEL-bound  $\alpha$ -lactalbumin probed by mass spectrometry. *Nature* 372, 646–651 (1994).
- Yang, J. J., Pitkeathly, M. & Radford, S. E. Far-UV circular dichroism reveals a conformational switch in a peptide fragment from the beta-sheet of hen lysozyme. *Biochemistry* 33, 7345–7353 (1994).
- Minor, D. L. Jr & Kim, P. S. Context-dependent secondary structure formation of a designed protein sequence. *Nature* 380, 730–734 (1996).
- Dobson, C. M. Finding the right fold. *Nature Struct. Biol.* 2, 513–517 (1995).
- Bychkova, V. E. & Pitsyn, O. B. Folding intermediates are involved in genetic diseases? *FEBS Lett.* 359, 6–8 (1995).
- Blake, C. C. F. et al. Human lysozyme protein domain P(132). *Structure* 382, 180–182 (1996).
- Chung, L. P., Keshav, S. & Gordon, S. Cloning the human lysozyme cDNA: inverted Alu repeat in the mRNA and in situ hybridization for macrophages and Paneth cells. *Proc. Natl Acad. Sci. USA* 85, 6227–6231 (1988).
- Osseman, E. E. & Lawlor, D. P. Serum and urinary lysozymes (muramidase) in monocytic and monomyelocytic leukemia. *J. Exp. Med.* 124, 921–951 (1966).
- Nanjo, F., Sakai, K. & Usui, T. p-nitrophenol pent-N'-acetyl-beta-chitosaminide as a novel synthetic substrate for the colorimetric assay of lysozyme. *J. Biochem.* 104, 255–258 (1988).
- Owiniowski, Z. in *Proceedings of the CCP4 Study Weekend* (eds Sawyer, L., Isaacs, N. & Bailey, S.) (SERC Daresbury Laboratory, Warrington, UK, 1993).
- CCP4 The CCP4 Suite: programs for protein crystallography. *Acta Crystallogr. D* 50, 760–763 (1994).
- Brünger, A. T. *X-PLOR* manual version 3.0 (Yale University, New Haven, CT, 1992).
- Jones, T. A., Zeng, J.-Y., Cowan, S. W. & Kjeldgaard, M. Improved methods for the building of protein models in electron density maps and the location of errors in these models. *Acta Crystallogr. A* 74, 110–119 (1991).
- Kraulis, P. J. *MOLSCRIPT* a program to produce both detailed and schematic plots of protein structures. *J. Appl. Crystallogr.* 24, 946–950 (1991).
- Perry, L. J. & Wetzel, R. Unpaired cysteine-54 interferes with the ability of an engineered disulfide to stabilize T4 lysozyme. *Biochemistry* 25, 733–739 (1986).
- Bai, Y., Milne, J. S., Mayne, L. & Englander, S. W. Primary structure effects on peptide group hydrogen exchange. *Proteins Struct. Funct. Genet.* 17, 75–86 (1993).
- Furukawa, J., Takano, K., Ogasahara, K., Yamagata, Y. & Yutani, K. The structure, stability, and folding process of amyloidogenic mutant human lysozyme. *J. Biochem.* 120, 1216–1223 (1996).

**Acknowledgements.** We thank G. Mertini for highly purified natural human lysozyme; V Emons and L. B. Lovat for electron microscopy; K. Harlos and L. C. Serpell for help with X-ray data collection; S. Lee and M. Bartlam for assistance with figures; I. D. Kerr and C. P. Pouting for sequence analysis; and A. K. Soutar for discussions. This work was supported by MRC programme and project grants (M.B.P., P.N.H. and C.C.F.B.), the EU (V.B.), the Royal Society (S.E.R. and C.N.R.), the Oxford Centre for Molecular Sciences (funded by the BBSRC, EPSRC and MRC, the Alzheimer Association of Ontario (P.E.F.) and an international research scholars award from the Howard Hughes Medical Institute (C.M.D.).

Correspondence should be addressed to M.B.P. (e-mail: mpp@pmms.ac.uk). Requests for molecular reagents should be addressed to D.R.B. (e-mail: drb@pmms.ac.uk) and for biophysical data to M.S. (e-mail: margo@chich.ac.uk). The variant-lysozyme coordinates have been deposited in the Protein Data Bank, accession no. 1UJZ for H36Thr and 1UYF for Asp67His.



# Therapeutic Potential of Chimeric Amyloid-reactive Monoclonal Antibody 11-1F4<sup>1</sup>

Alan Solomon,<sup>2</sup> Deborah T. Weiss, and  
Jonathan S. Wall

Human Immunology and Cancer Program, Department of Medicine,  
University of Tennessee Graduate School of Medicine, Knoxville,  
Tennessee 37920

## Abstract

**Purpose:** We had previously reported that certain of our murine (m) antihuman light chain monoclonal antibodies (mAbs) recognized an epitope common to AL and other types of amyloid fibrils. On the basis of this evidence, one such antibody, 11-1F4, was administered to mice bearing AL amyloidomas induced by s.c. injection of human AL extracts. The mAb bound to the amyloid and initiated an Fc-mediated cellular inflammatory response that led to rapid reduction in the tumor masses. To develop this reagent for clinical use, the 11-1F4 mAb was chimerized and its activity compared with that of the unmodified antibody.

**Experimental Design:** The chimeric (c) 11-1F4 mAb was produced in CHOdhfr-stable mammalian cell lines that had been transfected with a supervector DNA encoding the mouse 11-1F4 heavy and light chain variable regions (V<sub>H</sub>, V<sub>L</sub>) and human heavy and light chain constant regions (C<sub>H</sub>, C<sub>L</sub>). The antibody products were analyzed for their fibril binding activity and ability to effect amyloidolysis in two *in vivo* experimental models.

**Results:** The capability of the c11-1F4 mAb to interact with amyloid was demonstrated *in vitro*. Administration of this reagent into mice bearing human AL tumors or those with systemic AA deposits resulted in marked reduction in amyloid burden with no evidence of toxicity in the animals.

**Conclusions:** These results have led to the decision to produce GMP-grade c11-1F4 for a Phase I/II clinical trial in patients with primary (AL) amyloidosis where the effectiveness of the reagent could be determined. The use of amyloid-reactive antibodies would represent a novel approach in the treatment of individuals with this invariably fatal disorder.

## Introduction

Primary (AL) amyloidosis is a monoclonal plasma cell dyscrasia associated with the production of amyloidogenic immunoglobulin light chains that form fibrillar deposits in vital tissues; this relentless process leads to organ failure and death, usually within 9–36 months (1–5). Heretofore, treatment of patients with this disease had been limited to the use of anti-plasma cell chemotherapy given in conventional amounts or in high doses combined with autologous stem cell transplantation (6–12). Such efforts have, in some cases, extended survival; however, the overall prognosis remains poor.

As part of ongoing studies on the pathogenesis of primary (AL) amyloidosis and the use of immunotherapy as a means to eliminate amyloid deposits, we discovered that certain of our m<sup>3</sup>mAbs prepared against human light chain-related fibrils were capable of recognizing an amyloid-related, conformational epitope, as evidenced immunohistochemically and by ELISA. Furthermore, when one such reagent, the IgG1κ mAb 11-1F4, was administered to mice bearing human AL amyloidomas, the antibody bound to the amyloid and initiated an inflammatory response that led to elimination of the induced tumor (13).

To facilitate translation of these promising experimental findings into clinical practice, we requested assistance from the National Cancer Institute's RAID Program. Subsequently, RAID contracted with AERES Biomedical Ltd. (Mill Hill, London, United Kingdom) to chimerize the m11-1F4 amyloid-reactive mAb. Three CHO dhfr-stable cell lines were transfected with a supervector DNA specifying the murine V<sub>H</sub> and V<sub>L</sub> and human C<sub>H</sub> and C<sub>L</sub>. The resulting c11-1F4 mAbs produced by these mammalian cells were harvested, purified, and tested for their capacity to interact with amyloid in several *in vitro* and *in vivo* experimental systems. We now report the results of our studies where we have shown comparable fibril binding and effective, although somewhat reduced, amyloidolytic activity of the modified antibody as compared with its murine (native) counterpart.

## Materials and Methods

**PCR Cloning and Sequencing of the m11-1F4 Antibody Heavy and Light Chain Variable Region Genes.** Two clones (B2C4 and B2D6) from the SP2/0 hybridoma cell line producing the IgG1κ m11-1F4 amyloid-reactive mAb were furnished to AERES Biomedical Ltd. (Mill Hill). The cells were cultured in DMEM media (Life Technologies, Inc., Rockville, MD) supplemented with 20% (v/v) fetal bovine serum (Hy-

<sup>1</sup> Presented at the "Ninth Conference on Cancer Therapy with Antibodies and Immunoconjugates," October 24–26, 2002, Princeton, NJ. Supported, in part, by United States Public Health Service Research Grant CA10056 from the National Cancer Institute, Contract 21X5034A from Science Applications International Corporation-Frederick, and the Aslan Foundation. A. S. is an American Cancer Society Clinical Research Professor.

<sup>2</sup> To whom requests for reprints should be addressed, at University of Tennessee Medical Center, 1924 Alcoa Highway, Knoxville, TN 37920. Phone: (865) 544-9165; Fax: (865) 544-6865; E-mail: asolomon@mc.utmc.edu.

<sup>3</sup> The abbreviations used are: m, murine; c, chimeric; RAID, Rapid Access to Intervention Development; C<sub>H</sub>, heavy chain constant region; C<sub>L</sub>, light chain constant region; MTX, methotrexate; mAb, monoclonal antibody; V<sub>H</sub>, heavy chain variable region; V<sub>L</sub>, light chain variable region; AEF, amyloid-enhancing factor; BJP, Bence Jones protein.

clone, Logan, UT), penicillin/streptomycin, and L-glutamine (Life Technologies, Inc.). After growth to  $10^8$  viable cells, total RNA was isolated from each clone (RNA Isolation kit; Stratagene, La Jolla, CA), and first-strand cDNA was synthesized using the furnished *NotI*-d(T)<sup>18</sup> primer. The  $mV_H$  and  $V_L$  ( $V_K$ ) genes were then PCR amplified from each cDNA template, as described by Jones and Bendig (14) with AmpliTaq DNA polymerase. Separate PCRs were performed using different degenerate leader sequence-specific  $V_H$  and  $V_K$  and appropriate  $C_H$  and  $C_L$  primers (an equimolar mix of  $C\gamma 1$ ,  $C\gamma 2a$ ,  $C\gamma 2b$ ,  $C\gamma 3$ , and  $C\kappa$ ). The products were identified by electrophoresis on 1% agarose/Tris borate (pH 8.8) gels containing 0.5  $\mu$ g/ml ethidium bromide. Putatively positive products (~450 bp) were cloned directly into the pCR2.1 vector provided in the Topo TA Cloning kit (Invitrogen, Carlsbad, CA) and transformed into TOP10-competent cells using the protocol described by the manufacturer. Colonies that contained the plasmid with the 450-bp insert were selected by PCR screening using 17- and 21-mer oligonucleotide primers according to the method of Güssow and Clackson (15) and the double-stranded DNA was sequenced with the ABI PRISM 310 Genetic Analyzer and the ABI Prism BigDye terminator. Specifically designed PCR primers were used to modify the 5' and 3' ends of the 11-1F4  $V_H$  and  $V_K$  genes to obtain transient expression of their products in mammalian cells. The back primers introduced *HindIII* restriction and Kozak translation initiation sites, as well as an immunoglobulin leader sequence. The forward  $V_K$  primer provided a splice donor and *BamHI* restriction site and that for the  $V_H$ , the first 22 bp of the  $C\gamma 1$  gene, including an *ApaI* restriction site. The positive PCR products containing the correctly modified 11-1F4  $V_H$  and  $V_K$  genes were identified as previously noted and subcloned into their respective expression vectors as *HindIII*-*ApaI* (human  $\gamma 1$ , *Gm1* allotype) and *HindIII*-*BamHI* (human  $C\kappa$ , *Km3* allotype) fragments. The ligated  $V_K$  and  $V_H$  constructs were then used to transform DH5 $\alpha$  competent cells, and positive clones were selected by PCR screening.

**Construction of a Single Suprvector for Transient Expression of c11-1F4 mAb in COS Cells.** A single suprvector expressing both chains of the c11-1F4 antibody was constructed by ligating the *EcoRI* restriction enzyme digestion products of the heavy and light chain expression cassettes.

**Transient Expression of the c11-1F4 Antibody in COS Cells.** The c11-1F4 antibody was transiently expressed in ECACC/COS cells by cotransfection of each of the heavy and light chain vector constructs, as well as transfection of the single suprvector construct. After incubation for 72-h, the medium was collected, spun to remove cell debris, and analyzed by ELISA for chimeric antibody production and antigen binding.

**Quantification and Binding Analyses of the c11-1F4 Antibodies.** Whole IgG molecules present in COS cell supernatants were quantified using Nunc-Immuno MaxiSorp plates (Life Technologies, Inc., Gaithersburg, MD) in a capture ELISA. Antibody molecules were bound by an immobilized goat antihuman IgG Fc $\gamma$  fragment-specific antibody and detected by an antihuman  $\kappa$  light chain peroxidase-conjugated antibody (Sigma Chemical Co., St. Louis, MO). A standard curve was generated using known concentrations of a control IgG protein on the same plate. To test the capability of the

c11-1F4 antibodies to bind amyloid fibrils, a direct binding ELISA was used, as described previously (16).

**Transfection of CHOdhfr Mammalian Cells.** CHOdhfr cells (DUKS B11) were grown first in a nonselective media consisting of  $\alpha$ -MEM with ribonucleosides and deoxyribonucleosides (Life Technologies, Inc.), supplemented with 10% fetal clone II (Hyclone) and 50  $\mu$ g/ml gentamicin (Life Technologies, Inc.) in a 37°C, 5% CO<sub>2</sub> incubator. Aliquots of  $10^7$  cells/ml in PBS were transfected with 13  $\mu$ g of the 11-1F4 suprvector DNA at 1900V, 25  $\mu$ Farad capacitance using a Bio-Rad Gene Pulser. After a 24-h incubation in nonselective media, the cells were grown in the presence or absence of  $10^{-8}$  or  $10^{-9}$  M MTX in  $\alpha$ -MEM without ribo- or deoxyribonucleosides (Life Technologies, Inc.) supplemented with 10% dialyzed fetal bovine serum and 50 mg/ml gentamicin. The selective media were changed every 3–4 days until foci appeared. After repeated subculture and additional rounds of MTX amplification, three cell lines were selected on the bases of optimum growth and antibody production rates.

**Mycoplasma PCR Screen and Sterility Tests.** Media from the chosen cell lines were screened for the presence of *Mycoplasma* using a PCR-based kit. Testing for bacterial or fungal contamination was done by the Alamar Blue sterility assay (Serotech, Ltd., Raleigh, NC). Additionally, sterile flasks containing tryptic soy, Sabaraud, or thioglycollate broth were inoculated with cell suspensions and cultured for 3 weeks. As a control, media from cells grown in the absence of gentamicin and MTX also were tested.

**Determination of Production Rates of Selected CHOdhfr Stable Cell Lines during Exponential and Static Growth.** To measure antibody production under conditions of exponential growth, 75-cm<sup>2</sup> tissue culture flasks were seeded in duplicate with each cell line at a concentration of  $1 \times 10^5$  cells/ml (total medium volume = 20 ml) and incubated at 37°C under 5% CO<sub>2</sub>. After 24, 48, 72, and 96-h, the cell number was determined and the antibody concentration in the media measured by a quantitative ELISA (see above) and expressed as  $\mu$ g/ $10^6$  cells. For stable growth, duplicate flasks were seeded with each cell line at a concentration of  $1 \times 10^6$  cells/ml (total medium volume = 20 ml), and after 4 days, the cells were counted and the antibody concentration determined.

**Production and Purification of c11-1F4 mAb.** To have sufficient quantities of the c11-1F4 antibodies available for *in vitro* and *in vivo* studies, the three CHOdhfr-stable cell lines (22C1, 22C5, and 22D2) were grown for 1 month in single Integra CL1000 production flasks (Integra Biosciences, Ijamsville, MD) containing  $\alpha$ -MEM,  $10^{-6}$  M MTX, and 50  $\mu$ g/ml gentamicin. The supernatants were concentrated to ~5 ml, diluted 1:1 in Pierce Protein A binding buffer, and the antibody isolated using an Immunopure Plus Protein A Purification Kit (Pierce, Rockford, IL), as specified by the manufacturer. The eluted and neutralized material was then dialyzed in PBS overnight using Slide-A-Lyzer Dialysis cassettes (Pierce), sterile filtered, aliquoted into 1-ml volumes, and frozen at -20°C.

**Immunohistochemistry.** Immunohistochemical analyses were performed by the avidin-biotin complex technique (Vector Laboratories, New Bedford, MA) on 4- $\mu$ m thick deparaffinized sections of normal multitissue (BioGenex, San Ramon, CA) and AL-laden tissue mounted on poly-L-lysine-coated slides. The

Table 1 Properties of CHOdhfr cell line mAb products

Cell line	Stability (4°C, 37°C, -70°C) <sup>a</sup>	SDS PAGE <sup>a,b</sup>	Fibril binding assay <sup>a,b</sup>	Aggregation <sup>b</sup>	Dot blot <sup>c</sup>	Immunohistochemistry <sup>c</sup>
22C1	+,+,+	+	+	0	+	+
22C5	+,+,+	+	+	0	ND <sup>d</sup>	+
22D2	+,+,+	+	+	0	ND	+

<sup>a</sup> AERES data.<sup>b</sup> RAID data.<sup>c</sup> UT data.<sup>d</sup> ND, not determined.

primary reagents included the m or c11-1F4 mAbs; affinity-purified goat antimouse or human IgG horseradish conjugates were used as secondary antibodies (Bio-Rad, Hercules, CA) with diaminobenzidine (Vector Laboratories) as substrate.

**In Vivo Models.** Subcutaneous amyloidomas were induced in BALB/c mice by interscapular 100-mg injections of human amyloid fibrils extracted from the liver or spleen from patients with primary (AL) amyloidosis, as described previously (13). Systemic deposits of AA amyloid (secondary amyloidosis) were induced in BALB/c mice by s.c. 0.5-ml injections of AgNO<sub>3</sub> (1%) on days 1 and 10; additionally, on day 1, the animals received i.v. 100-μg doses of AEF, which consisted of AA fibrils extracted from the livers of amyloidotic mice (17).

## Results

**Generation of c11-1F4 Antibody.** Multiple PCR reactions designed to clone the m11-1F4 V<sub>H</sub> and V<sub>K</sub> genes yielded products of the expected size (~450 bp) from both the B2C4 and B2D6 hybridoma cell lines. Analyses of the PCR products from at least three clones from each yielded the expected heavy and light chain sequences. The modified murine V<sub>H</sub> and V<sub>K</sub> 11-1F4 gene constructs (see "Materials and Methods"), along with the human C<sub>γ</sub>1 and C<sub>κ</sub> constant region genes, were successfully cloned into their respective mammalian expression vectors and used for cotransfection of COS cells. A single supervector comprised of the immunoglobulin genes from both species also was prepared for this purpose. Because of the substantially higher expression levels achieved with the supervector, this construct was used to transfect CHOdhfr-mammalian cells that were subsequently cultured in media with or without MTX. Three of the amplified lines, 22C1, 22C5, and 22D2, had the highest rate of antibody production (50.6, 42.5, and 47 μg/10<sup>6</sup> cells/day, respectively) with approximate doubling times of 48–60 h. Although the three lines expanded at the same rate during exponential growth over 96 h, the production rate for 22C1 increased from 31 to 37 μg/10<sup>6</sup> cells/day over this period, whereas that of 22C5 and 22D2 decreased from 24 to 20 and 34 to 31 μg, respectively. During stable growth, the production rates, based on an average of the initial and 96-h viable cell count, were comparable (24.7, 21.5, and 20.5 μg/10<sup>6</sup> cells/day, respectively). Similarly, over the 1-month period of culture, the antibody concentrations in the media remained relatively stable. The three CHO cell lines (22C1, 22C5, and 22D2) and their products were uncontaminated by bacteria, fungi, or *Mycoplasma* and had acceptable endotoxin levels (0.7, 1.1, and 23.4 units/μg, respectively).

**In Vitro Analyses.** The properties of the three c11-1F4 mAbs are summarized in Table 1. By SDS-PAGE (Fig. 1) and Western blot analyses, these molecules were shown to have the molecular masses expected for chimeric IgG1 heavy- and κ-light chains. These analyses also demonstrated the stability of the antibody products after storage for 1–4 h at 4°C, 37°C, and 70°C. In other experiments, the binding of the c and m11-1F4 mAbs to synthetic AL amyloid fibrils was measured by ELISA where it was found to be comparable (Fig. 2). Additionally, the results of size exclusion HPLC indicated that the chimeric antibody preparations contained no appreciable protein aggregates, *i.e.*, they consisted almost entirely of IgG monomers (Fig. 3).

The c11-1F4 mAbs, as with the murine reagent, interacted only with fibrillar light chains but not with the soluble counterparts. As illustrated in Fig. 4, the 22C1 antibody reacted exclusively with the fibrils at concentrations as low as 1 μg/ml. A similar pattern was found with the m11-1F4 mAb. In studies of BJPs representative of the V<sub>κ</sub>1, V<sub>κ</sub>4, V<sub>λ</sub>6, and V<sub>λ</sub>8 subgroups, neither mAb recognized the κ1, λ6, and λ8 proteins; immunostaining of the κ4 component was expected because the original 11-1F4 reagent was produced by immunizing mice with V<sub>κ</sub>4 fibrils (13).

The capability of the c11-1F4 mAb to interact with human AL-containing deposits was tested immunohistochemically on tissues obtained from two patients with primary (AL) amyloidosis. As illustrated in Fig. 5, both the c and m11-1F4 reagents immunostained the vascular green birefringent congophilic areas in uterine and pancreatic tissues that were shown to contain κ4- and λ8-related amyloid deposits, respectively (as demonstrated using anti-V<sub>κ</sub>4 and V<sub>λ</sub>8 subgroup-specific mAbs).

Additionally, the reactivities of the c and m11-1F4 mAbs were tested against 15 different human specimens, including liver, spleen, kidney, heart, lung, intestine, muscle, pancreas, prostate, thyroid, testis/ovary, bladder, uterus, and brain. Diffusely mild to focally intense staining of hepatocytes, proximal renal tubules, and myocytes was noted. In contrast, far greater immunostaining was found when these tissues were studied with the chimeric IgG1κ anti-CD20 mAb Rituximab (Ref. 18; data not illustrated).

**In Vivo Analysis.** The efficacy of the IgG1κ c11-1F4 mAb to accelerate amyloidolysis in our *in vivo* amyloidoma model was compared with that of the murine parent. Because the 22C1-, 22C5-, and 22D2-derived c11-1F4 preparations exhibited equivalent reactivity with amyloid and there were limited quantities of each, the three were combined and used in our *in*

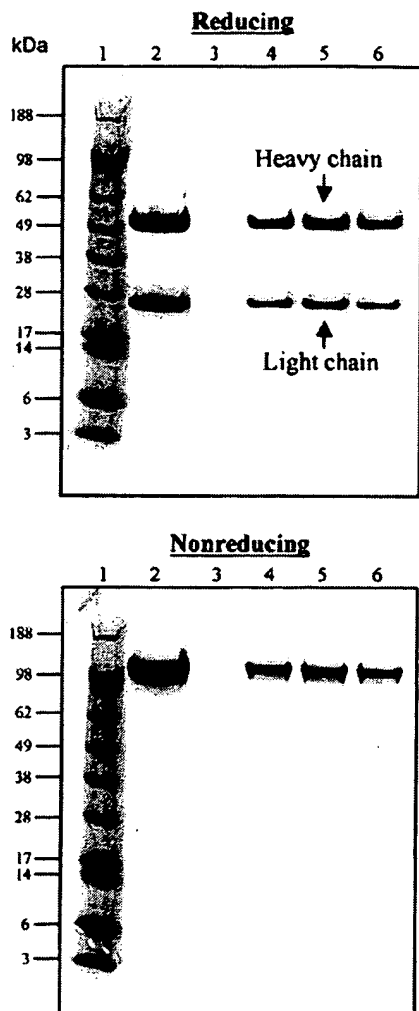


Fig. 1 Analyses by SDS-PAGE of c11-1F4 mAbs under reducing and nonreducing conditions (Coomassie blue-stained Novex bis tris 4–12% NuPage gels). Lane 1 contained protein standards of known molecular masses as indicated; Lane 2, a human IgG mAb; Lanes 4–6, 22C1, 22C5, and 22D2 mAbs, respectively. The locations of the immunoglobulin heavy and light chains are as indicated.

*vivo* experiments. Given the relatively large amount of amyloid extract required to produce a readily palpable amyloidoma (dry weight, 100 mg) and the scarcity of autopsy-derived samples, the numbers of animals used in each study was necessarily restricted to one pair of mice. In the first experiment, four sets were injected s.c. with a 1-ml volume of solution containing 100 mg of a human AL $\kappa$  extract (Ref. 19; patient HIG) that was comprised of fragments (~16 and 18 kDa) representing the major portion of the amyloidogenic precursor  $\kappa$ 1 light chain (BJP, HIG), as demonstrated by SDS-PAGE, Western blot, and chemical analyses. By dot blot, the c11-1F4 mAb, as with the murine reagent, reacted with amyloid HIG but not with the BJP. Forty-eight h after injection of the fibrillar extract, two of the four pairs were given an i.v. 100- $\mu$ g injection of either the m or cmAb; this treatment was repeated on days 4, 6, 8, 10, and 12

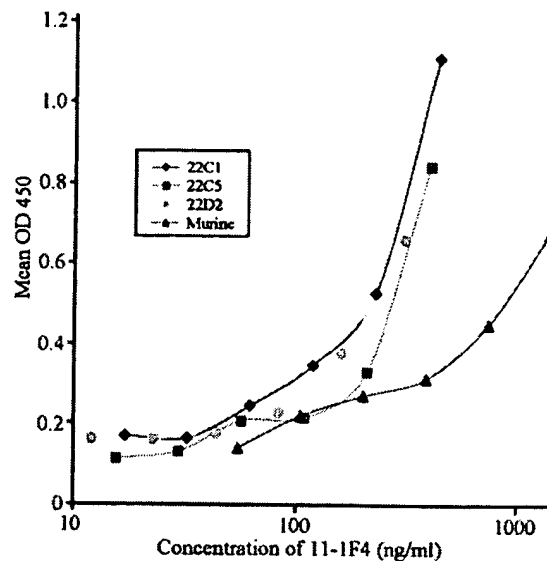


Fig. 2 *In vitro* reactivity of c11-1F4 antibodies. The c11-1F4 mAbs 22C1, 22C5, and 22D2 and m11-1F4 mAb were tested in a binding ELISA against synthetic light chain fibrils (JTO5) coated onto an ELISA plate.

(i.e., each mouse received a total of 600  $\mu$ g of antibody). For control purposes, similar doses of a monoclonal isotype matched (IgG1 $\kappa$ ) murine protein (MOPC 31C) were administered to the third set over the 12-day period, whereas the fourth was untreated. There were no obvious signs of toxicity in any of the mice.

Approximately 11 days postamyloid induction, the tumors in the mAb-injected mice began to decrease in size. One from each pair was euthanized on day 15 where it was noted that the amyloidomas from the 11-1F4-treated animals were obviously smaller than those from the 2 controls (Fig. 6). On day 16, 3 of the 4 remaining mice were sacrificed (1 control was kept for additional observation to determine the time when the amyloidoma would resolve in an untreated animal). As shown in Table 2, the wet weights of the residual amyloidomas in the 2 mice that received the m11-1F4 mAb were somewhat less than those from the animals that received the chimeric counterpart. In both cases, however, there was a marked reduction in size as compared with the controls, i.e., an average of 83 and 70%, respectively. The amyloidoma in the untreated animal did not become palpably smaller until day 24. On day 30, the mouse was sacrificed, and the mass of the remaining amyloidoma was found to be similar to those removed from the 11-1F4 mAb-treated animals on day 16.

The excised amyloidomas from the treated and control mice were divided in half: one portion was frozen in ornithine carbamyl transferase and the other was fixed in formalin and embedded in paraffin. Tissue (liver, spleen, and kidneys) from each animal was processed in similar fashion. Microscopic examination of Congo red-stained sections of the amyloidomas revealed the presence of green birefringent material in all samples, albeit considerably less in those obtained from the m and c11-1F4 mAb-treated animals. The most notable difference was

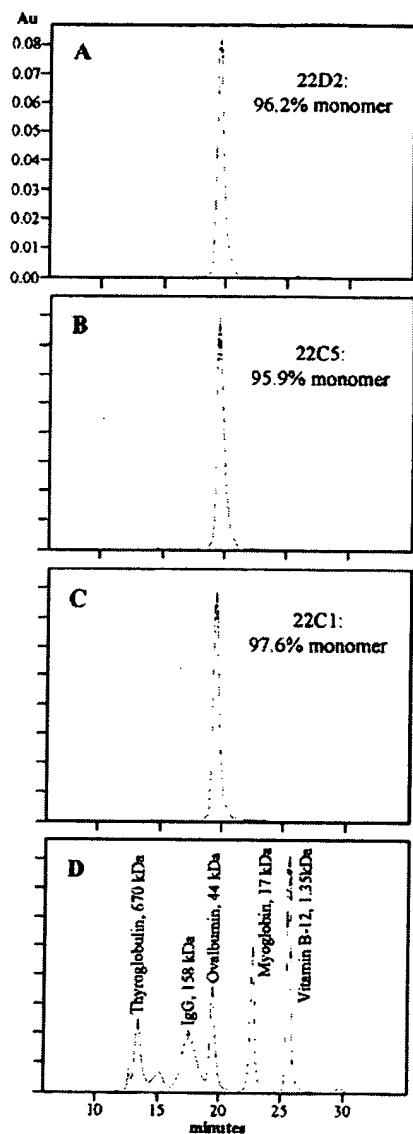


Fig. 3 HPLC analyses of c11-1F4 mAbs. Elution profiles of 22D2, 22C5, and 22C1 mAbs (A, B, and C, respectively) and protein standards (D) that were passed through a Toso Haas G 3000 SWx1 size exclusion chromatography column (elution buffer, PBS).

apparent in H&E- and cholesterae-treated specimens where the extent of macrophage, as well as activated neutrophil infiltration in the residual amyloidomas was far greater than that seen in controls. Furthermore, amyloid-bound c11-1F4 could be demonstrated immunohistochemically (data not illustrated). Other than the induced amyloid tumors, no gross pathological abnormalities were observed among the mice. Furthermore, the liver, spleen, and kidneys of the m and c11-1F4 mAb-treated and control animals appeared normal microscopically.

An identical protocol was used to compare the therapeutic efficacy of the c and m11-1F4 mAbs in mice injected with a human AL $\lambda$  (patient BAL) extract that predominantly contained a 16-kDa light chain fragment of amyloidogenic  $\lambda$ 3 BJP BAL.

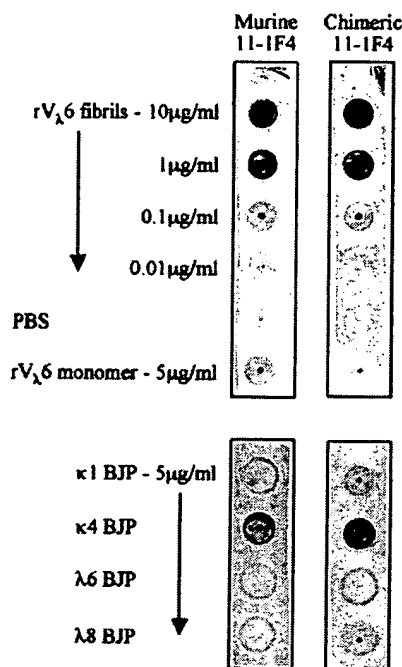


Fig. 4 Comparison by dot blot assay of the reactivities of m and c11-1F4 mAbs against fibrillar and soluble forms of light chains. *Top*: light chain fibrils were generated from a recombinant V $\lambda$ 6 protein and applied as "dots" at the concentrations indicated, as were PBS and the soluble V $\lambda$ 6 protein monomer. *Bottom*: human  $\kappa$ 1,  $\kappa$ 4,  $\lambda$ 6, and  $\lambda$ 8 Bence Jones proteins were likewise applied. Murine and c11-1F4 mAbs were used as primary reagents (5  $\mu$ g/ml) and goat antimouse and goat antihuman immunoglobulin horseradish peroxidase-labeled antibodies, respectively, were the secondary reagents. The reaction was developed with diaminobenzidine.

Because the amyloidoma in 1 of the m11-1F4 mAb-treated animals began to regress on day 12, 1 mouse from each of the four pairs was sacrificed on day 15. The masses of the amyloidomas removed from the m and c11-1F4 mAb-treated animals had decreased 75 and 15%, respectively, as compared with the control (Table 3). The remaining set was euthanized on day 21; in this case, the amyloidomas were reduced by 58 and 43%, respectively. The results of microscopic examination of the amyloidomas were similar to those described in the AL $\kappa$  HIG study.

We had previously demonstrated that the amyloid-reactive m11-1F4 mAb accelerated amyloidolysis in mice bearing AA hepatic and splenic deposits (13, 20). Because of the unavailability of animals with systemic AL amyloidosis, we tested the therapeutic efficacy of the c11-1F4 mAb (which had been shown immunohistochemically and by ELISA to react with AA fibrils) in the *in vivo* AA model. This form of amyloid was induced over a 10-day period by a standard protocol that included injections into 10 mice of silver nitrate and AA-derived fibrils, *i.e.*, AEF (Fig. 7). Five of these animals then received 100- $\mu$ g i.v. doses of the antibody on days 14, 17, 20, and 23, whereas the remaining 5 served as untreated controls. The animals were sacrificed on day 24 and the liver, spleen, and kidneys examined histochemically. The most pronounced inter-

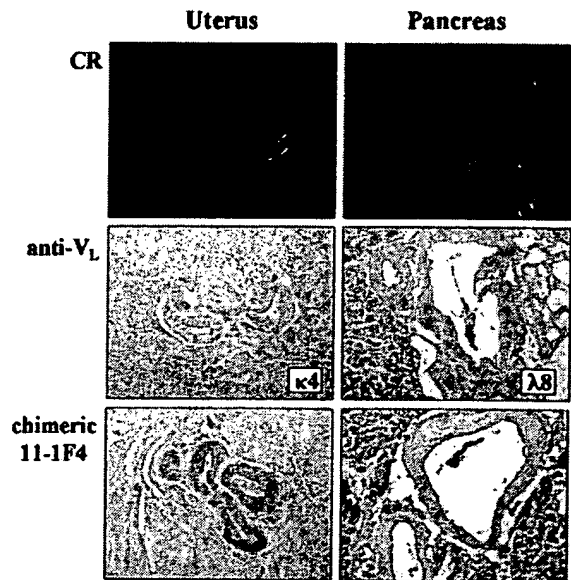


Fig. 5 Reactivity of c11-1F4 mAb with human vascular AL-containing amyloid deposits. The left and right panels illustrate the results obtained when uterine and pancreatic tissues from patients with  $\kappa$ 4- and  $\lambda$ 8-associated AL amyloidosis, respectively, were studied. (top: Congo red (CR) stain; middle: anti-V<sub>L</sub> subgroup-specific mAb; bottom: c11-1F4 mAb; original magnification,  $\times 200$ ).



Fig. 6 Monoclonal amyloid antibody 11-1F4-mediated resolution of a human AL $\kappa$  amyloidoma. Appearance of residual AL amyloid tumor (HIG) on day 15 in an untreated animal (control, left) and in mice given injections of m11-1F4 mAb, c11-1F4 mAb, or mIgG1 $\kappa$  protein MOPC 31C (control, right) 48 h after amyloidoma induction and then again on days 4, 6, 8, 10, and 12.

stitial congophilic deposits in both control and treated animals occurred within the spleen. The amount of this material was quantitated using image analysis and spectral segmentation techniques from 4- $\mu$ m thick Congo red-stained sections. As illustrated in Fig. 8, there was a statistically significant decrease ( $P = <.05$ ) in the mean splenic amyloid burden of the c11-1F4 mAb-treated mice versus untreated controls (amyloid burden index, 0.450 and 1.195, respectively). This reduction in splenic

Table 2 AL $\kappa$  (HIG) amyloidoma study

Antibody treatment	Weight of residual amyloidoma (g) <sup>a</sup>		Percentage of reduction <sup>b</sup>
Murine 11-1F4 mAb	0.02 <sup>c</sup>	0.17 <sup>d</sup>	97 <sup>c</sup> 68 <sup>d</sup>
Chimeric 11-1F4 mAb	0.16	0.18	73 66
Murine IgG1 $\kappa$ MOPC 31C	0.59	0.53	
None	0.56		

<sup>a</sup> Wet weight.  
<sup>b</sup> Compared with MOPC controls.  
<sup>c,d</sup> Days 15 and 16, respectively.

Table 3 AL $\lambda$  (BAL) amyloidoma study

Antibody treatment	Weight of residual amyloidoma (g) <sup>a</sup>		Percentage of reduction <sup>b</sup>
Murine 11-1F4 mAb	0.13 <sup>c</sup>	0.22 <sup>d</sup>	75 <sup>c</sup> 58 <sup>d</sup>
Chimeric 11-1F4 mAb	0.44	0.30	15 43
Murine IgG1 $\kappa$ MOPC 31C	0.52	0.53	
None	0.45		

<sup>a</sup> Wet weight.  
<sup>b</sup> Compared with MOPC controls.  
<sup>c,d</sup> Days 15 and 21, respectively.

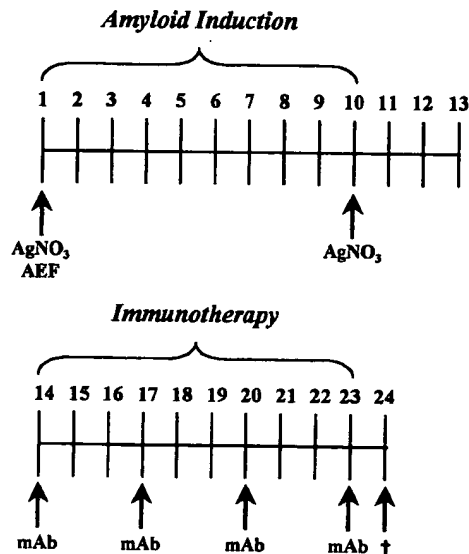


Fig. 7 Protocol for systemic AA amyloid induction and immunotherapy. AA amyloid was induced in mice by injections of silver nitrate (AgNO<sub>3</sub>) on days 1 and 10 and AA fibrils (AEF) on day 1. Groups of animals received either m or c11-1F4 mAbs at the times indicated. Another (control) group remained untreated.

amyloid was calculated to be 62%, as compared with 79% in the animals that received the m11-1F4 reagent.

### Discussion

On the basis of the results of the comparative immunological analyses (fibril binding, dot blot, and immunohistochemical assays), it was evident that the reactivity of the c11-1F4 mAb was identical to that of the original murine antibody. Moreover,

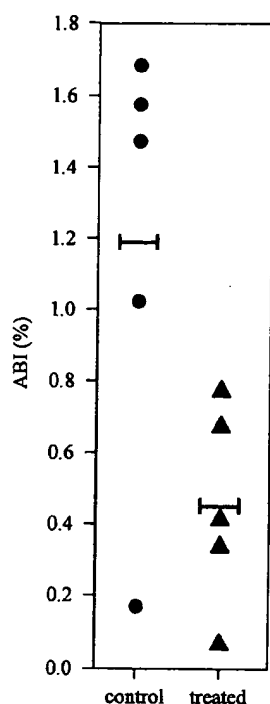


Fig. 8 Chimeric 11-1F4 mAb-induced resolution of systemic murine AA amyloid. Graphic representation of percent of AA amyloid remaining in splenic tissue obtained from mice that were injected with the c11-1F4 (treated) and those that received no antibody (control). The amyloid burden index (ABI) was calculated according to the following formula:  $ABI = CR + \text{area}/\text{total area} \times 100$ .

as demonstrated in studies involving mice bearing human AL amyloidomas or murine AA splenic deposits, the modified reagent, in which the mouse heavy and light chain constant region domains were replaced by their human counterparts, also was capable of accelerating amyloidolysis. Although the precise mechanism(s) responsible for this response is subject to additional investigation, we have shown that the Fc region of the 11-1F4 antibody molecule is essential to initiation of an immune effector response that leads to amyloid degradation (13); thus, we attribute the lesser degree of resolution achieved with the chimeric reagent in the two mouse models to the presence of human, rather than murine protein, in the Fc portion of the immunoglobulin molecule.

Notably, both types of 11-1F4 mAbs were capable of accelerating removal of the AL $\kappa$  and AL $\lambda$  amyloidomas. However, as generally found in our previous *in vivo* studies involving the murine reagent and four  $\kappa$ -type and eight  $\lambda$ -type extracts, the latter took somewhat longer to resolve (13). The factor(s) responsible for this difference remains to be determined.

With regard to potential toxicity, the c11-1F4 mAb, as with its murine counterpart, specifically recognized AL fibrils and failed to bind native light chains, with the exception of  $\kappa 4$  molecules. Presumably, this reactivity would not have an adverse effect clinically, given the fact that immunoglobulins bearing  $\kappa 4$  light chains represent <5% of the total human Ig $\kappa$  population (21). Furthermore, there were no abnormalities noted microscopically in the liver, spleen, or kidneys of the c11-1F4

mAb-treated animals, and in contrast to the c mAb Rituximab, this reagent had little or no reactivity with human tissue.

The demonstration of the effective performance of the c11-1F4 mAb molecule in these *in vitro* and *in vivo* studies has formed the basis to proceed with full-scale GMP production of this antibody for an eventual Phase I/II clinical trial involving patients with primary (AL) amyloidosis.

## Acknowledgments

We thank Dr. Siobhán O'Brien and Dr. Tarran Jones of AERES Biomedical Ltd. for preparing the c11-1F4 mAbs used in this study. We also thank Drs. Morris Kelsey, Barry Kobrin, Aparna Kolehkar, and other staff of the Biological Resource Branch and Biopharmaceutical Development Program, Division of Cancer Treatment and Diagnosis, National Cancer Institute-Frederick Cancer Research and Development Center for their scientific input and project oversight. We also thank Ms. Ronda Reed for secretarial assistance and Sallie Macy, Charles, L. Murphy, Dr. Lian Tang, Teresa Williams, Dennis Wolfenbarger, and Craig Wooliver for their technical contributions.

## References

- Solomon, A., and Weiss, D. T. Protein and host factors implicated in the pathogenesis of light chain amyloidosis (AL amyloidosis). *Amyloid. Int. J. Exp. Clin. Investig.*, 2: 269-279, 1995.
- Kyle, R. A., and Gertz, M. A. Primary systemic amyloidosis: clinical and laboratory features in 474 cases. *Semin. Hematol.*, 32: 45-59, 1995.
- Dhodapkar, M. V., Merlini, G., and Solomon, A. Biology and therapy of immunoglobulin deposition diseases. *Hematol. Oncol. Clin. N. Am.*, 11: 89-110, 1997.
- Falk, R. H., Comenzo, R. L., and Skinner, M. The systemic amyloidoses. *N. Engl. J. Med.*, 337: 898-909, 1997.
- Gertz, M. A., and Kyle, R. A. Amyloidosis: prognosis and treatment. *Semin. Arthritis Rheum.*, 24: 124-138, 1994.
- Skinner, M., Anderson, J., Simms, R., Falk, R., Wang, M., Libbey, C., Jones, L. A., and Cohen, A. S. Treatment of 100 patients with primary amyloidosis: a randomized trial of melphalan, prednisone, and colchicine versus colchicine only. *Am. J. Med.*, 100: 290-298, 1996.
- Kyle, R. A., Gertz, M. A., Greipp, P. R., Witzig, T. E., Lust, J. A., Lacy, M. Q., and Therneau, T. M. A trial of three regimens for primary amyloidosis: colchicine alone, melphalan and prednisone, and melphalan, prednisone, and colchicine. *N. Engl. J. Med.*, 336: 1202-1207, 1997.
- Dhodapkar, M. V., Jagannath, S., Vesole, D., Munshi, N., Naucke, S., Tricot, G., and Barlogie, B. Treatment of AL-amyloidosis with dexamethasone plus alpha interferon. *Leuk. Lymphoma*, 27: 351-356, 1997.
- Palladini, G., Anesi, E., Perfetti, V., Obici, L., Invernizzi, R., Balduini, C., Ascari, E., and Merlini, G. A modified high-dose dexamethasone regimen for primary systemic (AL) amyloidosis. *Br. J. Haematol.*, 113: 1044-1046, 2001.
- Comenzo, R. L., Vosburgh, E., Falk, R. H., Sanchowala, V., Reisinger, J., Dubrey, S., Dember, L. M., Berk, J. L., Akpek, G., LaValley, M., O'hara, C., Arkin, C. F., Wright, D. G., and Skinner, M. Dose-intensive melphalan with blood stem-cell support for the treatment of AL (amyloid light-chain) amyloidosis: survival and responses in 25 patients. *Blood*, 91: 3662-3670, 1998.
- Comenzo, R. L., Sanchowala, V., Fisher, C., Akpek, G., Farhat, M., Cerda, S., Berk, J. L., Dember, L. M., Falk, R., Finn, K., Skinner, M., and Vosburgh, E. Intermediate-dose intravenous melphalan and blood stem cells mobilized with sequential GM-CSF or G-CSF alone to treat AL (amyloid light chain) amyloidosis. *Br. J. Haematol.*, 104: 553-559, 1999.
- Comenzo, R. L., and Gertz, M. A. Autologous stem cell transplantation for primary systemic amyloidosis. *Blood*, 99: 4276-4282, 2002.

13. Hrnčić, R., Wall, J., Wolfenbarger, D. A., Murphy, C. L., Schell, M., Weiss, D. T., and Solomon, A. Antibody-mediated resolution of light chain-associated amyloid deposits. *Am. J. Pathol.*, 157: 1239–1246, 2000.
14. Jones, S. T., and Bendig, M. M. Rapid PCR-cloning of full-length mouse immunoglobulin variable regions. *Biotechnology*, 9: 579, 1991.
15. Güssow, D., and Clackson, T. Direct clone characterization from plaques and colonies by the polymerase chain reaction. *Nucleic Acids Res.*, 17: 4000, 1989.
16. Wall, J., Murphy, C. L., and Solomon, A. *In vitro* immunoglobulin light chain fibrillogenesis. *Methods Enzymol.*, 309: 204–217, 1999.
17. Lundmark, K., Westermark, G. T., Nyström, S., Murphy, C. L., Solomon, A., and Westermark, P. Transmissibility of systemic amyloidosis by a prion-like mechanism. *Proc. Natl. Acad. Sci. USA* 99: 6979–6984.
18. Maloney, D. G., Grillo-Lopez, A. J., White, C. A., Bodkin, D., Schilder, R. J., Neidhart, J. A., Janakiraman, N., Foon, K. A., Liles, T. M., Dallaire, B. K., Wey, K., Royston, I., Davis, T., and Levy, R. IDEC-C2B8 (Rituximab) anti-CD20 monoclonal antibody therapy in patients with relapsed low-grade non-Hodgkin's lymphoma. *Blood*, 90: 2188–2195, 1997.
19. Pras, M., Schubert, M., Zucker-Franklin, D., Rimon, A., and Franklin, E. C. The characterization of soluble amyloid prepared in water. *J. Clin. Investig.*, 47: 924–933, 1968.
20. Wall, J., Schell, M., Hrnčić, R., Macy, S., Wooliver, C., Wolfenbarger, D., Murphy, C., Donnell, R., Weiss, D. T., and Solomon, A. Treatment of amyloidosis using an anti-fibril monoclonal antibody: pre-clinical efficacy in a murine model of AA-amyloidosis. In: M. Bély and Á. Apáthy (eds.), *Amyloid and Amyloidosis*, IXth International Symposium on Amyloidosis, pp. 158–160. David Apathy, Budapest, Hungary, 2001.
21. Solomon, A., Weiss, D. T., Macy, S. D., Antonucci, R. A. Immunocytochemical detection of kappa and lambda light chain V region subgroups in human B-cell malignancies. *Am. J. Pathol.*, 137: 855–862, 1990.





THE AMERICAN ASSOCIATION OF  
PATHOLOGISTS AND BACTERIOLOGISTS

THE AMERICAN SOCIETY FOR  
EXPERIMENTAL PATHOLOGY

01. 02. 03. 04. 05. 06. 07. 08. 09. 10. 11. 12. 13. 14. 15. 16. 17. 18. 19. 20. 21. 22. 23. 24. 25. 26. 27. 28. 29. 30. 31. 32. 33. 34. 35. 36. 37. 38. 39. 40. 41. 42. 43. 44. 45. 46. 47. 48. 49. 50. 51. 52. 53. 54. 55. 56. 57. 58. 59. 60. 61. 62. 63. 64. 65. 66. 67. 68. 69. 70. 71. 72. 73. 74. 75. 76. 77. 78. 79. 80. 81. 82. 83. 84. 85. 86. 87. 88. 89. 90. 91. 92. 93. 94. 95. 96. 97. 98. 99. 100. 101. 102. 103. 104. 105. 106. 107. 108. 109. 110. 111. 112. 113. 114. 115. 116. 117. 118. 119. 120. 121. 122. 123. 124. 125. 126. 127. 128. 129. 130. 131. 132. 133. 134. 135. 136. 137. 138. 139. 140. 141. 142. 143. 144. 145. 146. 147. 148. 149. 150. 151. 152. 153. 154. 155. 156. 157. 158. 159. 160. 161. 162. 163. 164. 165. 166. 167. 168. 169. 170. 171. 172. 173. 174. 175. 176. 177. 178. 179. 180. 181. 182. 183. 184. 185. 186. 187. 188. 189. 190. 191. 192. 193. 194. 195. 196. 197. 198. 199. 200. 201. 202. 203. 204. 205. 206. 207. 208. 209. 210. 211. 212. 213. 214. 215. 216. 217. 218. 219. 220. 221. 222. 223. 224. 225. 226. 227. 228. 229. 230. 231. 232. 233. 234. 235. 236. 237. 238. 239. 240. 241. 242. 243. 244. 245. 246. 247. 248. 249. 250. 251. 252. 253. 254. 255. 256. 257. 258. 259. 260. 261. 262. 263. 264. 265. 266. 267. 268. 269. 270. 271. 272. 273. 274. 275. 276. 277. 278. 279. 280. 281. 282. 283. 284. 285. 286. 287. 288. 289. 290. 291. 292. 293. 294. 295. 296. 297. 298. 299. 300. 301. 302. 303. 304. 305. 306. 307. 308. 309. 310. 311. 312. 313. 314. 315. 316. 317. 318. 319. 320. 321. 322. 323. 324. 325. 326. 327. 328. 329. 330. 331. 332. 333. 334. 335. 336. 337. 338. 339. 340. 341. 342. 343. 344. 345. 346. 347. 348. 349. 350. 351. 352. 353. 354. 355. 356. 357. 358. 359. 360. 361. 362. 363. 364. 365. 366. 367. 368. 369. 370. 371. 372. 373. 374. 375. 376. 377. 378. 379. 380. 381. 382. 383. 384. 385. 386. 387. 388. 389. 390. 391. 392. 393. 394. 395. 396. 397. 398. 399. 400. 401. 402. 403. 404. 405. 406. 407. 408. 409. 410. 411. 412. 413. 414. 415. 416. 417. 418. 419. 420. 421. 422. 423. 424. 425. 426. 427. 428. 429. 430. 431. 432. 433. 434. 435. 436. 437. 438. 439. 440. 441. 442. 443. 444. 445. 446. 447. 448. 449. 450. 451. 452. 453. 454. 455. 456. 457. 458. 459. 460. 461. 462. 463. 464. 465. 466. 467. 468. 469. 470. 471. 472. 473. 474. 475. 476. 477. 478. 479. 480. 481. 482. 483. 484. 485. 486. 487. 488. 489. 490. 491. 492. 493. 494. 495. 496. 497. 498. 499. 500. 501. 502. 503. 504. 505. 506. 507. 508. 509. 510. 511. 512. 513. 514. 515. 516. 517. 518. 519. 520. 521. 522. 523. 524. 525. 526. 527. 528. 529. 530. 531. 532. 533. 534. 535. 536. 537. 538. 539. 540. 541. 542. 543. 544. 545. 546. 547. 548. 549. 550. 551. 552. 553. 554. 555. 556. 557. 558. 559. 560. 561. 562. 563. 564. 565. 566. 567. 568. 569. 570. 571. 572. 573. 574. 575. 576. 577. 578. 579. 580. 581. 582. 583. 584. 585. 586. 587. 588. 589. 590. 591. 592. 593. 594. 595. 596. 597. 598. 599. 600. 601. 602. 603. 604. 605. 606. 607. 608. 609. 610. 611. 612. 613. 614. 615. 616. 617. 618. 619. 620. 621. 622. 623. 624. 625. 626. 627. 628. 629. 630. 631. 632. 633. 634. 635. 636. 637. 638. 639. 640. 641. 642. 643. 644. 645. 646. 647. 648. 649. 650. 651. 652. 653. 654. 655. 656. 657. 658. 659. 660. 661. 662. 663. 664. 665. 666. 667. 668. 669. 670. 671. 672. 673. 674. 675. 676. 677. 678. 679. 680. 681. 682. 683. 684. 685. 686. 687. 688. 689. 690. 691. 692. 693. 694. 695. 696. 697. 698. 699. 700. 701. 702. 703. 704. 705. 706. 707. 708. 709. 710. 711. 712. 713. 714. 715. 716. 717. 718. 719. 720. 721. 722. 723. 724. 725. 726. 727. 728. 729. 730. 731. 732. 733. 734. 735. 736. 737. 738. 739. 740. 741. 742. 743. 744. 745. 746. 747. 748. 749. 750. 751. 752. 753. 754. 755. 756. 757. 758. 759. 760. 761. 762. 763. 764. 765. 766. 767. 768. 769. 770. 771. 772. 773. 774. 775. 776. 777. 778. 779. 780. 781. 782. 783. 784. 785. 786. 787. 788. 789. 790. 791. 792. 793. 794. 795. 796. 797. 798. 799. 800. 801. 802. 803. 804. 805. 806. 807. 808. 809. 810. 811. 812. 813. 814. 815. 816. 817. 818. 819. 820. 821. 822. 823. 824. 825. 826. 827. 828. 829. 830. 831. 832. 833. 834. 835. 836. 837. 838. 839.

[illegible]

## PRINTERS & PUBLISHERS

NOTICE: THIS MATERIAL MAY BE PROTECTED  
BY COPYRIGHT LAW (TITLE 17 U.S. CODE)

## ANIMAL MODEL FOR HUMAN DISEASE

Amyloidosis

**Animal Model: Spontaneous  
and Induced Amyloidosis**

Contributed by: Alan S. Cohen, MD and Tsuranobu Shirahama, MD, Department of Medicine, Boston University Medical Center, Boston, Mass.

### Biologic Features

*Species Involved (Strains, Breeds, etc).* Amyloid has been reported to occur spontaneously in a variety of animal species<sup>1</sup>—dogs,<sup>2</sup> cats,<sup>3</sup> mice,<sup>4</sup> birds<sup>5</sup> and many others. Several strains of mice (A/HeN, AALF, AL/N)<sup>6</sup> and the wild white Pekin ducks<sup>7</sup> are said to have a high spontaneous incidence.

Amyloidosis can be induced experimentally in many animal species—mice, hamsters, guinea pigs and rabbits, etc, although susceptibility to the amyloid-inducing regimen varies among species and strains.<sup>8,9</sup> Our present order of susceptibility to amyloid induction by casein injections in strains of mice is as follows: a) CBA/J, b) C57BL/6J, c) Swiss white (random bred from Charles River Laboratories), d) C<sub>3</sub>H/HeJ, e) Balb/cJ and f) SWR/J.

*Clinical or Phenotypic Characteristics as Applicable.* General weakness and loss of the body weight may occur, although there are no pathognomonic features. Animals may develop a nephrotic syndrome and associated illnesses; death from azotemia may occur.

### Pathologic Features

Intercellular deposition of amyloid which by light microscopy has a hyalin eosinophilic appearance. It stains with Congo red and shows

Publication sponsored by the Registry of Comparative Pathology of the Armed Forces Institute of Pathology and supported by Public Health Service Grant RR-00301 from the Division of Research Resources, US Department of Health, Education and Welfare, under the auspices of Universities Associated for Research and Education in Pathology, Inc. Supported by Grants AM-04599 and TI-AM-5285 from the National Institute of Arthritis and Metabolic Diseases, US Public Health Service, and by the Massachusetts chapter of the Arthritis Foundation, The John A. Hartford Foundation and the Arthritis Foundation.

characteristic green birefringence under polarized light after such staining. It is PAS-positive and demonstrates crystal violet and methyl violet *metachromasia*.<sup>1,9</sup> In the electron microscope, amyloid *in situ* consists of characteristic fibrils approximately 100 Å wide, indeterminate in length, rigid, nonbranching and often arranged in random array.<sup>1,10</sup> The deposition usually appears first in the perifollicular zone of the spleen, then in Disse's space in the liver and in the glomerular mesangial region in the kidney.<sup>1,10</sup>

When the animal is kept for a long period of time on an amyloid-inducing regimen, the deposition is wide-spread in a variety of organs, including the blood vessels.<sup>10</sup>

**Essentials for Definitive Recognition.** The recommended procedure for identification of amyloid deposits in tissue is: a) fixation of tissue in formalin, b) staining with alkaline Congo red, c) demonstration of the characteristic green birefringence for amyloid by polarizing microscopy and, if feasible d) demonstration of the characteristic amyloid fibrils by electron microscopy of osmium-fixed tissue sections (Figure 1).

**Experimental Procedures used.** A wide variety of methods for experimental induction of amyloidosis have been introduced.<sup>1,4,10</sup> At the present time, repeated injections of casein, as originated by Kuczynski in 1922,<sup>11</sup> seems to be an easily reproducible method. Generally, daily subcutaneous injections of 0.25 to 0.5 ml of 5 to 10% casein solution (which can be dissolved in approximately 0.05 N sodium hydroxide or 0.3 N sodium bicarbonate, with stirring and warming to 50 to 60 C) into mice usually produce amyloidosis in 3 to 4 weeks; 2 to 3 weekly injections of 1 to 2 ml of the casein solution into guinea pigs will induce amyloid within 2 to 4 months; while 2 to 3 weekly injections with 5 ml of the solution into rabbits will produce it within 3 to 5 months. These procedures, when established in a laboratory, are reproducible and induce amyloidosis in virtually 100% of the treated animals. Occasionally, longer periods of casein injection will be necessary before amyloid becomes apparent. However, the results are not always totally reproducible between laboratories; very subtle changes in the experimental conditions (for example, change of animal strains, change of the location of the laboratory, etc) can occasionally affect the induction of amyloid.<sup>4</sup>

#### Comparison with Human Disease

**Differences From and Similarities with the Human Model.** Experimentally induced amyloidosis in animals is comparable in virtually all respects with human amyloidosis<sup>12</sup> by histologic and electron microscopic standards.<sup>1,4,10,12</sup> It is likely that immunologic and biochemical differences will be discernible with future study.



Fig 1  
glomerul  
endot  
Inset—

De  
as de  
micro  
Pat  
Pro  
amyl  
need

Useful  
Sim  
and c  
of am  
Ani  
readil

Referen  
1. C.

n Journal  
Pathology

or such  
methyl  
in situ  
etermi-  
random  
ar zone  
nerular

nyloid-  
organs,

cedure  
ssue in  
of the  
oscopy  
fibrils  
1).

experi-  
At the  
nski in  
daily  
lution  
ide or  
) into  
injec-  
nduce  
15 ml  
These  
e and  
nally,  
nyloid  
repro-  
ental  
ation  
loid.<sup>4</sup>

xperi-  
ly all  
icro-  
mical

Vol. 68, No. 2  
August 1972

Animal Model for Amyloidosis 443

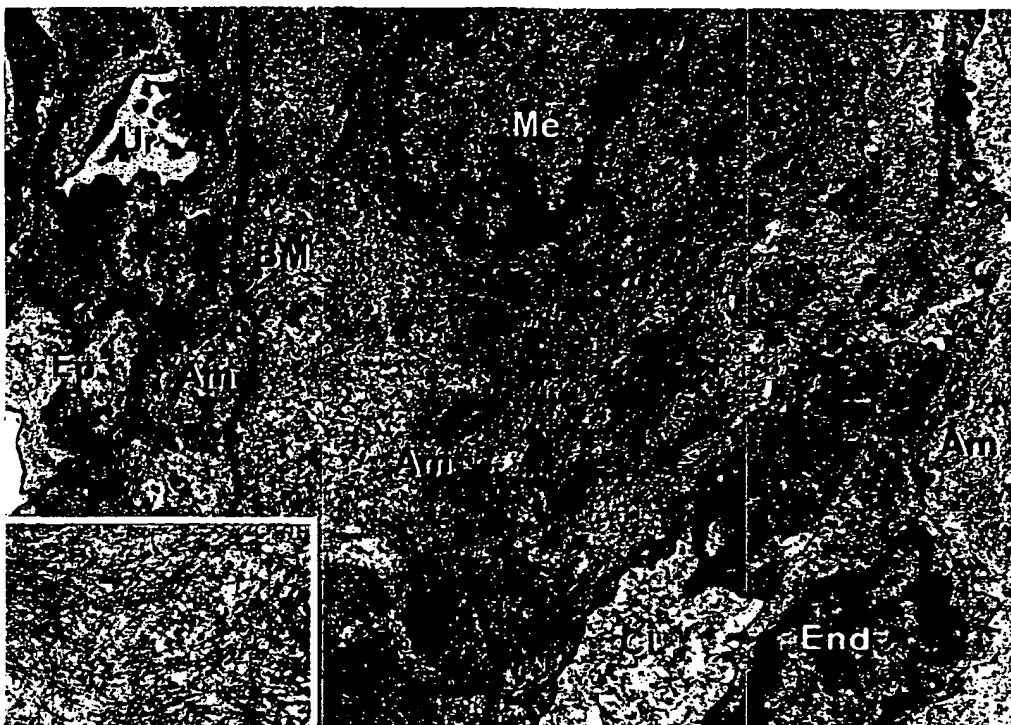


**Fig 1**—Amyloidosis experimentally induced by casein injections in a rabbit renal glomerulus. Am=amyloid fibrils, BM=basement membrane, CL=capillary lumen, End=endothelial cell, Ep=epithelial cell, Me=mesangial cell, Ur=urinary space ( $\times 6000$ ). Inset—A clearer demonstration of amyloid fibril structure ( $\times 24,000$ ).

**Definitive Diagnosis.** Recognition of amyloid deposition in the tissue, as defined by the appearance of green birefringence on polarization microscopy after Congo red staining.

**Pathologic Features.** As described above.

**Problems Needing Solutions.** More refined and faster methods for amyloid induction in reproducible fashion from laboratory to laboratory need to be established.

#### Usefulness and Availability of This Model

Since the model is quite comparable to human disease, it has been and can be used for studies of the course, pathogenesis and treatment of amyloid.

Animals (especially mice) suitable for experimental induction are readily available through commercial laboratories.

#### References

1. Cohen AS: The constitution and genesis of amyloid. International Review of

## 444 Cohen and Shirahama

American Journal  
of PathologyVol. 6:  
August

- Experimental Pathology, Vol 4. Edited by GW Richter, MA Epstein, New York, Academic Press, Inc. 1965, pp 159-243
2. Slanson DO, Gribble DH, Russell SW: A clinicopathological study of renal amyloidosis in dogs. *J Comp Pathol* 80:335-343, 1970
  3. Clark L, Seawright AS: Generalized amyloidosis in seven cats. *Pathol Vet* 6:117-134, 1969
  4. Sorenson GD, Helfner WA, Kirkpatrick JB: Experimental amyloidosis. Methods and Achievements in Experimental Pathology, Vol 1, Edited by E Bajusz, Basel, S Karger, 1966
  5. Cowan DG: Avian amyloidosis. *Pathol Vet* 5:51-58, 1968
  6. Ram JS, DeLellis RA, Glenner GG: Amyloid. VIII. On strain variability in experimental murine amyloid. *Proc Soc Exp Biol Med* 130:462-464, 1969
  7. Rigdon RH: Amyloidosis: spontaneous occurrence in white Pekin ducks. *Am J Pathol* 39:369-378, 1961
  8. Willerson JT, Asofsky R, Barth WF: Experimental murine amyloid. IV. Amyloidosis and immunoglobulins. *J Immunol* 103: 741-749, 1969
  9. Pearse AGE: Histochemistry, third edition, Vol 1. Boston, Little, Brown and Company, 1968, p 759
  10. Mandema E, Ruinen L, Scholten JH, Cohen AS (editors): Amyloidosis. Amsterdam, Excerpta Medica Foundation, 1968, p 463
  11. Kuczynski MH: Edwin Goldmanns Untersuchungen uber zellulare Vorgänge im Gefolge des Verdauungsprozesses auf Grund nachgelassener Präparate dargestellt und durch neue Versuche ergänzt. *Virchows Arch [Pathol Anat]* 239:185-302, 1922
  12. Cohen AS: Amyloidosis. *N Engl J Med* 277:522-530, 574-583, 628-638, 1967

Errata

McD  
rat ki  
in viv  
Am JPage  
are up  
be tur

Volume 24 Number 1, 2004

ISSN: 0895-8696

JOURNAL OF

# *Molecular Neuroscience*

Editor-in-Chief: **ILLANA GOZES, PhD***Special Issue*

Treating Alzheimer's Disease:  
New Directions in Drug Discovery  
and Development

*Guest Editors:*

Howard M. Fillit, MD

Lorenzo M. Refolo, PhD

ISOA

Univ. of Milan  
Bio-Medical  
Library

08 24 04



HUMANANA PRESS

HumanaJournals.com

*Journal of Molecular Neuroscience*  
Copyright © 2004 Humana Press Inc.  
All rights of any nature whatsoever reserved.  
ISSN0893-8696/04/24:167-172/\$25.00

☐ NOTICE: THIS MATERIAL MAY BE PROTECTED  
BY COPYRIGHT LAW (TITLE 17 U.S. CODE)

## ANTI-AMYLOID

# Novel Glycosaminoglycan Precursors as Antiamyloid Agents

## Part IV<sup>†</sup>

**Robert Kisilevsky,<sup>\*1,2</sup> Walter A. Szarek,<sup>3</sup> John Ancsin,<sup>1,2</sup>  
Rahul Vohra,<sup>3</sup> Zhanjiang Li,<sup>3</sup> and Sandra Marone<sup>3</sup>**

Departments of <sup>1</sup>Pathology and <sup>3</sup>Chemistry Queen's University, and <sup>2</sup>The Syl and Molly Apps  
Research Center Kingston General Hospital, Kingston, Ontario K7L 3N6, Canada

## Abstract

In vivo amyloids consist of two classes of constituents. The first is the disease-defining protein,  $\beta$ -amyloid (A $\beta$ ), in Alzheimer's disease. The second is a set of common structural components that usually are the building blocks of basement membrane (BM), a tissue structure that serves as a scaffold onto which cells normally adhere. In vitro binding interactions between one of these BM components and amyloidogenic proteins rapidly change the conformation of the amyloidogenic protein into amyloid fibrils. The offending BM component is a heparan sulfate (HS) proteoglycan, part of which is protein and the remainder a specific linear polysaccharide, which is the portion responsible for binding and imparting the typical amyloid structure to the amyloid precursor protein/peptide. Our past work has demonstrated that agents that inhibit the binding between HS and the amyloid precursor are effective antiamyloid compounds both in vitro and in vivo. Similarly, 4-deoxy analogs of glucosamine (a precursor of HS biosynthesis) are effective antiamyloid compounds both in culture and in vivo. Our continuing work concerns (1) the testing of our 4-deoxy compounds in a mouse transgenic model of Alzheimer's disease, and (2) the continuing design and synthesis of modified sugar precursors of HS, which when incorporated into the polysaccharide will alter its structure so that it affects its amyloid-inducing properties. Since our previous report, 22 additional compounds have been designed and synthesized based on the known steps involved in HS biosynthesis. Of these, 12 soluble compounds have been assessed for their effect on HS biosynthesis in hepatocyte tissue cultures. In addition, one anomer of a 4-deoxy-D-glucosamine analog, which possesses AA-amyloid inhibitory properties in vivo is in the process of being assessed for its anti-A $\beta$  activity using a murine transgenic model of brain A $\beta$  amyloidogenesis. The majority of the novel sugars prepared to date are analogs of N-acetylglucosamine. They have been modified at the 2-N, C-3, C-4, C-3 and C-4, or C-6 positions. One compound modified at the 2-N position (QS231), which inhibits HS synthesis in hepatocyte cultures, has shown marked enhancing properties *vis-à-vis* AA amyloid deposition in vivo. Very instructive results with regard to HS structure and its relation to AA amyloid deposition should be forthcoming from analyses of the AA-associated HS generated with this compound. Two additional compounds, QS431, modified at C-4, and QS610, modified at C-6, have been shown to have marked inhibitory and stimulatory effects, respectively, on hepatocyte HS synthesis. These compounds are presently being assessed in vivo in AA amyloid deposition models.

**Index Entries:** A $\beta$ ; amyloid; binding; glycosaminoglycans (GAGs); glucosamine analogs; heparan sulfate; SAA.

<sup>\*</sup>Author to whom all correspondence and reprint requests should be addressed. E-mail: kisilevsky@cliff.path.queensu.ca  
<sup>†</sup>For Parts I and II, see Kisilevsky R. and Szarek W.A. (2002a, 2002b, respectively); for Part III, see Kisilevsky et al. (2003).

## Introduction

### *Nature of Amyloid*

Amyloid is the term for extracellular fibrillar protein deposits that have a specific set of staining and structural characteristics. Amyloid deposits are involved in the pathogenesis of disorders such as Alzheimer's disease, adult-onset diabetes, joint destruction during prolonged hemodialysis, and several other rarer disorders. Although amyloids all look and stain the same in tissues, over 20 different protein types have been identified (Westermarck, 1997). In vivo, each amyloid is composed of two classes of components (Kisilevsky and Fraser, 1997): The first is the defining protein; the second is a set of common structural constituents. These include serum amyloid P, proteoglycans, usually perlecan (the basement membrane [BM] form of heparan sulfate [HS] proteoglycan [HSPG]), laminin, collagen IV, and apolipoprotein E. Substantial evidence indicates that interactions between the common components and the amyloidogenic protein play a role in amyloidogenesis (Kisilevsky and Fraser, 1997). Of particular importance are the glycosaminoglycans (GAGs) HS and/or heparin. In the cases of amyloids associated with inflammatory diseases (AA amyloid) and Alzheimer's disease ( $\beta$ -amyloid [ $A\beta$ ]), such amyloid-associated GAGs have been shown to have subtle changes in structure (Lindahl et al., 1995, 1996, 1999; Lindahl and Lindahl, 1997) and, when interacting with their respective amyloidogenic proteins, have the ability to alter their conformations so that they take on the structural characteristics typical of an amyloid (McCubbin et al., 1988; McLaurin et al., 1999a, 1999b; Kisilevsky and Fraser, 1997; Castillo et al., 1998).

### *Amyloidogenic Protein and Heparin/HS: Complementary Binding Domains*

The structural features of the HS-binding domain of serum amyloid A (SAA) and  $A\beta$  have been illustrated in our previous reports, Parts I and II (Kisilevsky and Szarek, 2002a, 2002b).

### *Rationale*

The rationale for the synthesis of novel GAG sugar precursors follows from the structure of heparin/HS and the biosynthetic steps that are responsible for their production (Lindahl et al., 1989). Altering the structure at the 4-position of either the glucosamine or the uronate residues would interfere with the growth of the GAG chain, as this position is necessary for the  $\alpha$ -(1  $\rightarrow$  4) linkages in the polysaccharide.

Alternatively, altering the structure at the 2-position of the uronate, or of the amino group of the glucosamine residue, would likely change the manner in which the growing polysaccharide chain is sulfated. In addition, because *N*-sulfonation is a required step in the proper epimerization and sulfation of the uronate, modification of glucosamine precursors at the amino group might result in modified or under-sulfated HS and, therefore, one that will probably not interact with amyloidogenic proteins/peptides.

## Materials and Methods

### *Chemical Syntheses*

Since the commencement of our project, 56 novel sugars have been designed and synthesized. The structures of many of these have been listed in previous publications. Some of the more recent compounds might have proprietary interest, for which reason their syntheses and structures are not presented in detail. Following favorable results from our in vitro testing in hepatocyte culture, considerable effort was placed on developing methodologies for the preparation of the larger quantities of an anomer of a 4-deoxy-glucosamine analog required for its in vivo testing as an anti- $A\beta$  amyloid compound in a mouse transgenic model of Alzheimer's disease. This study is now in progress.

During the past 12 mo, 22 compounds have been designed and synthesized based on the known steps involved in HS biosynthesis. Of these, 12 soluble compounds have been assessed for their effect on HS biosynthesis in hepatocyte tissue cultures. The effects of three of these compounds on HS biosynthesis and the effects of one on in vivo amyloidogenesis will be presented.

### *GAG Synthesis*

Mouse hepatocytes were isolated and placed in culture, as described previously (Subrahmanyam and Kisilevsky, 1988; Thomas et al., 1995; Berkin et al., 2000a, 2000b). These hepatocytes were cultured for 24 h in the absence or presence of varying concentrations of the novel sugar analogs. [ $^3$ H]Glucosamine and [ $^{35}$ S]SO<sub>4</sub> were used to monitor the synthesis and sulfation of the newly made HS, as described previously (Subrahmanyam and Kisilevsky, 1988; Thomas et al., 1995; Berkin et al., 2000a, 2000b).

### *Macrophage Tissue Culture Induction of AA Amyloid*

AA amyloid was induced in J774 mouse macrophage tissue cultures using a modification of the method described previously (Kluve-Beckerman et



## GAG Precursors as Anti-Amyloid Agents

169

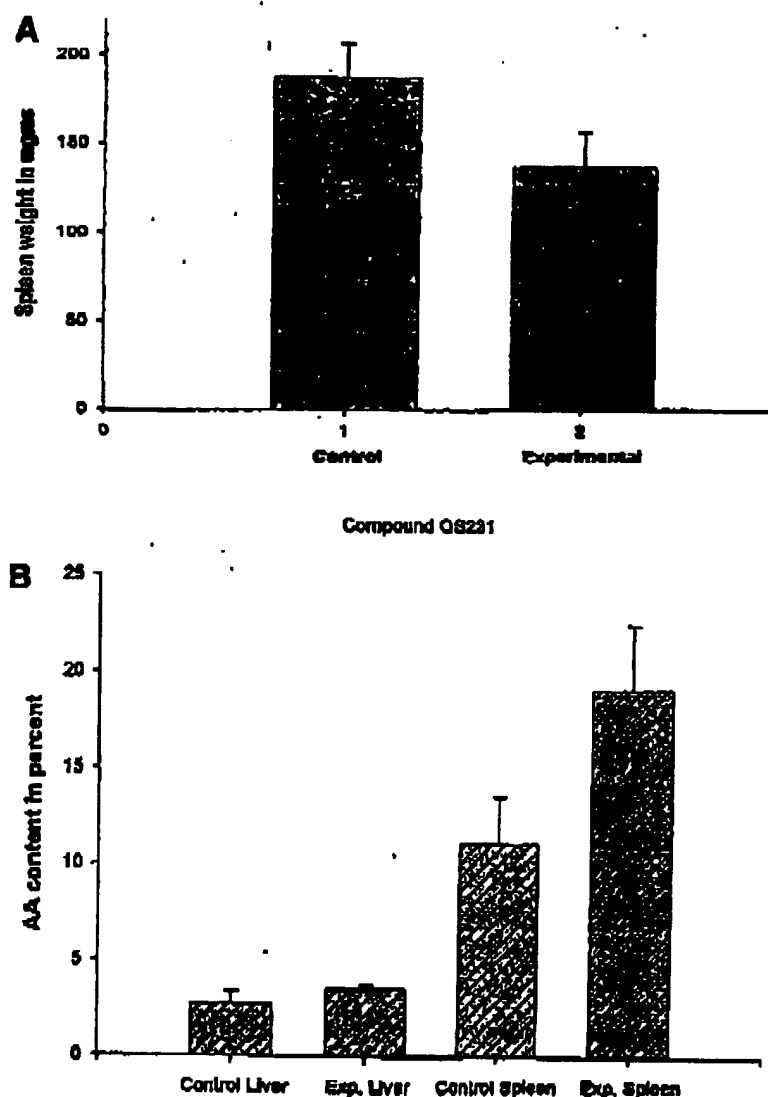


Fig. 1. Influence of compound QS231 on spleen weight during amyloid induction (A) and liver and spleen amyloid content (B).

al., 1999). Briefly, J774 cultures were grown to 75–80% confluence in RPMI medium for 24 h, following which the medium was changed to include 20  $\mu$ g amyloid-enhancing factor (AEF). After an additional 24 h, the medium was changed to include high-density lipoprotein/SAA (the AA amyloid precursor)  $\pm$  the compound of interest in appropriate concentrations. Cultures were maintained in this manner for 6 d, after which they were fixed and stained with Congo red.

#### *In Vivo* AA Amyloid Induction

AA amyloid was induced in 6- to 8-wk-old CD1 mice with AEF and AgNO<sub>3</sub> as an inflammatory stimulus, as described previously (Kisilevsky et al.,

1995). Twenty-four hours after induction, groups of 5 animals were treated with QS231 at 3 or 6 mg/dose, administered intravenously every 12 h, and sacrificed by CO<sub>2</sub> narcosis 5 d after the commencement of therapy. The quantity of amyloid/unit area of tissue (spleen and liver) was determined by image analysis, as described previously (Kisilevsky et al., 1995). Splenic amyloid was corrected for the change in spleen weight.

#### Results and Discussion

The inhibitory effect of QS231, a glucosamine analog with modification of a 2-N substituent, on HS synthesis has been reported in a previous posi-

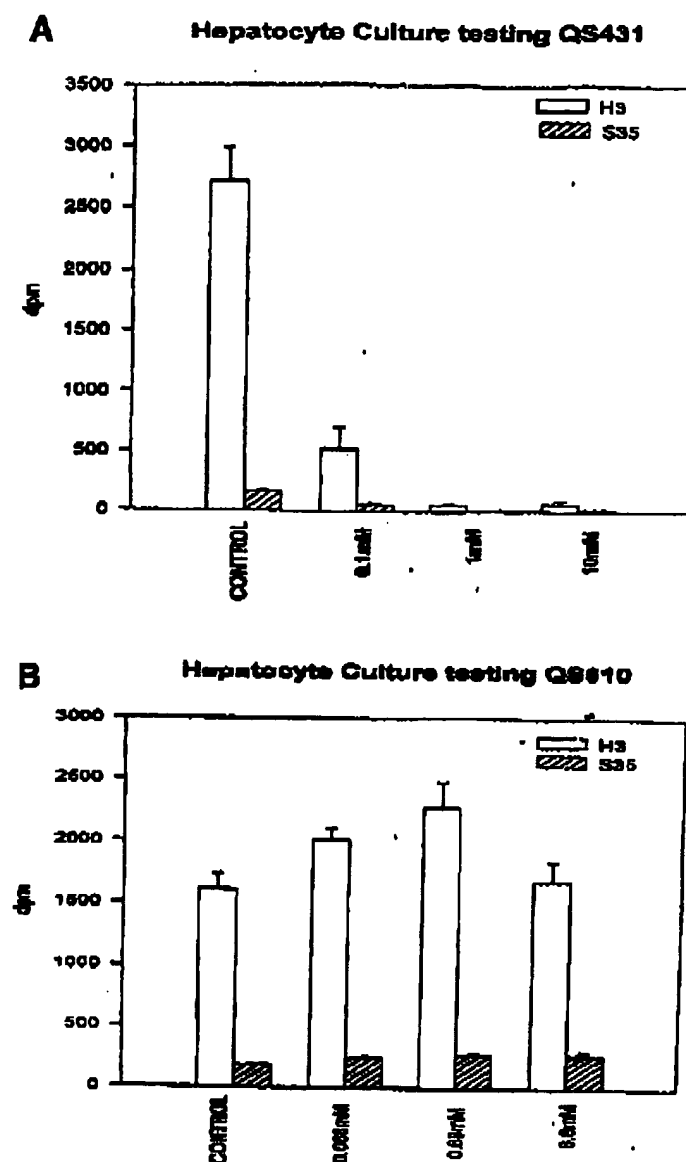


Fig. 2. The effects of different concentrations of compounds QS431 (A) and QS610 (B) on [ $^3\text{H}$ ] glucosamine and [ $^{35}\text{S}$ ]  $\text{SO}_4$  incorporation into hepatocyte heparan sulfate.

tion paper. Its effect on spleen weight during the induction of AA amyloidosis is illustrated in Fig. 1A. Spleen weights in untreated mice average 80 mg. Following amyloid induction over a 6-d period, and because of the systemic response to inflammation, spleens increase in size to about 180–185 mg. QS231 limited the splenic increase in weight to 130 mg, similar to that seen with many other compounds that inhibit HS biosynthesis. In contrast to other HS biosynthetic inhibitory agents tested in vivo that inhibited amyloid development, QS231 had a

marked enhancing effect on AA amyloid deposition (Fig. 1B). This surprising and fascinating result is potentially very instructive. These data have provided an opportunity to isolate and determine the structure of a specific amyloid-associated HS that enhances AA amyloid induction. Such structural information might indicate the critical elements that correlate with AA amyloidogenesis.

The effects of different concentrations of compounds QS431 and QS610 on [ $^3\text{H}$ ] glucosamine and [ $^{35}\text{S}$ ]  $\text{SO}_4$  incorporation into hepatocyte HS are illus-

## GAG Precursors as Anti-Amyloid Agents

171

trated in Fig. 2, A and B, respectively. QS431, an analog of glucosamine with a modified substituent at C-4, has a profound inhibitory effect on HS biosynthesis by hepatocytes in culture. This is similar to previous results that we have observed with anomers of a 4-deoxy-glucosamine analog, agents that have already been shown to inhibit in vivo amyloidogenesis (reported in Part III [Kisilevsky et al., 2003]). QS431 is now being assessed for anti-amyloid properties in culture and in vivo. QS610 and a related compound, QS611—glucosamine analogs with substituent modifications at C-6—both had stimulating properties on HS biosynthesis in hepatocyte cultures (exemplified by QS610 in Fig. 2B). As with the unexpected results with QS231, although QS610 and QS611 stimulate HS biosynthesis, they might be responsible for HS having a structure that will not support AA amyloidogenesis. These compounds are therefore being assessed for their effects on AA amyloidogenesis in culture and in vivo.

To date, the chemical design and synthetic procedures adopted are producing a range of desired compounds in good yield. Modifications in D-glucosamine have been made at the 2-N, C-3, C-4, C-6, or C-3 and C-4 positions. The most interesting results have emerged with modifications at the 2-N, C-4, or C-6 positions. Our in vivo results to date indicate that modification of HS structure might inhibit or enhance amyloid deposition and add further weight to our hypothesis that HS plays a major role in amyloidogenesis. Furthermore, the feasibility of preparing compounds and having the desired results in vitro and in vivo, in good yield by relatively inexpensive synthetic pathways, has been demonstrated. Several compounds that we have designed and synthesized, both in the past and present, are ones that have proven to alter amyloid deposition in vivo. As such, they represent promising lead candidates for the development of Alzheimer's disease therapeutics.

## Acknowledgments

This work was supported by grants from the Institute for the Study of Aging (R. K. and W. A. S.) and the Canadian Institutes of Health Research, grant MOP-3153 (R. K.). We also express our sincerest appreciation to Mrs. Ruth Tan and Mr. Lee Boudreau for their able assistance with various aspects of this project.

## References

- Berkin A., Szarek W. A., Plenkiewicz J., Szarek W. A., and Kisilevsky R. (2000a) Synthesis of 4-deoxy analogues of 2-acetamido-2-deoxy-D-glucose and 2-acetamido-2-deoxy-D-xylose and their effects on glycoconjugate biosynthesis. *Carbohydr. Res.* 325, 30–45.
- Berkin A., Szarek W. A., and Kisilevsky R. (2000b) Synthesis of 4-deoxy-4-fluoro analogues of 2-acetamido-2-deoxy-D-glucose and 2-acetamido-2-deoxy-D-galactose and their effects on cellular glycosaminoglycan biosynthesis. *Carbohydr. Res.* 326, 250–263.
- Castillo G. M., Cummings J. A., Yang W. H., Judge M. E., Sheardown M. J., Rimvall K., et al. (1998) Sulfate content and specific glycosaminoglycan backbone of perlecan are critical for perlecan's enhancement of islet amyloid polypeptide (amylin) fibril formation. *Diabetes* 47, 612–620.
- Kisilevsky R. and Fraser P. E. (1997) A $\beta$  amyloidogenesis: unique or variation on a systemic theme? *Crit. Rev. Biochem. Mol. Biol.* 32, 361–404.
- Kisilevsky R. and Szarek W. A. (2002a) Novel glycosaminoglycan precursors as anti-amyloid agents, in *Drug Discovery and Development for Alzheimer's Disease 2000*, Fillit, H. M., and O'Connell, A. W., eds., Springer, New York, pp. 98–105.
- Kisilevsky R. and Szarek W. A. (2002b) Novel glycosaminoglycan precursors as anti-amyloid agents. Part II. *J. Mol. Neurosci.* 19, 45–50.
- Kisilevsky R., Lemieux L. J., Fraser P. E., Kong X. Q., Hultin P. G., and Szarek W. A. (1995) Arresting amyloidosis in vivo using small-molecule anionic sulphonates or sulphates: implications for Alzheimer's disease. *Nature Med.* 1, 143–148.
- Kisilevsky R., Szarek W. A., Ancsin J., Bhat S., Li Z., and Marone S. (2003) Novel glycosaminoglycan precursors as anti-amyloid agents. Part III. *J. Mol. Neurosci.* 20, 291–297.
- Kluve-Beckerman B., Liepnieks J. J., Wang L. S., and Benson M. D. (1999) A cell culture system for the study of amyloid pathogenesis—amyloid formation by peritoneal macrophages cultured with recombinant serum amyloid A. *Am. J. Pathol.* 155, 123–133.
- Lindahl B. and Lindahl U. (1997) Amyloid-specific heparan sulfate from human liver and spleen. *J. Biol. Chem.* 272, 26091–26094.
- Lindahl B., Eriksson L., and Lindahl U. (1995) Structure of heparan sulphate from human brain, with special regard to Alzheimer's disease. *Biochem. J.* 306, 177–184.
- Lindahl B., Eriksson L., Spillmann D., Caterson B., and Lindahl U. (1996) Selective loss of cerebral keratan sulfate in Alzheimer's disease. *J. Biol. Chem.* 271, 16991–16994.
- Lindahl U., Kushke M., Lindholt K., and Oscarsson L. G. (1989) Biosynthesis of heparin and heparan sulfate. *Ann. New York Acad. Sci.* 556, 36–50.
- Lindahl B., Westling C., Gimenez-Gallego G., Lindahl U., and Salmivirta, M. (1999) Common binding sites for  $\beta$ -amyloid fibrils and fibroblast growth factor-2 in heparan sulfate from human cerebral cortex. *J. Biol. Chem.* 274, 30631–30635.
- McCubbin W. D., Kay C. M., Narindrasorasak S., and Kisilevsky R. (1988) Circular dichroism and fluorescence

- studies on two murine serum amyloid A proteins. *Biochem. J.* 256, 775-783.
- McLaurin J., Franklin T., Kuhns W. J., and Fraser P. E. (1999a) A sulfated proteoglycan aggregation factor mediates amyloid- $\beta$  peptide fibril formation and neurotoxicity. *Amyloid* 6, 233-243.
- McLaurin J., Franklin T., Zhang X. Q., Deng J. P., and Fraser P. E. (1999b) Interactions of Alzheimer amyloid- $\beta$  peptides with glycosaminoglycans—effects on fibril nucleation and growth. *Eur. J. Biochem.* 266, 1101-1110.
- Subrahmanyam L. and Kisilevsky R. (1988) Effects of culture substrates and normal hepatic sinusoidal cells on in-vitro hepatocyte synthesis of apo-SAA. *Scand. J. Immunol.* 27, 251-260.
- Thomas S. S., Plenkiewicz J., Ison E. R., Bols M., Zou W., Szarek W. A., and Kisilevsky R. (1995) Influence of monosaccharide derivatives on liver cell glycosaminoglycan synthesis: 3-deoxy-D-xylo-hexose (3-deoxy-D-galactose) and methyl (methyl 4-chloro-4-deoxy- $\beta$ -D-galactopyranosid)uronate. *Biochim. Biophys. Acta* 1272, 37-48.
- Westermarck P. (1997) Classification of amyloid fibril proteins and their precursors: an ongoing discussion. *Amyloid* 4, 216-218.

*Journal of Molecular Neuroscience*  
Copyright © 2003 Humana Press Inc.  
All rights of any nature whatsoever reserved.  
ISSN0895-8696/03/20:291-297/\$25.00

## ALZHEIMER'S THERAPEUTICS: Anti-Amyloid

# Novel Glycosaminoglycan Precursors as Anti-Amyloid Agents, Part III<sup>†</sup>

**Robert Kisilevsky,<sup>\*1,2</sup> Walter A. Szarek,<sup>3</sup> John Ancsin,<sup>1,2</sup> Shridhar Bhat,<sup>3</sup>  
Zhanjiang Li,<sup>3</sup> and Sandra Marone<sup>3</sup>**

Departments of <sup>1</sup>Pathology and Chemistry Queen's University, and <sup>2</sup>The Syl and Molly Apps  
Research Center Kingston General Hospital, Kingston, Ontario K7L 3N6 Canada

Received October 15, 2002; Accepted March 24, 2003

### Abstract

In vivo amyloids consist of two classes of constituents. The first is the disease-defining protein, e.g., amyloid  $\beta$  (A $\beta$ ) in Alzheimer's disease (AD). The second is a set of common structural components that usually are the building blocks of basement membrane (BM), a tissue structure that serves as a scaffold onto which cells normally adhere. In vitro binding interactions between one of these BM components and amyloidogenic proteins rapidly change the conformation of the amyloidogenic protein into amyloid fibrils. The offending BM component is a heparan sulfate (HS) proteoglycan (HSPG), part of which is protein, and the remainder is a specific linear polysaccharide that is the portion responsible for binding and imparting the typical amyloid structure to the amyloid precursor protein/peptide. Our past work has demonstrated that agents that inhibit the binding between HS and the amyloid precursor are effective anti-amyloid compounds both in vitro and in vivo. Similarly, 4-deoxy analogs of glucosamine (a precursor of HS biosynthesis) are effective anti-amyloid compounds both in culture and in vivo. Our continuing work concerns (1) the testing of our 4-deoxy compounds in a mouse transgenic model of AD, and (2) the continuing design and synthesis of modified sugar precursors of HS, which when incorporated into the polysaccharide will alter its structure so that it loses its amyloid-inducing properties. Since our previous report, 14 additional compounds have been designed and synthesized based on the known steps involved in HS biosynthesis. Of these, eight have been assessed for their effect on HS biosynthesis in hepatocyte tissue cultures, and the two anomers of a 4-deoxy-D-glucosamine analog have been assessed for their inflammation-associated amyloid (AA amyloid) inhibitory properties in vivo. The promising in vivo results with these two compounds have prompted studies using a murine transgenic model of brain A $\beta$  amyloidogenesis. A macrophage tissue-culture model of AA amyloidogenesis has been devised based on the work of Kluve-Beckerman et al. and modified so as to assess compounds in the absence of potential in vivo confounding variables. Preliminary results indicate that the anomers of interest also inhibit AA amyloid deposition in macrophage tissue culture. Finally, an in vitro technique, using liver Golgi (the site of HS synthesis) rather than whole cells, has been devised to directly assess the effect of analogs on HS biosynthesis. The majority of the novel sugars prepared to date are analogs of N-acetylglucosamine. They have been modified either at the 2-N, C-3, C-4, or C-3 and C-4 positions. Results with the majority of the 2-N analogs suggest that hepatocyte N-demethylases remove the N-substituent removal. Several of these have the desired effect on HS biosynthesis using hepatocyte cultures and will be assessed in the culture and in vivo AA amyloid models. To date 3-deoxy and 3,4-dideoxy analogs have failed to affect HS synthesis significantly. Compounds incorporating the 6-deoxy structural feature are currently being designed and synthesized.

**Index Entries:** A $\beta$ ; binding; glycosaminoglycans (GAGs); glucosamine analogs; heparan sulfate; SAA.

<sup>\*</sup>Author to whom all correspondence and reprint requests should be addressed. E-mail: kisilevsky@cliff.path.queensu.ca

<sup>†</sup>For Part I, see Kisilevsky and Szarek (2002a). For Part II, see Kisilevsky and Szarek (2002b).

## Introduction

### *Nature of Amyloid*

Amyloid is the term for extracellular fibrillar protein deposits that have a specific set of staining and structural characteristics. Amyloid deposits are involved in the pathogenesis of disorders such as Alzheimer's disease (AD), adult onset diabetes, joint destruction during prolonged hemodialysis, and several other rarer disorders. Although amyloids all look and stain the same in tissues, >20 different protein types have been identified (Westermarck, 1997). In vivo, each amyloid is composed of two classes of components (Kisilevsky and Fraser, 1997). The first is the defining protein; the second is a set of common structural constituents. These include serum amyloid P; proteoglycans, usually perlecan (the basement membrane form of heparan sulfate [HS] proteoglycan [HSPG]), laminin, collagen IV, and apolipoprotein E. Substantial evidence indicates that interactions between the common components and the amyloidogenic protein play a role in amyloidogenesis (Kisilevsky and Fraser, 1997). Of particular importance are the glycosaminoglycans (GAGs) HS and/or heparin. In the cases of amyloid associated with inflammatory diseases (AA amyloid) and AD (A $\beta$ ), such amyloid-associated GAGs have been shown to have subtle changes in structure (Lindahl et al., 1995, 1996, 1997, 1999); and when interacting with their respective amyloidogenic proteins, have the ability to alter their conformations so that they take on the structural characteristics typical of an amyloid (McCubbin et al., 1988; Kisilevsky and Fraser, 1997; Castillo et al., 1998; McLaurin et al., 1999a, 1999b).

### *Amyloidogenic Protein and Heparin/HS: Complementary Binding Domains*

The structural features of the HS binding domain of serum amyloid A (SAA) and A $\beta$  have been illustrated in our previous reports, Parts I and II (Kisilevsky and Szarek, 2002a, 2002b).

### **Rationale**

The rationale for the synthesis of novel GAG sugar precursors follows from the structure of heparin/HS, and the biosynthetic steps that are responsible for their production (Lindahl et al., 1989). Altering the structure at the 4 position of either the glucosamine or the uronate residues would interfere with the growth of the GAG chain, as this position is necessary for the  $\alpha$ -(1  $\rightarrow$  4) linkages in the polysaccha-

ride. Alternatively, altering the structure at the 2 position of the uronate, or of the amino group of the glucosamine residue, would likely change the manner in which the growing polysaccharide chain is sulfated. In addition, because N-sulfonation is a required step in the proper epimerization and sulfation of the uronate, modification of glucosamine precursors at the amino group may result in modified or undersulfated HS and therefore, one that will probably not interact with amyloidogenic proteins/peptides.

## Materials and Methods

### *Chemical Syntheses*

Since the commencement of our project, 34 novel sugars have been designed and synthesized (Table 1). Compounds 1–20 (other than 17B) were disclosed in our previous report. In our last report, only one of the two anomeric forms of compound 17 had been synthesized and tested. New synthetic strategies have since been devised that allowed the preparation of both anomers (17A and 17B). Following favorable results from our in vitro testing in hepatic culture, a considerable effort was placed on developing methodologies for the preparation of the larger quantities of 17A required for its in vivo testing as an anti-A $\beta$  compound in a mouse transgenic model of AD. In addition, a further 13 novel sugars have been prepared (Table 1). Of these 13 compounds, 21–27 have been assessed in hepatocyte cultures for their effects on HS biosynthesis. The remaining 6 compounds, 28–33, proved to be insoluble in culture media.

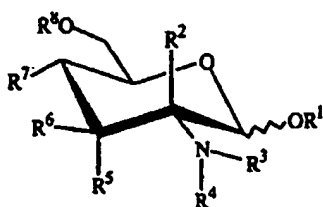
### *GAG Synthesis*

Mouse hepatocytes were isolated and placed in culture as described previously (Subrahmanyam and Kisilevsky, 1988; Thomas et al., 1995; Berkin et al., 2000a, 2000b). These were cultured for 24 h in the absence or presence of varying concentrations of the novel sugar analogs. [ $^3$ H]Glucosamine and [ $^{35}$ S]SO $_4$  were used to monitor the synthesis and sulfation of the newly made HS, as described previously (Subrahmanyam and Kisilevsky, 1988; Thomas et al., 1995; Berkin et al., 2000a, 2000b).

### *Macrophage Tissue Culture Induction of AA Amyloid*

AA amyloid was induced in J774 mouse macrophage tissue cultures using a modification of the method described previously (Kluve-Beckerman et al., 1999). Briefly J774 was grown to 75–80% conflu-

Table 1  
Structures of Glucosamine Analogs



| Compound | R <sup>1</sup> | R <sup>2</sup> | R <sup>3</sup> | R <sup>4</sup>   | R <sup>5</sup> | R <sup>6</sup>      | R <sup>7</sup>     | R <sup>8</sup>     |
|----------|----------------|----------------|----------------|--|----------------|---------------------|--------------------|--------------------|
| 1*       | H              | H              | H              | Me   | H              | OH                  | OH                 | H                  |
| 2*       | Ac             | H              | Ac             | Me   | H              | OAc                 | OAc                | Ac                 |
| 3*       | H              | H              | Me             | Me   | H              | OH                  | OH                 | H                  |
| 4*       | H              | H              | H              | <i>iso</i> -Pr   | H              | OH                  | OH                 | H                  |
| 5*       | H              | H              | H              | <i>p</i> -OMeBn  | H              | OH                  | OH                 | H                  |
| 6*       | H              | H              | H              | Ac   | H              | OSO <sub>3</sub> H  | OH                 | H                  |
| 7*       | Bn(α)          | H              | H              | Ac   | H              | OSO <sub>3</sub> H  | OH                 | H                  |
| 8*       | Bn(α)          | H              | H              | Ac   | H              | OSO <sub>2</sub> Me | OH                 | H                  |
| 9*       | Bn(α)          | H              | H              | Ac   | H              | OSO <sub>3</sub> H  | OSO <sub>3</sub> H | SO <sub>3</sub> H  |
| 10*      | H              | H              | H              | C(O)CF <sub>3</sub>  | H              | OH                  | OH                 | H                  |
| 11*      | H              | H              | H              | C(O) <i>tert</i> -Bu   | H              | OH                  | OH                 | H                  |
| 12*      | H              | H              | H              | Ac   | H              | H                   | OH                 | H                  |
| 13*      | Bn(α)          | H              | H              | Ac   | H              | H                   | OH                 | H                  |
| 14*      | H              | H              | H              | Ac   | F              | H                   | OH                 | H                  |
| 15*      | Bn(α)          | H              | H              | Ac   | F              | H                   | OH                 | H                  |
| 16*      | H              | H              | H              | Ac   | H              | OH                  | H                  | H                  |
| 17A*     | Ac(α)          | H              | H              | Ac   | H              | OAc                 | H                  | Ac                 |
| 17B      | Ac(β)          | H              | H              | Ac   | H              | OAc                 | H                  | Ac                 |
| 18*      | H              | H              | H              | Ac   | H              | H                   | H                  | H                  |
| 19*      | Bn(α)          | H              | H              | Ac   | H              | H                   | H                  | H                  |
| 20*      | Me(α)          | H              | H              | Ac   | H              | H                   | H                  | H                  |
| 21       | H              | H              |                | -CF <sub>2</sub> (CF <sub>2</sub> ) <sub>2</sub> CF <sub>2</sub> - | H              | OH                  | OH                 | H                  |
| 22       | H              | H              | H              | C(O)-(2-thienyl)   | H              | OH                  | OH                 | H                  |
| 23       | H              | H              | H              | SO <sub>2</sub> -Ph( <i>p</i> -Me)                                 | H              | OH                  | OH                 | H                  |
| 24       | H              | H              | H              | SO <sub>2</sub> Me   | H              | OH                  | OH                 | H                  |
| 25       | H              | H              | H              | SO <sub>2</sub> Et   | H              | OH                  | OH                 | H                  |
| 26       | H              | H              | H              | CO <sub>2</sub> <i>tert</i> -Bu                                    | H              | OH                  | OH                 | H                  |
| 27       | Me(α)          | H              | H              | Ac   | H              | OAc                 | H                  | H                  |
| 28**     | H              | H              |                | =CH-Ph( <i>p</i> -OMe)   | H              | OH                  | OH                 | H                  |
| 29**     | Ac(α)          | H              | H              | SO <sub>2</sub> Me   | H              | OAc                 | OAc                | Ac                 |
| 30**     | H              | H              | H              | CO <sub>2</sub> Bn   | H              | OH                  | OH                 | H                  |
| 31**     | Bn(α)          | H              | H              | Ac   | H              | OH                  | OH                 | C(Ph) <sub>3</sub> |
| 32**     | Bn(α)          | H              | H              | Ac   | H              | OSO <sub>3</sub> H  | OSO <sub>3</sub> H | H                  |
| 33***†   |                |                |                |  |                |                     |                    |                    |

\*Disclosed in previous reports (Kisilevsky and Szarek, 2002a and 2002b).

\*\*Did not dissolve in biological medium.

†Benzyl 2-acetamido-4,6-O-benzylidene-2,3-dideoxy-α-D-erythro-hex-2-enopyranoside.

Table 2  
Percent AA Amyloid per Unit Area of Tissue in Mice Treated Either with Compound 17A or 17B  
Normalized to the Untreated Controls<sup>a</sup>

| Compound  | Group    | Liver | Spleen | Spleen Wt.<br>(mg) | Spleen<br>corrected |
|-----------|----------|-------|--------|--------------------|---------------------|
| 17A/Exp 1 | Control  | 100   | 100    | 184                | 100                 |
|           | 6 mg/bid | 16.7  | 46.2   | 117                | 29.4                |
| 17A/Exp 2 | Control  | 100   | 100    | 177                | 100                 |
|           | 3 mg/bid | 121   | 106    | 136                | 81.4                |
|           | 6 mg/bid | 35.7  | 35.7   | 123                | 24.8                |
| 17B       | Control  | 100   | 100    | 192                | 100                 |
|           | 3 mg/bid | 83.8  | 66.4   | 148                | 51.2                |
|           | 6 mg/bid | 70.3  | 57.6   | 111                | 33.3                |

<sup>a</sup>The results in each experiment are the mean of five animals per group expressed as a percent of the untreated amyloid group. The spleen weights are expressed in mg. The five Corrected Spleen Amyloid accounts for the changes in spleen weight relative to the Controls (bold), which occur because of the treatment with compound 17A or 17B. Normal spleen weights in mice 6–8 wk of age are ~80 mg.

ence in RPMI medium for 24 h, after which the medium was changed to include 20  $\mu$ g amyloid-enhancing factor (AEF). After an additional 24 h, the medium was changed to include high-density lipoprotein (HDL)/SAA (the AA amyloid precursor)  $\pm$  the compound of interest in appropriate concentrations. Cultures were maintained in this manner for 6 d, after which they were fixed and stained with Congo red.

### In Vivo Amyloid Induction

AA amyloid was induced in 6- to 8-wk-old CD1 mice with AEF and AgNO<sub>3</sub> as an inflammatory stimulus, as described previously (Kisilevsky et al., 1995). Twenty-four hours after induction, groups of 5 animals were treated either with 17A or 17B at 3 or 6 mg/dose administered iv every 12 h and sacrificed by CO<sub>2</sub> narcosis 5 d after the commencement of therapy. The quantity of amyloid/unit area of tissue (spleen and liver) was determined by image analysis, as described previously (Kisilevsky et al., 1995). Splenic amyloid was corrected for the change in spleen weight as indicated in Table 2.

### Results

The effects of different concentrations of compounds 21–27 on [<sup>3</sup>H]glucosamine and [<sup>35</sup>S]SO<sub>4</sub> incorporation into hepatocyte HS are illustrated in Figures 1–7, respectively. Note that although not as effective as 17A and 17B, compound 24, which has

a 2-N-substituent that is not likely to be removed by liver demethylases, does have HS biosynthesis inhibitory properties.

The effect of the anomeric forms of compound 17 on AA amyloid deposition in vivo is illustrated in Table 2. Preliminary observations of the effect of 17B in the tissue-culture model of AA amyloid were extremely encouraging. Compound 17B inhibited amyloid deposition by 95% or more.

### Discussion

To date, the chemical design and synthetic procedures adopted are producing a range of desired compounds in good yield. Modifications in D-glucosamine have been made at the 2-amino group and at the C-3, C-4, C-6, and C-3 and C-4 positions.

As exemplified previously with compounds 1, 2, and 3, N-alkyl group substitutions in glucosamine provide data that can best be explained by the enzymatic N-dealkylation of the synthesized compounds. The net result is the generation of unlabeled glucosamine, which dilutes the labeled glucosamine pool, a feature appearing as a spurious inhibition of GAG synthesis. Strategic substituent modifications at the 2-amino position have been introduced to obviate removal of the N-substituent. Compound 24, possessing an N-sulfonamido substituent that cannot be removed by the liver N-dealkylases, is effective in inhibiting HS biosynthesis at concentrations advocating that it should be evaluated in vivo.



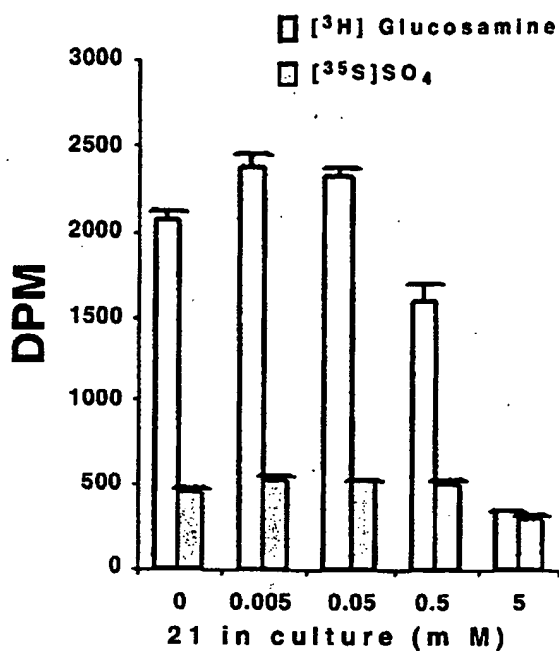


Fig. 1.

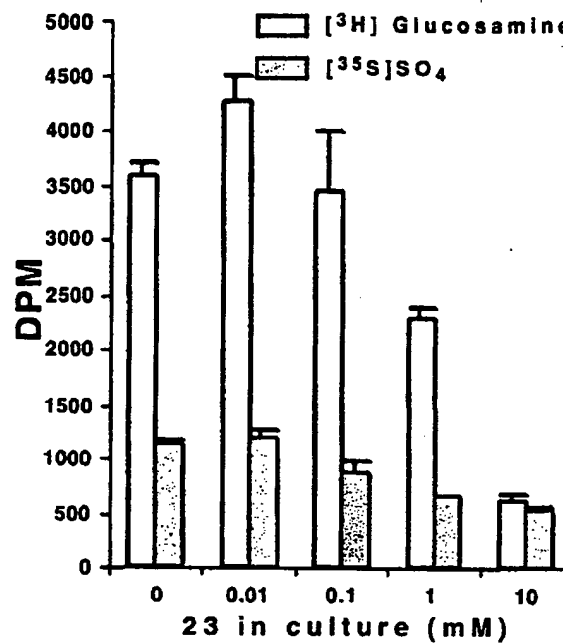


Fig. 3.

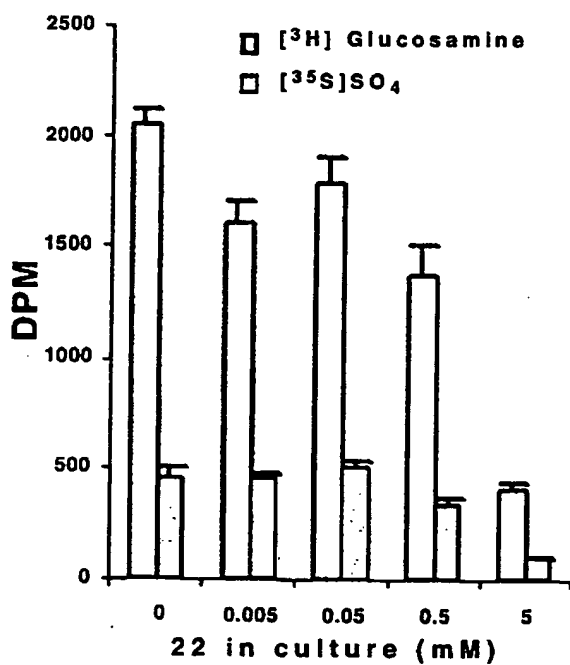


Fig. 2.

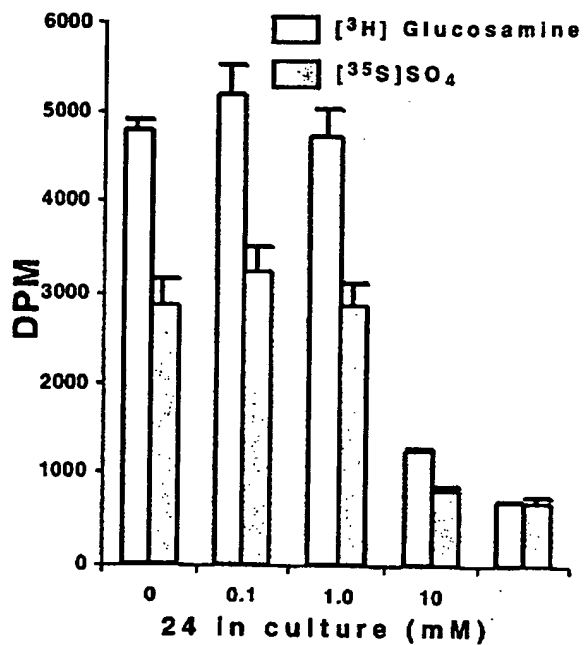


Fig. 4.

296

Kisilevsky et al.

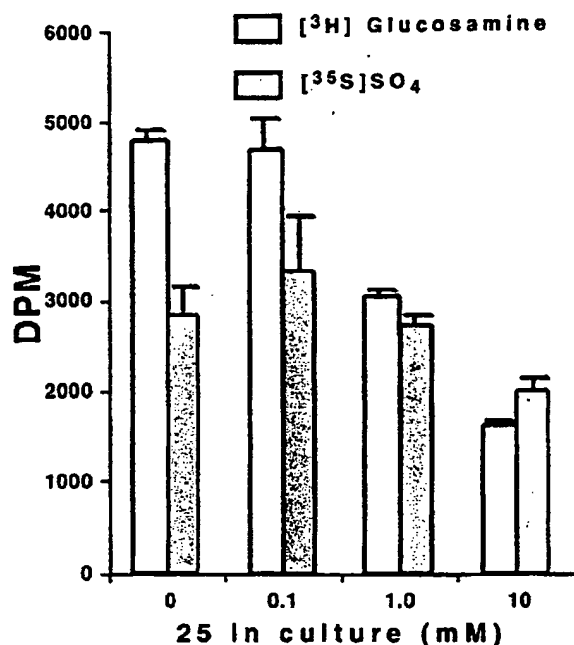


Fig. 5.

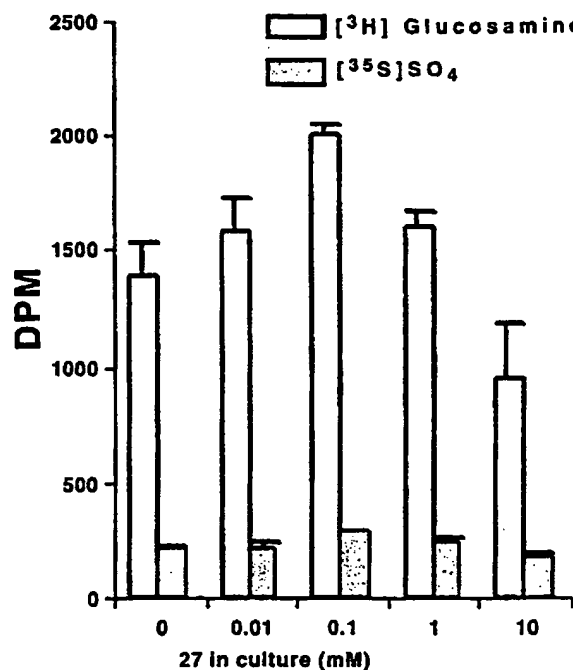


Fig. 7.

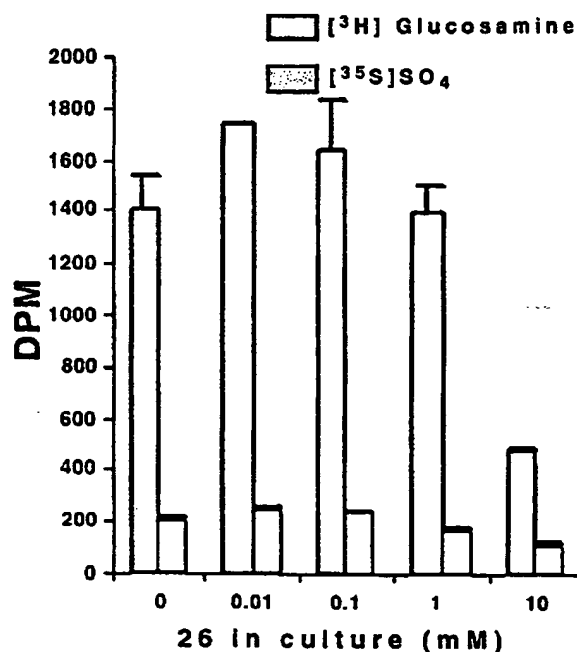


Fig. 6.

As shown in our previous position papers (Kisilevsky and Szarek, 2002a and 2002b), the effect of compound 17 (mixed anomers) on the biosyn-

thesis of liver HS can best be interpreted as truncating elongation of the growing GAG chain; the  $\alpha$ -anomer 17A was effective in substantially reducing the quantity of spleen and liver AA amyloid in an in vivo model of mouse AA amyloid induction. In such a model we have now shown that both 17A and the  $\beta$ -anomer 17B can, over a 5-d period, significantly reduce the quantity of AA amyloid accumulating in both the livers and spleens. Furthermore, preliminary results indicate that 17B at a concentration of 0.1 mM can virtually eliminate AA amyloid deposition in tissue culture, negating the possibility that these compounds act by reducing the concentration of SAA in vivo. These results add further weight to our hypothesis that HS plays a major role in amyloidogenesis. Inhibition of HS elongation by 17A or 17B identifies a strategy, and lead compounds, for the inhibition of amyloidogenesis. Large-scale syntheses have been developed in preparation for their assessment as inhibitors of A $\beta$  deposition in a mouse transgenic model of AD.

Our results to date have identified several compounds (17A, 17B, and 24) that have the desired effects in hepatocyte cultures. Compounds 17A and 17B truncate HS chain elongation, do not affect protein synthesis, and do inhibit AA amyloidogenesis in tissue culture and in vivo in both liver and spleen

(Table 2). Also, the feasibility of preparing compounds, having the desired results in vitro and in vivo, in good yield by relatively inexpensive synthetic pathways, has been demonstrated. The compounds that we have designed and synthesized both in the past and present are indeed compounds that have proven to be anti-amyloid active compounds in vivo. As such, they represent promising lead candidates for the development of AD therapeutics.

## Acknowledgments

This work was supported by grants from the Institute for the Study of Aging (R.K. and W.A.S.), the Canadian Institutes of Health Research, grant MOP-3153 (R.K.), and the Royal College of Physicians and Surgeons of Canada, Detweiler Traveling Fellowship (R.K.). We also express our sincerest appreciation to Mrs. Ruth Tan and Mr. Lee Boudreau for their able assistance with various aspects of this project.

## References

- Berkin A., Szarek M. A., Plenkiewicz J., Szarek W. A., and Kisilevsky R. (2000a) Synthesis of 4-deoxy analogues of 2-acetamido-2-deoxy-D-glucose and 2-acetamido-2-deoxy-D-xylose and their effects on glycoconjugate biosynthesis. *Carbohydr. Res.* 325, 30–45.
- Berkin A., Szarek W. A., and Kisilevsky R. (2000b) Synthesis of 4-deoxy-4-fluoro analogues of 2-acetamido-2-deoxy-D-glucose and 2-acetamido-2-deoxy-D-galactose and their effects on cellular glycosaminoglycan biosynthesis. *Carbohydr. Res.* 326, 250–263.
- Castillo G. M., Cummings J. A., Yang W. H., Judge M. E., Sheardown M. E., Sheardown M. J., Rimvall K., et al. (1998) Sulfate content and specific glycosaminoglycan backbone of perlecan are critical for perlecan's enhancement of islet amyloid polypeptide (amylin) fibril formation. *Diabetes* 47, 612–620.
- Kisilevsky R. and Fraser P. E. (1997) A $\beta$  amyloidogenesis: unique or variation on a systemic theme? *Crit. Rev. Biochem. Mol. Biol.* 32, 361–404.
- Kisilevsky R., Lemieux L. J., Fraser P. E., Kong X.-Q., Hultin P. G., and Szarek W. A. (1995) Arresting amyloidosis in vivo using small-molecular anionic sulphonates or sulphates: implications for Alzheimer's disease. *Nat. Med.* 1, 143–148.
- Kisilevsky R. and Szarek W. A. (2002a) Novel glycosaminoglycan precursors as anti-amyloid agents, in *Drug Discovery and Development for Alzheimer's Disease* 2000, Fillit H. M. and O'Connell A. W., eds., Springer, New York, pp. 98–105.
- Kisilevsky R. and Szarek W. A. (2002b) Novel glycosaminoglycan precursors as anti-amyloid agents, Part II. *J. Mol. Neurosci.* 19, 45–50.
- Kluve-Beckerman B., Liepnieks J. J., Wang L. S., and Benson M. D. (1999) A cell culture system for the study of amyloid pathogenesis—amyloid formation by peritoneal macrophages cultures with recombinant serum amyloid A. *Am. J. Pathol.* 155, 123–133.
- Lindhahl B., Eriksson L., and Lindahl U. (1995) Structure of heparan sulphate from human brain, with special regard to Alzheimer's disease. *Biochem. J.* 306, 177–184.
- Lindhahl B., Eriksson L., Spillman D., Caterson B., and Lindahl U. (1996) Selective loss of cerebral keratan sulfate in Alzheimer's disease. *Biochem. J.* 306, 177–184.
- Lindhahl B. and Lindahl U. (1997) Amyloid-specific heparan sulfate from human liver and spleen. *J. Biol. Chem.* 272, 26,091–26,094.
- Lindhahl B., Westling C., Gimenez-Gallego G., Lindahl U., and Salmivirta M. (1999) Common binding sites for  $\beta$ -amyloid fibrils and fibroblast growth factor-2 in heparan sulfate from human cerebral cortex. *J. Biol. Chem.* 274, 30,631–30,635.
- Lindhahl U., Kushke M., Lindholt K., and Oscarsson L. G. (1989) Biosynthesis of heparin and heparan sulfate. *Ann. N. Y. Acad. Sci.* 556, 36–50.
- McCubbin W. D., Kay C. M., Narindrasorasak S., and Kisilevsky R. (1988) Circular dichroism and fluorescence studies on two murine serum amyloid A proteins. *Biochem. J.* 256, 775–783.
- McLaurin J., Franklin T., Kuhns W. J., and Fraser P. E. (1999a) A sulfated proteoglycan aggregation factor mediates amyloid- $\beta$  peptide fibril formation and neurotoxicity. *Amyloid* 6, 233–243.
- McLaurin J., Franklin T., Zhang X. Q., Deng J. P., and Fraser P. E. (1999b) Interactions of Alzheimer amyloid- $\beta$  peptides with glycosaminoglycans—effects on fibril nucleation and growth. *Eur. J. Biochem.* 266, 1101–1110.
- Subrahmanyam L. and Kisilevsky R. (1988) Effects of culture substrates and normal hepatic sinusoidal cells on in-vitro hepatocyte synthesis of apo-SAA. *Scand. J. Immunol.* 27, 251–260.
- Thomas S. S., Plenkiewicz J., Ison E. R., Bols M., Zou W., Szarek W. A., and Kisilevsky R. (1995) Influence of monosaccharide derivatives on liver cell glycosaminoglycan synthesis: 3-deoxy-D-xylo-hexose (2-deoxy-D-galactose) and methyl (methyl 4-chloro-4-deoxy- $\beta$ -D-galactopyranosid)uronate. *Biochim. Biophys. Acta* 1272, 37–48.
- Westermarck P. (1997) Classification of amyloid fibril proteins and their precursors: an ongoing discussion. *Amyloid* 4, 216–218.

Volume 19 Nos. 1-2 August-October 2002 ISSN: 0895-8696

# Journal of **MOLECULAR NEUROSCIENCE**

ILLANA GOZLIS, Editor-in-Chief

## Drug Discovery in Alzheimer's Disease

*Special Double Issue*

*Guest Editors:*

Howard M. Fillit, MD

Alan W. O'Connell, PhD

Lorenzo M. Refolo, PhD

**ISOA**  
INSTITUTE FOR THE STUDY OF AGING

Univ. of Minn.  
Bio-Medical  
Library



Humana Press

[humanapress.com](http://humanapress.com)

*Journal of Molecular Neuroscience*  
 Copyright © 2002 Humana Press Inc.  
 All rights of any nature whatsoever reserved.  
 ISSN 0895-8696/02/19-45-50/\$11.50

? NOTICE: THIS MATERIAL MAY BE PROTECTED  
 BY COPYRIGHT LAW (TITLE 17 U.S. CODE)

## Novel Glycosaminoglycan Precursors as Anti-Amyloid Agents Part II<sup>†</sup>

Robert Kisilevsky<sup>\*1,2</sup> and Walter A. Szarek<sup>3</sup>

Departments of <sup>1</sup>Pathology and <sup>3</sup>Chemistry, Queen's University; and <sup>2</sup>The Syl and Molly Apps  
 Research Center, Kingston General Hospital, Kingston, Ontario K7L 3N6 Canada

Received September 20, 2001; Accepted October 16, 2001

### Abstract

In vivo amyloids consist of two classes of constituents. The first is the disease defining protein, e.g., A $\beta$  in Alzheimer's disease. The second is a set of common structural components that usually are the building blocks of basement membrane (BM), a tissue structure that serves as a scaffold onto which cells normally adhere. In vitro binding interactions between one of these BM components and amyloidogenic proteins rapidly change the conformation of the amyloidogenic protein into amyloid fibrils. The offending BM component is a heparan sulfate (HS) proteoglycan (HSPG), part of which is protein and the remainder a specific linear polysaccharide, which is the portion responsible for binding, and imparting the typical amyloid structure, to the amyloid precursor protein/peptide. Our past work has demonstrated that agents that inhibit the binding between HS and the amyloid precursor are effective anti-amyloid compounds both in vitro and in vivo. The present work is concerned with the design and synthesis of modified sugar precursors of HS, which, when incorporated into the polysaccharide, will alter its structure so that it loses its amyloid precursor protein/peptide-binding and fibril-inducing properties.

As part of our continuing study, since our previous report, 17 additional compounds have been designed and synthesized based primarily on the known steps involved in HS biosynthesis. In addition to the 4 reported last year, 10 more have been assessed in tissue culture for their inhibitory effect on heparan sulfate synthesis, and one of these has been assessed for its AA-amyloid inhibitory properties.

The majority of the novel sugars are analogues of N-acetylglucosamine. They have been modified either at the 4-OH, 3-OH, or 2-N positions. The majority of the 2-N analogues provide data suggesting that hepatocyte N-demethylases remove the N-substituents converting the 2-N analogues into the natural sugar, a process that dilutes the D-[<sup>3</sup>H] glucosamine tracer used to track heparan sulfate synthesis and thereby gives the impression that biosynthetic inhibition is occurring. To date 3-deoxy analogues have failed to affect heparan sulfate synthesis significantly. Compounds incorporating the 3,4-dideoxy structural feature are currently being assessed.

Using primary hepatocyte cultures, we reported previously that a 4-deoxy analogue is incorporated into HS and terminates its elongation. From the 4-deoxy series, one of the compounds has now been assessed in an in vivo model of AA-amyloid induction. This 4-deoxy analogue inhibited splenic AA amyloid deposition by at least 50%, and liver AA amyloid deposition by 85% when measured as amyloid/unit area of tissue. Furthermore, the spleen weights of the treated group were 1/2–1/3 of that in the untreated group indicating that the total splenic amyloid was 1/4–1/6 of that in the untreated group. The results provide further evidence that heparan sulfate is a critical factor in amyloidogenesis and modifications of sugar precursors of heparan sulfate synthesis may provide leads for therapeutic intervention in amyloidogenesis.

**Index Entries:** Glycosaminoglycan; heparan sulfate; glucosamine analogues; AA amyloidogenesis.

<sup>\*</sup>Author to whom all correspondence and reprint requests should be addressed. E-mail: kisilevsky@cliff.path.queensu.ca

<sup>†</sup>For Part I, see Kisilevsky R. and Szarek W. A. (2002), in *Drug Discovery and Development for Alzheimer's Disease* 2000, Pillit H. M. and O'Connell A. W., eds., Springer, New York, NY, pp. 98–105.

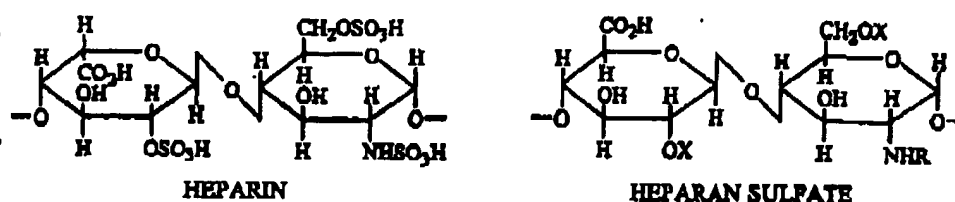


Fig. 1. Structural features of heparan sulfate/heparin.

## Introduction

### Nature of Amyloid

Amyloid is a term for extracellular fibrillar protein deposits that have a specific set of staining and structural characteristics. Amyloid deposits are involved in the pathogenesis of disorders such as Alzheimer's disease, adult onset diabetes, joint destruction during prolonged hemodialysis, and several other rarer disorders. Although, in tissues, amyloids all look and stain the same, over 20 different protein types have been identified (Westermarck, 1997). In vivo each amyloid is composed of two classes of components (Kisilevsky and Fraser, 1997). The first is the defining protein. The second is a set of common structural constituents. These include serum amyloid P, proteoglycans usually perlecan (the basement membrane form of heparan sulfate [HS] proteoglycan [HSPG]), laminin, collagen IV, and apolipoprotein E. A significant body of evidence has accumulated indicating that interactions between the common components on the one hand, and the amyloidogenic protein on the other, play a role in amyloidogenesis (Kisilevsky and Fraser, 1997). Of particular importance are the glycosaminoglycans (GAGs) HS and/or heparin. In the cases of amyloid associated with inflammatory diseases (AA amyloid) and Alzheimer's disease (A $\beta$ ), such amyloid-associated GAGs have been shown to have subtle changes in structure (Lindahl et al., 1995, 1996, 1997, 1999), and when interacting with their respective amyloidogenic proteins have the ability to alter their conformations so that they take on the secondary and fibrillar structural characteristics typical of an amyloid (McCubbin et al., 1988; McLaurin et al., 1999a, 1999b; Kisilevsky and Fraser, 1997; Castillo et al., 1998).

### Amyloidogenic Protein and Heparin/Heparan Sulfate: Complementary Binding Domains

The structural features of one HS binding domain of serum amyloid A (SAA) (the precursor to AA amyloid) necessary for HS binding are indicated below.

The critical amino acid residues have been identified (Ancsin and Kisilevsky, 1999), and are shown enlarged.

ADQEANRHGRSGKDPNYYRPPGLPAKY

An analogous domain has been identified in A $\beta$ (1-42) (C. Davidson and R. Kisilevsky, unpublished results) and is shown below.

DAEFRHDSGYEVHHQKLVFFAEDVGSNKGAIICLMVGGVVIA

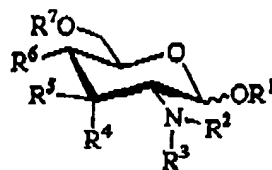
The general structural features of HS and heparin are indicated in Fig. 1. In HS, X may be H or SO<sub>3</sub>H, and R may be H, acetyl, or SO<sub>3</sub>H. Unpublished experimental work (J.B. Ancsin, C. Davidson, and R. Kisilevsky) has shown that the 6-OSO<sub>3</sub>H group on the glucosamine residue of heparin/HS is not necessary for binding to the HS binding domain of SAA. More critical are the 2-OSO<sub>3</sub><sup>-</sup> on the uronate residue, and the N-SO<sub>3</sub><sup>-</sup> of the glucosamine residue, both of which appear to be necessary for binding to SAA and A $\beta$ .

## Rationale

The rationale for the synthesis of novel GAG sugar precursors follows from the structure of heparin/HS, and the biosynthetic steps which are responsible for their production (Lindahl et al., 1989). Altering the structure at the 4-position of either the glucosamine or the uronate residues would interfere with the growth of the glycosaminoglycan chain, since this position is necessary for the  $\alpha$ -(1 $\rightarrow$ 4) linkages in the polysaccharide. Alternatively, altering the structure at the 2-position of the uronate, or of the amino group of the glucosamine residue, would likely change the manner in which the growing polysaccharide chain is sulfated. In addition, because N-sulfonation is a required step in the proper epimerization and sulfation of the uronate, modification of glucosamine precursors at the amino group will likely result in an undersulfated heparan sulfate product, and therefore one that will probably not interact with amyloidogenic proteins/peptides.

## Novel Glycosaminoglycan Precursors

Table 1  
Structures of Glucosamine Analogues



| Compound | R <sup>1</sup> | R <sup>2</sup> | R <sup>3</sup>         | R <sup>4</sup> | R <sup>5</sup>      | R <sup>6</sup>     | R <sup>7</sup>    |
|----------|----------------|----------------|------------------------|----------------|---------------------|--------------------|-------------------|
| 1*       | H              | H              | Me                     | H              | OH                  | OH                 | H                 |
| 2*       | Ac             | Ac             | Me                     | H              | OAc                 | OAc                | Ac                |
| 3*       | H              | Me             | Me                     | H              | OH                  | OH                 | H                 |
| 4        | H              | H              | isoPr                  | H              | OH                  | OH                 | H                 |
| 5        | H              | H              | p-OMeBn                | H              | OH                  | OH                 | H                 |
| 6        | H              | H              | Ac                     | H              | OSO <sub>3</sub> H  | OH                 | H                 |
| 7        | Bn(α)          | H              | Ac                     | H              | OSO <sub>3</sub> H  | OH                 | H                 |
| 8        | Bn(α)          | H              | Ac                     | H              | OSO <sub>3</sub> Me | OH                 | H                 |
| 9        | Bn(α)          | H              | Ac                     | H              | OSO <sub>3</sub> H  | OSO <sub>3</sub> H | SO <sub>3</sub> H |
| 10       | H              | H              | COCF <sub>3</sub>      | H              | OH                  | OH                 | H                 |
| 11       | H              | H              | CO <sub>tert</sub> -Bu | H              | OH                  | OH                 | H                 |
| 12       | H              | H              | Ac                     | H              | H                   | OH                 | H                 |
| 13       | Bn(α)          | H              | Ac                     | H              | H                   | OH                 | H                 |
| 14       | H              | H              | Ac                     | F              | H                   | OH                 | H                 |
| 15       | Bn(α)          | H              | Ac                     | F              | H                   | OH                 | H                 |
| 16       | H              | H              | Ac                     | H              | OH                  | H                  | H                 |
| 17       | Ac(α)          | H              | Ac                     | H              | OAc                 | H                  | Ac                |
| 18       | H              | H              | Ac                     | H              | H                   | H                  | H                 |
| 19       | Bn(α)          | H              | Ac                     | H              | H                   | H                  | H                 |
| 20       | Me(α)          | H              | Ac                     | H              | H                   | H                  | H                 |

\* Disclosed in previous report.

## Materials and Methods

## Chemical Syntheses

Since the commencement of our project 20 novel sugars have been designed and synthesized (Table 1). Compounds 1, 2, and 3 were disclosed in our previous report. At the time of our previous report compound 17 was a mixture of two anomers. A new synthesis has been designed that has afforded exclusively a single anomeric form. Sixteen additional novel sugars have been prepared (Table 1), as has a single anomeric form of 17.

## Glycosaminoglycan Synthesis

Mouse hepatocytes were isolated and placed in culture as described previously (Berkin et al., 2000a, 2000b; Subrahmanyam and Kisilevsky, 1988; Thomas et al., 1995). These were then cultured for 24 h in the absence or presence of varying concentrations of the novel sugar analogues. [<sup>3</sup>H]Glucosamine and [<sup>35</sup>S]SO<sub>4</sub> were used to monitor the synthesis and sulfation of the newly made HS as described previously

(Berkin et al., 2000a, 2000b; Subrahmanyam and Kisilevsky, 1988; Thomas et al., 1995).

## In Vivo AA Amyloid Induction

AA amyloid was induced in 6–8-wk-old CD1 mice with amyloid enhancing factor and AgNO<sub>3</sub>, as an inflammatory stimulus, as described previously (Kisilevsky et al., 1995). Twenty-four hours after induction 5 animals were treated with 17 (single anomer), 6 mg/dose administered intravenously every 12 h, and sacrificed by CO<sub>2</sub> narcosis 5 d after the commencement of therapy. The quantity of amyloid/unit area of tissue (spleen and liver) was determined by image analysis as described previously (Kisilevsky et al., 1995).

## Results

The effects of different concentrations of compounds 1, 2, 3, (6 and 7), (12 and 13), (5 and 11), on [<sup>3</sup>H] glucosamine and [<sup>35</sup>S] SO<sub>4</sub> incorporation into hepatocyte heparan sulfate are illustrated in Figs. 2,

48

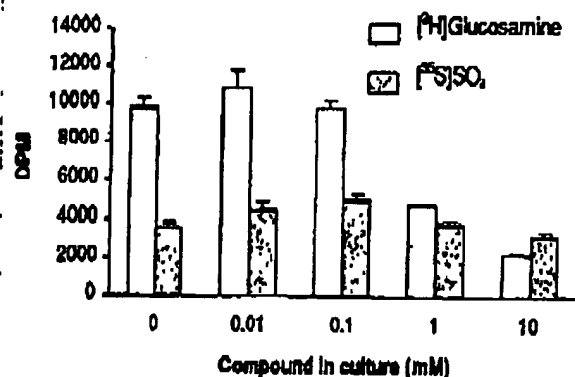


Fig. 2. Effect of increasing concentration of compound 1 on [<sup>3</sup>H]glucosamine and [<sup>35</sup>S]SO<sub>4</sub> incorporation into hepatocyte heparan sulfate.

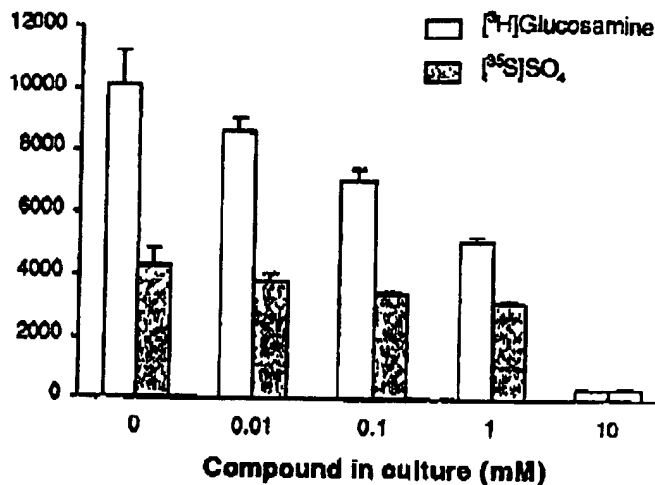


Fig. 3. Effect of increasing concentration on compound 2.

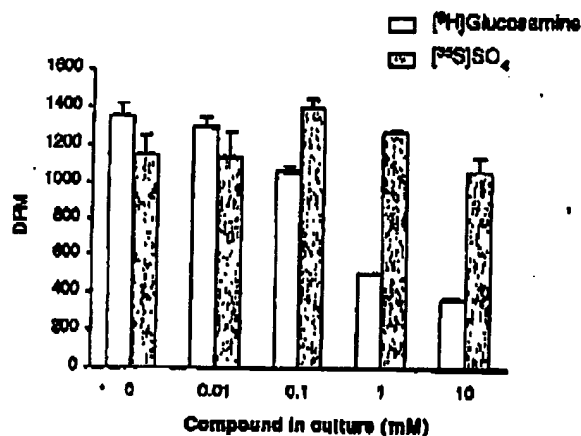


Fig. 4. Effect of increasing concentration of compound 3.

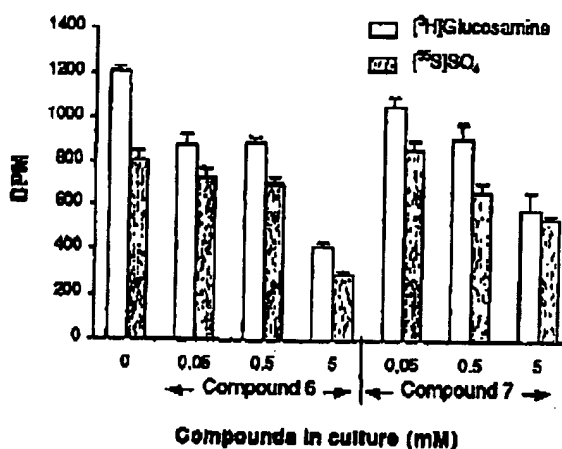


Fig. 5. Effects of increasing concentrations of compounds 6 and 7.

3, 4, 5, 6, and 7, respectively. For comparison the effect of increasing concentrations of glucosamine on [<sup>3</sup>H] glucosamine and [<sup>35</sup>S] SO<sub>4</sub> incorporation into hepatocyte heparan sulfate are illustrated in Fig. 8. Note that the effects of 1, 2, 3, 6, and 7 on [<sup>3</sup>H] glucosamine and [<sup>35</sup>S] SO<sub>4</sub> incorporation are similar to the effect of increasing glucosamine concentrations (Fig. 8). Note that compounds 5, 11, 12, and 13 have relatively little effect on [<sup>3</sup>H] glucosamine and [<sup>35</sup>S] SO<sub>4</sub> incorporation except at the highest concentration.

The effect of the single anomeric form of compound 17 on AA amyloid deposition is illustrated in Table 2.

## Discussion

The chemical design and synthetic procedures adopted produced the desired compounds in good

yield, the minimum being 60–65% based on the starting material. The structures of the compounds were validated by elemental analysis, NMR spectroscopy and mass spectrometry.

As shown in our previous report the effect of compound 17 (mixed anomers), or the de-O-acetylated counterpart since 17 presumably undergoes intracellular de-O-acetylation, on the biosynthesis of liver heparan sulfate can best be interpreted as terminating elongation of the growing glycosamino-glycan chain. We have now shown that this compound can, over a 5-d period, significantly reduce the quantity of AA amyloid accumulating in both the livers and spleens when mice are exposed to an AA amyloid induction protocol. These results add further weight to our hypothesis that heparan sulfate plays a sig-



### Novel Glycosaminoglycan Precursors

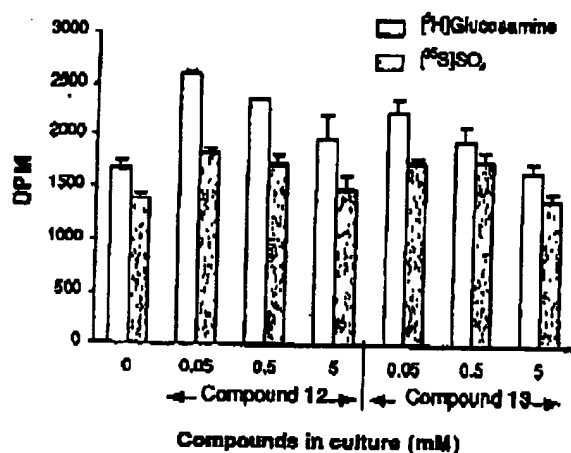


Fig. 6. Effects of increasing concentrations of compounds 12 and 13.

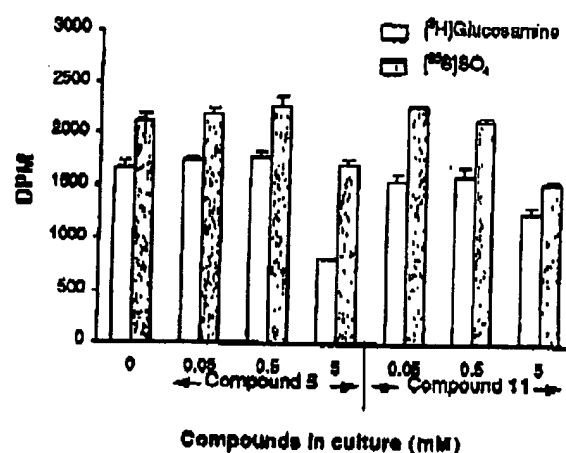


Fig. 7. Effects of increasing concentrations of compound 5 and 11.

nificant role in amyloidogenesis. Inhibition of heparan sulfate elongation by 17 identifies an additional strategy and lead compound for the inhibition of amyloidogenesis.

As exemplified with compounds 1, 2, and 3, *N*-alkyl group substitutions in glucosamine provide data that can best be explained by the enzymatic de-*N*-alkylation of the synthesized compounds. The net result is the generation of unlabeled glucosamine, which dilutes the labeled glucosamine pool, a feature appearing as a spurious inhibition of glycosaminoglycan synthesis. Nevertheless, modifications can be introduced at this site to obviate removal of the *N*-substituent; this approach is in progress.

As exemplified by compounds 12 and 13, 3-deoxy compounds have relatively little effect on hepatocyte heparan sulfate synthesis whereas -SO<sub>3</sub> substitutions at this location have a modest inhibitory effect at high concentrations. Compounds 18 and 20 are examples of 3,4-dideoxy glucosamine analogues, which are currently being assessed for their effect on heparan sulfate synthesis.

Our preliminary results have identified a specific anomer of compound 17, which has the desired results in tissue culture, truncates heparan sulfate chain elongation, does not affect protein synthesis, and does inhibit AA amyloidogenesis in both liver and spleen by 75–85%. These data are in keeping with the chemical design and synthetic objectives set out in our original proposal. They indicate the feasibility of preparing the desired compounds in good yield by the relatively inexpensive synthetic pathways chosen for this purpose and have the desired results in vitro and in vivo.

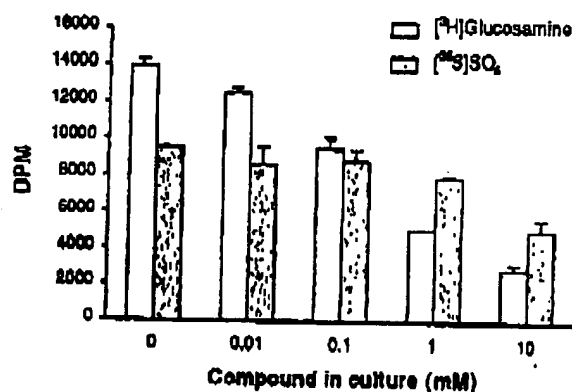


Fig. 8. Effect of increasing concentration of glucosamine

Table 2  
The Percent AA Amyloid per Unit Area of Tissue in Mice Treated with Compound 17 and in Untreated Controls<sup>a</sup>

| Treatment group    | Spleen    | Liver     |
|--------------------|-----------|-----------|
| Controls           | 9.3 ± 1.5 | 1.2 ± 0.4 |
| 17 (single anomer) | 4.3 ± 0.9 | 0.2 ± 0.1 |

<sup>a</sup>The values are the mean ± SEM of 5 animals per group. For both spleens and livers, 0.02 < *p* < 0.05.

### Acknowledgments

This work was supported by grants from the Natural Sciences and Engineering Research Council of Canada (WAS), the Medical Research Council of Canada, grant MT-3153 (RK), and the Institute for the Study of Aging (RK and WAS). We also express

our sincerest appreciation to Drs. Shridhar Bhat, Zhanjiang Li, Sandra Marone, Ali Berkin, and Mrs. Ruth Tan for their able assistance with various aspects of this project.

## References

- Ancsin J. B. and Kisilevsky R. (1999) The heparin/heparan sulfate-binding site on apo-serum amyloid A: Implications for the therapeutic intervention of amyloidosis. *J. Biol. Chem.* 274, 7172-7181.
- Berkin A., Szarek M. A., Plenkiewicz J., Szarek W. A., and Kisilevsky R. (2000a) Synthesis of 4-deoxy analogues of 2-acetamido-2-deoxy-D-glucose and 2-acetamido-2-deoxy-D-xylose and their effects on glycoconjugate biosynthesis. *Carbohydr. Res.* 323, 30-45.
- Berkin A., Szarek W. A., and Kisilevsky R. (2000b) Synthesis of 4-deoxy-4-fluoro analogues of 2-acetamido-2-deoxy-D-glucose and 2-acetamido-2-deoxy-D-galactose and their effects on cellular glycosaminoglycan biosynthesis. *Carbohydr. Res.* 326, 250-263.
- Castillo G. M., Cummings J. A., Yang W. H., et al. (1998) Sulfate content and specific glycosaminoglycan backbone of perlecan are critical for perlecan's enhancement of islet amyloid polypeptide (amylin) fibril formation. *Diabetes* 47, 612-620.
- Kisilevsky R. and Fraser P. E. (1997) A $\beta$  amyloidogenesis: unique or variation on a systemic theme? *Crit. Rev. Biochem. Mol. Biol.* 32, 361-404.
- Kisilevsky R., Lemieux L. J., Fraser P. E., Kong X. Q., Hultin P. G., and Szarek W. A. (1995) Arresting amyloidosis in vivo using small-molecule anionic sulphonates or sulphates: implications for Alzheimer's disease. *Nature Med.* 1, 143-148.
- Lindahl B., Eriksson L., and Lindahl U. (1995) Structure of heparan sulphate from human brain, with special regard to Alzheimer's disease. *Biochem. J.* 306, 177-184.
- Lindahl B., Eriksson L., Spillmann D., Caterson B., and Lindahl U. (1996) Selective loss of cerebral keratan sulfate in Alzheimer's disease. *J. Biol. Chem.* 271, 16991-16994.
- Lindahl B. and Lindahl U. (1997) Amyloid-specific heparan sulfate from human liver and spleen. *J. Biol. Chem.* 272, 26091-26094.
- Lindahl B., Westling C., Gimenez-Gallego G., Lindahl U., and Salmivirta M. (1999) Common binding sites for  $\beta$ -amyloid fibrils and fibroblast growth factor-2 in heparan sulfate from human cerebral cortex. *J. Biol. Chem.* 274, 30631-30635.
- Lindahl U., Kushke M., Lindholt K., and Oscarsson L. G. (1989) Biosynthesis of heparin and heparan sulfate. *Ann. NY Acad. Sci.* 556, 36-50.
- McCubbin W. D., Kay C. M., Narindrasorasak S., and Kisilevsky R. (1988) Circular dichroism and fluorescence studies on two murine serum amyloid A proteins. *Biochem. J.* 256, 775-783.
- McLaurin J., Franklin T., Kuhns W. J., and Fraser P. E. (1999a) A sulfated proteoglycan aggregation factor mediates amyloid- $\beta$  peptide fibril formation and neurotoxicity. *Amyloid* 6, 233-243.
- McLaurin J., Franklin T., Zhang X. Q., Deng J. P., and Fraser P. E. (1999b) Interactions of Alzheimer amyloid- $\beta$  peptides with glycosaminoglycans: effects on fibril nucleation and growth. *Euro. J. Biochem.* 266, 1101-1110.
- Subrahmanyam L. and Kisilevsky R. (1988) Effects of culture substrates and normal hepatic sinusoidal cells on in-vitro hepatocyte synthesis of apo-SAA. *Scand. J. Immunol.* 27, 251-260.
- Thomas S. S., Plenkiewicz J., Ison E. R., Bols M., Zou W., Szarek W. A., and Kisilevsky R. (1995) Influence of monosaccharide derivatives on liver cell glycosaminoglycan synthesis: 3-deoxy-D-xylo-hexose (3-deoxy-D-galactose) and methyl (methyl 4-chloro-4-deoxy- $\beta$ -D-galactopyranosid) uronate. *Biochim. Biophys. Acta* 1272, 37-48.
- Westermarck P. (1997) Classification of amyloid fibril proteins and their precursors: an ongoing discussion. *Amyloid* 4, 216-218.

## Acceleration of amyloid protein A amyloidosis by amyloid-like synthetic fibrils

KATARZYNA JOHAN\*, GUNILLA WESTERMARK\*, ULLA ENGSTRÖM†, ÅSA GUSTAVSSON\*, PER HULTMAN\*, AND PER WESTERMARK\*‡

\*Division of Molecular and Immunological Pathology, University Hospital, S-581 85 Linköping, Sweden; and †Ludwig Institute for Cancer Research, Uppsala Branch, S-751 24 Uppsala, Sweden

Communicated by Donald F. Steiner, University of Chicago, Chicago, IL, December 24, 1997 (received for review April 7, 1997)

**ABSTRACT** Amyloid protein A (AA) amyloidosis is a consequence of some long-standing inflammatory conditions, and subsequently, an N-terminal fragment of the acute phase protein serum AA forms  $\beta$ -sheet fibrils that are deposited in different tissues. It is unknown why only some individuals develop AA amyloidosis. In the mouse model, AA amyloidosis develops after  $\approx 25$  days of inflammatory challenge. This lag phase can be shortened dramatically by administration of a small amount of amyloid extract containing an as yet undefined amyloid-enhancing factor. In the present study, we show that preformed amyloid-like fibrils made from short synthetic peptides corresponding to parts of several different amyloid fibril proteins exert amyloidogenic enhancing activity when given i.v. to mice at the induction of inflammation. We followed i.v. administered, radiolabeled, heterologous, synthetic fibrils to the lung and to the perifollicular area in the spleen and found that new AA-amyloid fibrils developed on these preformed fibrils. Our findings thus show that preformed, synthetic, amyloid-like fibrils have an *in vivo* nidus activity and that amyloid-enhancing activity may occur, at least in part, through this mechanism. Our findings also show that fibrils of a heterologous chemical nature exert amyloid-enhancing activity.

Secondary or amyloid protein A (AA) amyloidosis is a life-threatening systemic disease in which deposits of amyloid can be found in most tissues of the body. The main constituent of the amyloid deposits is a fibril formed by  $\beta$ -pleated sheets of protein AA, the latter of which is an N-terminal 44- to  $\approx 100$ -amino acid cleavage product of the 104 amino acid precursor serum AA (SAA) (for review, see ref. 1). In humans, there are at least three different SAA genes coding for SAA1, SAA2 and SAA4, respectively (2). SAA1 and SAA2 are acute phase reactant high density apolipoproteins. These are expressed mainly by the liver, but SAA4 is expressed in several different tissues (3, 4). N-terminal fragments of SAA1 and SAA2 give rise to protein AA and polymerize to amyloid fibrils in humans. SAA is a conserved protein, and AA amyloidosis occurs, with varying frequency, in many mammalian species and in some birds (for review, see refs. 5 and 6). The mouse (*Mus musculus*) is prone to develop AA amyloidosis and is the most commonly used animal model for AA amyloidosis. The two mouse SAA isoforms of high density lipoprotein, SAA1 and SAA2, are both acute phase reactants, but only SAA2 is amyloidogenic and is found as protein AA in the fibrils (7, 8).

The plasma concentration of SAA is normally low both in humans and in mice, but the SAA concentration rises quickly at an acute inflammation as a response to cytokines, especially interleukin-1, interleukin-6, and tumor necrosis factor  $\alpha$  (for

review, see ref. 9), to levels as high as 1 mg/ml. When inflammation subsides, the SAA concentration gradually returns to normal. In humans, AA amyloidosis most commonly occurs in individuals with long term active inflammatory disease, which, in developed countries, usually is rheumatoid arthritis. In developing countries, the common cause of AA amyloidosis is a chronic infectious disease among which tuberculosis, leprosy, and malaria predominate (10). However, most individuals with these chronic inflammatory diseases never develop AA amyloidosis despite the high plasma concentration of SAA. It is still unclear why only a subset of individuals develops AA amyloidosis. In contrast to the disease in the mouse, there is so far no definite proof of a specific amyloid-prone SAA variant in humans, although some SAA isotypes may be over represented as amyloid fibrils (11, 12). Therefore, in addition to high concentrations of an amyloidogenic protein, other factors are important in the pathogenesis of AA amyloidosis.

AA amyloidosis can be easily induced experimentally in many strains of mice by a prolonged inflammatory challenge, e.g. s.c. injections of silver nitrate or casein (13). It also was observed several decades ago that an extract of mouse amyloid tissue, given i.v. with the simultaneous induction of inflammation, dramatically shortens the time for AA amyloid to develop (14). The same effect can be achieved by injection of cells from mice with AA amyloidosis (15). Despite many efforts, the active component [called "amyloid enhancing factor" (AEF)] has never been isolated or defined. It has, however, been suggested to act like the infectious protein in scrapie-related cerebral diseases (16). Because a general consensus concerning how amyloid deposits develop includes the role of a nidus, we previously tested (17) the effect of synthetic amyloid-like fibrils made from short peptides on the time necessary for amyloid induction and found an AEF-like effect of these fibrils. We now present strong evidence that AEF-like activity is exerted by synthetic amyloid-like fibrils by serving as a nidus on which new AA amyloid fibrils form.

### MATERIALS AND METHODS

**Mice.** Outbred female NMRI mice were purchased from Bomholtgard Breeding and Research Center (Ry, Denmark). The mice were 10–16 weeks of age and had free access to water and pellets (Type R 36; Lactamin, Vadstena, Sweden).

**Peptides.** C-terminally amidated peptides were synthesized as described (18). The following peptides, previously shown to be highly fibrillogenic *in vitro*, were used: a peptide corresponding to positions 20–29 of human islet amyloid polypeptide with an added N-terminal tyrosine residue [Tyr-islet amyloid polypeptide(20–29)] (19) and the following regions of

The publication costs of this article were defrayed in part by page charge payment. This article must therefore be hereby marked "advertisement" in accordance with 18 U.S.C. §1734 solely to indicate this fact.

© 1998 by The National Academy of Sciences 0027-8424/98/952558-6\$2.00/0  
PNAS is available online at <http://www.pnas.org>.

Abbreviations: AA, amyloid protein A; AEF, amyloid enhancing factor; SAA, serum amyloid A; TTR, transthyretin.

‡To whom reprint requests should be addressed. e-mail: perwe@pai.liu.se.

human transthyretin (TTR): TTR(10–20), TTR(24–35), TTR(105–115) and TTR(115–124) (20).

**In Vitro Fibril Formation.** Fibrils were made *in vitro* as described elsewhere (19, 20). In brief, synthetic peptides were dissolved in 10% acetic acid at a concentration of 10 mg/ml and were left for 24 hr at room temperature. The peptide solutions then were neutralized to pH 7 with 25% NH<sub>4</sub>OH. After 30 min, samples from each of the solutions were dried on glass slides, stained with Congo red, and evaluated for green birefringence in polarized light, which was found with all materials. Negatively stained samples were also studied by electron microscopy to verify presence of amyloid-like fibrils. The fibril preparations were diluted with distilled water to a concentration of 1 mg/ml and were stored at +4°C.

**Labeling of Synthetic Fibrils with <sup>125</sup>I.** Because TTR contains a tyrosine residue at position 116, the peptide TTR(115–124) was chosen for labeling. Labeling with Na<sup>125</sup>I (100 mCi/ml; Amersham) was performed with the chloramine-T method (21). Na<sup>125</sup>I (5 µl) was dispensed into an Eppendorf plastic tube placed within a lead cylinder. HCl (5 µl of 10 mM) then was added to the iodide solution, immediately followed by 150 µl of freshly made TTR(115–124) peptide solution (10 mg/ml in 10% acetic acid) and 25 µl of chloramine T-solution (5.2 mg/ml in distilled water). The solutions were mixed, and after 10 min, 40 µl sodium metabisulfite solution (4.8 mg/ml in distilled water) was added, followed 30 sec later by the addition of 20 µl of sodium iodide (10 mg/ml in distilled water).

For formation of labeled fibrils, the above peptide solution was neutralized with ammonia and left for 30 min at room temperature. Bound and free <sup>125</sup>I were separated by dilution of the fibril suspension with distilled water followed by centrifugation at 100,000 × g for 15 min. This latter procedure was repeated once. The presence of birefringent Congoophilic material was verified as described above. The pelleted material was diluted with distilled water to the volume of 1.5 ml (1 mg/ml; specific activity 1.4 mCi/mg) and was used in the experiments.

**Preparation of AA Fibril Supernatants Used for AEF Activity.** AEF was prepared from the livers of mice with severe systemic AA amyloidosis as described (17). In brief, liver tissue was homogenized in 0.15 M NaCl, followed by centrifugation at 15,000 × g for 30 min at 4°C. Homogenization and centrifugation of the pellet were repeated 10 times. Amyloid fibrils subsequently were extracted with distilled water (22), and pooled supernatants from the second and third water extractions were used as AEF. The total protein concentration was 1.32 mg/ml as determined by a protein assay kit (Bio-Rad).

**Induction of Amyloidosis.** Mice were divided into six groups, with 10 animals in each group to determine the AEF effect of the synthetic fibril preparations. Each mouse in the experimental groups received a single injection of 0.1 ml of AEF or 0.1 ml of the synthetic fibril suspension into the lateral tail vein. Both types of fibril suspensions were sonicated briefly before injection to reduce possible aggregates. A control group of 30 animals received an i.v. injection of 0.1 ml of vehicle (10% acetic acid neutralized with 25% NH<sub>4</sub>OH and diluted 10 times with distilled water). These i.v. injections were followed immediately by an s.c. dorsal injection of 0.5 ml of 1% AgNO<sub>3</sub> as an inflammatory stimulus. AgNO<sub>3</sub> injections (0.1 ml) were repeated on day 7 and, for remaining animals, on day 14. Seven animals from each of the experimental groups and the control groups were killed on day 10, and the remaining animals of each group were killed on day 16. Tissue samples from spleen were fixed in 10% neutral buffered formalin and embedded in paraffin. In another experiment, 12 mice received TTR(24–35) fibrils i.v., and another 13 mice received the same amount of the peptide dissolved in dimethyl sulfoxide. In both groups of animals, the injections were followed by dorsal injections of 0.1 ml of 1% AgNO<sub>3</sub> exactly as above, and all mice were killed on day 16.

Table 1. C-terminally amidated synthetic peptides used for *in vitro* formation of amyloid-like fibrils

| Peptide      | Amino acid sequence          |
|--------------|------------------------------|
| IAPP(20–29)  | YSNFGAILSS-NH <sub>2</sub>   |
| TTR(10–20)   | CPLMKVLDVAV-NH <sub>2</sub>  |
| TTR(24–35)   | PAINVAVHVFRK-NH <sub>2</sub> |
| TTR(105–115) | YTIAALLSPYS-NH <sub>2</sub>  |
| TTR(115–124) | SYSTTAVVTN-NH <sub>2</sub>   |

**Fate of Synthetic Fibrils *in Vivo*.** The fate of injected fibrils was followed by using a group of 11 mice injected i.v. with 0.1 ml of <sup>125</sup>I-iodinated TTR(115–124) fibrils, followed immediately by an s.c. injection of 0.5 ml of 1% AgNO<sub>3</sub>. The mice subsequently were given 0.1 ml of 1% AgNO<sub>3</sub> s.c. on days 7 and 14. Three mice died immediately after the i.v. injection of iodinated TTR fibrils. Of the remaining mice, one mouse was killed on each of days 1, 6, 11 and 20, and four mice were killed on day 22. Samples from spleen, liver, kidneys, lungs, and thyroid were fixed in 10% neutral buffered formalin for 24 hr and embedded in paraffin or were fixed in 10% neutral buffered formalin for 24 hr and subsequently infiltrated in 5% sucrose in 0.05 M Tris-Cl buffer (pH 8.0) containing 0.15 M NaCl (Tris-buffered saline), and then snap-frozen in Tissu-Tek OCT Compound embedding medium (Histolab, Västra Frölunda, Sweden). Small samples of lung tissue from mice killed on days 20 and 22 were fixed for 2 hr at room temperature in 4% paraformaldehyde and 0.5% glutaraldehyde in 0.1% sodium cacodylate buffer (pH 7.4) containing 0.1% sucrose. Thereafter, the samples were dehydrated for electron microscopy and embedded in Epon (Agar Aids, Essex, UK) polymerized at 60°C or Unicryl or Lowicryl K4M (Polysciences) photopolymerized at –20°C.

**Antisera.** Antiserum against the synthetic peptide TTR(115–124) was raised in a rabbit as described elsewhere (23). Antiserum to TTR(115–124) is amyloid-specific, i.e., it reacts only with TTR in, or purified from, amyloid deposits (23). Antiserum to mouse protein AA was raised in rabbits as described elsewhere (17). Goat antiserum to mouse amyloid P component kindly was provided by M. B. Pepys, London, U.K.

**Light Microscopy.** Paraffin sections (10 µm) and cryostat sections (10 µm) were stained with alkaline Congo red and hematoxylin (24) and subsequently were examined for the presence of amyloid, indicated by green birefringence with polarized light. The amount of amyloid in the paraffin sections of spleen was graded as described (17).

**Macroautoradiography.** Air-dried cryostat sections (10 µm) of thyroid, spleen, liver, kidney and lung from the mice injected with <sup>125</sup>I-labeled TTR(115–124) fibrils were placed on Kodak X-OmatAR x-ray film in an x-ray cassette with x-ray intensifying screens at –70°C for 7 days.

**Microautoradiography.** Air-dried cryostat sections (10 µm) were coated with Hypercoat LM-1 autoradiographic emulsion (Amersham), air dried, and exposed in light proof boxes at +4°C for 6, 10, or 18 weeks. Slides without sections were coated with autoradiographic emulsion, air dried, and subse-

Table 2. Splenic amyloid deposits induced by treatment with AgNO<sub>3</sub> and different synthetic peptide fibrils compared with controls treated with AgNO<sub>3</sub> and vehicle or AEF

| Treatment    | Mice, n | Mice with amyloid | Amyloid grade |
|--------------|---------|-------------------|---------------|
| TTR(10–20)   | 10      | 1                 | 1+            |
| TTR(24–35)   | 10      | 3                 | 1+–3+         |
| TTR(105–115) | 10      | 2                 | 1+–3+         |
| TTR(115–124) | 10      | 5                 | 2+            |
| IAPP(20–29)  | 10      | 2                 | 2+            |
| AEF          | 10      | 10                | 3+–4+         |
| Vehicle      | 28      | 1                 | 1+            |

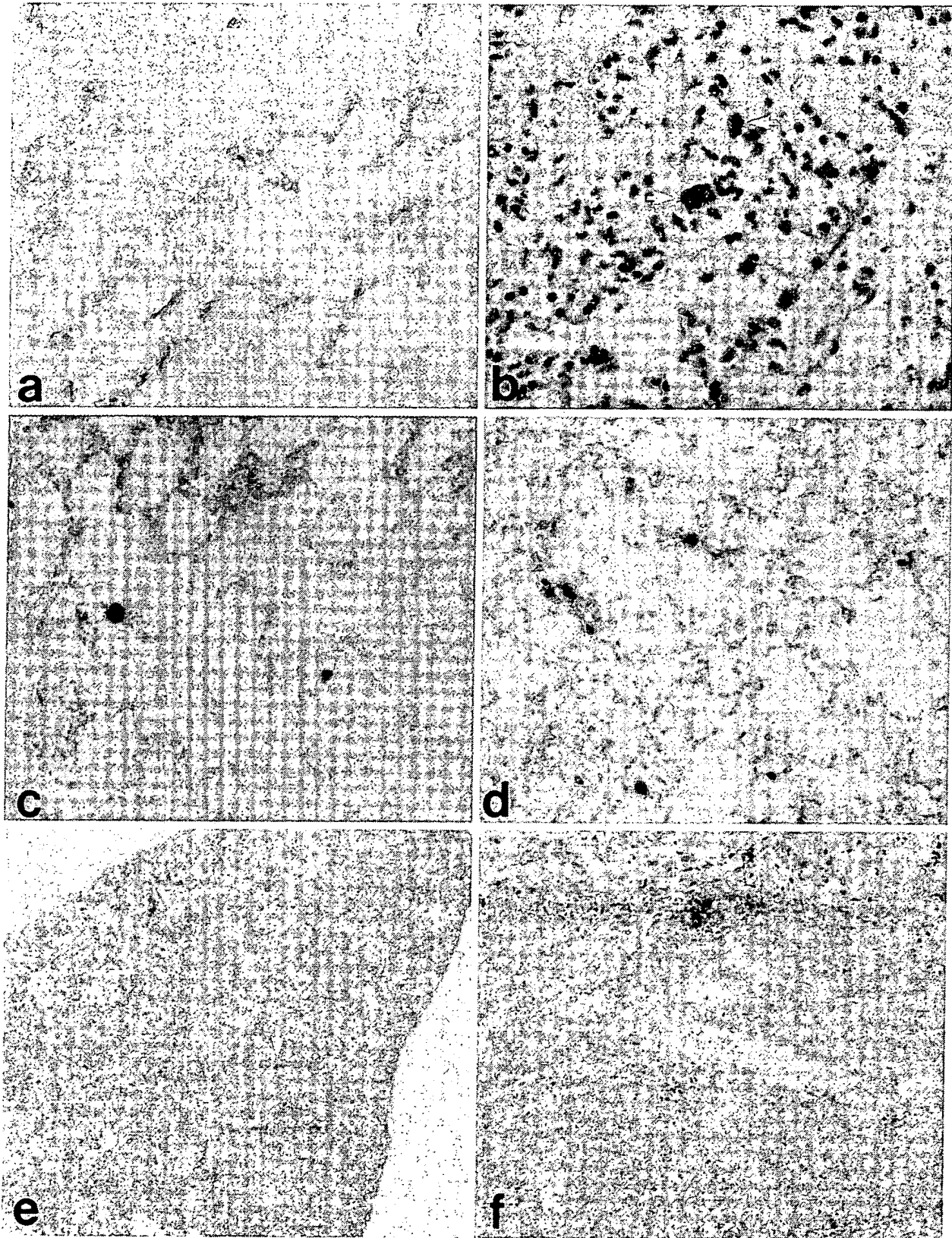


FIG. 1. (a-d): Lung tissue from a mouse given synthetic TTR(115-124) fibrils i.v. Small amyloid deposits (arrows) occasionally were found in vascular lumina stained with Congo red and viewed in polarized light (a) and labeled with antiserum to mouse protein AA and to the synthetic peptide TTR(115-124) (b and c). (d-f) Tissues taken from a mouse that had received <sup>125</sup>I-labeled TTR(115-124) fibrils i.v. 22 days before it was killed. (d) Lung tissue with several radioactivity labeled spots corresponding to the minute amyloid deposits. e A section of the spleen and silver grains occur perifollicularly at the amyloid deposits. (f) Close-up of e at the arrow.

quently exposed together with the coated sections to serve as control autoradiographs. The slides were developed in Kodak D-19 developer, fixed in Kodak Unifix fixer for 4 min, and washed in two changes of distilled water. The sections were immediately post-stained with hematoxylin. To investigate whether silver injected as  $\text{AgNO}_3$  reduced the autoradiographic emulsion, sections from one of the experimental mice that had received silver nitrate s.c. but no labeled fibrils were coated and exposed for 2 hr and then were processed as described above.

**ImmunoGold Electron Microscopy.** Semithin sections were cut from blocks embedded in Unicryl, Lowicryl, and Epon. The sections were exposed on Kodak X-OmatAR x-ray film in the same way as described above. Ultrathin sections were cut thereafter from the blocks containing radioactive deposits as determined by macroautoradiography. Consecutive sections from Unicryl- or Lowicryl-embedded blocks were mounted on Formvar-coated (Ladd Research Industries, Burlington, VT) nickel grids and used for single indirect ImmunoGold labeling. The sections from Epon-embedded blocks were placed on uncoated nickel grids and used for double indirect ImmunoGold labeling.

Before immunolabeling, all of the sections were incubated with 5% BSA in Tris-buffered saline for 30 min to block nonspecific binding sites. For single immunolabeling, the sections then were transferred onto a drop of rabbit antiserum against mouse AA, TTR(115–124), or mouse serum amyloid P-component (all diluted 1:200) and incubated overnight at room temperature in a humidity chamber. After washing in 0.05 sodium phosphate buffer (pH 7.4) containing 0.15 M NaCl (PBS) and blocking in 5% BSA in Tris-buffered saline for 10 min, the sections were incubated with 10 nm of colloidal gold-labeled goat anti-rabbit IgG (Biocell Laboratories) for 1 hr at room temperature. Thereafter, the sections were washed in PBS, rinsed in distilled water, and counterstained with 5% uranyl acetate and lead citrate.

For double immunolabeling, one face of the grid was performed as described above, applying rabbit anti-AA antiserum followed by 10 nm of colloidal gold labeled goat anti-rabbit IgG. The other face of the grid then was labeled with rabbit anti-TTR(115–124) antiserum, and the reaction was visualized with 20 nm of protein A gold particles (Biocell Laboratories). Care was taken not to wet the opposite face during the incubations. The sections were counterstained only on one face with uranyl acetate and lead citrate. The sections were viewed in a JEOL 1200 electron microscope at 80 kV.

**Statistical Analysis.** For statistical comparison between groups, Fisher's exact test was used with INSTAT 2.01 software.

## RESULTS

**Fibrils.** All synthetic peptides formed Congoophilic aggregates *in vitro* that exhibited green birefringence in polarized light. The extracted murine AA amyloid fibrils used as AEF showed strong green birefringence after Congo red staining.

**In Vivo Effects of Injected Synthetic Peptide Fibrils and AEF.** Injection (i.v.) of fibrils made from TTR(10–20), TTR(24–35), TTR(105–115), TTR(115–124), or islet amyloid polypeptide(20–29) induced accelerated amyloid deposition in mice given  $\text{AgNO}_3$  as detected with Congo red staining (Table 2). Of 50 mice that received synthetic fibrils, 13 developed amyloidosis, whereas 1 of 28 surviving control mice that received vehicle had only minute amyloid deposits ( $P = 0.01$ ). In all animals, the amyloid deposits were localized in the perifollicular areas of the spleen. Amyloid deposits also were detected perifollicularly in the spleen of all mice treated with AEF and  $\text{AgNO}_3$ . The deposits in the latter group were moderate in six mice and extensive in four mice.

In the experiment in which the same peptide [TTR(24–35)] was injected in a fibrillar or nonfibrillar form, none of the 13

mice given nonfibrillar peptide showed amyloid on day 16, whereas 4 of 12 mice injected with fibrils had splenic amyloid deposits ( $P < 0.04$ ).

**Effects of TTR(115–124) Fibrils Labeled with  $^{125}\text{I}$ .** No splenic amyloid was detected in mice that died immediately after injections or in mice killed on days 1, 6, or 11, as determined by Congo red staining. All of the mice killed on days 20 ( $n = 1$ ) and 22 ( $n = 4$ ) had small to extensive amyloid deposits perifollicularly in the spleen. Three of the mice had hepatic amyloid deposits that were localized to the central vein areas. One mouse showed severe generalized amyloidosis with amyloid deposition not only in the spleen and liver but also in the kidneys, lungs, and thyroid.

Small congophilic deposits were seen in some sections of lungs of animals (killed on days 20 and 22) that had received TTR(115–124) fibrils (Fig. 1*a*). These amyloid deposits reacted strongly with antiserum to TTR(115–124) (Fig. 1*c*) immunohistochemically, and somewhat weaker immunoreactivity was observed with antiserum to amyloid P component (not shown). There was also a strong reaction with antiprotein AA antiserum (Fig. 1*b*). No staining was detected with normal rabbit serum, and the tissues from an untreated control mouse showed no reaction with the antisera used.

**Distribution of  $^{125}\text{I}$ -Labeled TTR(115–124) Fibrils.** In the mouse killed on day 1, macroautoradiography showed strong

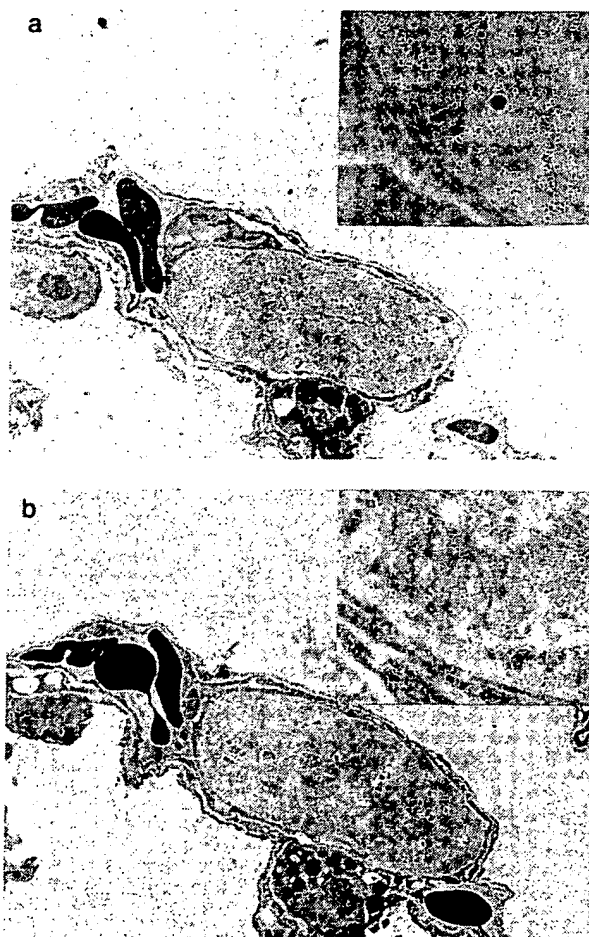


FIG. 2. Electron microscopical picture of an amyloid deposit in the lung of a mouse that had received TTR(115–124) fibrils i.v. at the induction of amyloidosis and was killed on day 22. The fibrils are labeled with antiserum to TTR(115–124) (*a*) and mouse protein AA (*b*). Both antisera label the fibrils specifically. ( $\times 5,000$ ). (Insets) Parts of the deposits. ( $\times 37,500$ ).



focal radioactivity in the lungs and liver and moderate multifocal areas of radioactivity in the spleen. The mice killed on days 6, 11, 20, and 22 showed strong focal radioactivity in the lungs. Only weak multifocal radioactivity was detected in spleen from mice killed on days 6 and 11, and very weak radioactivity was present in the spleen sections from three of five mice killed on days 20 and 22. No radioactivity was detected in the livers of the mice killed on days 6, 11, 20, or 22.

Microautoradiography verified the results obtained by macroautoradiography. Microautoradiography showed varying amounts of silver grains distributed in diffuse perifollicular patterns in spleen sections from the three mice killed on days 20 and 22 (Fig. 1 *e* and *f*). The radioactivity was localized to the areas of spleen in which amyloid deposits were detected by Congo red staining and by immunohistochemistry. Varying numbers of focally distributed heavy accumulations of silver grains were present in the lungs of all animals (Fig. 1*d*). The thyroid glands had very strong concentration of silver grains confined to the follicles. No silver reduction was observed in the autoradiographs of the livers. The silver precipitate in the tissues originating from the injected  $\text{AgNO}_3$  easily was discriminated from the silver grains in the film.

**Immunoelectron Microscopy of Lung Tissue.** Lung tissue was chosen for the immunoelectron microscopic study because the strongly radioactivity-labeled and well demarcated amyloid deposits were easy to find. Such deposits were found at the electron microscopic level in the lungs from three of five mice receiving  $^{125}\text{I}$ -labeled TTR(115–124) fibrils i.v. The small deposits were rounded and almost always were surrounded by basal membrane-like material and appeared to be located within lumina of small blood vessels (Fig. 2). The amyloid fibrils had no definite organization and varied somewhat in morphology. In some deposits, thicker fibrils were evident, whereas in others the fibrils were uniformly thin (not shown).

Immunolabeling with antiserum to TTR(115–124) varied. Thicker fibrils showed a very strong labeling with antiserum to TTR(115–124) (Fig. 2*a*) and only slight labeling with antiserum to mouse protein AA (Fig. 2*b*). The opposite phenomenon was observed with thin fibrils (not shown). In double immunolabeling experiments [in which one face of the section was incubated with antiserum to TTR(115–124) and the other with antiserum to mouse protein AA], labeling with both antisera was clearly evident in the amyloid deposits (Fig. 3). However, the proportion of labeling with the different antisera varied in that a strong labeling with anti TTR(115–124) was

followed by a weaker protein AA labeling and vice versa. Thus, of 19 different deposits studied, protein AA immunoreactivity predominated in 7, and TTR immunoreactivity predominated in 12. All deposits were labeled with antiserum to amyloid P-component.

## DISCUSSION

In this study, we show that preformed fibrils made from synthetic peptides and given in small doses i.v. in mice shorten the lag phase between an inflammatory stimulus and development of AA amyloidosis and, consequently, have amyloid-enhancing effects. By the use of radioactivity-labeled synthetic fibrils, we followed injected synthetic fibrils to the lung and spleen. Some fibril aggregates were trapped in lung capillaries and formed small distinctive amyloid foci that could be identified by Congo red staining. By double ImmunoGold labeling, we were able to show that these amyloid foci not only contained the synthetic fibrils but also murine protein AA fibrils. Likewise, we found that early perifollicular splenic amyloid deposits contained radioactivity labeled material, indicating that synthetic fibrils not only were trapped in the lung but also were present at an area known to be a target for the first deposits in murine experimental AA amyloidosis (25). Sections of kidney and liver, organs in which amyloid deposits occur later (25), exhibited no radioactivity.

Formation of amyloid fibrils is supposed to occur as an off-pathway event from specific near-native protein intermediates at the folding–unfolding pathway (26). A nucleation mechanism is believed to be of importance because seeding a solution of amyloid fibril proteins like  $\beta$ -protein (27) or islet amyloid polypeptide (28) with preformed fibrils made from the homologous proteins strongly enhances the speed by which new fibrils are formed. This fibril growth follows first-order kinetics (29, 30). The nucleation mechanism is similar to that implicated in the prion model of “infectivity”; the protein with abnormal tertiary structure serves as template for other protein molecules (16, 31). However, in prion diseases, the infectivity may be dissociated from the formation of amyloid fibrils (32). The formation of the nucleus in the amyloidogenesis in general is, however, poorly understood, but it should be noted that in the present experiments only peptides in their fibrillar form exerted amyloid-enhancing effects.

The finding that amyloid-like fibrils synthetically made from heterologous proteins enhanced the development of AA amyloidosis presumably by acting as *nidi* is of great interest. This finding raises the provocative question of whether other components in addition to amyloid fibrils can act as *nidi* in the amyloidogenesis. One of the major and unsolved questions in the pathogenesis of human AA amyloidosis asks why only some individuals with longstanding inflammatory conditions and high SAA plasma concentration develop amyloid deposits. It is known from the mouse (33) and the mink (1, 34) that several SAA isoforms exist and that they vary strongly in amyloidogenicity. Such a mechanism may exist also in humans (11, 12) but is probably less important because in most instances, human AA amyloid is derived from common SAA isotypes also present in individuals who do not develop amyloidosis. Therefore, other factors in addition to a suitable SAA must be of importance in the human amyloidogenesis. The mechanism found in the present study in which exogenous substances enhance AA-amyloidogenesis in an experimental mouse model may be true also in the human situation. Hypothetically, an exogenous substance may form a *nidus* on which the first AA fibrils form. Such a mechanism could explain why only a fraction of individuals with longstanding high plasma SAA concentration get AA amyloidosis. Furthermore, similar mechanisms may be important not only in AA amyloidosis but also in other types of amyloid deposits.

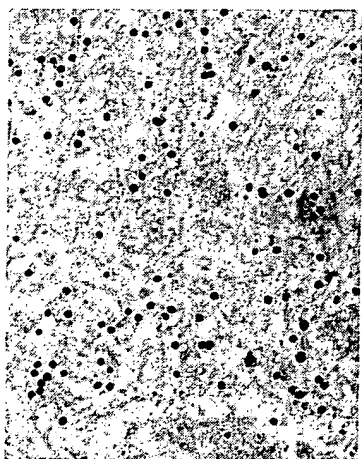


FIG. 3. Double immunolabeling of a lung amyloid deposit with antiserum to TTR(115–124) (20 nm of gold particles) and to mouse protein AA (10-nm gold particles). This deposit seems to consist mainly of synthetic TTR fibrils, but specific protein AA-labeling also is seen. ( $\times 80,000$ .)

We thank Maric-Louise Eskilsson and Christer Bergman for skilled technical assistance. This work was supported by the Swedish Medical Research Council (Project 5941) and the Amyl Foundation.

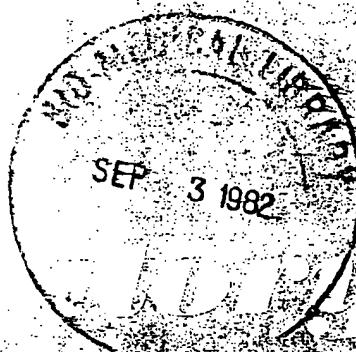
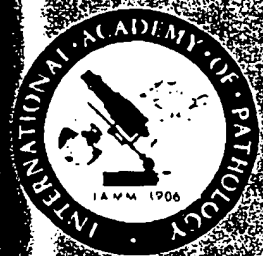
1. Husby, G., Marhaug, G., Dowton, B., Sletten, K. & Sipe, J. D. (1994) *Amyloid* **1**, 119–137.
2. Whitehead, A. S., de Beer, M. C., Steel, D. M., Rits, M., Lelias, J. M., Lane, W. S. & de Beer, F. C. (1992) *J. Biol. Chem.* **267**, 3862–3867.
3. Benditt, E. P. & Meek, R. L. (1989) *J. Exp. Med.* **169**, 1841–1846.
4. Meek, R. L., Urieli-Shoval, S. & Benditt, E. P. (1994) *Proc. Natl. Acad. Sci. USA* **91**, 3186–3190.
5. Zschiesche, W. & Jakob, W. (1989) *Pharmacol. Ther.* **41**, 49–83.
6. Johnson, K. H., Westermark, P., Sletten, K. & O'Brien, T. D. (1996) *Amyloid* **3**, 270–289.
7. Hoffman, J. S., Ericsson, L. H., Eriksen, N., Walsh, K. A. & Benditt, E. P. (1984) *J. Exp. Med.* **159**, 641–646.
8. Shiroo, M., Kawahara, E., Nakanishi, I. & Migita, S. (1987) *Scand. J. Immunol.* **26**, 709–716.
9. McAdam, K. P. W. J., Raynes, J. G., Alpers, M. P., Westermark, G. T. & Westermark, P. (1998) *Papua New Guinea Med. J.*, in press.
10. McAdam, K. P. W. J. (1978) *Papua New Guinea Med. J.* **21**, 69–78.
11. Baba, S., Masago, S. A., Takahashi, T., Kasama, T., Sugimura, H., Tsugane, S., Tsutsui, Y. & Shirasawa, H. (1995) *Hum. Mol. Genet.* **4**, 1083–1087.
12. Westermark, P., Sletten, K., Westermark, G. T., Raynes, J. & McAdam, K. P. (1996) *Biochem. Biophys. Res. Commun.* **223**, 320–323.
13. Skinner, M., Shirahama, T., Benson, M. D. & Cohen, A. S. (1977) *Lab. Invest.* **36**, 420–427.
14. Willerson, J. T., Gordon, J. K., Talal, N. & Barth, W. F. (1969) *Arthritis Rheum.* **12**, 232–240.
15. Werdelin, O. & Rønne, P. (1966) *Acta Pathol. Microbiol. Scand.* **68**, 1–18.
16. Gajdusek, D. C. (1994) *Ann. N. Y. Acad. Sci.* **724**, 173–190.
17. Ganowiak, K., Hultman, P., Engström, U., Gustavsson, Å. & Westermark, P. (1994) *Biochem. Biophys. Res. Commun.* **199**, 306–312.
18. Gustavsson, Å., Engström, U. & Westermark, P. (1991) *Biochem. Biophys. Res. Commun.* **175**, 1159–1164.
19. Westermark, P., Engström, U., Johnson, K. H., Westermark, G. T. & Betsholtz, C. (1990) *Proc. Natl. Acad. Sci. USA* **87**, 5036–5040.
20. Gustavsson, Å., Engström, U. & Westermark, P. (1997) *Amyloid* **4**, 1–12.
21. Hunter, W. M. (1978) *Handb. Exp. Immunol. Immunochem.* **14.1**–14.40.
22. Pras, M., Schubert, M., Zucker-Franklin, D., Rimon, A. & Franklin, E. C. (1968) *J. Clin. Invest.* **47**, 924–933.
23. Gustavsson, Å., Engström, U. & Westermark, P. (1994) *Am. J. Pathol.* **144**, 1301–1311.
24. Puchtler, H., Sweat, F. & Levine, M. (1962) *J. Histochem. Cytochem.* **10**, 355–364.
25. Shirahama, T. & Cohen, A. S. (1980) *Am. J. Pathol.* **99**, 539–550.
26. Wetzel, R. (1994) *Trends Biotechnol.* **12**, 193–198.
27. Jarrett, J. T. & Lansbury, P. T. (1993) *Cell* **73**, 1055–1058.
28. Ashburn, T. T. & Lansbury, P. T. (1993) *J. Am. Chem. Soc.* **115**, 11012–11013.
29. Naiki, H., Higuchi, K., Nakakuki, K. & Takeda, T. (1991) *Lab. Invest.* **65**, 104–110.
30. Esler, W. P., Stimson, E. R., Ghilardi, J. R., Vinters, H. V., Lee, J. P., Mantyh, P. W. & Maggio, J. E. (1996) *Biochemistry* **35**, 749–757.
31. Cohen, F. E., Pan, K.-M., Huang, Z., Baldwin, M., Fletterick, R. J. & Prusiner, S. B. (1994) *Science* **264**, 530–531.
32. Wille, H., Baldwin, M. A., Cohen, F. E., DeArmond, S. J. & Prusiner, S. B. (1996) in *The Nature and Origin of Amyloid Fibrils*, eds. Bock, G. R. & Goode, J. A. (Wiley, New York), pp. 181–201.
33. Meek, R. L., Hoffman, J. S. & Benditt, E. P. (1986) *J. Exp. Med.* **163**, 499–510.
34. Foyen Bruun, C., Rygg, M., Nordstoga, K., Sletten, K. & Marhaug, G. (1994) *Scand. J. Immunol.* **40**, 337–344.



ISSN 0023-6837

Volume 47 • Number 2 • August 1982

LAINAW 47 (2) 111-214 (1982)



Current  
Periodical  
Room

# *International Investigation*

OFFICIAL JOURNAL OF  
THE UNITED STATES-CANADIAN DIVISION OF  
THE INTERNATIONAL ACADEMY OF PATHOLOGY



THE WILLIAMS & WILKINS COMPANY, Baltimore, Md.

ase

955

NOTICE: THIS MATERIAL MAY BE PROTECTED  
BY COPYRIGHT LAW (TITLE 17 U.S. CODE)

0023-6837/82/4702-0139\$02.00/0

LABORATORY INVESTIGATION

Copyright © 1982 by the United States-Canadian Division of the International Academy of Pathology

Vol. 47, No. 2, p. 139, 1982

Printed in U.S.A.

# Further Characterization of Amyloid-Enhancing Factor

M. A. AXELRAD, M.D., PH.D., R. KISILEVSKY, M.D., PH.D., J. WILLMER, M.D.,  
S. J. CHEN, M.Sc., AND M. SKINNER, M.D.

*Departments of Pathology and Biochemistry, Queen's University and Kingston General Hospital, Kingston, Ontario, and The Arthritis and Connective Tissue Disease Section, The Thorndike Memorial Laboratory and the Division of Medicine, Boston City Hospital and University Hospital, Boston University School of Medicine, Boston, Massachusetts*

Amyloid-enhancing factor (AEF) is a transferable activity that in CBA/J mice reduces the induction time of splenic amyloid deposition to 48 hours. Azocasein, or AgNo<sub>3</sub>, can induce AEF in the spleen and liver. In the liver several subcellular organelles possess this activity. This is likely due to AEF's adherent properties. AEF is most effective when given by the intravenous route. After intravenous injection, AEF particulates localize to the perifollicular areas of the spleen and Kupffer cells in the liver. The effects of AEF administration persist for at least 4 weeks. AEF can be solubilized in 4 M glycerol, is not the amyloid A protein, and is not likely to be the serum amyloid P component. The extract can be fractionated by Sepharose 4B column chromatography. The active component is of high molecular weight, and tentative identification by disc electrophoresis has been made.

**Additional key words:** Casein, Inflammation, Liver, Spleen.

Examination of the immune system during the induction of amyloid prompted several laboratories, in the recent past, to undertake transfer of tissue or cells in an attempt to induce amyloid deposition in isogeneic recipients. These "transfer experiments" met with variable success and have been adequately reviewed by Hardt and Ranlov (7). Various cells, primarily from spleen but also liver, and subcellular particles, such as nuclei, were shown to have such activity, but there was no general agreement as to the nature of the enhancing factor, although there has been one report of a small molecular weight protein having these enhancing properties (11). Although the central importance of this "enhancing" activity has been alluded to by Janigan (9), it has not been the subject of much investigation during the last 5 to 6 years.

Our own previous work with amyloid-enhancing factor (AEF) (1, 2, 3, 15, 17) has indicated that the active component is a protein (1, 2), that AEF can always be demonstrated approximately 24 to 48 hours prior to the deposition of amyloid (2), and that AEF activity is present in sonicated as well as viable spleen cells (2, 15, 17). To further characterize AEF, in the present report we have examined the following questions. (1) Does any particular cell organelle possess AEF activity? (2) Does the route of administration of AEF play any role in its effectiveness? Where do AEF particulates localize after intravenous injection? (3) What combinations of AEF and inflammation are effective in producing amyloid in

48 hours? (4) In what manner can AEF activity be solubilized from tissue? Does the extract possess amyloid (AA) and/or serum amyloid P(SAP) protein? (5) Do either AA or SAP possess AEF activity? And finally, (6) Can one fractionate the AEF extracts to partially purify AEF?

## MATERIALS AND METHODS

### ANIMALS

All animals were CBA/J female mice weighing 20 to 25 gm.

### AEF

AEF was prepared as described previously (14). Briefly, AEF was derived from spleens of animals which, after azocasein injections, had just commenced amyloid deposition. The spleens were teased in ice-cold Hanks' balanced salt solution, the debris was allowed to settle, and the cell suspension was removed and centrifuged at  $650 \times g$  for 10 minutes at 4° C. The cell pellet was resuspended in Hanks' balanced salt solution to a final concentration of  $50 \times 10^6$  cells per ml., disrupted by sonification, and stored at -20° C.

**Subcellular Localization.** Where subcellular fractions were examined for AEF activity, fresh normal or AEF-containing livers were homogenized in 2.5 volumes of 0.3 M tris(hydroxymethyl)aminomethane (Tris)-HCl, pH 7.5,

0.15 M  $\text{NH}_4\text{Cl}$  and 3.5 mM  $\text{Mg}(\text{CH}_3\text{COO}^-)_2$ , and 0.1 M sucrose per gram of tissue, and the homogenate was centrifuged at  $15,000 \times g$  for 10 minutes at  $4^\circ \text{C}$ . The postmitochondrial supernatant was (1) centrifuged at  $100,000 \times g$  for 1 hour, providing a microsomal pellet and a  $100,000 \times g$  supernatant; (2) treated with 0.15 ml. of 10 per cent Na deoxycholate per ml. of postmitochondrial supernatant and subsequently centrifuged in a discontinuous sucrose gradient at 40,000 r.p.m. for 4 hours at  $4^\circ \text{C}$ . as described previously (12), with the polyribosomes being recovered as a pellet. These polyribosomes monitored by electron microscopy have previously been shown to be pure and without membrane contamination (18); and (3) incubated with puromycin and KCl as described by Rolleston (26), then layered on a discontinuous sucrose gradient, and spun at 40,000 r.p.m. for 4 hours at  $4^\circ \text{C}$ . The ribosomes accumulated as a pellet, and the endoplasmic reticulum membranes left at the interface could be harvested by centrifugation. These membranes have had 85 to 90 per cent of their ribosomal RNA removed as monitored by RNA determinations.

The fractions noted (postmitochondrial supernatant, microsomal pellet,  $100,000 \times g$  supernatant, polyribosomes and membranes), were resuspended in phosphate-buffered saline to a concentration of 4 mg. per ml. Each of the fractions was then tested for AEF activity.

**AEF Solubilization.** Spleens and livers used for the solubilization of AEF were obtained from CBA retired breeders which had received 15 azocasein injections (0.5 ml. of a 7 per cent solution) subcutaneously once daily, Monday to Friday. These spleens and livers were used immediately or frozen at  $-20^\circ \text{C}$ . and used when necessary. AEF was extracted with 8 ml. of 0.5 M KCl, or 4 M glycerol, 10 mM Tris-HCl, pH 7.5, per gram of spleen. Four milliliters of extractant was used per gram of liver. The tissues were homogenized in Potter-Elvehjem vessels, shaken for 1 hour at  $4^\circ \text{C}$ ., and then centrifuged at  $250,000 \times g$  for 1 hour at  $4^\circ \text{C}$ . The supernatants were harvested and extensively dialyzed against phosphate-buffered saline.

Where the supernatant from glycerol extracts was fractionated, 5 to 7.5 ml. were applied directly to either a  $2.6 \times 100\text{-cm.}$  or a  $2.6 \times 200\text{-cm.}$  Sepharose 4B column previously equilibrated in 4 M glycerol, 10 mM Tris-HCl, pH 7.5. The eluant was monitored at 280 nm., and the individual fractions, comprising the various peaks, were pooled and concentrated using an Amicon pressure dialysis cell and a PM 10 membrane. Prior to injection the fractions were extensively dialyzed against phosphate-buffered saline. All operations were at  $4^\circ \text{C}$ .

Protein determinations were performed using the BioRad protein assay kit and bovine serum albumin as the standard.

**AEF Administration.** Unless otherwise indicated, AEF, either crude or partially purified, was always administered intravenously with prior sonification. In the vast majority of cases, AEF was given immediately before the subcutaneous inflammatory stimulus (either azocasein or  $\text{AgNO}_3$ ). In a few experiments the AEF preceded the inflammatory stimulus by varying periods of time, and in some experiments it followed the inflammatory stimulus by 24 hours.

## LIGHT AND ELECTRON MICROSCOPIC LOCALIZATION OF AEF-CONTAINING PARTICULATES AFTER INJECTION

A microsomal pellet from liver possessing AEF activity was prepared and labeled by reductive methylation using formaldehyde and  $\text{NaB}^3\text{H}_4$  (New England Nuclear) as described previously (19). After the chemical manipulation, the microsomal preparation was extensively washed in phosphate-buffered saline and the activity was again monitored. No loss of activity occurred. After the intravenous injection of 1 mg. of labeled material the animals were sacrificed 2 minutes later, and portions of liver and spleen were prepared for light and electron microscopic autoradiography by a modification of the method of Ludwin (23).

Tissues for light microscopic autoradiography were fixed in formalin, embedded in paraffin, sectioned at 6  $\mu\text{m.}$ , deparaffinized, and dipped in Kodak NT B-3 emulsion. After 2 to 4 weeks the slides were developed in Microdol and fixed in 24 per cent sodium thiosulfate. The sections were then stained with hematoxylin and eosin by the method of Kopriwa and Leblond (21).

Tissues for electron microscopic autoradiography were prepared by the method of Kopriwa (20). These were fixed in glutaraldehyde, embedded in Epon, the sections placed on celloidin-coated slides, and dipped in Ilford L4 emulsion. After 5 months they were developed in Kodak D-19 developer, fixed in 24 per cent sodium thiosulfate, and rinsed. The sections were transferred to grids, stained with uranyl acetate, and examined with a Hitachi H500 electron microscope.

## ELECTROPHORESIS

Electrophoresis was performed in 5 per cent polyacrylamide gels as described previously (14), except that all materials were dissolved in 4 M glycerol, 10 mM Tris-HCl, pH 7.5. Gels were stained with 0.25 per cent Amido black in 7 per cent acetic acid and destained electrophoretically.

## TISSUE PREPARATION AND AMYLOID QUANTITATION

Spleens were fixed in 10 per cent buffered formalin, embedded in paraffin, sectioned at 6  $\mu\text{m.}$ , and stained by the alkaline Congo red method (25). Under crossed polars the area of visible amyloid (red-green birefringent zones) was measured by morphometric analysis using a radicle in one of the eyepieces of a microscope and the point count technique of Weibel, Kistler, and Scherle (31). Each group contained at least three spleens, and three fields were examined per spleen, 120 points per field. The results are expressed as the percentage of sectional area covered by amyloid.

## PREPARATION OF AZOCASEIN

This was prepared as described previously (10), and 0.5 ml. of a 7 per cent solution was used for subcutaneous injection.

## SILVER NITRATE

A 2 per cent solution was prepared using doubly distilled and deionized water, and 0.5 ml. was used for subcutaneous injection.

Iso  
S  
bee  
10  
ser  
buf  
hot  
buf  
abs  
Seq  
yle  
tra  
(24  
AN  
wh  
tio  
in  
Fre  
ma  
foll  
IM  
S  
SA  
ant  
3 n  
hou  
cha  
QU  
I  
180  
in  
ing  
we  
of  
coc  
Ve  
foll  
sie  
qu  
I  
in  
azo  
hot  
wa  
15)  
pre  
fra  
I  
liv  
sul  
(m  
sor  
ses  
ob  
of  
act

ON OF  
TIONctivity  
using  
ar) as  
ipula-  
ashed  
again  
he in-  
al the  
ons of  
ectron  
of thewere  
d at 6  
emul-  
ed in  
ulfate.  
n andwere  
were  
ctions  
ord L4  
Kodak  
ulfate,  
ained  
H500acryl-  
at all  
s-HCl,  
black  
oreti-ON  
nalin,  
ed by  
olars  
ones)  
idicle  
point  
(31).  
three  
The  
area, and  
eousy dis-  
d for

## ISOLATION OF SAP

SAP was isolated from the serum of mice that had been pretreated with a 0.5-ml. subcutaneous injection of 10 per cent casein 24 hours prior to being bled. The serum was mixed with Sepharose 4B in 0.01 M Tris-buffered saline, 0.002 M calcium chloride, pH 8.0, for 18 hours at 4° C. The mixture was washed with the same buffer until the effluent solution was free of material absorbing at 280 nm. SAP was then eluted from the 4B Sepharose with 0.01 M Tris-buffered saline, 0.01 M ethylenediaminetetraacetic acid (EDTA). SAP was freed of trace contamination by gel filtration on ultragel AcA34 (24).

## ANTIBODY TO MOUSE SAP

Antisera to mouse SAP was prepared in New Zealand white female rabbits by three weekly intradermal injections of 0.1 mg. of mouse SAP which had been dissolved in 0.01 M Tris-buffered saline and emulsified in complete Freund's adjuvant. Three weeks later a fourth intradermal injection was given, and the animal was bled the following week.

## IMMUNODIFFUSION

SAP was identified by double diffusion versus anti-SAP in a gel containing 1 per cent agar. Antigen and antibody wells were approximately 5 mm. apart and were 3 mm. in diameter. The agar plate was incubated for 2 hours at 37° C. and then at room temperature in a moist chamber. Readings were taken at 18 to 24 hours.

## QUANTITATIVE IMMUNOELECTROPHORESIS

Rocket immunoelectrophoresis (22) was performed on 180 × 80-mm. glass plates in a gel of 1 per cent agarose in 0.075 M Veronal buffer, 0.01 M EDTA, pH 8.6, containing 3 per cent rabbit antimouse SAP. Two-millimeter wells were filled with 3  $\mu$ l. of sample along one long side of the plate. Electrophoresis was performed on a water-cooled platform for 6 hours at 200 volts with the same Veronal buffer. The plates were washed in normal saline, followed by water, then dried, and stained with Coomassie blue. A standard curve was prepared using known quantities of purified mouse SAP.

## RESULTS

In a preliminary communication (2) we indicated that, in spleens of animals which had been treated daily with azocasein for 7 to 8 days, AEF activity appeared 24 to 48 hours prior to the appearance of amyloid. The activity was present both in viable and sonicated cells (2, 3, 14, 15). The presence of AEF activity in sonicated cells prompted us to examine whether any particular cell fraction possessed the AEF activity.

Using liver our observations indicated that normal liver did not contain any AEF activity. However, every subcellular fraction of AEF-containing liver examined (microsomes, ribosomes, and membranes devoid of ribosomes), except the 100,000 × g cell supernatant, possessed such activity. These findings, as well as previous observations by others on the diverse cellular distribution of enhancing activity (cf. reference 7), suggest that the active material can associate with particulates in an

indiscriminate fashion. This was tested by incubating fine iron filings with spleen homogenates containing AEF, the filings being recovered with magnets. AEF did indeed associate with the filings, and after intravenous injection the filings were located primarily in the perifollicular area. AEF activity remains associated with these iron filings *in vivo*, since in other experiments we demonstrated that iron filings with AEF could be passaged from one animal to another, retaining their AEF activity. The localization of AEF-containing particulates was also examined by labeling liver microsomes containing AEF activity and subsequently performing autoradiography on sections of liver and spleen. Not surprisingly, the labeled particulates were cleared by Kupffer cells in liver and by cells in the perifollicular region of the spleen. In the spleen, silver grains were not found in lymphocytes but exclusively in the processes of phagocytic cells (Fig. 1).

## ROUTE OF AEF ADMINISTRATION

Since the AEF activity was not demonstrable in the 100,000 × g supernatant fractions (the soluble fractions) but was associated with particulates, the route of administration could be important in determining the presence of such activity. This was borne out by the observation (Table 1) that subcutaneous administration of AEF factor was ineffective. The best route of administration was the intravenous one. An intermediate result was seen on intraperitoneal administration of AEF.

## WHAT COMBINATION OF AEF AND INFLAMMATION IS EFFECTIVE IN PRODUCING AMYLOID?

In the experiments previously described AEF and an inflammatory stimulus (AgNO<sub>3</sub> or azocasein) were administered within minutes of each other. A variety of experiments were also performed to examine the effect of each treatment alone and the temporal relationship that may be necessary for AEF and inflammation to induce amyloid. These may be summarized as follows.

1. Over a 48-hour period an inflammatory stimulus (AgNO<sub>3</sub> or azocasein) of and by itself is insufficient to produce splenic amyloid (Table 2), although it does cause a marked increase in SAA levels (16, 17). Longer periods of inflammation (7 to 10 days) using azocasein or AgNO<sub>3</sub> lead both to splenic amyloid deposition and AEF activity (2).

2. AEF by itself, even after repeated intravenous injections, never induces amyloid, nor does it raise SAA levels (17).

3. AEF may be administered 4 weeks before the inflammatory stimulus with splenic amyloid occurring within 48 hours of the injection of the inflammatory stimulus (data not shown).

4. In the presence of an elevated level of SAA, previously induced by an AgNO<sub>3</sub> injection, significant splenic amyloid deposition occurs within 48 hours of the administration of AEF (Table 2).

## EXTRACTION AND PURIFICATION OF AEF

The studies already described as well as our preliminary results demonstrating that AEF is likely to be a protein (1, 2) were done with crude material (sonicated



FIG. 1. Electron microscopic autoradiograph of spleen after administration of labeled AEF containing microsomes showing grains (ar-

rows) in a process of phagocytic cell. Centrally placed lymphocyte is devoid of grains.  $\times 15,900$ .

TABLE 1. ROUTE OF ADMINISTRATION OF AMYLOID-ENHANCING FACTOR<sup>a</sup>

|                           | Sectional area covered by amyloid |     |
|---------------------------|-----------------------------------|-----|
|                           | %                                 |     |
| Subcutaneous (over thigh) | 0                                 | (3) |
| Intraperitoneal           | $10.8 \pm 0.5$                    | (3) |
| Intravenous               | $20.5 \pm 2.1$                    | (3) |

<sup>a</sup> Animals received AEF ( $25 \times 10^6$  sonicated spleen cells) by various routes, followed immediately by a daily dose of azocasein, 0.5 ml. of a 7 per cent solution for 2 days. The animals were killed 48 hours after the AEF and the spleens assessed for amyloid. The results are the means  $\pm$  S.E. of the number of animals in parentheses.

spleen cells or postmitochondrial supernatant from homogenized liver). More satisfying and precise results can only be obtained with a purified AEF preparation. High concentrations of KCl (0.5 M) or 4 M glycerol were found

TABLE 2. EFFECT OF AMYLOID-ENHANCING FACTOR ON SPLENIC AMYLOID DEPOSITION IN ANIMALS WITH A PREVIOUSLY ESTABLISHED ACUTE INFLAMMATORY REACTION<sup>a</sup>

| Group                               | Sectional area covered by amyloid |     |
|-------------------------------------|-----------------------------------|-----|
|                                     | %                                 |     |
| 1. AgNO <sub>3</sub>                | 0                                 | (3) |
| 2. AEF alone                        | 0                                 | (3) |
| 3. AgNO <sub>3</sub> + AEF (24 hr.) | $0.1 \pm 0.1$                     | (3) |
| 4. AgNO <sub>3</sub> + AEF (48 hr.) | $14.0 \pm 2.7$                    | (3) |

<sup>a</sup> Group 1 received AgNO<sub>3</sub> (0.5 ml. of a 2 per cent solution) subcutaneously and was sacrificed 48 hours later; group 2 received AEF as  $25 \times 10^6$  sonicated spleen cells and was sacrificed 48 hours later; group 3 received AgNO<sub>3</sub>, as group 1, followed 24 hours later by AEF. The animals were sacrificed 24 hours after receiving AEF; group 4 received AgNO<sub>3</sub>, as groups 1 and 3, followed 24 hours later by AEF. The animals were sacrificed 48 hours after the AEF. The results are the means  $\pm$  S.E. of the number of animals in parentheses.

to be  
erol  
tion  
liver  
by K  
clear  
speci  
since  
purifi  
tions  
main  
the  
peak  
glyce  
Peak  
glyce  
hem  
lecul  
the  
were  
indic  
Gl  
cont.  
resis  
glyce  
diffe  
pres  
pres  
sent  
the  
band  
poly  
activ

% Sectional Area Covered by Amyloid

FIG.  
peak  
extra

to be effective in solubilizing the activity, with the glycerol being much more effective than the KCl. For extraction of AEF the spleen proved to be a better source than liver. Dose-response curves of AEF extracted from spleen by KCl, and glycerol, are demonstrated in Figure 2. It is clear that the glycerol-extracted material has a higher specific activity than that attained with KCl. We have since focused on the glycerol extract for our subsequent purification. Material extracted in glycerol when fractionated on Sepharose 4B column provided us with five main protein peaks (Fig. 3). Peak 2, Figure 3, had by far the highest specific activity (Table 3). The activity of peak 2 plotted in relation to the activities of whole glycerol and KCl extracts is also indicated in Figure 2. Peak 2 activity is much higher than equivalent doses of glycerol or KCl extracts. Peak 4 is endogenous splenic hemoglobin with a molecular weight of 68,000. The molecular weight exclusion of Sepharose 4B in glycerol is of the order of  $1 \times 10^6$ . Although molecular weight markers were not used to calibrate this column the results clearly indicate a high molecular weight for the active fraction.

Glycerol-extracted material from normal and AEF-containing spleens was also subjected to disc electrophoresis in 5 per cent polyacrylamide gels containing 4 M glycerol. The electrophoretic patterns (Fig. 4) showed a difference in the slowly migrating region. A protein band present in the AEF preparation (Fig. 4, arrow) was not present in the normal extract. This protein band represented the major component in peak 2, the fraction with the highest AEF activity. Elution of the identical protein band indicated in Figure 4, from a scaled-up 5 per cent polyacrylamide slab gel, provided a protein with AEF activity.

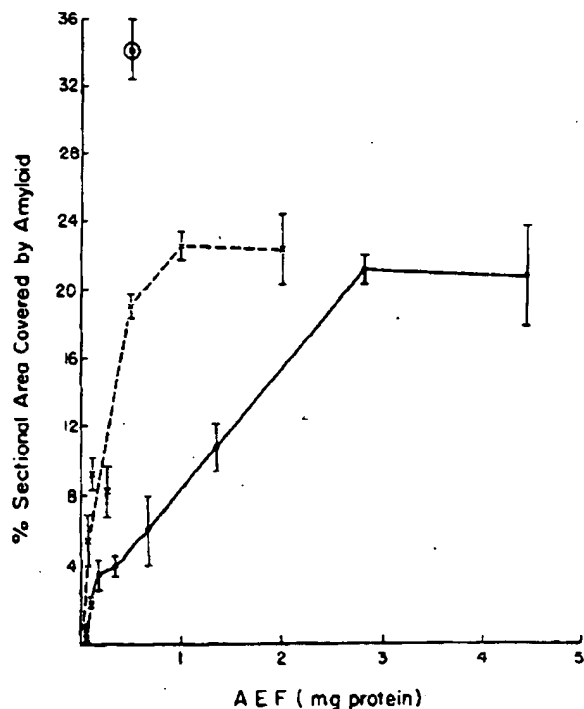


FIG. 2. Dose-response curves of AEF extracted with 0.5 M KCl (●—●) and 4 M glycerol (x—x). ○ represents activity of 500 µg. of peak 2 obtained from a Sepharose 4B fractionation of 4 M glycerol extract (see Fig. 3). Note increasing specific activity.

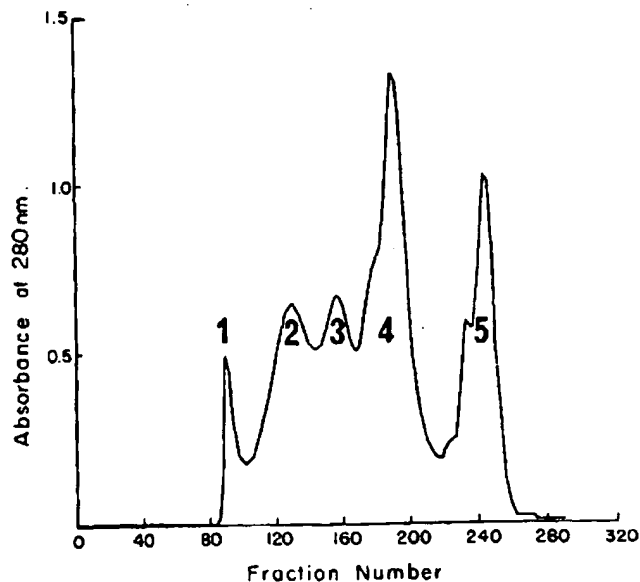


FIG. 3. Sepharose 4B fractionation of 4 M glycerol, 10 mM Tris HCl, pH 7.5, extract of AEF-containing spleens. Seven milliliters of extract were applied to a 2.6 × 200-cm. Sepharose 4B column previously equilibrated in the glycerol buffer. Peaks (1 to 5) are numbered from the left. Peak 4 is hemoglobin, molecular weight 68,000. Most AEF activity is present in Peak 2.

TABLE 3. AMYLOID-ENHANCING FACTOR ACTIVITY IN 500 µg. OF PROTEIN FROM PEAKS OF AMYLOID-ENHANCING FACTOR SEPARATED BY SEPHAROSE 4B CHROMATOGRAPHY<sup>a</sup>

| Peak | Sectional area covered by amyloid % |     |
|------|-------------------------------------|-----|
| 1    | 19.3 ± 3.3                          | (9) |
| 2    | 31.4 ± 3.1                          | (8) |
| 3    | 14.4 ± 1.9                          | (9) |
| 4    | 0                                   | (9) |
| 5    | 0                                   | (9) |

<sup>a</sup> The fractions constituting each of the peaks in Figure 3 were pooled, concentrated, and dialyzed extensively against phosphate-buffered saline. Five hundred micrograms of protein from each peak were administered intravenously as AEF, followed by a single subcutaneous injection of AgNO<sub>3</sub>, 0.5 ml. of a 2 per cent solution. The animals were killed 48 hours later and the spleens assessed for amyloid deposition. The results are the means ± S.E. of the number of animals in parentheses.

#### RELATIONSHIP OF AEF TO AA AND SAP

The glycerol AEF extracts previously described were obtained from spleens that have AA deposits. Although we have shown that AEF activity in spleen appears prior to the morphologic demonstration of AA deposits (2), it was still possible that submicroscopic or dissolved quantities of AA could have been present in these preparations. After intravenous injection it can be argued that this AA would provide a nidus in the recipient's spleen for further AA deposition.

For these reasons AEF glycerol extracts were examined for AA cross-reactive material. Neither glycerol extracts from liver (performed by M. Pepys) nor those from spleen possessed such cross-reactive proteins as assessed by immunodiffusion.



For the reasons mentioned a further possibility that had to be considered was that AEF represented the SAP protein, a protein found in association with amyloid. As can be seen from the double immunodiffusion (Fig. 5), splenic glycerol extracts possess large quantities of SAP. Similar observations have been made with liver glycerol extracts (performed by M. Pepys). However, after fractionation of the splenic glycerol extracts on Sepharose 4B columns, it became apparent that the AEF activity could be dissociated from the peak containing the bulk of the SAP (Tables 3 and 4). Further, using antibodies directed against SAP and immunoperoxidase staining, we were not able to demonstrate SAP in tissue until the amyloid (AA in type) was actually deposited itself. This confirms similar observations made by Baltz, Dyck, and Pepys (4). SAP and AA seem to be deposited in the

TABLE 4. QUANTITY OF SERUM AMYLOID P IN VARIOUS PEAKS OF AMYLOID-ENHANCING FACTOR SEPARATED BY SEPHAROSE 4B CHROMATOGRAPHY<sup>a</sup>

| Sample peaks | Height of reaction |
|--------------|--------------------|
|              | mm.                |
| 1            | 4.9                |
| 2            | 3.1                |
| 3            | 15.3               |
| 4            | 2.6                |
| 5            | 0                  |

<sup>a</sup> The four fractions constituting the tops of each peak in Figure 3 were pooled and assessed for SAP content using rocket immunoelectrophoresis. The data represent the mean height of the precipitin lines from duplicate samples.



FIG. 4. Electrophoresis of 4 M glycerol extracts from (A) normal spleens, (B) AEF-containing spleens, (C) peak 2, Figure 3. Arrow indicates band with AEF activity.

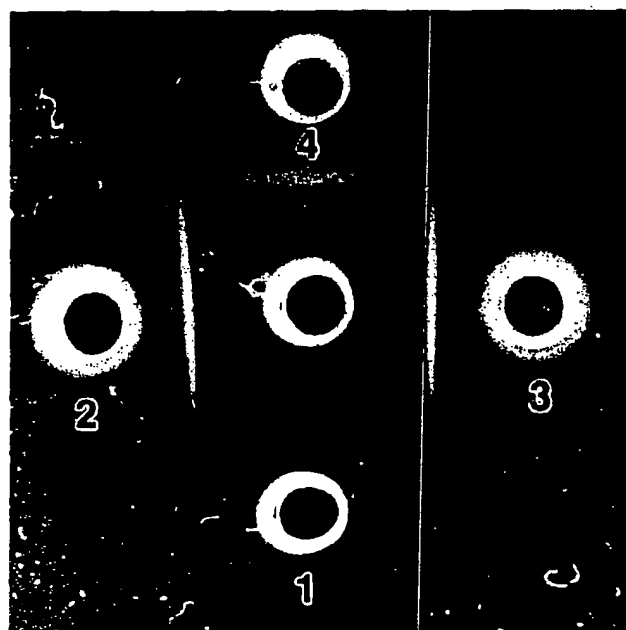


FIG. 5. Immunodiffusion of glycerol-extracted AEF versus anti-SAP (center well). Well 1, glycerol extract of normal spleen; Wells 2 and 3, glycerol extracts of AEF-containing spleen; and Well 4, purified SAP.

tissues at approximately the same time, whereas AEF activity appears in the spleen prior to either of these two components (2). Neither purified human tissue SAP, purified mouse serum SAP, nor purified mouse AA possess AEF activity.

## DISCUSSION

Our initial interest in the AEF stemmed from our observation that spleen cells derived from amyloidotic animals when transferred to isogeneic recipients would allow the recipients to deposit amyloid in 48 hours, but only if an inflammatory reaction was provoked in these animals (3, 15, 17). While trying to show that AEF was dependent upon cellular functions, experiments were also performed with sonicated spleen cells. Much to our surprise, in the presence of an inflammatory reaction these sonicated cells functioned quite as well as the intact cells themselves (2, 15, 17). We concluded that a cellular component, rather than the metabolic activity of the transferred cells, was responsible for AEF activity. We were also able to demonstrate by enzymatic inactivation that AEF is a protein (1, 2). Further, with a constant dose of AEF the amount of amyloid deposition in the spleen in 48 hours was dependent upon the intensity of the inflammatory stimulus (15). Conversely, when a constant inflammatory stimulus was used, the amount of amyloid deposited in 48 hours varied as a function of the dose of AEF (2). With longer periods of azocasein administration (10 to 15 days), one could demonstrate AEF activity not only in the spleen but also in liver and bone marrow.

Our definition of AEF activity in previous reports (1, 2, 3, 15, 17) and in the present communication is a functional one. AEF is a transferable activity which in CBA/J mice reduces the induction time of splenic amy-

loid de-  
copy.  
marke  
sition  
AE  
prior  
sibilit  
tial re  
amylo  
amylo  
neces  
shown  
depos  
in AE  
recipi  
devel

It is  
of the  
Teilu  
activi  
as do  
perio  
areas  
hydra  
appea  
solub  
ones  
as ac  
tion i  
origi  
these  
favor  
numl  
tive i  
ing A  
emph  
gene

Af  
cellu  
ticul  
enat  
prob  
nent  
the  
have  
nent  
Not  
nent  
origi  
quer  
prol  
anal  
prot  
is a  
this

A  
4 M  
org  
mec  
acti  
four  
mai

loid deposition to 48 hours, as visualized by light microscopy. The striking feature of AEF activity is its ability to markedly decrease the induction time of amyloid deposition in CBA/J mice.

AEF appears in the donors approximately 48 hours prior to the amyloid (2). This raises the interesting possibilities that (1) AEF plays a crucial and perhaps essential role in the development of inflammation-associated amyloid, and (2) the lag phase, which is always seen in amyloid induction protocols, may represent the time necessary for the appearance of this factor. As we have shown (2, 13) once AEF is present in the spleen, amyloid deposition progresses rapidly and with the same kinetics in AEF donors and recipients. The rapid response of the recipients probably occurs because the lag phase for AEF development has been bypassed.

It is tempting to speculate that AEF is the culmination of the first phase of amyloid deposition as described by Teilum (29) and others (7). The appearance of AEF activity precedes AA deposition in much the same way as does the histologic appearance of pyroninophilic and periodic acid-Schiff-positive cells in the perifollicular areas of spleen (6, 29, 30). This indicates that a carbohydrate-containing substance is seen in cells prior to the appearance of AA. In this regard the glycerol and KCl solubilization techniques used for AEF extraction are ones used for extraction of lysosomal glycoproteins, such as acid phosphatase (8). Whether this temporal association is simply fortuitous or of significance in the cellular origin of AEF remains to be determined. In recent years, these perifollicular cells have been largely ignored in favor of the splenic lymphocytes. The increase in the number of periodic acid-Schiff-positive cells with repetitive inflammatory stimulation (30), as well as the increasing AEF activity with such stimulation (2), suggests that emphasis should be placed on these cell types in the genesis of AEF.

After disruption of AEF-containing liver various intracellular organelles possess AEF activity. Exogenous particulates (e.g., iron filings) when added to spleen homogenates also acquire AEF activity. Disruption of the liver probably allows the AEF to associate with cell components it does not usually encounter. This likely explains the previous findings of others in which transfer activities have been associated with many different cell components and macromolecular complexes (cf. reference 7). Not until antibodies can be raised to the active component are we likely to determine the cell and organelle of origin by immunohistochemical techniques. The subsequent distribution of this material in the animal receiving prolonged inflammatory stimuli will also be amenable to analysis. The localization of AEF activity to a specific protein band in the 4 M glycerol acrylamide gels (Fig. 4) is a first step in providing us with the necessary tools for this immunohistochemical localization.

AEF can be extracted in a soluble form in 0.5 M KCl or 4 M glycerol. For injection purposes removal of the KCl or glycerol by dialysis and its replacement by physiologic media invariably results in the precipitation of AEF activity. In crude cell homogenates AEF is also always found as a particulate. We feel this may indicate the manner in which AEF exists *in vivo*. The observation of

others (5) of necrosis of periodic acid-Schiff-positive and pyroninophilic cells in the perifollicular area with the consequent phagocytosis of cellular particulates would be the *in vivo* counterpart to the clearing of AEF from the circulation after its intravenous injection. If so, this localization would play a significant role in determining the initial anatomical distribution of amyloid in the spleen.

It should be emphasized that AEF is not likely to be a new and unnatural cellular component. AEF is probably a quantitative change in a normal cellular constituent. Using intact spleen cells we have observed that  $1 \times 10^8$  normal cells can reduce the amyloid induction time in CBA/J mice to approximately 4 days (3). An equivalent result can be obtained from  $2 \times 10^4$  cells from amyloidotic animals. If this ratio of cells is a true reflection of the quantitative difference of the active component, one is dealing with a 5000-fold increase in AEF in the amyloidotic animals.

Our initial observations with AEF were made with crude cellular preparations from spleen that contained both AA and SAP, a protein found in association with AA. Either of these could have been responsible for the AEF activity. There is little, if any, soluble AA in the glycerol preparation, as determined by immunodiffusion, and purified AA does not have AEF activity. It is also highly unlikely that amyloid fibrils are present in the glycerol extract as the extract is centrifuged at high gravitational forces ( $250,000 \times g$ ) for fairly long periods of time. Any fibrils would be pelleted under such conditions. For these reasons we feel that AEF is not AA that has been cleared by the recipient's spleen and that subsequently serves as a nidus for further AA deposition.

The role of SAP in relation to AEF activity cannot be answered conclusively. We can dissociate most of the AEF activity from the bulk of the SAP (Tables 3 and 4), although each fraction that possesses AEF activity also possesses SAP. Further, pure human or mouse SAP does not have AEF activity. Although it seems that pure SAP is not the AEF, one is still left with the possibility that SAP is associated with other proteins in the form of a macromolecular complex. Against this possibility is the observation that AEF activity appears in the spleen prior to SAP (2, 4). It should be possible to subject the active protein band from the 4 M glycerol acrylamide gels to sodium dodecyl sulfate gel electrophoresis to determine whether this band consists of a single large polypeptide, multiple subunits of one polypeptide, or a complex of several different polypeptides of which SAP is a constituent.

The occurrence of AEF and its effect on amyloid deposition raises many other questions. (1) Does AEF represent the recently described inducer of SAA (27)? This is unlikely because AEF is not soluble in physiologic solutions, whereas the SAA inducer apparently is; AEF appears late in the course of the usual induction protocols (5 to 6 days), whereas SAA appears early (hours); and when AEF is administered intravenously it does not lead to an increase in circulating SAA (17). Thus, although inflammation is apparently responsible for the appearance of both AEF and SAA, they are not related in an obvious, causal manner. In addition, recent evidence

i-SAP  
and 3,  
SAP.

AEF  
two  
SAP,  
pos-

our  
dotic  
ould  
, but  
, these  
' was  
' also  
' sur-  
these  
cells  
lular  
f the  
' We  
ation  
stant  
the  
ty of  
cont-  
nt of  
f the  
imin-  
AEF  
bone

ts (1,  
is a  
ch in  
amy-



suggests that the SAA inducer is interleukin I (28). (2) Is AEF peculiar to the CBA/J strain? Previous work involving transfer factors has been done with strains other than CBA/J mice (e.g., C3H and C57B1 (cf. reference 7)), although all of our experience has been with the CBA strain. A similar factor has been noted in A/J mice (32). Whether these factors are identical or simply similar in end result remains to be determined. But, clearly, strains other than CBA possess "enhancing factors." (3) Is the variable strain and species susceptibility to AA deposition related to genetically different AEFs or the manner in which AEF is handled metabolically? We have had no experience in this regard. Cross-strain experiments in which AEF derived from CBA/J mice was used in A/J recipients were only marginally effective in inducing rapid amyloid deposition. CBA/J AEF given to C3H/HeJ mice is very effective (R. Kisilevsky, unpublished data). (4) What role does AEF play normally? This will not be answered until its cell of origin is determined.

The significance of our observations lie not only with the reduced induction time but also with the extreme reproducibility and synchrony that AEF confers on the model being used. Virtually 100 per cent of the animals respond positively, and the quantity of the amyloid deposited and its kinetics vary little in replicate experiments. Such a model should be particularly useful in examining various aspects of AA deposition, for example doing precursor-product studies. AA deposition is reduced to a specific period of 24 hours (the second 24 hours), whereas the usual protocols require 7 to 10 days. The appearance of AEF, its effect on the induction of amyloid, and the kinetics of AA deposition would tie together many features of the first and second phases of this deposition.

**Acknowledgments:** We wish to thank Dr. M. B. Pepys, Immunological Medicine Unit, Royal Postgraduate Medical School, Hammersmith Hospital, London, England, for assaying our liver glycerol extracts for AA and SAP.

Date of acceptance: March 8, 1982.

This work was supported by grants from the Medical Research Council of Canada (MT-3153) and from the United States Public Health Service, National Institute of Arthritis, Metabolism, and Digestive Diseases (AM 04599 and AM 07014), National Institute of Health Multipurpose Arthritis Center (AM 20613), from the General Clinical Research Centers Branch of the Divisions of Research Resources, National Institute of Health (RR 533), from the Massachusetts chapter of the Arthritis Foundation, and from the Arthritis Foundation.

Address reprint requests to: R. Kisilevsky, M.D., Department of Pathology, Queen's University, Kingston, Ontario, Canada K7L 3N6.

#### REFERENCES

1. Axelrad MA, Kisilevsky R: Biological characterization of amyloid enhancing factor (abstr). *Proc Can Fed Biol Soc* 21:122, 1978
2. Axelrad MA, Kisilevsky R: Biological characterization of amyloid enhancing factor. In *Amyloid and Amyloidosis*. Proceedings of the Third Symposium on Amyloidosis, Povia de Varzim, Portugal, 1979, edited by Glenner GC, Costa PP, deFreitas AF, pp 527-533. Amsterdam, Excerpta Medica, 1980
3. Axelrad M, Kisilevsky R, Beswetherick S: Acceleration of amyloidosis by syngeneic spleen cells from normal donors. *Am J Pathol* 78:277, 1975
4. Baltz ML, Dyck RF, Pepys MB: Amyloid P-component in mice injected with casein: identification in amyloid deposits and in cytoplasm of hepatocytes. *Immunology* 41:59, 1980
5. Claesson MH, Hardt F: Quantitative studies on the decay of lymphoid cells during the development of casein-induced immune amyloidosis. *Acta Pathol Microbiol Scand (A)* 80:125, 1972
6. Druet RL, Janigan DT: Experimental amyloidosis: rates of induction, lymphocytes depletion and thymic atrophy. *Am J Pathol* 49:911, 1966
7. Hardt F, Ranlov P: Transfer amyloidosis. *Int Rev Exp Pathol* 16:273, 1976
8. Jacobs FA, Flynn TG, Clarke AF: Characterization of separated prostatic acid phosphatase forms in normal and castrated rats. *Mol Cell Endocrinol* 18:177, 1980
9. Janigan DT: Pathogenetic mechanisms in protein-induced amyloidosis. *Am J Pathol* 55:379, 1969
10. Janigan DT, Druet RL: Experimental amyloidosis: role of antigenicity and rapid induction. *Am J Pathol* 48:1013, 1966
11. Keizman I, Rimon A, Sohar E, Gafni J: Amyloid accelerating factor. *Acta Pathol Microbiol Scand (A)* 233:172-177, 1972
12. Kisilevsky R: The regulatory parameter of protein synthesis most affected by ethionine and cycloheximide: a comparison of computer and *in-vivo* studies. *Biochim Biophys Acta* 272:463, 1972
13. Kisilevsky R: Accelerated amyloid deposition: the effect of DMSO or colchicine treatment (abstr). *Lab Invest* 44:34, 1981
14. Kisilevsky R, Axelrad M, Brunet S, Richards M: Effects of amyloid induction on plasma protein turnover, and its implications. *Am J Pathol* 83:299, 1976
15. Kisilevsky R, Axelrad M, Corbett W, Brunet S, Scott F: The role of inflammatory cells in the pathogenesis of amyloidosis. *Lab Invest* 37:544, 1977
16. Kisilevsky R, Benson MD: SAA induction does not require the spleen. *Lab Invest* 44:84, 1981
17. Kisilevsky R, Benson MD, Axelrad MA, Boudreau L: The effect of a liver protein synthesis inhibitor on plasma SAA levels in a model of accelerated amyloid deposition. *Lab Invest* 41:206, 1979
18. Kisilevsky R, Skinozuka H, Bennedetti EL, Shull KH, Farber E: Ribosomal alterations following ethionine intoxication. *Lab Invest* 28:8, 1973
19. Kisilevsky R, Weiler L, Treloar MA: An analysis of alterations in ribosomal conformation using reductive methylation. *J Biol Chem* 253:7101, 1978
20. Kopriwa BM: A reliable, standardized method for ultrastructural electron microscopic radioautography. *Histochemie* 37:1, 1973
21. Kopriwa BM, Leblond CP: Improvements in the coating technique of radioautography. *J Histochem Cytochem* 10:269, 1962
22. Laurell CB: Quantitative estimation of proteins by electrophoresis in agarose gel containing antibodies. *Anal Biochem* 15:45, 1966
23. Ludwin SK: An autoradiographic study of cellular proliferation in remyelination of the central nervous system. *Am J Pathol* 95:683, 1979
24. Pepys MB, Dash AC, Munn EA, Feinstein A, Skinner M, Cohen AS, Gewurz H, Osmand AP, Painter RH: Isolation of amyloid P-component (protein AP) from normal serum as a calcium dependent binding protein. *Lancet* 1:1029, 1977
25. Puchtler H, Sweat F, Levine M: On the binding of Congo red by amyloid. *J Histochem Cytochem* 10:355, 1962
26. Rolleston FS: The binding of ribosomal subunits to endoplasmic reticulum membranes. *Biochem J* 129:721, 1972
27. Selinger MJ, McAdam KPWJ, Kaplan MM, Sipe JD, Vogel SN, Rosenstreich DL: Monokine-induced synthesis of serum amyloid A protein by hepatocytes. *Nature* 285:489, 1980
28. Szein MB, Vogel SN, Sipe JD, Murphy PA, Mizel SB, Oppenheim J, Rosenstreich DL: The role of macrophages in the acute-phase response: SAA inducer is closely related to lymphocyte activating factor and endogenous pyrogen. *Cell Immunol* 63:164, 1981
29. Teilum G: Studies on pathogenesis of amyloidosis. II. Effect of nitrogen mustard in inducing amyloidosis. *J Lab Clin Med* 43:367, 1954
30. Teilum G: Periodic acid-schiff-positive reticulo-endothelial cells producing glycoprotein. *Am J Pathol* 32:945, 1956
31. Weibel ER, Kistler GS, Scherle WF: Practical stereological methods for morphometric cytology. *J Cell Biol* 30:23, 1966
32. Wohlgethan JR, Cathcart ES: Amyloid resistance in A/J mice: studies with a transfer model. *Lab Invest* 42:663, 1980



Volume 36 • Number 4 • April 1977

LAINAW 36 (4) 363-484 (1977)



EDITOR

Robert H. Hepinstall

ASSOCIATE EDITOR

John K. Bolanoff

EDITORIAL BOARD

Murray R. Abell

Rosario L. Basterga

Sergio A. Bencosme

Earl P. Benditt

Ellis S. Benson

Oranwood Bowden

Peter M. Burkholder

Jacob Churg

Ramzi S. Cotran

Harlan I. Firlinger

Peter J. Goldblatt

Joseph Graham

Rolla B. Hill, Jr.

Grover M. Hutchins

Robert B. Jennings

Nathan Kaufman

Jerome Klicavans

Gordon K. Klattworth

Charles Kahn, III

David Lagnoff

Peter W. Lampert

Robert J. Lukes

Vincent T. Marchesi

N. Scott McNutt

M. James Phillips

C. Barry Pierce

Coarad L. Pirani

Lynne M. Reid

William C. Roberts

David M. Robertson

Emanuel Rubin

Dante G. Scarpelli

Theodor K. Shukla

Samuel S. Spicer

Donald J. Srobooda

Robert D. Terry

Benjamin F. Trump

Emil R. Unanue

John H. Yardley

# A JOURNAL OF PATHOLOGY

The Williams & Wilkins Company BALTIMORE, MD.

NOTICE: THIS MATERIAL MAY BE PROTECTED  
BY COPYRIGHT LAW (TITLE 17 U.S. CODE)

LABORATORY INVESTIGATION  
Copyright © 1977 by the International Academy of Pathology

Vol. 36, No. 4, p. 420, 1977  
Printed in U.S.A.

# Murine Amyloid Protein AA in Casein-Induced Experimental Amyloidosis

MARTHA SKINNER, M.D., TSURANOBU SHIRAHAMA, M.D., MERRILL D. BENSON, M.D., AND  
ALAN S. COHEN, M.D.

*Arthritis and Connective Tissue Disease Section, Evans Department of Clinical Research,  
University Hospital, and the Thorndike Memorial Laboratory and Division of Medicine, Boston  
City Hospital, Boston, Massachusetts 02118*

Amyloidosis was induced in mice by 25 subcutaneous injections of casein. The splenic amyloid fibrils were identified by electron microscopy to be closely associated with reticular cells. After isolation of the fibrils by simple physical techniques, their ultrastructure revealed single filaments of 80 to 100 Å width, which were rigid, nonbranching, and of indeterminate length. This is comparable to previous studies on human preparations.

The amyloid fibrils were dissociated by solution in guanidine and chromatography. The resultant amyloid fibril protein was characterized as to its molecular weight, amino acid analysis, and amino-terminal sequence. It was thus definitely identified as protein AA, the major component of secondary amyloidosis. An antibody to this protein, murine AA, identified a cross-reacting mouse serum protein SAA and indicated a species specificity when tested against human preparations.

A comparison is made with the AA protein in another murine model as well as AA proteins from human, guinea pig, monkey, and mink amyloidosis.

Additional key words: Amino acid sequence, High resolution microscopy, Serum AA (SAA).

Murine amyloidosis induced by the chronic administration of casein, endotoxin, and other agents has been used as a model for the study of human systemic amyloidosis for many years (2, 6, 7, 10, 11). This model has been presumed to be comparable to secondary amyloidosis which is associated with chronic inflammatory disease. This similarity has not been proven biochemically and thus its use as the definitive model with regard to the pathogenesis of systemic amyloid has been limited. Primary and secondary human amyloid as well as amyloid of animal origin show identical tinctorial properties when examined by light microscopy. By electron microscopy they all appear to be composed of long nonbranching fibrils of approximately 80 to 100 Å in width (23). Amino acid sequence analysis, however, has determined a difference between the components of human primary and secondary amyloid fibrils. Primary fibrils have been found to be homologous to variable segments of immunoglobulin light chains whereas secondary fibrils are composed of a substance called protein AA which has a unique amino acid sequence (3, 9, 14, 16). In addition, a serum protein SAA, immunologically cross-reactive with protein AA, has been found in the sera of all normal and amyloidotic humans and animals (1, 4, 18, 21, 25). Normal sera have SAA in minute quantities whereas sera from amyloidotic persons or those with inflammatory diseases have elevated levels.

Our report provides a detailed morphologic study of casein-induced murine amyloid with chemical and immunologic analyses of the isolated fibril protein. The N-terminal sequence identifies it as a secondary or protein AA type of amyloid. It is compared to the human AA, guinea pig AA, monkey AA, a mouse AA induced by *Candida albicans*, and the amyloid fibrils of spontaneous mouse amyloid. Its relationship to a murine SAA precursor is discussed.

## MATERIALS AND METHODS

### INDUCTION OF AMYLOID

Amyloidosis was induced in 20 CBA/J mice (Jackson Laboratories, Bar Harbor, Maine) by daily subcutaneous injections of 0.5 ml. of 10 per cent casein for 5 weeks. Small portions of their spleens and livers were prepared for light and electron microscopy and the remaining portions were frozen at -20° C. for further study.

### ISOLATION OF AMYLOID FIBRILS

A modification in the isolation procedure of Pras *et al.* (20) was used as follows. The amyloidotic spleens were pooled and homogenized in 200 ml. of normal saline in a blender at low speed for 10 seconds. The mixture was centrifuged at 15,000 r.p.m. 4° C. for 30 minutes. The

supernatant was decanted and the sediment was rehomogenized with fresh saline and centrifuged in the same manner. This procedure was repeated 10 to 15 times until the tissue was free of soluble components as determined by an optical density of the supernatant solution of less than 0.1 at 280 nm. The sediment was then homogenized in 200 ml. of deionized water in the same manner followed by centrifugation at 15,000 r.p.m. 4° C. for 1 hour. The supernatant was saved and the sediment rehomogenized in 200-ml. aliquots of deionized water and centrifuged two more times in the same manner. The sediment remaining after the third wash was rehomogenized in 100 ml. of deionized water and centrifuged at 12,000 r.p.m. 4° C. for 2 hours. Amyloid fibrils which were suspended in the water were recovered from the second, third, and fourth supernatants by lyophilization.

#### LIGHT AND ELECTRON MICROSCOPY

For light microscopy, small pieces of tissue from spleens and livers were examined. Formalin-fixed paraffin sections were stained with Congo red and hematoxylin and examined under conventional and polarized light. For electron microscopy, small pieces of tissue from three spleens and three livers, by random selection, were prepared as follows. Tissues were double-fixed with aldehyde and osmium fixatives, and Epon-embedded thin sections were stained with uranyl acetate and lead citrate and examined in a Siemens-Elmiskop I.

An aliquot of the isolated amyloid fibrils was also prepared for light and electron microscopy. For light microscopy, a drop of water-suspended material was placed on a gelatin-coated microscopic slide, air-dried, fixed with 10 per cent formalin, stained with Congo red and hematoxylin and examined with conventional and polarized light. For electron microscopy, the material was spread on a carbon-coated grid, shadow-casted with platinum-palladium or negatively stained with phosphotungstate or uranyl salt and examined in a Siemens-Elmiskop I electron microscope (23).

#### CHROMATOGRAPHY

Isolated amyloid fibrils were added to 4 M guanidine, pH 7.5, allowed to stand with occasional stirring at 4° C. for 24 hours and centrifuged. The supernatant solution of amyloid fibrils was chromatographed on a 90- by 2.5-cm. G-100 Sephadex column (Pharmacia Fine Chemicals, Inc., Piscataway, New Jersey) in 4 M guanidine, pH 7.5. The chromatographic peaks were dialyzed against distilled water and recovered by lyophilization. The larger retarded peak was dialyzed using Spectrapor no. 8 membrane tubing (Spectrum Medical Industries, Inc., Los Angeles, California).

#### MOLECULAR WEIGHT DETERMINATION

Disc gel electrophoresis was performed in 0.1 per cent sodium dodecyl sulfate, 10 per cent acrylamide, and compared to molecular weight standards: lysozyme (14,000),  $\gamma$ -globulin light chain (23,000) (Schwarz-Mann Corporation, Orangeburg, New York), and pepsin

(35,000) (Worthington Biochemical Corporation, Freehold, New Jersey) (29).

#### AMINO ACID ANALYSIS

Amino acid analyses of the isolated amyloid fibrils and the protein in each peak from the G-100 Sephadex column were performed on a JEOL-5AH analyzer after hydrolysis in 6 N HCl at 110° C. for 20 hours (28).

#### SEQUENCE STUDIES

Five milligrams of murine Peak 3, 700 ml. of *N,N*-dimethyl-*N*-allylamine (Pierce Biochemicals, Rockford, Illinois), 3 mg. of 4-sulfophenylisothiocyanate (Beckman Laboratories, Palo Alto, California), and 70 ml. of tributylamine (Pierce Biochemicals) were reacted according to the procedure of Braunitzer, Schrank, and Ruhfus (5) in the reaction cup of a Beckman 890C sequencer. The sequencing procedure was then carried out according to the method of Edman and Begg (8) using a slow-peptide program (no. 071472 Beckman Laboratories). The phenylthiohydantoin amino acid residues were identified on a Beckman 65 gas chromatograph



FIG. 1. a, Light micrograph of CBA/J mouse spleen after 25 injections of casein. Large amounts of a homogeneous material can be seen around a follicle. b, Identical area viewed under polarizing light. In color the birefringence is of the classic green type. Congo red and hematoxylin;  $\times 100$ .

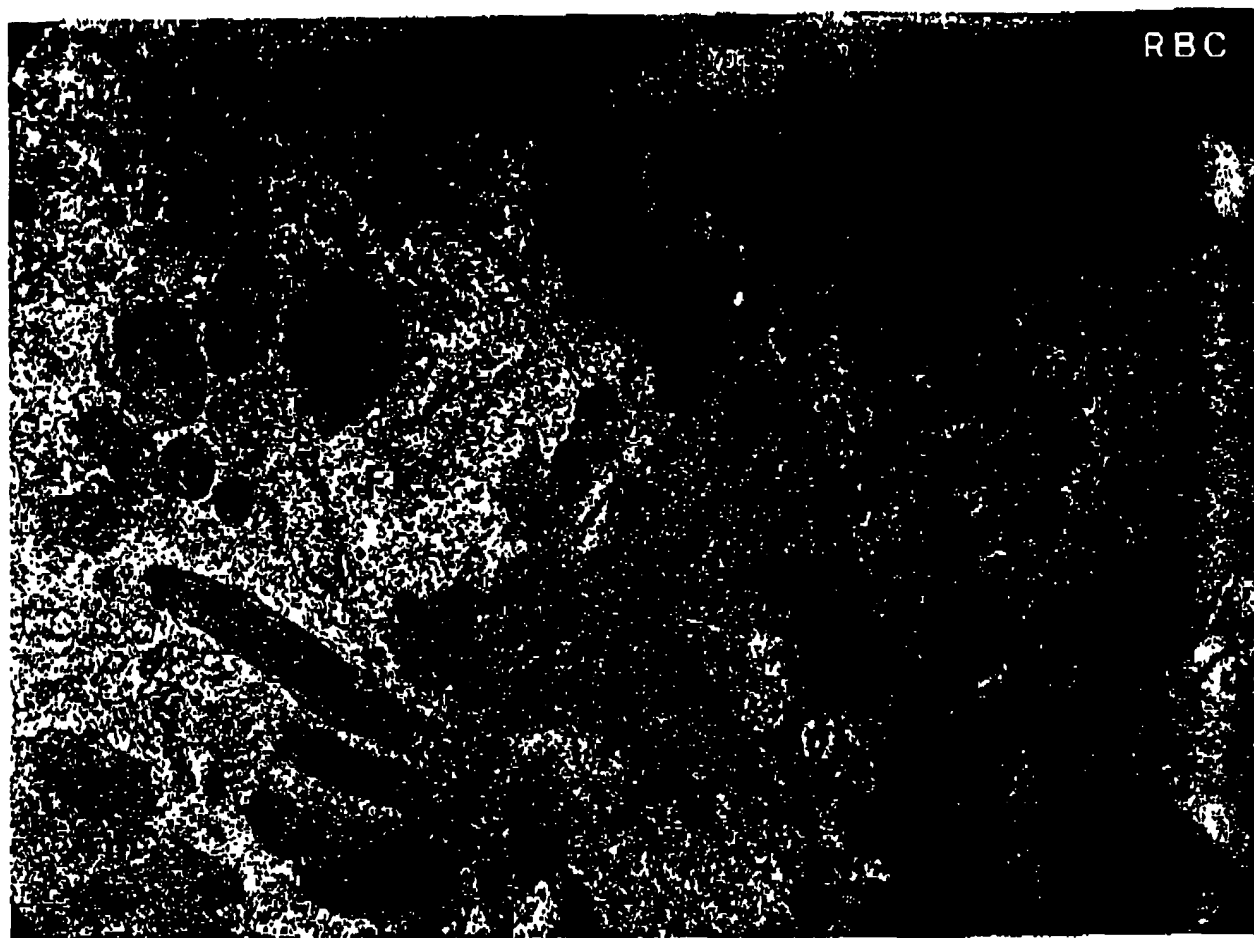


FIG. 2. Electron micrograph of mouse spleen after 25 casein injections. A fixed reticular cell (FRC) is seen; it contains many deep cytoplasmic invaginations (asterisk) in longitudinal or oblique sections and contains bundles of well oriented amyloid fibrils (Am).

Numerous inclusions (I) are also noted. SLRC, Sinus lining reticular cell; Sin, sinus; RBC, red blood cell. (Conventional electron microscopic preparation.) Uranyl acetate and lead citrate;  $\times 10,000$ .

(19). Each phenylthiohydantoin residue after sequence degradation was converted to its free amino acid by hydrolysis in 57 per cent hydriotic acid (Fisher Scientific Company, Pittsburgh, Pennsylvania) at  $125^{\circ}\text{C}$ . for 20 hours and the identity confirmed by amino acid analysis (27).

#### ANTIBODY FORMATION

Antisera were produced in New Zealand White rabbits by the intradermal injection of 0.1 mg. of Peak 3 protein in complete Freund's adjuvant. The animals were boosted with repeat intradermal injections of the same antigen at 4 and 6 weeks and bled 1 week later.

#### IMMUNODIFFUSION

The protein in each peak from the G-100 Sephadex column was tested by double diffusion in agar against antiserum to the Peak 3 protein. In addition, the murine amyloid fractions were tested against anti-human protein AA and human AA was tested against anti-murine Peak 3 protein.

#### RESULTS

At the end of the 25-day injection period the spleen and liver were markedly infiltrated with a homogenous eosinophilic Congo red positive substance by light microscopy (Fig. 1a and b). By electron microscopy, deposits of amyloid fibrils were closely associated with the reticuloendothelial cells (Fig. 2). Deep cytoplasmic invaginations were seen in the cells which contained bundles of well oriented amyloid fibrils. Also, in the cytoplasm of these cells, inclusions were seen which have recently been described and are considered to be the transitional forms between the primary type of dense bodies and the cytoplasmic invaginations containing amyloid fibrils (24).

The amyloid-rich spleens totaling 4.0 gm. in wet weight were pooled for isolation of amyloid fibrils. The wet weight was equivalent to approximately 800 mg. of dry weight and after the isolation procedure yielded 140 mg. of amyloid fibrils. High resolution electron microscopy of the isolated murine amyloid fibrils demonstrated them to be comparable with fibrils from human preparations (Fig. 3). Fibrils were seen as single fila-

ab:  
me

me  
no  
gr  
sic

0.1  
7.5  
in  
pe:  
Pe  
of:

(Tr  
ral  
sec  
ind

pre  
asp  
rel:  
anc  
E  
mu  
ban  
(Fi



FIG. 3. Electron micrograph of isolated murine amyloid fibrils, shadow-casted with platinum-palladium, demonstrating single filaments (arrows) of 80 to 100 Å in width, which appear rigid, non-

branching, and of indeterminate length. Lateral aggregates of filaments (open arrows) with occasional twisting are also noted.  $\times 60,000$ .

ments of 80 to 100 Å in width, which appeared rigid, nonbranching, and of indeterminate length. Lateral aggregates of the filaments could be seen with an occasional twisting evident.

The amyloid fibrils were dissolved in 4 M guanidine, 0.1 M tris (hydroxymethyl) aminomethane (Tris), pH 7.5, and chromatographed on a Sephadex G-100 column in the same buffer. A void volume and two retarded peaks were obtained (Fig. 4). The second retarded peak, Peak 3, was the largest single component and consisted of 35 per cent of the recovered material.

Amino acid analyses of each peak were carried out (Table 1). The protein in Peak 3 was noted to be comparable to human protein AA, the major component of secondary amyloid and the protein AA from casein-induced amyloidosis in guinea pigs, both of which were prepared in our laboratory. There were large amounts of aspartic acid, glutamic acid, glycine, and alanine and relatively low amounts of threonine, proline, valine, and leucine. No cystine was present.

By sodium dodecyl sulfate disc gel electrophoresis the murine Peak 3 protein was seen as two closely aligned bands and is shown in comparison to human protein AA (Fig. 5). The larger amount of murine protein appeared

to be in the slightly slower migrating band and molecular weight calculations were based on the center point of this larger band. The molecular weight of 10,000 for murine Peak 3 protein (or AA) is slightly higher than the molecular weight of human AA which has been reported by many investigators as 8,500 (3, 9, 14, 16) (Fig. 6).

Amino acid sequence analysis of the murine Peak 3 protein (or AA) was determined to 26 residues (Table 2). Since the protein had been coupled to sulfophenylisothiocyanate prior to sequence analysis, no amino acid was recovered in the ethylacetate phase of the first residue for analysis by gas chromatography. However, after hydriotic acid hydrolysis of the aqueous phase and amino acid analysis, serine and a very small amount of arginine were recovered. Thus it would seem that murine AA lacked an N-terminal arginine, a finding which has been noted in protein AA from other species. Phenylalanine was recovered as the second residue with a yield of 141.5 nmoles as calculated from gas chromatographic standards. Tryptophan and tyrosine were tentatively identified as residue numbers 17 and 20, respectively, because gas chromatographic identity could be made but yields were too low to quantitate.

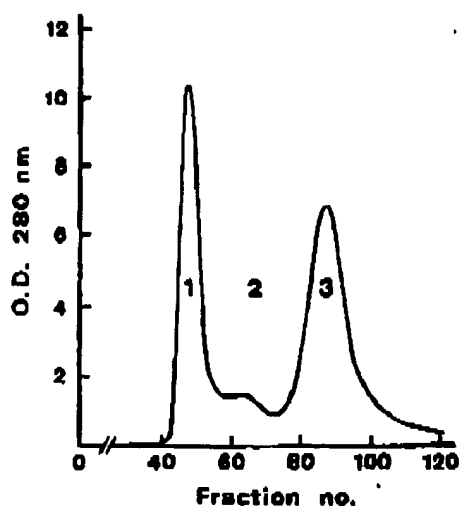


FIG. 4. Gel chromatography of murine amyloid fibrils through Sephadex G-100 (2.5 cm. by 90 cm.) eluted with 4 M guanidine-HCl, 0.1 M Tris, pH 7.5, and collected in 8 ml.-fractions.

TABLE 1. AMINO ACID ANALYSES (RESIDUES PER 100 RESIDUES)

|               | Murine amyloid after chromatography |        |        | Human amyloid protein AA | Guinea pig amyloid protein AA (26) |
|---------------|-------------------------------------|--------|--------|--------------------------|------------------------------------|
|               | Peak 1                              | Peak 2 | Peak 3 |                          |                                    |
| Lysine        | 6.7                                 | 5.5    | 5.3    | 4.7                      | 5.0                                |
| Histidine     | 2.5                                 | 2.2    | 3.0    | 2.2                      | 2.0                                |
| Arginine      | 6.6                                 | 6.2    | 7.2    | 10.3                     | 8.3                                |
| Aspartic acid | 6.5                                 | 9.9    | 11.6   | 12.7                     | 10.6                               |
| Threonine     | 3.5                                 | 5.1    | 2.7    | 1.3                      | 2.7                                |
| Serine        | 4.1                                 | 5.9    | 3.8    | 5.5                      | 5.4                                |
| Glutamic acid | 14.8                                | 14.8   | 13.3   | 8.5                      | 11.9                               |
| Proline       | 6.8                                 | 4.5    | 2.1    | 2.6                      | 3.5                                |
| Glycine       | 5.9                                 | 9.0    | 14.9   | 12.0                     | 10.6                               |
| Alanine       | 4.5                                 | 8.6    | 13.9   | 16.1                     | 15.6                               |
| Cystine       | 2.7                                 | 1.3    | 0      | 0                        | 0.4                                |
| Valine        | 7.3                                 | 5.2    | 2.0    | 3.0                      | 3.6                                |
| Methionine    | 2.3                                 | 2.3    | 3.0    | 1.2                      | 3.2                                |
| Isoleucine    | 5.6                                 | 4.0    | 3.8    | 4.3                      | 2.4                                |
| Leucine       | 10.8                                | 7.7    | 1.3    | 4.0                      | 5.5                                |
| Tyrosine      | 3.9                                 | 3.0    | 4.0    | 3.5                      | 4.0                                |
| Phenylalanine | 5.8                                 | 4.9    | 9.2    | 7.8                      | 5.0                                |

A comparison of this sequence with protein AA from other species was made by aligning serine at position 2 (Table 3). Twenty-three of the 27 residues were identical with the sequence of human protein AA thus giving an 85 per cent homology. The substitutions occurred at positions 7, isoleucine for leucine; 12, glutamic acid for aspartic acid; 15, glycine for arginine; and 22, threonine for serine. All of the substitutions represent first or third base changes of the genetic codon scheme, thus indicating a similar side chain character for each substituted amino acid. Also for comparison, the proteins AA from guinea pig, monkey, mink and a preparation of mouse amyloid induced by *Candida albicans* are included (Table 3) and discussed below.

Four of five rabbits produced antibody within 7 weeks of initial immunization with murine Peak 3 (or AA) and all were specific for murine protein AA. Sera from casein-treated CBA/J mice were tested and found to contain a component which cross-reacted identically with

isolated protein AA when tested against the antiserum to murine Peak 3 (Fig. 7). No reaction was seen with normal CBA/J serum, human protein AA, normal human serum, or amyloidotic human serum. Conversely antiserum to the human protein AA did not react with the murine Peak 3 or the casein-treated murine serum, indicating a species specificity.

## DISCUSSION

Casein injections in the CBA/J murine model have been shown to induce a secondary or protein AA type of amyloidosis. Histologically and with Congo red staining, the amyloid has the classic fibrillar appearance and green birefringence. On electron microscopy the mouse spleen tissue section fibrils were extracellular, 80 to 100 Å in cross-section, and the deposits were seen closely associated with the reticuloendothelial cells. The deep cytoplasmic invaginations of the reticuloendothelial cells containing the amyloid fibrils have been considered to be the site of amyloid fibril formation (Fig. 2) (12, 24). On high resolution microscopy after isolation, the fibrils were rigid, nonbranching, of indeterminate length, and identical with all other isolated amyloid fibrils.

The fibril component of the murine amyloid, protein AA, was found to cross-react with immunologic identity

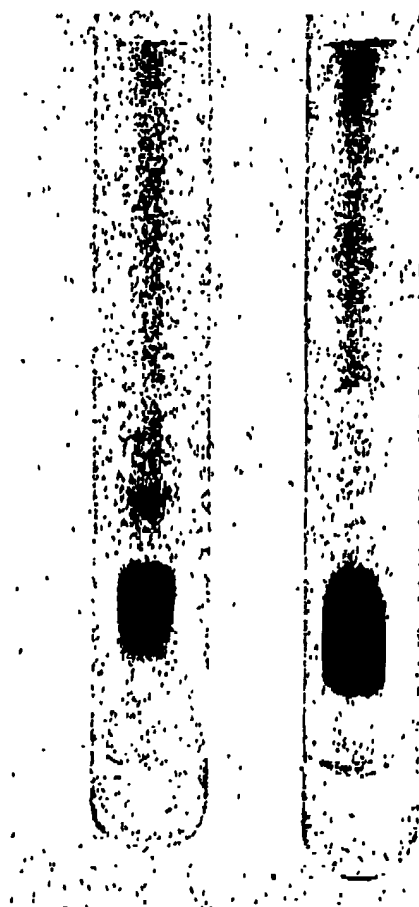


FIG. 5. Ten per cent acrylamide sodium dodecyl sulfate disc gel electrophoresis of murine protein AA (left) and human protein AA (right).

Fig. 5. Ten per cent acrylamide sodium dodecyl sulfate disc gel electrophoresis of murine protein AA (left) and human protein AA (right).

with human amyloid protein AA. In and prote path prote howe ogy, (Tab guin AA (His begin AA (alan alan An disea prote mole It oth for tr En imen prote

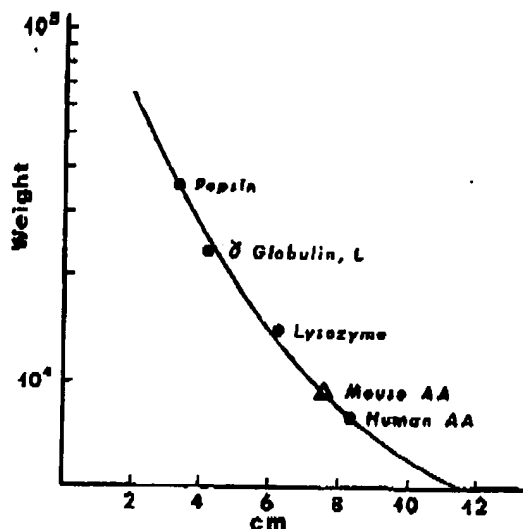


FIG. 8. Molecular weights as determined by migration in centimeters of proteins in 10 per cent acrylamide sodium dodecyl sulfate gel electrophoresis. The murine AA ( $\Delta$ ) was slightly larger than the human AA.

with a component in murine serum, SAA, when they were tested against the antiserum to murine AA. In human studies SAA has been found in only minute quantities in normal sera, but SAA is markedly elevated in secondary amyloidosis as well as in acute and chronic inflammatory conditions. The size of SAA appears to be approximately 100,000 daltons in comparison to that of 8,500 daltons for tissue AA. When the human and murine models were compared, a definite species specificity was found in testing SAA and AA with anti-AA. Because of its elevated levels with disease and its immunologic identity to AA, SAA has been presumed to be the precursor in the pathogenesis of secondary amyloid fibrils.

Intact SAA has not yet been isolated in any species and thus sequence data of the high molecular weight protein are not available to aid in understanding the pathogenesis of tissue AA. The N-terminal variations of protein AA among the various species are of interest, however, for in spite of their obvious sequence homology, there appears to be an N-terminal heterogeneity (Table 3). Amyloid secondary to casein injection in guinea pigs has been shown to be composed of protein AA with an additional 5 amino acid N-terminal peptide (His-Ala-Lys-Gly-Glu) prior to the usual AA sequence beginning Arg-Ser-Phe (26). It varied from the human AA prototype at positions 3, with isoleucine for phenylalanine; 8, with lysine for glycine; 14, with proline for alanine; and 18, with leucine for tryptophan.

Amyloidosis secondary to a chronic granulomatous disease in a monkey was also found to be primarily protein AA. However, approximately 22 per cent of the molecules lacked the N-terminal arginine residue (13). It otherwise was identical with the human AA except for tryptophan rather than phenylalanine at position 3.

Endotoxin has been used to induce amyloidosis experimentally in mink. The amyloid fibril was identified as protein AA from a characteristic amino acid analysis

and aligned beginning at residue 17 by partial sequence of two cyanogen bromide fractions. Interestingly, like the guinea pig and monkey, it has an N-terminal variation from the usual sequence with a blocked N-terminal (15). Other differences from human AA include tyrosine for tryptophan at position 18 and tyrosine for arginine at position 25.

A study has recently been reported using *Candida albicans* to induce amyloidosis in C57BL/K mice (10). The experimental amyloid produced was protein AA and had minimal variations when compared to the casein-induced murine amyloid of the present study. A lack of N-terminal arginine was noted, and the amino acids at positions 7, 12, 15, and 22, which varied from the human and other species, were similar to those found in the CBA/J casein-induced amyloidosis. Glycine at position 2 was the only variation from the present study.

Other studies using the murine model include one in which amyloidosis was produced experimentally by four methods (*Mycobacterium butyricum*, casein, casein plus Freund's adjuvant, and endotoxin). In addition, amyloid had developed spontaneously in noninbred male Swiss mice (general purpose mice). Chemical analysis on the spontaneous mouse amyloid showed an amino acid analysis characteristic of protein AA, but an N-terminal which was unreactive to dinitrofluorobenzene (11).

A spontaneously occurring amyloid in aged SJL mice has recently been studied, and it appears that an amyloid which is not protein AA occurs in that species (22).

TABLE 2. SEQUENTIAL DEGRADATION OF MURINE AA

| Step no. | Deduced residue | Gas chromatography | nmoles            | Amino acid analysis |
|----------|-----------------|--------------------|-------------------|---------------------|
| 1        | Ser             | — <sup>a</sup>     | —                 | Ser, Arg            |
| 2        | Phe             | Phe                | 141.5             | Phe                 |
| 3        | Phe             | Phe                | 164.0             | Phe                 |
| 4        | Ser             | Ser                | 59.8              | Ser                 |
| 5        | Phe             | Phe                | 154.0             | Phe                 |
| 6        | Ile             | Ile                | 126.0             | Ile                 |
| 7        | Gly             | Gly                | 98.2              | Gly                 |
| 8        | Glu             | Glu                | 147.9             | Glu                 |
| 9        | Ala             | Ala                | 122.6             | Ala                 |
| 10       | Phe             | Phe                | 104.6             | Phe                 |
| 11       | Gln             | Glu                | 75.6              | Glu                 |
| 12       | Gly             | Gly                | 39.9              | Gly                 |
| 13       | Ala             | Ala                | 97.6              | Ala                 |
| 14       | Gly             | Gly                | 45.6              | Gly                 |
| 15       | Asp             | Asp                | 53.9              | Asp                 |
| 16       | Met             | Met                | 48.0              | —                   |
| 17       | Trp             | Trp                | N.C. <sup>b</sup> | —                   |
| 18       | Arg             | —                  | —                 | Arg                 |
| 19       | Ala             | Ala                | 37.6              | Ala                 |
| 20       | Tyr             | Tyr                | N.C.              | Tyr                 |
| 21       | Thr             | —                  | —                 | Thr                 |
| 22       | Asp             | Asp                | 19.5              | Asp                 |
| 23       | Met             | Met                | 40.0              | —                   |
| 24       | ( )             | —                  | —                 | —                   |
| 25       | Glu             | Glu                | 14.8              | Glu                 |
| 26       | Ala             | Ala                | 27.1              | Ala                 |

<sup>a</sup> — Residue could not be determined.

<sup>b</sup> N.C., Not calculated.

<sup>c</sup> ( ) Indeterminant by GC or AAA.



TABLE 3. AMINO ACID SEQUENCE OF CASEIN-INDUCED MURINE AMYLOID PROTEIN AA AND COMPARISON WITH HUMAN AA, GUINEA PIG AA, MONKEY AA, AND MINK AA

|                    | 1         | 2   | 3   | 4   | 5   | 6   | 7      | 8   | 9       | 10     | 11  |
|--------------------|-----------|-----|-----|-----|-----|-----|--------|-----|---------|--------|-----|
| Murine AA          | (Arg)-    | Ser | Phe | Phe | Ser | Phe | Ile    | Gly | Glu     | Ala    | Phe |
| Human Protein AA   | Arg       | Ser | Phe | Phe | Ser | Phe | Leu    | Gly | Glu     | Ala    | Phe |
| Guinea Pig AA (26) | His       | Ala | Lys | Gly | Glu | Arg | Ser    | Ile | Phe     | Ser    | Ala |
| Monkey AA (13)     | Arg       | Ser | Trp | Phe | Ser | Phe | Leu    | Gly | Glu     | Ala    | Gly |
| Mink AA (15)       | (blocked) |     |     |     |     |     |        |     |         |        |     |
| Murine AA (10)     |           |     |     |     |     |     |        |     |         |        |     |
|                    | 12        | 13  | 14  | 15  | 16  | 17  | 18     | 19  | 20      | 21     | 22  |
| Murine AA          | Glu       | Gly | Ala | Gly | Asp | Met | (Trp)- | Arg | Ala     | (Tyr)- | Thr |
| Human              | Asp       | Gly | Ala | Arg | Asp | Met | Trp    | Arg | Ala     | Tyr    | Ser |
| Guinea Pig         | ( )       | Gly | Pro | ( ) | Asp | Met | Leu    | ( ) | Ala/Ser |        |     |
| Monkey             | Asp       | Gly | Ala | Arg | Asp | Met | Trp    | Arg | Ala     | Tyr    | Ser |
| Mink               |           |     |     |     |     |     |        |     |         |        |     |
| Murine AA          | Glu       | Gly | Ala | Gly | Asp | Met | Trp    | Arg | Ala     | Tyr    | Thr |

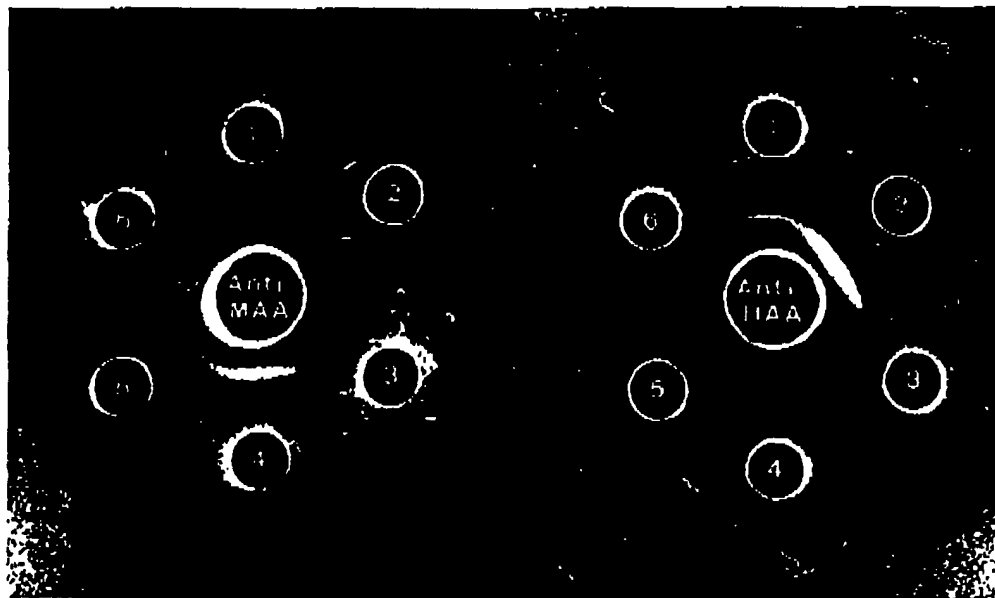


FIG. 7. Double diffusion in agar of antiserum to murine AA (MAA) (left) and antiserum to human AA (HAA) (right) versus 1, amyloidotic human serum; 2, human AA; 3, normal human serum;

4, murine AA; 5, serum from casein-treated CBA/J mouse; and 6, normal murine serum.

The amyloid fibril component was of larger size and had an amino acid analysis unlike that of protein AA. In addition, the amyloid fibril protein did not react with antiserum to mouse AA.

These N-terminal variations suggest the hypothesis that the protein AA, if it is derived from the larger SAA precursor, may represent a cleavage of the C-terminal portion of SAA. Attempts to isolate the intact SAA, an 80,000 to 180,000 molecular weight protein, from human serum have been unsuccessful. Several investigators have partially degraded it by formic acid and isolated a 12,000 to 14,000 molecular weight protein (1, 17, 21, 25).

One N-terminal sequence of the degraded SAA has been identical with the usual human protein AA (21). This would make a carboxy-terminal cleavage of AA from SAA less likely unless one postulates both an amino and a carboxy-terminal cleavage in the pathogenesis of AA from SAA. It will be important to see the total sequence of the 12,000 to 14,000 molecular weight protein and also the N-terminal sequence of the larger SAA in order to clarify this problem.

In summary, amyloidosis has been induced in CBA/J mice with casein. The amyloid found has had the classic tinctorial and electron microscopic properties when

ACTION

Vol. 36, No. 4, 1977

## MURINE AMYLOID PROTEIN AA

42

compared to human amyloidosis. By amino acid analysis and N-terminal sequence analysis, it was found to be primarily composed of protein AA comparable to secondary amyloidosis. An antibody prepared to the murine protein AA identified a cross-reacting serum component, SAA, analogous to the human system. The murine model for AA and its relationship to SAA can contribute significantly to our understanding of the human secondary amyloid fibril protein.

**Acknowledgments:** The authors wish to acknowledge the excellent technical assistance of Christina Carr and Orville Rodgers and the photographic assistance of David Feigenbaum.

**Date of acceptance:** December 7, 1976. A portion of this work was presented in abstract form on June 10, 1976 at the American Rheumatism Association Meeting, Chicago, Illinois.

These investigations were supported by grants from the United States Public Health Service, National Institute of Arthritis and Metabolic Diseases (AM-04599 and T1-AM-8285), from the General Clinical Research Centers Branch of the Division of Research Resources, National Institutes of Health (RR-433), from the Massachusetts Chapter of the Arthritis Foundation, from the Arthritis Foundation, and from the John A. Hartford Foundation.

Dr. Benson's present address is: Indiana University School of Medicine, Indianapolis, Indiana 46202.

Address reprint requests to: Martha Skinner, M.D., University Hospital, Arthritis Section, 75 B. Newton St., Boston, Massachusetts 02118.

## REFERENCES

- Anders RF, Nordstoga K, Natvig JB, Husby G: Amyloid-related serum protein SAA in endotoxin-induced amyloidosis of the mink. *J Exp Med* 143:578, 1976
- Baumal R, Ackermann A, Wilson B: Immunoglobulin biosynthesis in myeloma-associated and casein-and-endotoxin-induced murine amyloidosis. *J Immunol* 114:1785, 1975
- Benditt EP, Eriksen N, Hermanson MA, Ericsson LH: The major proteins of human and monkey amyloid substance: common properties including unusual N-terminal amino acid sequences. *FEBS Lett* 19:169, 1971
- Benson MD, Skinner M, Lian J, Cohen AS: "A" protein of amyloidosis: isolation of a cross-reacting component from serum by affinity chromatography. *Arthritis Rheum* 18:315, 1975
- Brannitzer G, Schrank B, Buhfus A: Versuche zum vollständigen und automatischen Abbau von Peptiden nach der Quadrolmethode. *Hoppe Seylers Z Physiol Chem* 351:1589, 1970
- Cohen AS, Cathcart ES: Casein-induced experimental amyloidosis. *Methods Achiev Exp Pathol* 5:307, 1972
- Cohen AS, Shirahama T: Animal model for human disease: spontaneous and induced amyloidosis. *Am J Pathol* 68:441, 1972
- Edman P, Begg G: A protein sequencer. *Eur J Biochem* 1:80, 1967
- Ein D, Kimura S, Glanzer GG: An amyloid fibril protein of unknown origin: partial amino acid sequence analysis. *Biochem Biophys Res Commun* 48:496, 1972
- Eriksen N, Ericsson LH, Pearall N, Lagunoff D, Benditt EP: Mouse amyloid protein AA: homology with nonimmunoglobulin protein of human and monkey amyloid substance. *Proc Natl Acad Sci USA* 73:964, 1976
- Glennner GG, Page D, Isaraky C, Harada M, Cuatrecasas P, Eanes ED, DeLellis RA, Keiser HR: Murine amyloid fibril protein: isolation, purification and characterization. *J Histochem Cytochem* 19:16, 1971
- Guett B, Ghidoni JJ: The site of formation and ultrastructure of amyloid. *Am J Pathol* 43:837, 1963
- Hermanson MA, Kuhn RW, Walsh KA, Neurath H, Eriksen N, Benditt EP: Amino acid sequence of monkey amyloid protein A. *Biochemistry* 11:2934, 1972
- Husby G, Natvig JB, Michaelsen TE, Sletten K, Høst H: Unique amyloid protein subunit common to different types of amyloid fibril. *Nature* 244:363, 1973
- Husby G, Natvig JB, Sletten K, Nordstoga K, Anders RF: An experimental model in mink for studying the relation between amyloid fibril protein AA and the related serum protein SAA. *Scand J Immunol* 4:811, 1975
- Levin M, Franklin EC, Frangione B, Pras M: The amino acid sequence of a major nonimmunoglobulin component of some amyloid fibrils. *J Clin Invest* 51:2778, 1972
- Linke RP, Sipe JD, Pollock PS, Ignaczak TF, Glennner GG: Isolation of a low-molecular weight serum component antigenically related to an amyloid fibril protein of unknown origin. *Proc Natl Acad Sci USA* 72:1473, 1975
- McAdam KPWJ, Sipe JD: Serum precursor of murine amyloid protein: an acute phase reactant in response to polyclonal B cell mitogens. *Fed Proc* 35:1650, 1976
- Pisano JJ, Bronsart TJ: Analysis of amino acid phenylthiohydantoin by gas chromatography. *J Biol Chem* 244:5597, 1969
- Pras M, Schubert M, Zucker-Franklin D, Rimon A, Franklin EC: The characterization of soluble amyloid prepared in water. *J Clin Invest* 47:924, 1968
- Rosenthal CJ, Franklin EC, Frangione B, Greenspan J: Isolation and partial characterization of SAA—an amyloid-related protein from human serum. *J Immunol* 118:1415, 1976
- Scheinberg MA, Cathcart ES, Eastcott JW, Skinner M, Benson M, Shirahama T, Bennett M: The SJL/J mouse: a new model for spontaneous age-associated amyloidosis. *Lab Invest* 35:47, 1976
- Shirahama T, Cohen AS: High-resolution electron microscopic analysis of the amyloid fibril. *J Cell Biol* 33:679, 1967
- Shirahama T, Cohen AS: An analysis of the close relationship of lysosomes to early deposits of amyloid: ultrastructural evidence in experimental mouse amyloidosis. *Am J Pathol* 73:97, 1973
- Sipe JD, Ignaczak TF, Pollock PS, Glennner GG: Amyloid fibril protein AA: purification and properties of the antigenically related serum component as determined by solid phase radioimmunoassay. *J Immunol* 116:1151, 1976
- Skinner M, Cathcart ES, Cohen AS, Benson MD: Isolation and identification by sequence analysis of experimentally induced guinea pig amyloid fibrils. *J Exp Med* 140:871, 1974
- Smithies O, Gibson DM, Fanning RM, Goodflesh JM, Gilman JM, Ballantyne DC: Quantitative procedures for use with the Edman-Begg sequencer: partial sequence of two unusual immunoglobulin light chains, Ref and Sac. *Biochemistry* 10:4912, 1971
- Spackman DH, Stein WH, Moore S: Automatic recording apparatus for use in the chromatography of amino acids. *Anal Chem* 30:1190, 1958
- Weber K, Osborn M: The reliability of molecular weight determinations by dodecyl sulfate-polyacrylamide gel electrophoresis. *J Biol Chem* 244:4406, 1967

and 6,

been  
This  
from  
and  
ence  
also  
er to

3A/J  
asic  
han



# Techniques to study amyloid fibril formation in vitro

Melanie R. Nilsson\*

*Department of Chemistry, McDaniel College, Eaton Hall, 2 College Hill, Westminster, MD 21157, USA*

Accepted 5 March 2004

Available online 7 June 2004

## Abstract

Amyloid fibrils are ordered aggregates of peptides or proteins that are fibrillar in structure and contribute to the complications of many diseases (e.g., type 2 diabetes mellitus, Alzheimer's disease, and primary systemic amyloidosis). These fibrils can also be prepared in vitro and there are three criteria that define a protein aggregate as an amyloid fibril: green birefringence upon staining with Congo Red, fibrillar morphology, and  $\beta$ -sheet secondary structure. The purpose of this review is to describe the techniques used to study amyloid fibril formation in vitro, address common errors in the collection and interpretation of data, and open a discussion for a critical review of the criteria currently used to classify a protein aggregate as an amyloid fibril.

© 2004 Elsevier Inc. All rights reserved.

**Keywords:** Amyloid fibrils; Protein aggregation; Congo Red; FTIR; TEM; Criteria; Classification; Review; Techniques; Thioflavin T

## 1. Introduction

Amyloidosis describes a group of diseases that are characterized by the deposition of amyloid fibrils and other biological molecules (called a plaque or amyloid deposit) that kills cells or prevents them from functioning properly [1,2]. Amyloid can be identified using a radioactive tracer in vivo or at post-mortem by the staining of tissue sections with Congo Red [3–5]. The location of the deposits varies and typically governs the observed symptoms. In Alzheimer's and prion disease, for example, these deposits are in the brain and result in dementia. In type 2 diabetes mellitus, the deposits are formed in the pancreas and contribute to  $\beta$ -cell dysfunction. Alternatively, the deposits can occur in multiple locations, which is observed in primary systemic amyloidosis.

Amyloid fibrils are ordered aggregates of a normally soluble peptide or protein. More than 20 different peptides/proteins have been identified in amyloid fibrils in vivo [6]. Amyloid fibrils can also be produced in vitro by

subjecting disease-associated or non-disease associated peptides/proteins to destabilizing conditions [7,8]. The presence of amyloid fibrils (either ex vivo or in vitro) is defined by three criteria: green birefringence upon staining with Congo Red, fibrillar morphology, and  $\beta$ -sheet secondary structure [9]. An in vitro sample that satisfies these three criteria is shown in Fig. 1.

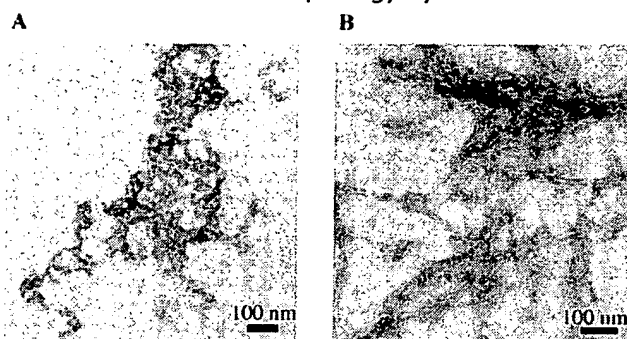
A major impetus for the characterization of in vitro amyloid fibrils is to test the 'amyloid hypothesis,' which asserts that amyloid fibrils or the formation of amyloid fibrils is a causative factor in disease onset and/or progression [10]. This hypothesis has been supported by the demonstration that amyloid fibrils and amyloid fibril intermediates (Fig. 2) are toxic to cell cultures [11,12]. The study of amyloid fibril formation in vitro, however, has applications beyond the relationship of fibrils to human disease. The characterization of the process of protein misfolding that occurs as a prelude to fibril formation has provided insights into normal protein folding and the evolution of protein folding [13–15]. Furthermore, the highly ordered arrangement of proteins in amyloid fibrils has sparked considerable interest in the use of amyloid fibrils for nanotechnology and other applications in materials science [16,17].

\* Fax: 1-410-386-4613.

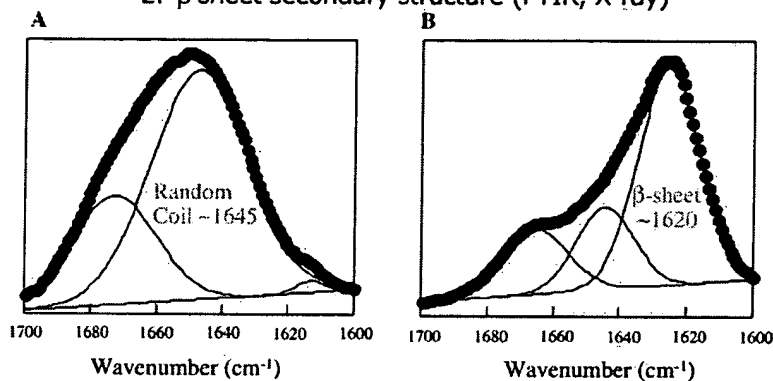
E-mail address: [mnilsson@mcdaniel.edu](mailto:mnilsson@mcdaniel.edu).

## Characterization of Amyloid Fibrils

### 1. Fibrillar morphology by TEM



### 2. $\beta$ -sheet secondary structure (FTIR, X-ray)



### 3. Birefringence upon staining with Congo Red

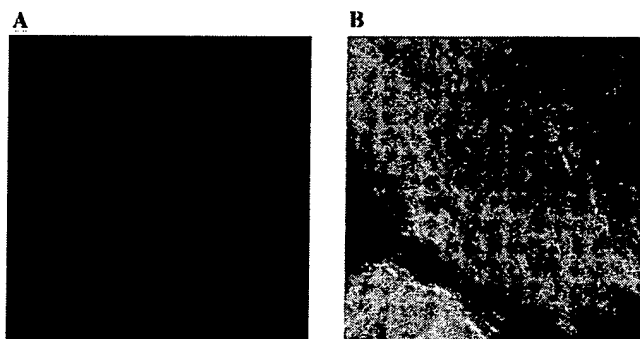


Fig. 1. A protein aggregate formed in vitro that satisfies the three criteria to define the sample as amyloid fibrils is shown on the right and clearly demonstrates fibrillar morphology by TEM,  $\beta$ -sheet secondary structure by FTIR, and green birefringence under polarized light upon staining with Congo Red. The protein aggregate on the left does not satisfy any of these criteria. Reprinted with permission from [23,58].

## 2. Techniques, trouble shooting, and critical analysis of amyloid fibril criteria

### 2.1. Overview of techniques

In vitro studies are typically performed using pure protein samples or protein in the presence of other components found in amyloid deposits. The techniques discussed in this review are presented in the context of the study of the protein component alone, but can easily

be extended to studies in which different additives are present. Two aspects of amyloid fibril formation can be characterized in vitro; the determination of the structure of the fibril and the process of fibril formation (i.e., mechanism and kinetics). Both processes begin with the characterization of the component peptide or protein by traditional techniques used to study protein structure. However, since many amyloid-forming peptides and proteins are highly prone to aggregate in vitro, techniques which require low sample concentration (e.g.,

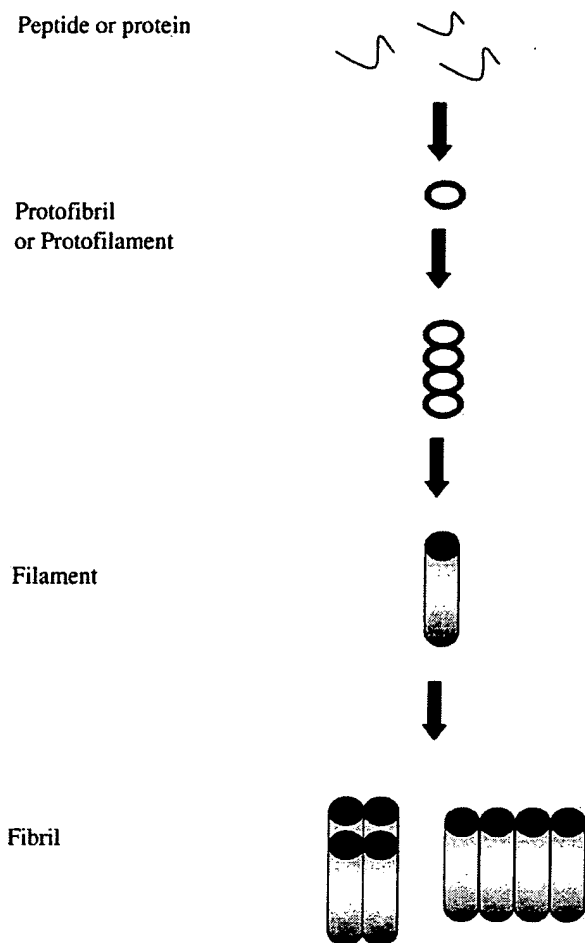


Fig. 2. Schematic diagram of the assembly processes that have been observed during amyloid fibril formation in vitro. *Note.* Not all peptides and proteins have been shown to have a protofibril or protofilament intermediate state.

circular dichroism spectroscopy) are utilized most frequently to maintain the molecule in a monomeric form. Once information about the initial secondary structure is known, the protein can be subjected to conditions to promote aggregation into amyloid fibrils. The exact conditions are highly variable and sample dependent. Once conditions that promote fibril formation are established, the kinetics of the process can be examined by assaying the solution for fibrils at specific time intervals. The most common techniques to identify the presence of amyloid fibrils are Thioflavin T (ThT)<sup>1</sup> fluorescence,

Congo Red binding, transmission electron microscopy (TEM), and Fourier transform infrared spectroscopy (FTIR). (Note: although ThT fluorescence is not one of the 'defining' criteria for amyloid fibrils, it is relatively well accepted as an indicator of the presence of amyloid fibrils.) These procedures for detection are typically new applications of old techniques, so the application of these methods to the examination of fibrils will be highlighted.

## 2.2. Sample preparation

The single biggest obstacle in the examination of peptides and proteins that form amyloid fibrils is sample preparation. There have been numerous reports of batch to batch variability and poor reproducibility of experiments both within and among laboratories with many different proteins [18]. Several different factors can contribute to this variability. The first issue to consider is the purity of the peptide or protein sample. Impurities can affect the kinetics of aggregation [19–21] and, unfortunately, there is no way to predict if a sample impurity will increase, decrease, or have no effect on aggregation. To prevent chemical degradation of pure samples, proper storage conditions are important. Typically, peptides are most stable when stored as a lyophilized powder, under N<sub>2</sub>, in a desiccator, in the freezer (–20 °C). However, even under these conditions, some peptides can undergo chemical modifications [21]. Therefore, the purity of the sample should be examined prior to each experiment. Proteins are also prone to chemical modification over time and should likewise be properly stored and carefully examined for chemical modification.

The next aspect of sample preparation is to assess the ion-pairing agent used in the peptide/protein purification process since the ion pair can affect the kinetics of aggregation. The purification, particularly of peptides, is performed using buffers that contain either HCl or trifluoroacetic acid (TFA). Since peptides are charged molecules, the negative ion present from the acid (Cl<sup>–</sup> or TFA<sup>–</sup>) forms an ion pair with the positively charged N-terminus or side chains of the peptide. These two reagents lead to ion pairs that differ in size (Cl<sup>–</sup> < TFA<sup>–</sup>) and hydrophobicity (Cl<sup>–</sup> < TFA<sup>–</sup>) and, consequently, can have a significant effect on amyloid fibril formation. The Aβ<sub>1–40</sub> peptide, for example, has been shown to be random coil by CD if prepared from TFA but β-sheet if purified using HCl [22]. Equally dramatic effects of ion pairing agents on the ability of IAPP<sub>24–29</sub> to form amyloid fibrils have also been reported [23].

Another important aspect of sample preparation is the removal of pre-formed aggregates from purified peptide and protein samples. Amyloid fibril formation typically follows nucleation–polymerization kinetics but the presence of a pre-formed aggregate or fibril 'seed'

<sup>1</sup> Abbreviations used: CD, circular dichroism spectroscopy; DDI, distilled and deionized; DMSO, dimethyl sulfoxide; DTGS, deuterated triglycine; FTIR, Fourier transform infrared spectroscopy; HFIP, 1,1,1,3,3,3-hexafluoro-2-propanol; HPLC, high performance liquid chromatography; LN<sub>2</sub>, liquid nitrogen; MCT, mercury cadmium telluride; PTA, phosphotungstic acid; RP-HPLC, reversed phase HPLC; TEM, transmission electron microscopy; TFA, trifluoroacetic acid; TFE, 2,2,2-trifluoroethanol; ThT, thioflavin T; UA, uranyl acetate.

dramatically alters the observed kinetics as shown in Fig. 3 [24]. Aggregates are removed by filtration using a syringe filter (20 nm) or centrifugation, but the aggregates must be larger than the filter size or dense enough to form a pellet to be removed. Organic solvents (DMSO, dimethyl sulfoxide; TFE, trifluoroethanol; and HFIP, hexafluoroisopropanol), strong acids (TFA, formic acid), and concentrated base (NaOH,  $\text{NH}_4\text{OH}$ ) have also been used for solubilization of pre-formed aggregates. Formic acid, however, should be avoided because it can result in the formylation of serine [25]. Organic solvents should be used with caution because they can dramatically alter the secondary structure and aggregation properties of proteins and peptides. DMSO is very hygroscopic and wet DMSO can, in some cases, promote aggregation [26]. TFE and HFIP can also promote non-native  $\beta$ -sheet interactions [27]. In addition, organic solvents can cause leaching of plastic tubes and should be used only in glass containers. A couple of other notes of caution about filtering samples warrant mention. First, fibrils can pass through syringe filters, even a 20 nm filter. If the filtered material is examined by TEM, long fibrils (which presumably pass edge-wise through the filter) and short fibril fragments (i.e., mechanically broken fibrils) are often present (MRN/DPR unpublished results). Second, most commercially avail-

able syringe filters are prepared with wetting agents that absorb significantly below 220 nm. This can make quality CD spectra below 220 nm difficult to obtain. Therefore, syringe filters should be prewashed with DDI water prior to sample filtration.

On a final note, many samples that are assayed for amyloid formation are incubated in phosphate buffer at physiological pH and temperature for a given period of time. These conditions can promote fibril formation in some systems but also provide ideal conditions for bacterial growth. Bacterial growth can also readily occur in samples that contain amyloid fibrils (MRN/DPR unpublished results). Both ThT and Congo Red can bind to bacteria and result in false positive results. Bacterial growth can be minimized by adding 0.05% sodium azide, performing the incubation at 4 °C, autoclaving buffers, or by growing the sample in  $\text{D}_2\text{O}$  instead of  $\text{H}_2\text{O}$ .  $\text{D}_2\text{O}$  is a good substitute for water since it is only about 10% more viscous, allows for easy FTIR analysis, and inhibits bacterial growth.

### 2.3. Strategy and techniques for detecting amyloid fibril formation

To determine if a peptide or protein will form amyloid fibrils, a systematic approach can be used which

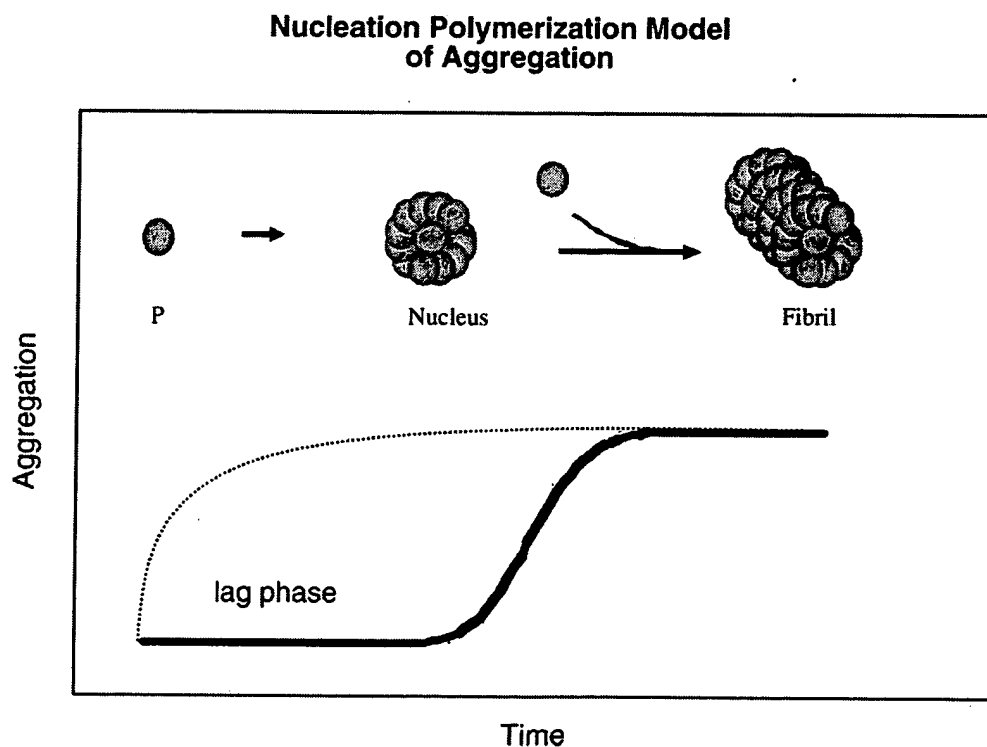


Fig. 3. The aggregation of a protein (P) into amyloid fibrils typically begins with a 'lag phase' in which no aggregation is observed. During this time, the entropically unfavorable process of initial association occurs. Once the aggregation process begins and a critical nucleus is formed, the aggregation proceeds rapidly into amyloid fibrils (solid line). The lag phase, however, can be overcome (dotted line) by the addition of a pre-formed nucleus (i.e., an aliquot of solution containing pre-formed fibrils). This schematic represents the 'nucleation-polymerization' kinetics for amyloid fibril formation [24], but other similar kinetic processes have also been reported [59].

minimizes cost but maximizes sensitivity. The sample is incubated under a variety of different solution conditions (pH, temperature, and ionic strength) which are suspected to promote fibril formation. Each sample is visually examined for an increase in viscosity, gel formation, or the appearance of a precipitate. Once a change in viscosity or a gel/precipitate is observed, the sample is analyzed by the Thioflavin T (ThT) assay and the Congo Red assays. If a positive result is obtained by either assay, the sample should be examined for the presence of fibrils by TEM. If fibrils are present, the final step is to determine if there is  $\beta$ -sheet secondary structure either by FTIR or X-ray fiber diffraction [28].

*The Thioflavin T (ThT) Assay* measures the change in fluorescence intensity of ThT upon binding to amyloid fibrils. The enhanced fluorescence can be observed by fluorescence microscopy or by fluorescent spectroscopy; the spectroscopic assay is described in Procedure 1. The spectroscopic assay is commonly used to monitor fibril formation over time, but the assay is not strictly quantitative [29] and differences in binding have been observed for samples after lyophilization [60].

**Procedure 1:** Thioflavin T spectroscopic assay [29]

1. Prepare a ThT stock solution by adding 8 mg ThT to 10 mL phosphate buffer (10 mM phosphate, 150 mM NaCl, pH 7.0) and filter through a 0.2  $\mu$ m syringe filter. This stock solution should be stored in the dark and is stable for about one week.
2. Dilute the stock solution into the phosphate buffer (1 mL ThT stock to 50 mL buffer) on the day of analysis to generate the working solution.
3. Measure the fluorescence intensity of 1 mL working solution by excitation at 440 nm (slitwidth 5 nm) and emission 482 nm (slitwidth 10 nm), averaging over 60 s.
4. Add an aliquot of untreated protein solution (5–10  $\mu$ L) to the cuvette, stir for 1 min, and measure the intensity over 60 s. This serves as the control sample.
5. Repeat steps 3–4 with 5–10  $\mu$ L of the aggregated protein solution. A measured intensity above the control sample is indicative of amyloid fibrils.
6. Note: the ThT assay can also be performed in multi-well plates [29] or in situ [30].

False negatives can occur if the fibrils are packed together in such a way that the surface for ThT binding is not present. The aggregation kinetics for islet amyloid polypeptide, for example, have a lag phase followed by an initial increase in ThT intensity during fibril formation and then a decrease in ThT intensity [31]. This is likely a result of the formation of mat-like assemblies of fibrils which are difficult to sample and lack ThT binding sites (MRN/AC unpublished results). False positives can be observed due to ThT binding to amorphous aggregates or bacteria.

*The Congo Red birefringence assay* was developed for the examination of in situ and ex vivo amyloid and was

later extended to the examination of in vitro samples (Procedure 2). Many things exhibit birefringence but are not amyloid; buffer salts (phosphate and urea) are inherently birefringent and appear as intense white birefringence, hair or other fibers exhibit birefringence but are often multicolored. This technique is relatively subjective and a known fibrillar sample should be used as a control. There is also a Congo Red spectrophotometric assay which is more objective, less prone to misinterpretation, and can be easily combined with the microscopic analysis (Procedure 3).

**Procedure 2:** Congo Red birefringence assay [5]

1. Prepare the staining solution: prepare a solution of 80% EtOH: 20% DDI water and add a saturating amount of NaCl. Stir this solution for a few minutes and filter away the excess NaCl. Add a saturating amount of Congo Red, stir, and filter to obtain the final working solution [32]. Congo Red can be used straight from the manufacturer or can be recrystallized from 50% EtOH:50% DDI water prior to use [33]. The staining solution should be used on the day of preparation or can be stored if 0.05% sodium azide is added to inhibit bacterial growth.
2. Air-dry 10  $\mu$ L of the aggregated protein solution onto a glass microscope slide.
3. Place 200–400  $\mu$ L of the staining solution onto the dried protein sample. Wait a few seconds and then blot away the excess solution with a lint-free Kimwipe (or hardened filter paper), being careful not to touch the sample, and allow the stained sample to dry at room temperature.
4. Examine the stained sample using polarized light microscopy. The microscope should have high quality, strain-free lenses for optimal performance. If the polarizers are aligned, the material stained with Congo Red will appear reddish pink (the affinity for Congo Red is known as congophilia). If the polarizers are crossed at a 90° angle to each other, the background of the sample will turn black. Any bright spots that appear are a result of birefringence (the sample bends the light in such a way that it can pass through the upper polarizer to reach your eye). The detection of yellow/green birefringence is considered a positive result for the presence of amyloid. The absence of such birefringence is a negative result. The birefringence under crossed polarizers should match the areas of Congo Red staining observed under visible light.

**Procedure 3:** Congo Red spectroscopic assay [34]

1. Prepare a 7 mg/mL solution of Congo Red in buffer (5 mM potassium phosphate, 150 mM NaCl, pH 7.4) and filter through a 0.2  $\mu$ m syringe filter immediately prior to use.
2. Zero a UV-Vis spectrophotometer between 400 and 700 nm at room temperature with a sample of 1 mL phosphate buffer in a disposable cuvette.

3. Add 5  $\mu$ L of the Congo Red solution to the phosphate buffer, scan between 400 and 700 nm and record the spectrum.
4. Add 5–10  $\mu$ L of protein solution to the cuvette and incubate for 30 min at room temperature. At this stage, a red precipitate may become visible. Mix the contents of the cuvette by pipetting the solution up and down and then record the spectrum between 400 and 700 nm.
5. Mathematically subtract the Congo Red spectrum from the protein + Congo Red spectrum. A maximal spectral difference at 540 nm is indicative of amyloid fibrils.
6. To use this sample for the microscopic analysis, transfer the protein + Congo Red solution from the cuvette to an Eppendorf, centrifuge at 12,000–14,000 rpm to pellet the fibrils, wash the fibrils with water, resuspend the fibrils in a small amount of water, and place on a glass microscope slide. Let the sample air-dry and analyze under polarized light (Procedure 2, step 4).

Birefringence upon staining with Congo Red is used as a method for the identification of amyloid fibrils but many issues regarding this technique remain unresolved. Deposits could be overlooked due to the thickness of the sample, orientation of the deposits, or problems with the equipment or use of the equipment [35,36]. Therefore, Congo Red birefringence may be useful for the identification of amyloid deposits, but Cooper asserts that using this technique exclusively would result in false negative results and other techniques should be used [35]. Although this warning was issued long ago by a pioneer in the amyloid field, Congo Red birefringence remains a primary criterion for amyloid fibril identification both in vivo and in vitro. If a sample does not show birefringence upon staining with Congo Red but exhibits all other properties of amyloid, it is currently not likely to be classified as amyloid.

The mechanism of interaction between Congo Red and amyloid fibrils is not well understood. It has been suggested that the interaction may be from an oligomer of Congo Red molecules not a single monomer [37]. Furthermore, Congo Red has been shown to bind to soluble proteins, not just insoluble amyloid fibrils [38] and recent advances in microscopic methods have revealed that the core of amyloid deposits do not show birefringence after staining with Congo Red [61]. Congo Red has several functional groups (Fig. 4) that could potentially interact with amyloid fibrils by: (1) hydrogen bonding with the primary amino groups acting as H-bond donors, (2) ionic interactions via the sulfonate, (3) hydrophobic interactions between the aromatic rings and the fibril, (4) steric intercalation of the dye between  $\beta$  sheets, or (5) a combination of these interactions. There is no reason to assume a priori that the mechanism of interaction will be the same for ex vivo versus in

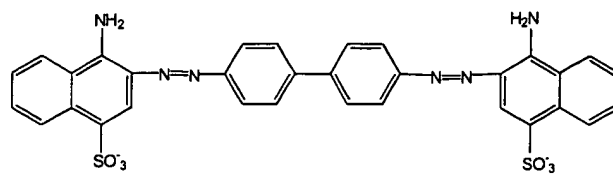


Fig. 4. Chemical structure of Congo Red.

vitro preparations or for amyloid fibrils of different peptide/protein compositions. There is substantial evidence, in fact, that amyloid fibrils of different compositions bind Congo Red by different mechanisms. The binding of Congo Red to poly-L-lysine, for example, is pH dependent and the mechanism of interaction has been proposed to be an electrostatic charge pairing between the positively charged lysine side chains and the negatively charged sulfonate groups of the Congo Red molecule [34]. Other peptides such as insulin and A $\beta$  have been proposed to interact with Congo Red by hydrophobic interactions [39]. Studies in which the binding of Congo Red and Congo Red analogs to fibrils composed of different peptides revealed substantially different binding affinities, suggesting the dye interacts by different mechanisms depending on the component peptide [40]. Additionally, the molecular packing of fibrils can obscure ThT binding and may also obscure Congo Red binding. This phenomenon has been previously noted in tissue samples and pretreatment with alkaline alcohol has been shown to break hydrogen bonds and result in significantly enhanced Congo Red birefringence [5].

In order for Congo Red birefringence to be justifiably used as the primary criterion for amyloid identification, it should bind to all amyloid deposits by the same mechanism such that the dye is detecting a common motif, not unique interactions with specific amino acids. There is now substantial evidence that Congo Red does not bind amyloid deposits by the same mechanism and may, therefore, not detect some deposits that are amyloid because of amino acid composition or even fibril packing motifs. Thus, although deposits that exhibit birefringence upon staining with Congo Red generally have the other characteristics of amyloid deposits (the assay is specific), many deposits have the other characteristics of amyloid deposits but do not show birefringence with Congo Red (the assay is not sensitive) [41–45,62]. For these reasons, the use of Congo Red birefringence as a rigid criterion for the identification of amyloid fibrils in vitro should be critically reconsidered.

*Transmission electron microscopy (TEM)* is used to detect the presence of fibrils. For quality TEM data, the composition of the protein sample solution must not damage the EM grids and excessive salt should be avoided since salt crystals can obscure the identification of fibrils. The grids for amyloid fibril detection can be



made of copper or nickel with 200–400 mesh spacing. The grids are first covered in formvar and subsequently carbon coated. Staining is typically performed with a 2% solution of uranyl acetate (UA) in water (Procedure 4). Phosphotungstic acid (PTA) at pH 7.0 can also be used for staining fibril samples but significantly improved resolution for fibrillar samples has not been observed with PTA compared to UA. Many things on an EM grid are artefacts that can be mistaken for protein aggregates. For example, blemishes on formvar caused by some solvents or by a poor formvar coating can appear to be interesting shaped protein aggregates. Folded formvar can look like fibrils but is easily distinguished from authentic fibrils by a dramatic change upon focusing due to the depth of the folded formvar. Dense uranyl acetate crystals are occasionally present and are not related to the protein composition of the sample. A completely blank grid is observed if the formvar has torn (which occurs if too high a concentration of sample is used) or if all the protein remained in solution and did not settle on the grid. The lack of any protein adsorption to the grid is typically a good indication that there is little to no protein aggregation, amyloid or otherwise.

**Procedure 4:** Negative staining of amyloid fibrils for TEM [46]

1. Prepare a solution of 2% uranyl acetate in DDI water. This solution can be stored for several weeks at 4 °C. On the day of sample staining, spin the uranyl acetate solution at 12,000 rpm for 3 min to pellet any unsolubilized uranyl acetate.
2. Place 3  $\mu$ L of protein sample on the grid. After 3 min, apply a torn edge of hardened, ashless filter paper at the edge of the grid to absorb the remaining liquid (this process is known as wicking).
3. Immediately (i.e., do not let the sample dry on the grid), place 3  $\mu$ L of staining solution on the grid, wait 3 min, wick away excess solution, and air dry.
4. The grids can be immediately examined or stored in an EM grid case prior to examination. The grids are imaged using an electron microscope operating at 80 keV. Scan at low magnification (10–12,000 $\times$ ) to get an idea of the overall sample composition and then examine the finer details of the fibrils at higher magnification (25,000 $\times$ ). Amyloid fibrils are typically linear, unbranching, and 5–10 nm in width.

Glenner noted that “amyloid fibrils [in disease] may take forms and have dimensions differing from those previously described” and concluded that “no strict dimension can be placed on the amyloid fibril” [47]. This statement likewise extrapolates to amyloid fibrils formed in vitro. On a single grid of a protein fibril sample produced in vitro, it is possible to observe aggregates that are amorphous, spherical, fibrillar or higher-order assemblies of fibrils such as two fibrils wound around each other, lateral assemblies that form sheet-like deposits, and rope-like assemblies of many

fibrils wound together [48]. This raises several issues: (1) Does there need to be a specific amount of the fibrillar deposit to define the sample as amyloid? (2) The distinct assembly patterns suggest that the fibrils formed from different peptides have fibril surfaces that are very different. Does the surface heterogeneity among fibrils affect the ability of fibrils to bind ThT or Congo Red?

*Fourier transform infrared (FTIR) spectroscopy* is used to detect the presence of  $\beta$ -sheet secondary structure. Typically, the sample is examined before and after aggregation and an increase in  $\beta$ -sheet secondary structure is observed upon amyloid fibril formation. For FTIR analysis, sample preparation is very important. First, the ion pairing agent used in the purification of the peptide or protein needs to be IR compatible. Commercial peptides generally have TFA as the ion pair but TFA has an infrared vibration that interferes with the analysis of protein/peptide secondary structure and, therefore, must be exchanged to another ion pair (Procedure 5, step 1). Next, the residual water adsorbed to the peptide or protein needs to be exchanged to D<sub>2</sub>O. This step is not designed to fully deuterate the protein/peptide because, if the peptide or protein is subjected to conditions to fully deuterate the sample, this may lead to a different FTIR spectrum by prematurely inducing aggregation. The peptide or protein is then analyzed by FTIR in D<sub>2</sub>O and a spectrum recorded; this procedure is repeated after fibril formation. The choice of sample holder and scanning parameters for FTIR analysis varies, but a dismountable sample cell (which can be thoroughly and easily cleaned) and a minimum of 64 scans encompassing the range of 1500–1800 cm<sup>-1</sup> is ideal. The amide I band, which is used to assign secondary structure, occurs in the region between 1600 and 1700 cm<sup>-1</sup>. However, many interesting side chain vibrations occur on the edge of this range and detection between 1500 and 1800 cm<sup>-1</sup> will allow these vibrations to be observed. The most common detectors are DTGS and MCT. DTGS is particularly stable and, therefore, provides superior water vapor subtraction while the MCT detector is more sensitive but generally less stable and needs to be cooled with LN<sub>2</sub>.

**Procedure 5:** FTIR analysis of amyloid fibrils

1. Exchange the ion pairing agent: dissolve the peptide/protein in 5 mM HCl, freeze in liquid nitrogen (LN<sub>2</sub>), lyophilize, and repeat this process 4–5 times. Alternatively, the peptide/protein can be repurified by RP-HPLC using HCl instead of TFA in the buffers.
2. Exchange the residual H<sub>2</sub>O to D<sub>2</sub>O: dissolve the peptide in a small amount of D<sub>2</sub>O, incubate at room temperature for 30 min, freeze (LN<sub>2</sub>), and lyophilize.
3. Amyloid fibrils should be formed in D<sub>2</sub>O with the pD adjusted with DCl/NaOD. As a general rule, it

is difficult to get quality FTIR spectra from fibrils formed in  $\text{H}_2\text{O}$  and then exchanged to  $\text{D}_2\text{O}$ .

- 4a. Data acquisition in  $\text{D}_2\text{O}$ : purge sample chamber for 20 min, take a scan of the empty chamber (as a background), purge for 20 min, take a scan of the same  $\text{D}_2\text{O}$  solution used for sample preparation, purge for 20 min, take a scan of the sample, and subtract the  $\text{D}_2\text{O}$  spectrum from the sample spectrum\*.
- 4b. Data Acquisition in the solid state: purge sample chamber for 20 min, take a scan of the empty chamber (as a background), purge for 20 min, take a scan of the empty sample cell, purge for 20 min, dry the peptide or fibril sample onto the sample cell window using a gentle stream of nitrogen and take a scan of the sample, and subtract the  $\text{D}_2\text{O}$  spectrum from the sample spectrum\*.
5. Examine the Amide I region ( $1600\text{--}1700\text{ cm}^{-1}$ ) of the sample spectrum.  $\beta$ -sheet secondary structure is detected by the presence of a band near  $1620\text{ cm}^{-1}$ .
6. Note: FTIR can be performed in  $\text{H}_2\text{O}$  instead of  $\text{D}_2\text{O}$ , but very high sample concentrations are required and the high sample concentration can make it difficult to obtain a sample spectrum of the monomeric peptide/protein.

\*Some FTIR instruments do not require purging to eliminate water vapor (e.g., Perkin Elmer Spectrum One).

The interpretation of an FTIR spectrum should begin with an examination of the primary sequence of the protein/peptide. Side chains such as Asn and Gln, which are common in amyloid-forming and prion proteins [63], have IR vibrations that overlap in the amide I band. Therefore, an estimate of the total contribution of the spectrum from the side-chain vibrations and where these vibrations typically appear should be determined [49]. The peaks in the spectrum can be identified by curve fitting of the original spectrum, Fourier self deconvolution which narrows the bands, or by analyzing the 2nd derivative of the FTIR spectrum which highlights the points of inflection (i.e., the peaks) of the original spectrum. For curve-fit analysis, it is important to note that a given spectrum typically will not have a unique fit. Therefore, the spectrum should be fit using the minimum number of curves necessary, the maxima of the curve-fit peaks should correlate with the maxima visible in the raw data, and typically the curve-fit peaks should have similar widths, i.e., full-width at half-height (FWHH) values. The integration of the area of the component bands used to generate the final curve fit can provide an estimate of the relative percentages of secondary structure present (Fig. 1). A 2nd derivative spectrum should only be presented in conjunction with the original spectrum. The second derivative amplifies the peak positions but, if there is poor water subtraction, the noise is also amplified and leads to a skewed

data set (unless the data is smoothed, which is not encouraged).

The assignment of a peak at a given wavenumber to a given secondary structure should be done with caution since the FTIR analysis of protein secondary structure is still largely empirical. Thus, it is *not* possible to assign an FTIR spectrum a priori unless the percent of secondary structural elements is already known from another technique. The assignment of turns is particularly ambiguous. As a rule of thumb, however, a peak near  $1645\text{ cm}^{-1}$  is indicative of random coil,  $1655\text{ cm}^{-1}$  of  $\alpha$ -helix, and  $1620\text{--}1640\text{ cm}^{-1}$  of  $\beta$  sheet [50–52]. Stronger hydrogen bonding results in a shift to lower wavenumbers and, therefore, amyloid fibrils often have  $\beta$  sheet peaks below  $1620\text{ cm}^{-1}$ . FTIR has also been used to suggest that the  $\beta$ -sheets in amyloid fibrils are largely anti-parallel but some have been assigned a parallel orientation (e.g., insulin and calcitonin) [47,53]. The assignment of an anti-parallel  $\beta$ -sheet is based on the observation of a peak near  $1680\text{ cm}^{-1}$  that arises due to transition dipole coupling [54] and is absent in a parallel  $\beta$ -sheet. However, the assignment of the  $1680\text{ cm}^{-1}$  peak to transition dipole coupling can be ambiguous in some cases since the second band observed for a random coil structure in  $\text{D}_2\text{O}$  also occurs in this region [50].

There are two interesting issues to consider regarding the use of  $\beta$ -sheet secondary structure (detected by FTIR or X-ray diffraction) as a criterion for amyloid fibril identification; the hydration state of the sample and the amount of  $\beta$ -sheet secondary structure necessary to qualify a sample as an amyloid fibril. The current amyloid criteria do not include any specifications regarding these parameters and, therefore, they are interpreted using the widest possible range, i.e., any hydration state and any percentage of  $\beta$ -sheet structure is acceptable. It is widely known, however, that the  $\beta$ -sheet content of a dried sample is often significantly higher than a hydrated sample and, therefore, the analysis of fibrils in the solid state often facilitates the observation of  $\beta$ -sheet secondary structure [23,55]. This observation leads to speculation regarding the factors that are important in the observation of  $\beta$ -sheet structure [64]. Furthermore, the effect of sample hydration and aggregation on the extinction coefficients for secondary structural elements in an FTIR spectrum is unknown. The current assumption is that the extinction coefficients for all secondary structural elements are the same, which is likely true for folded proteins but not necessarily for aggregated protein samples. It is probable, in fact, that protein aggregation may decrease the extinction coefficient for  $\beta$ -sheet secondary structure which would result in an ‘apparent’ decrease in  $\beta$ -sheet content. Therefore, the  $\beta$ -sheet structure criterion will need to remain broadly defined until a correlation between sample state and extinction coefficients is established.

### 3. Proposal for revised criteria for the identification of in vitro amyloid fibrils

The growing literature of fibrillar deposits that deviate from the criteria for standard amyloid fibrils highlights the need for a re-evaluation of the techniques currently used to identify amyloid fibrils in vitro. Since many other properties have been identified to be associated with amyloid fibrils, it seems reasonable that a new classification system for in vitro amyloid fibrils may be warranted. As a possible new classification scheme, the following criteria are proposed:

- (A) Fibrillar morphology.
- (B) Fibrils that are entirely  $\alpha$ -helical are excluded.
- (C) A total score of 4 must be achieved by satisfying a combination of the following criteria. Only one item per category can count toward the final score (i.e., Congo Red binding by either the spectroscopic or the microscopic assay yields two points; these two criteria cannot be combined to achieve four points.)

| Characteristic  | Score for a positive test |
|---|---------------------------|
| $\beta$ -sheet secondary structure in hydrated or dried samples | 2                         |
| Congo Red binding (via microscopic or spectroscopic assay)      | 2                         |
| ThT or ThS binding  | 2                         |
| Gel formation   | 1                         |
| Protofibril intermediate or seeded kinetics                     | 1                         |
| Low solubility in denaturant or protease resistance             | 1                         |

This classification system would include the current classification of an in vitro amyloid fibril (i.e., the sum of  $\beta$ -sheet secondary structure and Congo Red binding yields the necessary 4 points) but this system extends the boundaries to include other properties that have become associated with amyloid fibrils. The all  $\alpha$ -helical aggregates [56,57] are excluded because, at this point, they are unique and seem to warrant their own separate category. However, continual revision of this scheme could lead to a broader classification of in vitro amyloid such that a more complete understanding of this class of aggregate will emerge as new discoveries are made.

### Acknowledgments

I am grateful to Anne Clark and Mark Krebs for technical advice, helpful discussions, and a critical review of the manuscript. I am also grateful to Dan Raleigh (DPR) and Anne Clark (AC) for access to

unpublished data and Chris Dobson for financial support during manuscript preparation.

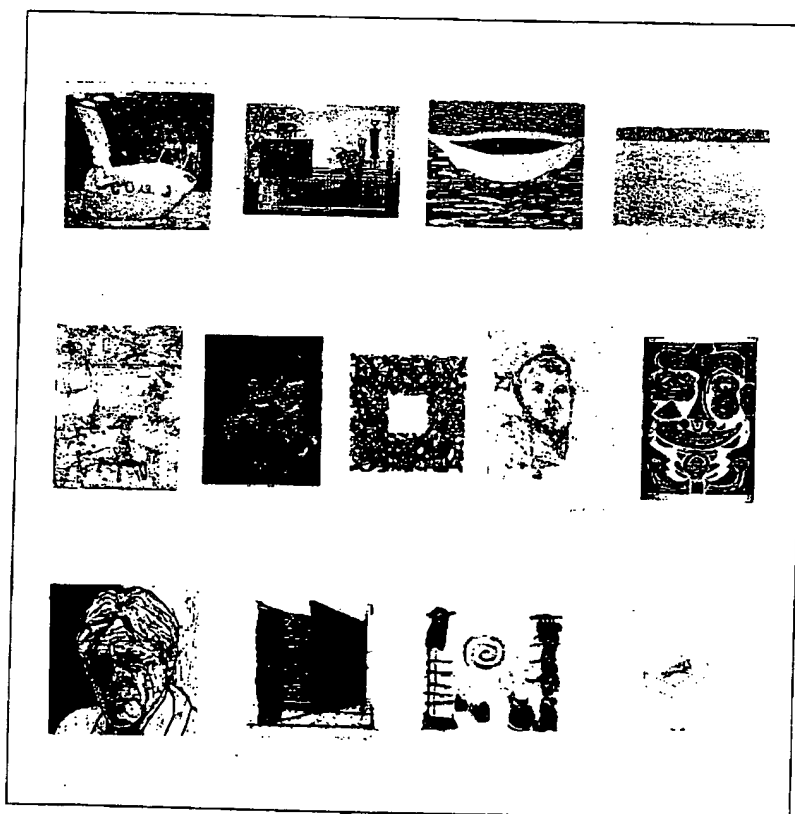
### References

- [1] R. Kisilevsky, P.E. Fraser, *Crit. Rev. Biochem. Mol. Biol.* 32 (1997) 361–404.
- [2] J.D. Sipe, *Crit. Rev. Clin. Lab. Sci.* 31 (1994) 325–354.
- [3] P.N. Hawkins, M.B. Pepys, *Eur. J. Nucl. Med.* 22 (1995) 595–599.
- [4] C. Aprile, G. Marinone, R. Saponato, C. Bonino, G. Merlini, *Eur. J. Nucl. Med.* 22 (1995) 1393–1401.
- [5] H. Puchtler, F. Sweat, M. Levine, *J. Histochem. Cytochem.* 10 (1962) 355–364.
- [6] P. Westermark, *Amyloid: Int. J. Exp. Clin. Invest.* 4 (1997) 216–218.
- [7] F. Chiti, P. Webster, N. Taddei, A. Clark, M. Stefani, G. Ramponi, C.M. Dobson, *Proc. Natl. Acad. Sci. USA* 96 (1999) 3590–3594.
- [8] M.R.H. Krebs, D.K. Wilkins, E.W. Chung, M.C. Pitkeathly, A.K. Chamberlain, J. Zurdo, C.V. Robinson, C.M. Dobson, *J. Mol. Biol.* 300 (2000) 541–549.
- [9] J.D. Sipe, A.S. Cohen, *J. Struct. Biol.* 130 (2000) 88–98.
- [10] J.W. Kelly, *Nat. Struct. Biol.* 9 (2002) 323–325.
- [11] B.A. Yankner, L.K. Duffy, D.A. Kirschner, *Science* 250 (1990) 279–282.
- [12] B. Caughey, P.T. Lansbury Jr., *Annu. Rev. Neurosci.* 26 (2003) 267–298.
- [13] C.M. Dobson, *Philos. Trans. R. Soc. Lond. B* 356 (2001) 133–145.
- [14] R. Wetzel, *Cell* 86 (1996) 699–702.
- [15] P.T. Lansbury Jr., *Proc. Natl. Acad. Sci. USA* 96 (1999) 3342–3344.
- [16] H.A. Lashuel, S.R. LaBrenz, L. Woo, L.C. Serpell, J.W. Kelly, *J. Am. Chem. Soc.* 122 (2000) 5262–5277.
- [17] C.E. MacPhee, C.M. Dobson, *J. Am. Chem. Soc.* 122 (2000) 12707–12713.
- [18] C. Soto, E.M. Castano, R.A. Kumar, R.C. Beavis, B. Frangione, *Neurosci. Lett.* 200 (1995) 105–108.
- [19] L. Hou, I. Kang, R.E. Marchant, M.G. Zagorski, *J. Biol. Chem.* 277 (2002) 40173–40176.
- [20] V.N. Uversky, G. Yamin, P.O. Souillac, J. Goers, C.B. Glaser, A.L. Fink, *FEBS Lett.* 517 (2002) 239–244.
- [21] M.R. Nilsson, M.D. Driscoll, D.P. Raleigh, *Protein Sci.* 11 (2002) 342–349.
- [22] I. Kaneko, S. Tutumi, *J. Neurochem.* 68 (1997) 438–439.
- [23] M.R. Nilsson, D.P. Raleigh, *J. Mol. Biol.* 294 (1999) 1375–1385.
- [24] J.D. Harper, P.T. Lansbury Jr., *Annu. Rev. Biochem.* 66 (1997) 385–407.
- [25] R. Orlando, P.T. Kenny, M.G. Zagorski, *Biochem. Biophys. Res. Commun.* 184 (1992) 686–691.
- [26] M. Jackson, H.H. Mantsch, *Biochim. Biophys. Acta* 1078 (1991) 231–235.
- [27] A. Dong, J. Matsuura, M.C. Manning, J.F. Carpenter, *Arch. Biochem. Biophys.* 355 (1998) 275–281.
- [28] M. Sunde, L.C. Serpell, M. Bartlam, P.E. Fraser, M.B. Pepys, C.C.F. Blake, *J. Mol. Biol.* 273 (1997) 729–739.
- [29] H. LeVine, *Amyloid: Int. J. Exp. Clin. Invest.* 2 (1995) 1–6.
- [30] J. Wall, C.L. Murphy, A. Solomon, *Methods Enzymol.* 309 (1999) 204–217.
- [31] G.T. Westermark, S. Gebre-Medhin, D.F. Steiner, P. Westermark, *Mol. Med.* 6 (2000) 998–1007.
- [32] D.F. Moriarty, D.P. Raleigh, *Biochemistry* 38 (1999) 1811–1818.
- [33] P.C. Bedaux, P.J.O. Kerssemakers, C.A.M. Meijers, *Pharm. Weekblad* 98 (1963) 189–195.
- [34] W.E. Klunk, J.W. Pettegrew, D.J. Abraham, *J. Histochem. Cytochem.* 37 (1989) 1273–1282.

- [35] J.H. Cooper, *J. Clin. Pathol.* 22 (1969) 410–413.
- [36] M.T. Elghetany, A. Saleem, K. Barr, *Ann. Clin. Lab. Sci.* 19 (1989) 190–195.
- [37] M. Skowronek, B. Stopa, L. Konieczny, J. Rybarska, B. Piekarska, E. Szneler, G. Bakalarski, I. Roterman, *Biopolymers* 46 (1998) 267–281.
- [38] R. Khurana, V.N. Uversky, L. Nielsen, A.L. Fink, *J. Biol. Chem.* 276 (2001) 22715–22721.
- [39] D.B. Carter, K.C. Chou, *Neurobiol. Aging* 19 (1998) 37–40.
- [40] T.T. Ashburn, H. Han, B.F. McGuinness, P.T. Lansbury Jr., *Chem. Biol.* 3 (1996) 351–358.
- [41] C.B. Caputo, P.E. Fraser, I.E. Sobel, D.A. Kirschner, *Arch. Biochem. Biophys.* 292 (1992) 199–205.
- [42] G. Ratnaswamy, E. Koepf, H. Bekele, H. Yin, J.W. Kelly, *Chem. Biol.* 6 (1999) 293–304.
- [43] J.T. Jarrett, P.T. Lansbury Jr., *Biochemistry* 31 (1992) 12345–12352.
- [44] T.A. Lutz, J.S. Rand, *J. Comp. Pathol.* 116 (1997) 157–170.
- [45] P.N. Hawkins, 10 years experience with serum amyloid P component scintigraphy, in: *Proceedings of the IXth International Symposium on Amyloidosis*, Budapest, 2001, pp. 238–241.
- [46] E.H. Nielsen, M. Mybo, S.-E. Svehaug, *Methods Enzymol.* 309 (1999) 491–496.
- [47] G.G. Glenner, *Prog. Histochem. Cytochem.* 13 (1981) 1–35.
- [48] C.S. Goldsburly, G.J.S. Cooper, K.N. Goldie, S.A. Müller, E.L. Saafi, W.T.M. Gruijters, M.P. Misur, A. Engel, U. Aebi, J. Kistler, *J. Struct. Biol.* 119 (1997) 17–27.
- [49] Y.N. Chirgadze, O.V. Fedorov, N.P. Trushina, *Biopolymers* 14 (1975) 679–694.
- [50] Y.N. Chirgadze, B.V. Shestopalov, S.Y. Venyaminov, *Biopolymers* 12 (1973) 1337–1351.
- [51] C.R. Middaugh, H. Mach, J.A. Ryan, G. Sanyal, D.B. Volkin, 1995. *Methods in Molecular Biology*, vol. 40: Protein Stability and Folding: Theory and Practice, Humana Press Inc., pp. 137–156.
- [52] M. Jackson, H.H. Mantsch, *Crit. Rev. Biochem. Mol. Biol.* 30 (1995) 95–120.
- [53] H.H. Bauer, M. Müller, J. Goette, H.P. Merkle, U.P. Fringeli, *Biochemistry* 33 (1994) 12276–12282.
- [54] W.H. Moore, S. Krimm, *Proc. Natl. Acad. Sci. USA* 72 (1975) 4933–4935.
- [55] W. Turnell, R. Sarra, J.O. Baum, D. Caspi, M.L. Balz, M.B. Pepys, *Mol. Biol. Med.* 3 (1986) 409–424.
- [56] M. Sadqi, F. Hernandez, U. Pan, M. Perez, M.D. Schaeberle, J. Avila, V. Munoz, *Biochemistry* 41 (2002) 7150–7155.
- [57] L. Bousset, N.H. Thomson, S.E. Radford, R. Melki, *EMBO* 21 (2002) 2903–2911.
- [58] M.R. Nilsson, C.M. Dobson, *Biochemistry* 42 (2003) 375–382.
- [59] J.W. Kelly, *Nat. Struct. Biol.* 7 (2000) 824–826.
- [60] M.J. Bonifacio, Y. Sakaki, M.J. Saraiva, *Biochi. Biophys. Acta.* 1316 (1996) 35–42.
- [61] L.W. Jin, K.A. Claborn, M. Kurimoto, M.A. Geday, I. Maezawa, F. Sohraby, M. Estrada, W. Kaminsky, B. Kahr, *Proc. Natl. Acad. Sci. USA* 100 (2003) 15294–15298.
- [62] S. Chen, V. Berthelie, J.B. Hamilton, B. O’Nuallain, R. Wetzel, *Biochemistry* 41 (2002) 7391–7399.
- [63] M.D. Michelitsch, J.S. Weissman, *Proc. Natl. Acad. Sci. USA* 97 (2000) 11910–11915.
- [64] A. Kishimoto, K. Hasegawa, H. Suzuki, H. Taguchi, K. Namba, M. Yoshida, *Biochem. Biophys. Res. Commun.* 315 (2004) 739–745.

# *Netherlands* The Journal of Medicine

PUBLISHED IN COLLABORATION WITH THE NETHERLANDS ASSOCIATION OF INTERNAL MEDICINE



AL AMYLOIDOSIS

PSEUDOMALABSORPTION OF LEVOTHYROXINE

CEREBRAL MALARIA

MENINGOCOCCAL PERICARDITIS

Univ. of Minn.  
Bio-Medical  
Library

04 23 04

## REVIEW

NOTED THIS JOURNAL MAY BE REPRODUCED  
BY ANY PERSON OR ORGANIZATION

# Diagnostic and therapeutic approach of systemic amyloidosis

B.P.C. Hazenberg<sup>1\*</sup>, I.I. van Gameren<sup>1</sup>, J. Bijzet<sup>1</sup>, P.L. Jager<sup>2</sup>, M.H. van Rijswijk<sup>1</sup>

Departments of <sup>1</sup>Rheumatology and <sup>2</sup>Nuclear Medicine, University Hospital Groningen, the Netherlands, tel.: +31 (0)50-361 34 32, fax: +31 (0)50-361 93 08, e-mail: b.p.c.hazenberg@int.azg.nl, \* corresponding author

## ABSTRACT

Amyloidosis is a group of diseases, all characterised by deposition of protein fibrils with a  $\beta$ -sheet structure. This structure generates affinity of amyloid for Congo red dye and is resistant to proteolysis. Three types of systemic amyloidosis are important for the clinician: AA (related to underlying chronic inflammation), AL (related to underlying monoclonal light chain production) and ATTR amyloidosis (related to old age or underlying hereditary mutations of transthyretin). Signs and symptoms vary considerably among the three types and the choice of treatment differs completely.

A stepwise approach in diagnosis and therapy is presented. When amyloidosis is suspected the first step is histological proof of amyloid and the second is proof of systemic involvement. The next two steps are determination of the type of amyloid followed by detection of the precursor protein. The fifth step is a thoughtful clinical evaluation, necessary for assessment of prognosis and therapy. Subsequently, the choice of therapy is based on the 'precursor-product' concept. In the final step, the effects of therapy on the underlying disease as well as on the amyloidosis are assessed during follow-up. In this evaluation serum amyloid P component (SAP) scintigraphy helps to show organ involvement and therapy response.

their insolubility, resistance to proteolysis and binding affinity for Congo red dye and the consequent green birefringence with polarised light. Amyloid fibrils are derived from different protein precursors. Extracellular deposition of amyloid fibrils in organs and tissues results in loss of organ function and may cause prominent swelling of the affected organ or tissue. Deposition of amyloid can be localised (restricted to one organ or site of the body) or systemic (in various organs and tissues throughout the body). The various clinical pictures of systemic amyloidosis are related to the type of precursor protein involved.<sup>1,2</sup> Terms such as primary and secondary amyloidosis have become obsolete, because all types of amyloid are secondary to the production of a specific precursor. Therefore the old nomenclature has been replaced by a new one based on the protein precursor.<sup>3</sup> In this article the clinician will find a stepwise approach to diagnosis, clinical evaluation and background of therapy in patients with suspected systemic amyloidosis. Readers who want to know more about clinical aspects and molecular mechanisms of the systemic amyloidoses are referred to the review articles of Falk *et al*<sup>4</sup> and Merlini and Belotti.<sup>5</sup>

## CLASSIFICATION

Although localised deposition of amyloid plays an important role in the development of widespread serious diseases such as Alzheimer's disease ( $\beta$ -protein in the plaques) and diabetes mellitus type II (amylin in the islands of Langerhans), this article focuses on the systemic types of amyloidosis. There are four major types.<sup>1,3</sup>

## INTRODUCTION

Amyloidosis is a group of diseases all characterised by deposition of proteinaceous fibrils with a molecular  $\beta$ -sheet structure.<sup>1</sup> This structure of the fibrils is responsible for

### AA amyloidosis

This type is caused by longstanding inflammation. Serum amyloid A protein (SAA), an acute phase reactant, is the precursor protein. Renal manifestations, such as proteinuria (progressing to nephrotic syndrome) and loss of renal function (progressing to renal failure), are observed very frequently (about 90% of cases). Less frequent manifestations are autonomic neuropathy, hepatomegaly and cardiomyopathy.

### AL amyloidosis

AL amyloidosis is caused by a plasma cell dyscrasia. Lambda or kappa immunoglobulin light chain is the precursor protein of this type. Clinical manifestations are very diverse, such as cardiomyopathy, hepatomegaly, splenomegaly, nephrotic syndrome, renal failure, orthostatic hypotension, diarrhoea, peripheral and autonomic neuropathy, arthropathy, carpal tunnel syndrome (CTS) and glossomegaly. The diversity of manifestations (and their combinations) depends on the severity of deposition in the various organs and tissues.

### ATTR amyloidosis

Various autosomal dominant hereditary point mutations of the precursor protein transthyretin (TTR) cause this type. Transthyretin, formerly called prealbumin because of its electrophoretic profile, is an acronym of a transport protein of thyroid hormone and retinol-binding protein. More than 80 of these mutations have been described. Prominent clinical manifestations are (familial) peripheral and autonomic neuropathy, but cardiomyopathy, renal failure and eye involvement (vitreous opacities) are also often observed. Severe cardiomyopathy can be the presenting sign in some of the TTR mutations. In very old age, normal ('wild-type') TTR can also behave as precursor protein. This so-called senile systemic amyloidosis is characterised by a slowly progressive cardiomyopathy.

### AB $\beta$ 2M amyloidosis

This type is caused by renal failure and longstanding (i.e. at least 5 to 10 years) dialysis with decreased clearance of beta-2-microglobulin ( $\beta$ 2M).  $\beta$ 2M is the precursor protein of this type. Clinical manifestations are arthropathy, such as tenosynovitis, shoulder pain, CTS, periarticular cysts, pathological fractures and destructive spondyloarthropathy. Synovial tissue biopsy is the method to detect amyloid. Kidney transplantation stops the disease.<sup>4,5</sup>

AB $\beta$ 2M amyloidosis is a disabling disease that should be recognised and treated. This article, however, describes only the first three types (AA, AL and ATTR) of systemic amyloidosis because these types are often unexpected, difficult to diagnose, with variable involvement of many different organs and tissues and often pose the problem of finding the most appropriate therapy.

### PROOF OF AMYLOID

The first step is to detect amyloid. The diagnosis of amyloid is based on proof of its presence in tissue. This can be shown in a positive Congo red stained tissue specimen with the characteristic apple-green birefringence in polarised light (see figure 1). The abdominal subcutaneous fat aspiration is the most elegant and least inconvenient method for this purpose, with a sensitivity ranging between 54%<sup>6</sup> and 82%<sup>7,8</sup> and a specificity of 100%.

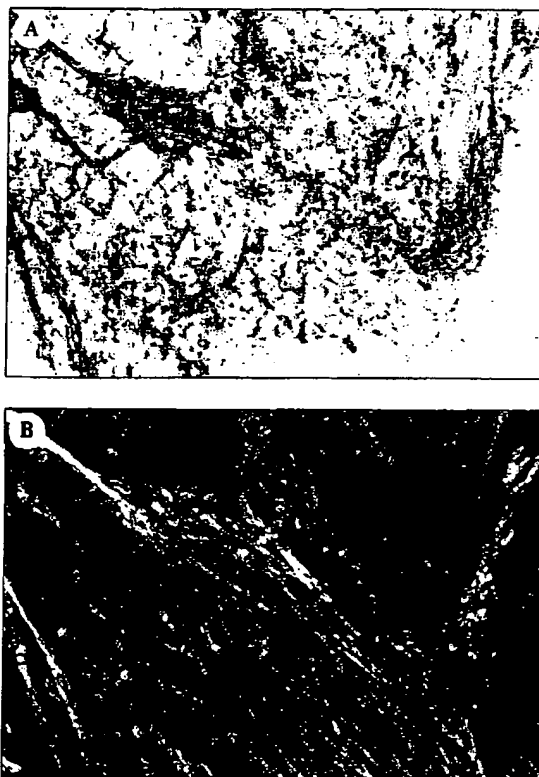


Figure 1A and B

Example of an abdominal subcutaneous fat aspirate, stained with Congo red, magnification 30x.

A: When viewed in normal light, amyloid is stained red.

B: The same specimen viewed in polarised light: amyloid shows apple-green birefringence.

These figures are similar to those of the well-known rectum biopsy.<sup>8</sup> If the primary biopsy site (fat or rectum) is negative for amyloid and there is strong suspicion of amyloidosis, a biopsy of the other tissue is useful to increase the chance of detecting amyloid. A bone marrow biopsy can also be used, but has a disappointingly low sensitivity of 50 to 60%.<sup>8</sup> When all biopsies are negative but a strong suspicion of amyloidosis still exists, a biopsy of the affected organ or tissue is indicated.<sup>1,9</sup>

## SYSTEMIC DEPOSITION

Amyloid deposition can be local or systemic. Therefore the second step is to check for systemic deposition. Some sites are exclusively involved in systemic amyloidosis, such as kidneys, liver, nerves, abdominal fat and spleen. If such a site is positive for amyloid, systemic involvement is established. Localised amyloid can often be found in other sites of the body, including the eyelid, cardiac atria, larynx, ureter and skin. In these cases amyloid must be undetectable elsewhere in the body to confirm localised amyloidosis. Most other sites (bone marrow, heart, bowel, lung, joint, etc.) are nearly always involved in systemic amyloidosis. In this situation it is recommended to demonstrate amyloid in two different organs or tissues. For this demonstration, however, it is sufficient to have histological proof at one site (such as bone marrow, skin or rectum) and clinical involvement (such as nephrotic syndrome, hepatomegaly, macroglossia, or cardiomyopathy) at the other site.<sup>10</sup>

## TYPE OF AMYLOID

After verification of presence of systemic amyloid, the third step is determination of the type of amyloid. In many cases the type of amyloid can be assessed with high probability from the medical history and clinical picture. Amyloidosis in a patient with longstanding rheumatoid arthritis and nephrotic syndrome is almost certainly the AA type. Someone with polyneuropathy who belongs to a family with hereditary amyloidosis probably has ATTR amyloidosis. And in a patient with characteristic shoulder pads and glossomegaly it is hard to imagine something other than AL amyloidosis. Nevertheless, even in these patients with strong clinical evidence for a particular type of amyloid, more solid confirmation of the specific type of amyloid should be determined. The clinical consequences of incorrect typing of amyloid can be considerable: prognosis and therapy of the three major types of systemic amyloidosis are completely different.

Immunohistochemistry of a biopsy is helpful to characterise the type of amyloid by using specific antibodies (see figures 2 and 3). In AA amyloidosis this technique is sufficient, provided sensitive and specific monoclonal antibodies are used, such as mcr<sup>10</sup> and Reu.86.2.<sup>11,12</sup>

However, in ATTR amyloidosis and especially in AL amyloidosis this method is less reliable than in AA amyloidosis. This is caused by heterogeneity of amyloid deposits, loss of epitopes in the fibril structure, lower sensitivity and specificity of (polyclonal) antibodies and nonspecific adherence of immunoglobulins to amyloid deposits or the background.<sup>10</sup> Lack of a positive family



Figure 2A and B

Rectum biopsy of a patient with AA amyloidosis, magnification 30x. Small deposits of amyloid can be seen in the epithelial border and in the submucosa in the walls of blood vessels.

A: Amyloid is red in the Congo red stain.

B: Amyloid is brown in the immunoperoxidase stain with monoclonal antibodies against SAA (Reu.86.2).

history does not exclude ATTR amyloidosis as shown by a considerable number of 'sporadic' cases that have been described.<sup>13</sup> Therefore presence of a TTR mutation (by DNA analysis) must be established in all cases of ATTR amyloidosis. The only exclusion for this requirement is old age (>80 years) and a typical clinical picture of senile systemic amyloidosis (i.e. slowly progressive cardiomyopathy). In patients with AL amyloidosis, a monoclonal plasma cell dyscrasia with overproduction of lambda or kappa light chain must be present. It can be detected in bone marrow (clonal dominance by immunophenotyping of plasma cells), urine (Bence Jones proteins, immunofixation of concentrated urine) and blood (M-protein, immunofixation and the free light chain assay). However, a monoclonal gammopathy of undetermined significance (MGUS) is frequently present in healthy older persons,



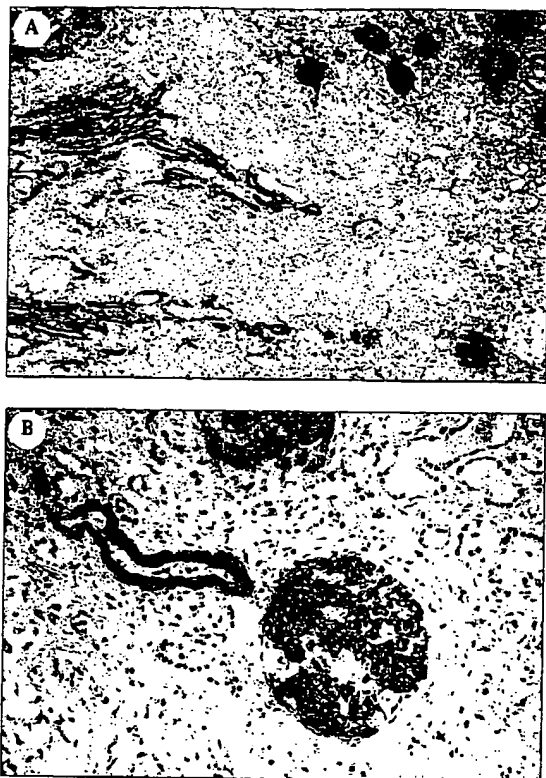


Figure 3A and B

Kidney tissue of a patient with AA amyloidosis.

Amyloid is brown in the immunoperoxidase stain with monoclonal antibodies against SAA (Reu.86.2).

A: Overview with glomeruli and vasa recta, magnification 10x.

B: Detail, glomerulus, magnification 40x.

ranging from 2% in persons of 50 to 3% in persons of 70 years.<sup>14</sup> Thus detection of MGUS does not exclude other types than AL amyloidosis. It is important to notice that the clinical picture of ATTR amyloidosis and AL amyloidosis can sometimes be similar, such as in cases with polyneuropathy, autonomic neuropathy, cardiomyopathy and carpal tunnel syndrome. In such a clinical picture it is therefore not sufficient to show the presence of a plasma cell dyscrasia but also necessary to exclude a TTR mutation before AL amyloidosis can be diagnosed.<sup>15</sup>

## PRECURSOR PROTEIN

After establishing the type of amyloid it is time for the fourth step, i.e. to look for a precursor protein in the blood. Detection of a precursor protein and measuring its serum concentration is important for therapy. In AA amyloidosis the precursor protein is SAA, an acute phase

reactant. The behaviour of SAA during inflammation is comparable with C-reactive protein (CRP), a protein that can be assessed in routine clinical practice. In ATTR amyloidosis the precursor protein is a mutated TTR. This can be detected by isoelectric focusing.<sup>1</sup> In AL amyloidosis a recently described assay shows the presence of free lambda and kappa precursor proteins in blood using specific antibodies raised against normally hidden epitopes in the complete immunoglobulin.<sup>13</sup>

## CLINICAL EVALUATION

The fifth step is to obtain a reliable understanding of the 'amyloid load', i.e. affected organs and tissues and severity of amyloid deposition in vital organs (such as heart, liver and kidneys). One should not forget to ask about the family history, impotence, orthostatic complaints, loss of sensibility, fatigue, weight loss and bowel problems. Physical examination should also focus on signs such as orthostatic blood pressure, friability of skin, glossomegaly, arthropathy, hepatomegaly, splenomegaly, oedema, cardiac failure and loss of sensibility and muscle strength of extremities. A thoughtful systematic clinical approach is helpful. The heart can be examined with electrocardiography (signs of low voltage and pseudo-anteroseptal infarction), chest X-ray (normally sized heart despite signs of cardiac failure), echocardiography (thickness of septum and ventricular walls), 24-hour Holter registration (conduction, rhythm and heart rate variability) and a MUGA scan (ejection fraction). The kidneys can be examined with serum albumin, creatinine clearance, urine sediment and proteinuria, whereas serum albumin, liver enzymes such as alkaline phosphatase, bilirubin, coagulation tests and cholinesterase can be used to examine the liver. Thyroid-stimulating hormone can be used for the thyroid and fasting cortisol for the adrenal glands. Autonomic function tests ('Ewing battery') and heart rate variability are ways of evaluating autonomic neuropathy.<sup>16,17</sup> Electromyography can be used to assess peripheral neuropathy. Abdominal ultrasound may be helpful to evaluate size and echogenicity of liver, spleen and kidneys. Not all of the examinations mentioned above need to be employed because often it is obvious that clinical organ involvement is not present at all. However, echocardiography should be considered in all patients, even in those without cardiac symptoms. Serum amyloid P component (SAP) scintigraphy is a technique that has been developed in London by Pepys and Hawkins for specific evaluation of amyloidosis.<sup>18,19</sup> All amyloid deposits contain SAP, a glycoprotein that belongs to the pentraxin family and binds in a calcium-dependent way to all amyloid deposits independently of the protein of origin. The <sup>125</sup>I-labelled SAP scan can show specific uptake in organs such as liver, spleen, kidneys,

adrenals, bone marrow and joints (see figure 4 for some examples). However, myocardium does not show specific uptake, probably because of the combination of high background activity of tracer still present in the blood pool and decreased permeability in cardiac tissue of this tracer with a high molecular weight.<sup>18</sup> Measurement of SAP retention after 24 or 48 hours combined with the intensity of organ uptake on images provides a quantitative estimate of amyloid load in an individual patient that might be used to monitor effect of therapy in this patient.<sup>19</sup> The technique is only available in a few centres.

than one year.<sup>19</sup> Median survival in AL amyloidosis in case of symptomatic cardiomyopathy is four to six months, with kidney involvement about two years and with CTS more than three to four years. Patients with AA amyloidosis have a median survival of two to four years.<sup>19</sup> However, survival depends greatly on the activity of the underlying inflammation.<sup>20</sup> Patients with ATTR amyloidosis may survive up to 10 to 15 years.<sup>1</sup>

## THERAPY

The current basis of therapy is the so-called 'precursor-product' concept.<sup>21</sup> The central idea of this concept is that further growth of amyloid deposits will cease when the supply of necessary precursor proteins is put to a stop. Therefore, in AA amyloidosis the treatment is aimed at decreasing SAA serum levels to normal basal values (below 3 mg/l). This aim can only be achieved by a complete suppression or eradication of the underlying chronic inflammation. Examples are surgical treatment of chronic osteomyelitis and antibiotic treatment of infectious diseases such as tuberculosis and leprosy. In chronic inflammatory diseases such as rheumatoid arthritis and Crohn's disease effective suppression of inflammation (resulting in a substantial decrease of serum SAA levels below 10 mg/l) can be difficult, but should be attempted.<sup>20</sup> To achieve this goal, cytostatic drugs can be used (such as methotrexate, azathioprine, cyclophosphamide, or chlorambucil), but also anti-TNF (tumour necrosis factor) drugs (such as infliximab, adalimumab and etanercept). In patients with TRAPS (TNF-receptor-associated periodic syndrome) etanercept (acting as a soluble TNF receptor) seems to be a rational treatment because of the abnormal function of the mutated TNF receptor.<sup>22</sup> The interleukin-1-receptor antagonist anakinra may be highly effective in cryopyrin-related diseases such as familial cold urticaria and Muckle-Wells syndrome.<sup>23</sup> Colchicine has a central place in the treatment of familial Mediterranean fever (FMF), not only by reducing the frequency and severity of attacks, but also by preventing the development of AA amyloidosis.<sup>24</sup> Dimethylsulphoxide (DMSO) was first thought to dissolve amyloid fibrils, but turned out to be an anti-inflammatory agent.<sup>25</sup> The anti-amyloid effect in AA amyloidosis appeared to be mediated by lowering SAA serum levels.<sup>21,25,26</sup>

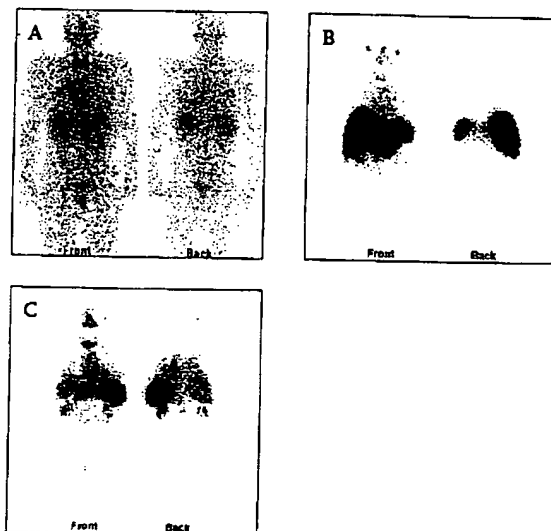


**Figure 4A, B and C**  
SAP (Serum Amyloid P component) scintigraphy 24 hours after intravenous injection of <sup>125</sup>I-SAP, total body uptake front (left images) and back (right images).  
A: Healthy control with minor nonspecific uptake (radioactive degradation products including free iodine) in stomach, bladder and minimal uptake in the (blocked) thyroid.  
B: Intense uptake in liver and spleen in a patient with AL amyloidosis.  
C: Uptake in spleen and kidney in a patient with AA amyloidosis.

## PROGNOSIS

The last step before determining therapy is assessment of prognosis. Generally prognosis is poor if the disease is untreated. The prognosis depends upon the type of amyloid, severity of amyloid deposition, number of vital organs affected, presence of symptomatic cardiomyopathy, severity of the underlying disease and response to therapy of the underlying disease. Patients with untreated AL amyloidosis have the worst prognosis, with a median survival of less

than one year.<sup>19</sup> Median survival in AL amyloidosis in case of symptomatic cardiomyopathy is four to six months, with kidney involvement about two years and with CTS more than three to four years. Patients with AA amyloidosis have a median survival of two to four years.<sup>19</sup> However, survival depends greatly on the activity of the underlying inflammation.<sup>20</sup> Patients with ATTR amyloidosis may survive up to 10 to 15 years.<sup>1</sup>

## SUPPORTIVE TREATMENT

Beside treatment aimed at the underlying disease, it is necessary to give supportive treatment for loss of organ function caused by amyloid deposition. In cardiac involvement the clinician should be extremely careful when using digoxin and calcium-channel blockers (their affinity to amyloid in the heart may enhance toxicity) and with cisapride for bowel motility problems (because of the risk of 'torsade des pointes'). Amyloid involvement of the heart primarily leads to right-sided heart failure; therefore the clinician should be careful with volume depletion (the problem is more an inflow than an outflow problem). Patients with symptomatic bradycardia may need implantation of a pacemaker. Nephrotic syndrome can be treated with salt restriction, careful use of diuretics and angiotensin-converting enzyme (ACE) inhibitors or nonsteroidal anti-inflammatory drugs. Orthostatic hypotension is difficult to treat. Fludrocortisone should be tried first and sometimes erythropoietin may also be helpful to treat this condition. Amitriptyline can be used for neuropathic pain; however, it should be used with caution (because of its possible effects on blood pressure and rhythm) in patients with cardiomyopathy. Adequate oral or intravenous feeding is mandatory in patients with significant weight loss, debilitating diarrhoea, absorption problems, or intestinal pseudo-obstruction. Various problems can cause diarrhoea, such as disturbed bowel motility, bacterial overgrowth, bile salt malabsorption and massive bowel wall infiltration with amyloid. Multisystem involvement results in a mix of serious problems and in such a situation it is almost impossible to find an appropriate treatment for all symptoms.<sup>1</sup>

## EFFECT OF TREATMENT

The final step after the establishing therapy is the measurement of effect. This is especially true for patients with such an intangible disease as systemic amyloidosis.<sup>30</sup> The essence of the 'precursor-product' concept is that no further accumulation of amyloid deposits will occur after successful standstill of the supply of precursor proteins. Besides, the hope is that the body will be able to remove some of the amyloid deposits still present. Repeated measurements after specific time intervals can give an idea of the effect of therapy. It is important to note that two different processes should be monitored in this way.

Firstly, the underlying process with its precursor protein should be monitored: serum SAA, free kappa or lambda light chain and mutated ATTR in AA, AL and ATTR amyloidosis, respectively. If treatment is successful SAA levels should fall below 10 mg/l, free kappa and lambda levels and kappa/lambda ratio should return to normal reference ranges and mutant TTR should not be detectable in the blood.

Secondly, the process of amyloid accumulation should be assessed by measuring the 'amyloid load'. For this measurement quantitative abnormal clinical signs should be monitored, such as serum albumin, alkaline phosphatase, bilirubin, creatinine clearance, proteinuria, ventricular wall thickness, ejection fraction, conduction and rhythm, heart rate variability, Ewing battery results and the size of enlarged organs, such as liver, spleen and kidneys. The abdominal subcutaneous fat aspiration can be repeated at each time point to get an idea of the severity of the presence of amyloid or its disappearance from tissue.<sup>30</sup> SAP scintigraphy, if abnormal at presentation, is the method of choice to monitor amyloid load in the individual patient.<sup>18,20,30,31</sup> Although differences among the leading research groups are small, response criteria are currently not standardised. Comparing results of therapy will become much easier if the international amyloid community is able to create a generally accepted set of criteria for response, stable disease and progressive disease for the different types of systemic amyloidosis.

## TREATMENT PERSPECTIVES

The 'precursor-product' concept focuses on the prevention of further deposition of amyloid. Clinical research is directed to developing new drugs that can interfere with amyloid deposition or can stimulate the removal of amyloid deposits. A promising new drug for patients with AA amyloidosis is sodium-1,3-propane-disulfonate (Fibrillex). This drug is a glycosaminoglycan-mimetic drug that binds to SAA. This binding may prohibit binding of SAA to glycosaminoglycans in tissue.<sup>32</sup> A multinational phase II/III trial started in 2001 and results are to be expected in the summer of 2005. In AL amyloidosis

4'-iodo-4'-deoxydoxorubicin (IDOX) may have effect in soft tissue involvement, although definite proof has to be awaited.<sup>33</sup> CPHPC is another drug that leads to depletion of SAP from the circulation.<sup>34</sup> If this mechanism indeed stops accumulation of amyloid, it may be very useful for all types of systemic amyloidosis. However, clinical results are not available yet. Diflunisal is worth mentioning, which might be useful as stabilising ligand in patients with ATTR amyloidosis. This drug stabilises *in vitro* the TTR tetramer in blood and prohibits its degradation into amyloidogenic dimers and monomers.<sup>35</sup>

A completely different approach is vaccination. Research has been focused on conformational epitopes present in all types of amyloid that might be used for vaccination.<sup>36</sup> If this hypothesis turns out to be valid, it can be used for patients with all types of systemic amyloidosis. What is more, in the future preventive vaccination might be considered in people at risk for the development of amyloidosis.

## CONCLUSION

A systematic, stepwise evaluation of patients with systemic amyloidosis helps to get a grip on this intangible disease. Histological proof of amyloid, verification of systemic involvement, assessment of the particular type of amyloid and its precursor form the background for a thoughtful clinical evaluation. New techniques such as <sup>125</sup>I-SAP scintigraphy may have a place in this evaluation. The 'precursor-product' concept is still the current basis of treatment, but research is aimed at finding new ways to attack amyloid.

## NOTE

Most data were presented at the Immunology symposium on Systemic Diseases in Groningen, 14 February 2003 and at the Internal Medicine Congress in Maastricht, 15 May 2003.

## REFERENCES

- Falk RH, Comenzo RL, Skinner M. The systemic amyloidoses. *N Engl J Med* 1997;337:898-909.
- Westermarck P, Benson MD, Buxbaum JN, et al. Amyloid fibril protein nomenclature - 2002. *Amyloid J Protein Folding Disord* 2002;9:197-200.
- Merlini G, Bellotti V. Molecular mechanisms of amyloidosis. *N Engl J Med* 2003;349:583-96.
- Kay J. B2-microglobulin amyloidosis. *Amyloid Int J Exp Clin Invest* 1997;4:187-211.
- Kamphuis ACA, Geerlings W, Hazenberg BPC, Thijn CJ. Annual evaluation of hip joints and hands for radiographic signs of Aβ2M-amyloidosis in long-term hemodialysis patients. *Skeletal Radiol* 1994;23:421-7.
- Bredvdeld FC, Markusse HM, MacFarlane JD. Subcutaneous fat biopsy in the diagnosis of amyloidosis secondary to chronic arthritis. *Clin Exp Rheumatol* 1989;7:407-10.
- Klemi PJ, Sorsa S, Happonen RP. Fine-needle aspiration biopsy from subcutaneous fat. An easy way to diagnose secondary amyloidosis. *Scand J Rheumatol* 1987;16:429-31.
- Kyle RA, Gertz MA. Primary systemic amyloidosis: Clinical and laboratory features in 474 Cases. *Semin Hematol* 1995;32:45-59.
- Janssen S, Rijswijk MH van, Meijer S, Ruinen L, Hem GK van der. Systemic amyloidosis: a clinical survey of 144 cases. *Neth J Med* 1986;29:376-85.
- Röcken C, Sletten K. Amyloid in surgical pathology. *Virchows Arch* 2003;443:3-16.
- Hazenberg BPC, Grond J, Top D van de, Bijzet J, Limburg PC, Rijswijk MH van. Detection of amyloid AA in rectal biopsies with a new monoclonal anti-human SAA antibody (Reu.86.2). *Kidney Int* 1991;40:976-7.
- Hazenberg BPC, Limburg PC, Bijzet J, Rijswijk MH van. A quantitative method for detecting deposits of amyloid A protein in aspirated fat tissue of patients with arthritis. *Ann Rheum Dis* 1999;58:96-102.
- Lachmann HJ, Booth DR, Booth SE, et al. Misdiagnosis of hereditary amyloidosis as AL (primary) amyloidosis. *N Engl J Med* 2002;346:1786-91.
- Kyle RA, Therneau TM, Rajkumar SV, et al. A long-term study of prognosis in monoclonal gammopathy of undetermined significance. *N Engl J Med* 2002;346:564-9.
- Lachmann HJ, Gallimore R, Gillmore J, et al. Outcome in systemic AL amyloidosis in relation to changes in concentration of circulating free immunoglobulin light chains following chemotherapy. *Br J Haematol* 2003;122:78-84.
- Reyners AKL, Hazenberg BPC, Haagsma EB, Tio RA, Reitsma WD, Smit AJ. The assessment of autonomic function in patients with systemic amyloidosis: methodological considerations. *Amyloid Int J Exp Clin Invest* 1998;5:193-9.
- Reyners AKL, Hazenberg BPC, Reitsma WD, Smit AJ. Heart rate variability as a predictor of mortality in patients with AA and AL amyloidosis. *Eur Heart J* 2002;23:157-61.
- Hawkins PN, Lavender JP, Pepys MB. Evaluation of systemic amyloidosis by scintigraphy with <sup>125</sup>I-labeled serum amyloid P component. *N Engl J Med* 1990;323:508-13.
- Jager PL, Hazenberg BPC, Franssen EJP, Limburg PC, Rijswijk MH van, Piers DA. Kinetic studies with Iodine-123-labeled serum amyloid P component in patients with systemic AA and AL amyloidosis and assessment of clinical value. *J Nucl Med* 1998;39:699-706.
- Gillmore JD, Lovat LB, Persey MR, Pepys MB, Hawkins PN. Amyloid load and clinical outcome in AA amyloidosis in relation to circulating concentration of serum amyloid A protein. *Lancet* 2001;358:24-9.
- Rijswijk MH van. Amyloidosis. Groningen: University of Groningen, 1981.
- Dode C, Hazenberg BPC, Pecheux C, et al. Mutational spectrum in the MEYF and TNFRSF1A genes in patients suffering from AA amyloidosis and recurrent inflammatory attacks. *Nephrol Dial Transplant* 2002;17:1212-7.
- Hawkins PN, Lachmann HJ, McDermott MF. Interleukin-1-receptor antagonist in the Muckle-Wells syndrome. *N Engl J Med* 2003;348:2583-4.
- Zemer D, Pras M, Sohar E, Modan M, Cabili S, Gafni J. Colchicine in the prevention and treatment of the amyloidosis of familial Mediterranean fever. *N Engl J Med* 1986;314:1001-5.
- Rijswijk MH van, Ruinen L, Donker AJ, de Blecourt JJ, Mandema E. Dimethylsulfoxide in the treatment of AA amyloidosis. *Ann N Y Acad Sci* 1983;411:67-83.
- Iwakiri R, Sakemi T, Fujimoto K. Dimethylsulfoxide for renal dysfunction caused by systemic amyloidosis complicating Crohn's disease. *Gastroenterology* 1999;117:1031-2.
- Comenzo RL, Vosburgh E, Falk RH, et al. Dose-intensive melphalan with blood stem-cell support for the treatment of AL (Amyloid light-chain) amyloidosis: Survival and responses in 25 patients. *Blood* 1998;91:3662-70.
- Skinner M, Santhorawala V, Seldin DC, et al. High-dose melphalan and autologous stem-cell transplantation in patients with AL amyloidosis: an 8-year study. *Ann Intern Med* 2004;140:85-93.
- Ericzon B-C, Larsson M, Herlenius G, Wilczek HE, on behalf of reporting members of the FAPWTR. Report from the Familial Amyloidotic Polyneuropathy World Transplant Registry (FAPWTR) and the Domino Liver Transplant Registry (DLTR). *Amyloid J Protein Folding Disord* 2003;10(suppl 1):67-76.

30. Cameren II van, Hazenberg BPC, Jager PL, Smit JW, Vellenga E. AL amyloidosis treated with induction chemotherapy with VAD followed by high dose melphalan and autologous stem cell transplantation. *Amyloid J Protein Folding Disord* 2002;9:165-74.
31. Hawkins PN, Richardson S, MacSweeney JE, et al. Scintigraphic quantification and serial monitoring of human visceral amyloid deposits provide evidence for turnover and regression. *QJM* 1993;86:365-74.
32. Inoue S, Hultin PG, Szarek WA, Kisilevsky R. Effect of poly(vinylsulfonate) on murine AA amyloid: a high-resolution ultrastructural study. *Lab Invest* 1996;74:1081-90.
33. Gertz MA, Lacy MQ, Dispenzieri A, et al. A multicenter phase II trial of 4'-iodo-deoxydoxorubicin (IDOX) in primary amyloidosis (AL). *Amyloid J Protein Folding Disord* 2002;9:24-30.
34. Pepys MB, Herbert J, Hutchinsonson WL, et al. Targeted pharmacological depletion of serum amyloid P component for treatment of human amyloidosis. *Nature* 2002;417:254-9.
35. Hammarstrom P, Wiseman RL, Powers ET, Kelly JW. Prevention of transthyretin amyloid disease by changing protein misfolding energetics. *Science* 2003;299:713-7.
36. Hrnčić R, Wall J, Wolfenbarger DA, et al. Antibody-mediated resolution of light chain-associated amyloid deposits. *Am J Pathol* 2000;157:1239-46.

**Teveten®** bevat eprosartan mesylaot overeenkomend met 400 of 600 mg eprosartan (als vrije base) per tablet. **Farmacotherapeutische groep:** Angiotensine-II receptor antagonist. **Indicatie:** Essentiële hypertensie. **Dosering:** 600 mg éénmaal daags. Wanneer de daling van de bloeddruk onvoldoende is, kan de dosis worden verhoogd tot 800 mg, of kan een ander antihypertensivum worden toegevoegd (zoals een thiazide-diureticum of een calciumantagonist). **Inname met of zonder voedsel.** **Contra-indicaties:** gebleken overgevoeligheid voor één der bestanddelen van het product. Zwangerschap en lactatie. Ernstig verminderde leverfunctie. **Speciale waarschuwingen en voorzorgen:** voorzichtigheid geboden bij ernstig gestoorde nierfunctie (creatinineklaring < 30 ml/min), dialysepatiënten en bij coronaire hartziekten. **Algemeen:** voor producten die het RAS-systeem beïnvloeden zijn voorzorgen te nemen: bij aorta- en mitralisklep stenose, bij hypertrofische cardiopathie, bij stenose van de renale arterie(n), na een niertransplantatie, bij gelijktijdig gebruik van kaliumsparende diuretica of kaliumzouten evenals bij verminderde nierfunctie en medicatie die de kaliumspiegel kunnen verhogen (kaliumspiegel controleren), bij ernstige hartinsufficiëntie (hartfunctie controleren), bij ernstige natrium- en/of volumedepletie (leer depletie corrigeren), niet aanbevelen bij primair hyperaldosteronisme. **Interacties:** voorzichtig combineren met lithium. **Bijwerkingen:** Incidenties vergelijkbaar met die van placebo. Angio-oedeem is een enkele keer waargenomen. **Aard en inhoud van de verpakking:** Teveten® 400, 56 tabletten in blisters, Teveten® 600, 14 of 28 tabletten in blisters. **RVG-ars:** Teveten® 400 RVG 22260, Teveten® 600 RVG 23983. **Vergoeding:** wordt volledig vergoed binnen het GVS. **Afleveringsstatus:** UR. **Datering:** deel 1B: 8 nov '99. Volledige productinformatie is op aanvraag verkrijgbaar. **Solvay Pharma B.V., Postbus 501, 1380 AM Mesp. Tel. 020 - 02 33 800 Fax: 0294 - 43 24 11 E-mail: nlpharma@solvay.com**

www.beterleven.nl  SOLVAY PHARMA

FROM

(FRI) 2 4 2005 13:13/ST. 13:03/NO. 5560118826 P 20

Number 3

31 October 1997

# JMB

## JOURNAL OF MOLECULAR BIOLOGY

Univ. of Minn.  
Bio-Medical  
Library

1. 1 97.



ACADEMIC PRESS

273 (3) 503-764 ISSN 0022-2836



0022-2836(199710)273:3;1-U

**JMB**NOTICE: THIS MATERIAL MAY BE PROTECTED  
BY COPYRIGHT LAW (TITLE 17 U.S. CODE)

## Common Core Structure of Amyloid Fibrils by Synchrotron X-ray Diffraction

Margaret Sunde\*, Louise C. Serpell, Mark Bartlam, Paul E. Fraser  
Mark B. Pepys and Colin C. F. Blake

Laboratory of Molecular  
Biophysics, University of  
Oxford, Rex Richards Building  
South Parks Road, Oxford  
OX1 3QU, UK

Tissue deposition of normally soluble proteins as insoluble amyloid fibrils is associated with serious diseases including the systemic amyloidoses, maturity onset diabetes, Alzheimer's disease and transmissible spongiform encephalopathy. Although the precursor proteins in different diseases do not share sequence homology or related native structure, the morphology and properties of all amyloid fibrils are remarkably similar. Using intense synchrotron sources we observed that six different *ex vivo* amyloid fibrils and two synthetic fibril preparations all gave similar high-resolution X-ray fibre diffraction patterns, consistent with a helical array of  $\beta$ -sheets parallel to the fibre long axis, with the strands perpendicular to this axis. This confirms that amyloid fibrils comprise a structural superfamily and share a common protofilament substructure, irrespective of the nature of their precursor proteins.

© 1997 Academic Press Limited

\*Corresponding author

Keywords: amyloid; fibre; X-ray diffraction; protofilament; structure

### Introduction

Amyloidosis is the extracellular deposition of insoluble protein fibrils leading to tissue damage and disease (Pepys, 1996; Tan *et al.*, 1995; Kelly, 1996). The fibrils form when normally soluble proteins and peptides self-associate in an abnormal manner (Kelly, 1997). Amyloid is associated with serious diseases including systemic amyloidosis, Alzheimer's disease, maturity onset diabetes, and the prion-related transmissible spongiform encephalopathies (Table 1). There is no specific treatment for amyloid deposition and these diseases are usually fatal. The subunits of amyloid fibrils may be wild-type, variant or truncated proteins, and

similar fibrils can be formed *in vitro* from oligopeptides and denatured proteins (Bradbury *et al.*, 1960; Filshie *et al.*, 1964; Burke & Rougvie, 1972). The nature of the polypeptide component of the fibrils defines the character of the amyloidosis.

Despite large differences in the size, native structure and function of amyloidogenic proteins, all amyloid fibrils are of indeterminate length, unbranched, 70 to 120 Å in diameter, and display pathognomonic green birefringence when viewed in polarized light after staining with Congo Red (Pepys, 1996). Early X-ray diffraction examinations of amyloid fibrils (Borlar *et al.*, 1967; Eanes & Glenner, 1968) gave simple patterns with 4.7 to 4.8 Å meridional reflections and 10 Å equatorial reflections, arising from the molecular spacings present within the regularly repeating, ordered structural elements of the fibrils. They are characteristic of a cross- $\beta$  structure (Pauling & Corey, 1951) in which the polypeptide chain is organized in  $\beta$ -sheets arranged parallel to the fibril axis with their constituent  $\beta$ -strands perpendicular to the fibril axis. This distinctive fibre diffraction pattern led to the amyloidoses being called the  $\beta$ -fibrilloses (Glenner, 1980a,b), and the fibril protein of Alzheimer's disease was named the  $\beta$ -protein before its secondary structure was known (Glenner & Wong, 1984). The characteristic cross- $\beta$  diffraction pattern, together with the fibril appearance and tinctorial

Present addresses: M. Sunde, Oxford Centre for Molecular Sciences, University of Oxford, New Chemistry Laboratory, South Parks Road, Oxford OX1 3QT, UK; L. C. Serpell, Center for Research in Neurodegenerative Diseases, University of Toronto, Tanz Neuroscience Building, Queen's Park Crescent West, Toronto M5S 3H2, Canada; P. E. Fraser, Center for Research in Neurodegenerative Diseases and Department of Medical Biophysics, University of Toronto, Tanz Neuroscience Building, Queen's Park Crescent West, Toronto M5S 3H2, Canada; M. B. Pepys, Immunological Medicine Unit, Royal Postgraduate Medical School, Hammersmith Hospital, Du Cane Road, London W12 0NN, UK.

Table 1. Diversity of amyloid fibril proteins

| Clinical syndrome                                 | Fibril subunit  | Cross- $\beta$ pattern | Structure of precursor  | Reference to structure         |
|---|---|------------------------|-------------------------|--------------------------------|
| Monoclonal protein systemic (AL) amyloidosis      | Full-length or fragments of V <sub>L</sub> domain of Ig light chain | +                      | All $\beta$             | Schormann <i>et al.</i> (1995) |
| Reactive systemic (AA) amyloidosis                | 76-residue N-terminal fragment of amyloid A protein                 | +                      | $\alpha/\beta$          | Turnell <i>et al.</i> (1986b)  |
| Familial amyloidotic polyneuropathy               | Full-length or fragments of transthyretin variants                  | +                      | All $\beta$             | Handlton <i>et al.</i> (1993)  |
| Hereditary apoAI amyloidosis                      | N-terminal fragments (~90 residues) of apoAI variants               | +                      | ( $\alpha/\beta$ )      | Nolle & Altknecht (1997)       |
| Hereditary lysozyme amyloidosis                   | Full-length lysozyme variants                                       | +                      | $\alpha+\beta$          | Booth <i>et al.</i> (1997)     |
| Type II diabetes mellitus                         | 37-residue fragment of islet-amyloid polypeptide                    | +                      | Unknown                 |                                |
| Alzheimer's disease                               | 1-39 to 43 residue A $\beta$ protein                                | +                      | $\alpha, \beta$ or coil | Barrow <i>et al.</i> (1992)    |
| Insulin-related amyloid                           | Full-length wild-type insulin                                       | +                      | $\alpha+\beta$          | Adams <i>et al.</i> (1969)     |
| Transmissible spongiform encephalopathies         | Full-length or fragments of prion protein                           | +                      | $\alpha+\beta$          | Harrison <i>et al.</i> (1997)  |
| Medullary carcinoma of the thyroid                | Fragments of calcitonin   | +                      | Unknown                 |                                |
| Senile systemic amyloidosis                       | Full-length or fragments of wild-type transthyretin                 | +                      | Unknown                 |                                |
| Hemodialysis-related amyloidosis                  | Full-length, wild-type $\beta_2$ -microglobulin                     | +                      | All $\beta$             | Blake <i>et al.</i> (1978)     |
| Isolated atrial amyloidosis                       | Atrial natriuretic factor   | +                      | All $\beta$             | Becker & Reeke (1985)          |
| Hereditary cerebral amyloid angiopathy            | 110-residue fragment of variant cystatin-C                          | +                      | Unknown                 |                                |
| Finnish hereditary amyloidosis                    | 71-residue fragment of gelsolin variants                            | +                      | $\alpha+\beta$          | Bode <i>et al.</i> (1988)      |
| Hereditary fibrinogen $\alpha$ -chain amyloidosis | Fragments of fibrinogen $\alpha$ -chain variants                    | +                      | $\alpha/\beta$          | Burfield <i>et al.</i> (1996)  |

Key to symbols: +, this variant; -, no diffraction evidence; ( $\alpha/\beta$ ), secondary structure prediction.



properties are now the accepted diagnostic hallmarks of amyloid, and suggest that the fibrils, although formed from quite different protein precursors, share a degree of structural similarity.

In order to determine the extent and nature of this similarity we have used intense synchrotron X-ray beams to obtain the first high-resolution diffraction patterns from a range of different *ex vivo* and synthetic amyloid fibrils. Amyloid fibrils were isolated from patients with, respectively: monoclonal  $\lambda$  immunoglobulin light chain amyloidosis (Pepys, 1996); reactive systemic amyloid A protein amyloidosis (Pepys, 1996) and hereditary amyloidosis caused by Leu60Arg variant apolipoprotein A-I (Soutar *et al.*, 1992); Asp67His variant lysozyme (Pepys *et al.*, 1993; Booth *et al.*, 1997); and two different transthyretin variants, Val30Met and Gly47Val (Booth *et al.*, 1994). Synthetic fibrils were prepared from a peptide corresponding to residues 10 to 19 ( $\beta$ -strand A) of transthyretin, and from a peptide with the sequence of residues 20 to 29 of the islet-associated polypeptide (IAPP).

### The high-resolution meridional X-ray pattern and a common repeat on the fibril axis

The synchrotron X-ray diffraction patterns from these different fibril preparations are shown in Figure 1 and the spacings of the reflections are listed in Table 2. These high-resolution patterns are dominated by the cross- $\beta$  reflections but they also contain groups of additional reflections that have not been observed previously in other amyloid diffraction patterns. Despite the known, large differences in the lengths and folding conformations of the polypeptide chains of the precursors, the major features of the diffraction patterns from the various amyloid fibrils are clearly very similar.

The meridional diffraction pattern derives from the ordered molecular structures along the length of the amyloid fibril. The presence of reflections on the meridian out to 2 Å indicates that the individual fibrils have highly ordered internal structures along the fibre axis. The intense reflection at 4.7 to 4.8 Å that dominates the meridional diffraction patterns of amyloid fibrils is derived from the mean separation of the hydrogen-bonded  $\beta$ -strands that are arranged perpendicular to the fibre axis in the cross- $\beta$  structure (Figure 2). In addition to this intense reflection, the synchrotron radiation has also revealed several weaker, higher-angle reflections, occurring in this range of diverse amyloids, that have not been reported previously. These reflections include a second order of the 4.7 to 4.8 spacing, at 2.4 Å.

In some of the amyloid samples (Figure 1(b), (d), (e) and (f)), the intense "4.7 Å" reflection can be seen to be a close doublet, with components at 4.82 Å and 4.63 Å. In patterns where this doublet cannot be resolved its presence can be inferred from the observation that the calculated first order of the

second harmonic of the 4.7 Å spacing, found at 2.39 to 2.41 Å, maps to the extreme inner edge of the intense 4.7 Å reflection, leaving space for a 4.6 Å component within the overall intensity envelope. The weaker, higher-angle reflections occur at closely similar spacings in the different samples. For example, reflections with spacings of 3.2 Å, 2.8 to 2.9 Å, 2.22 to 2.27 Å and 2.00 to 2.02 Å occur frequently, and reflections with spacings of 2.39 to 2.41 Å (the second order of the intense 4.82 Å reflection) are present in all of the amyloid samples that we have examined at high resolution. Because these reflections are very weak, even in relatively well oriented patterns, their absence from certain images may simply indicate that they are too weak to be observed above the noise level in those patterns. The observed similarity over the medium- and high-angle regions of the meridional X-ray pattern can only occur if the fibrils have well-defined and closely similar molecular structures, at least insofar as their ordered core components are concerned.

The observed meridional spacings can be fitted to the same repeat distance for each pattern, namely 115 Å (Table 2). The observed spacings for many of the reflections can also be fitted to a fundamental repeat of 28.8 to 29.9 Å to give orders of diffraction of 6 through 14 for spacings from 4.8 Å to 2.00 Å. However, this fit does not include all observed reflections. It is possible to include these if it is assumed that the 28.8 to 28.9 Å distance represents a pseudo-repeat and that the true repeat is four times as long, being 115.1 to 115.6 Å. As Table 2 indicates, all of the observed meridional reflections can be indexed on this longer repeat and this indexing can be carried out separately for the diffraction patterns from each type of amyloid fibril to give almost identical repeat distances. The ability to index the meridional spacings from each different fibril preparation to essentially the same unit cell edge indicates a close similarity in the underlying core molecular structure of all of these samples. This similarity is evidence that the protofilament structure of amyloid fibrils is common across the diverse range of fibril samples examined here, regardless of the constituent protein or the number of protofilaments making up the fibril.

The most intense features of the X-ray patterns we show here correspond to those previously reported for other amyloid fibrils (Table 1), including those from full-length (Kirschner *et al.*, 1986; Gorevic *et al.*, 1987) and fragments of the Alzheimer's disease A $\beta$  peptide (Kirschner *et al.*, 1987; Fraser *et al.*, 1991; Inouye *et al.*, 1993), amyloid A protein (Turnell *et al.*, 1986a), calcitonin (Gilchrist & Bradshaw, 1993), insulin (Burke & Rougvie, 1972), and synthetic peptides of transthyretin (Jarvis *et al.*, 1993) and the prion protein (Come *et al.*, 1993; Tagliavini *et al.*, 1993; Nguyen *et al.*, 1995). The lack of high-resolution data, beyond the basic cross- $\beta$  reflections, has limited further analysis of the molecular structures of these fibrils.

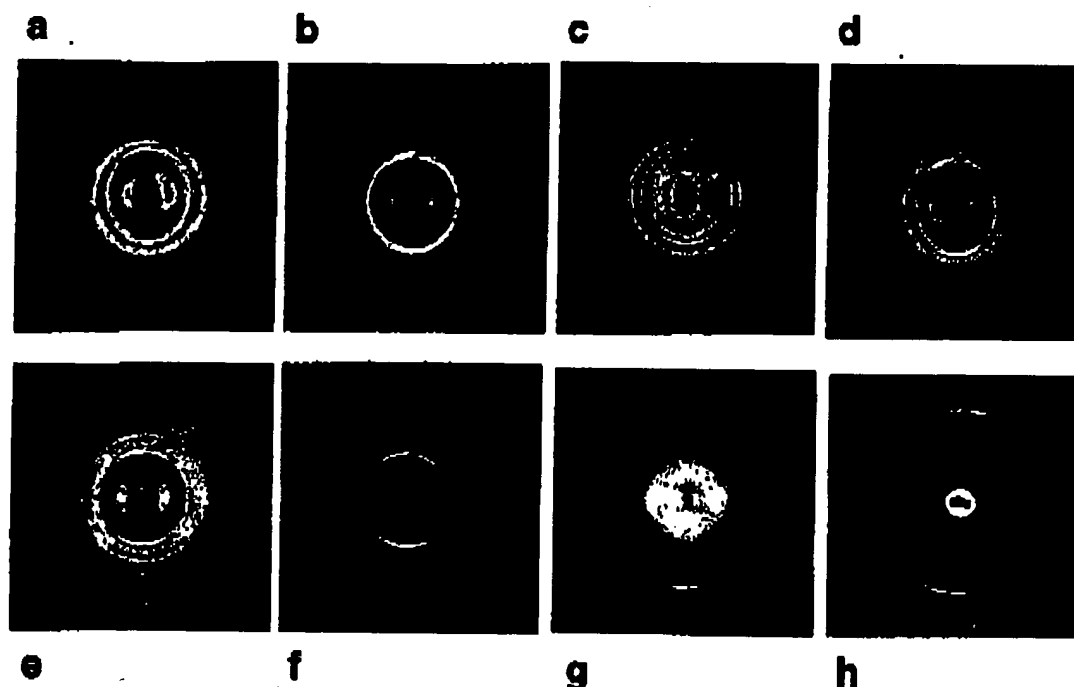


**Figure 1.** X-ray fibre diffraction patterns from *ex vivo* and synthetic amyloid fibrils. X-ray fibre diffraction patterns from eight different types of amyloid fibril, prepared as described below. The meridional axis (direction parallel to the fibril axis) is the vertical axis in this display. Amyloid fibril samples as follows: (a) ATTR2, Gly47Val transthyretin; (b) ATTR1, Val30Met transthyretin; (c) AAPOAI, Leu60Arg apolipoprotein A-I; (d) AL, monoclonal  $\lambda$  immunoglobulin light chain; (e) FTTR, peptide with the sequence of the A-strand of human transthyretin; (f) FIAPP, peptide with the sequence of residues 20 to 29 of the islet-associated polypeptide; (g) AA, amyloid A protein; (h) ALys, Asp67His lysozyme. Amyloid fibrils were isolated, as described by Nelson *et al.* (1991), from spleens of patients with different types of systemic amyloidosis and prepared for X-ray examination on a stretch frame. A droplet of fibril suspension (5 to 10 mg/ml in distilled water) was placed between two tubes and allowed to dry at room temperature, during which time the distance between the ends of the capillaries was increased slowly, by small increments, to stretch out the fibrils and encourage alignment. The peptides were synthesized by standard peptide synthesis chemistry and were dissolved in distilled water at a concentration of 10 mg/ml to produce amyloid fibrils. The solution, in a siliconized capillary tube, was then placed in a 2 T magnetic field to facilitate alignment of the fibrils during their formation and was allowed to dry at room temperature for about ten days. X-ray fibre diffraction patterns were collected at user station ID2 on beamline 4 at the European Synchrotron Research Facility (ESRF) at Grenoble, France (wavelength 0.9515 Å), at station 7.2 at the Synchrotron Radiation Source (SRS) at Daresbury, UK (wavelength 1.488 Å) or in-house using a Cu K $\alpha$  Rigaku rotating-anode source (wavelength 1.5418 Å). All images were collected on MARResearch image plate X-ray detectors (180 or 300 mm diameter). Various exposure times were used for the different samples to optimize the detection of reflections. The images were collected on different beamlines, with varying wavelengths, beam-stops and sample-to-detector distances; these variations account for the differences in relative intensities and positions of the beam stop between images. The fibre diffraction patterns were analysed using the display program IPDSEP, run on a Hewlett Packard workstation (ESRF) and a Digital workstation (Oxford). Spacings were measured in triplicate and on both sides of the patterns. False colour images were produced with the program PROFIDA (Lorenz & Holmes, 1993).

### Differences in the equatorial reflections

The equatorial X-ray reflections relate to the fibril structure perpendicular to the fibre direction. Because the crystalline order in fibres is usually much lower in directions perpendicular to the fibre axis than parallel to the axis, the equatorial reflections from amyloid fibrils are weaker and broader than their meridional equivalents (Figure 1, Table 3). Early diffraction studies of amyloid (Bonar *et al.*, 1967; Earnes & Glenner, 1968) demonstrated a single equatorial reflection with a spacing

of about 10 Å. As the intensities of the equatorial reflections are determined by the structure of the fibrils projected down the fibre axis, this reflection has been identified as representing the spacing of the  $\beta$ -sheets in the amyloid fibril.

The use of synchrotron radiation has revealed a more detailed equatorial diffraction pattern in which there are both additional reflections and also greater spatial resolution of the previously observed reflections. The synchrotron patterns do, however, exhibit broad maxima at around 10 Å and 5 Å, characteristic of  $\beta$ -sheets separated by

Table 2. Meridional reflections

| Order    | ATTR1  | ATTR2  | AL     | AApoAI | ALys   | AA     | FTTR   | FIAPP  |
|----------|--------|--------|--------|--------|--------|--------|--------|--------|
| 24       | 4.84   | 4.84   | 4.82   | 4.79   | 4.80   | 4.78   | 4.80   | 4.83   |
| 25       | 4.84   | 4.80   | 4.82   | 4.64   | 4.63   | 4.60   | 4.58   | 4.60   |
| 26       |        |        |        | 4.42   | 4.46   |        |        |        |
| 27       |        |        |        |        |        |        |        |        |
| (n-)     | 4.10   |        | 4.18   | 4.12   | 4.13   | 4.14   |        |        |
| 28       |        |        |        |        |        |        |        |        |
| 29       |        |        |        |        |        |        |        |        |
| 30       |        |        |        |        |        |        |        |        |
| (o-m)    | 3.83   | 3.85   | 3.86   |        |        |        |        | 3.83   |
| 31       |        |        |        | 3.73   | 3.74   | 3.72   | 3.71   |        |
| 32       |        |        | 3.61   |        |        |        |        |        |
| 33       |        |        |        |        |        |        |        |        |
| 34       |        |        |        | 3.40   |        |        |        |        |
| 35       |        |        |        |        |        |        |        |        |
| 36       |        |        |        |        |        |        | 3.21   |        |
| 37       |        |        |        | 3.19   |        |        |        |        |
| 38       |        |        |        |        |        |        |        |        |
| 39       |        |        |        |        |        |        |        |        |
| 40       |        |        |        | 2.90   |        |        |        |        |
| 41       |        | 2.82   |        |        |        |        | 2.82   |        |
| 42       |        |        |        |        |        |        |        |        |
| 43       |        |        |        |        |        |        |        |        |
| 44       |        |        |        |        |        |        | 2.61   |        |
| 45       |        |        |        |        |        |        |        |        |
| 46       |        |        |        |        |        |        |        |        |
| 47       |        |        |        |        |        |        |        |        |
| 48       | 2.39   | 2.41   | 2.41   | 2.39   | 2.40   |        | 2.39   | 2.41   |
| 49       |        |        |        |        |        |        |        |        |
| 50       |        |        |        |        |        |        |        |        |
| 51       |        |        | 2.27   |        |        |        | 2.25   |        |
| 52       |        |        |        |        |        |        |        | 2.22   |
| 53       |        |        |        | 2.17   |        |        |        |        |
| 54       |        |        |        |        |        |        |        |        |
| 55       |        |        |        |        |        |        |        |        |
| 56       |        |        |        |        |        |        |        |        |
| 57       |        |        |        |        |        |        |        |        |
| 58       |        |        |        | 2.00   |        |        | 2.00   |        |
| cell     | 115.37 | 115.39 | 115.61 | 115.48 | 115.56 | 115.12 | 115.13 | 115.48 |
| $\sigma$ | 0.59   | 0.37   | 0.099  | 0.46   | 0.28   | 0.61   | 0.47   | 0.35   |

Spacing (in Å) of all meridional reflections measured from diffraction patterns, with the corresponding order of the indexed reflections. Calculated cell edge dimension (along the meridian) given for each fibril sample (with standard deviation). Samples as follows: ATTR1, Val30Met variant transthyretin; ATTR2, Gly47Val variant transthyretin; AL, monoclonal  $\lambda$  immunoglobulin light chain; AApoAI, Leu60Arg variant apolipoprotein A-I; ALys, Asp67His variant lysozyme; AA, amyloid A protein; FTTR, peptide with the sequence of the A-strand of wild-type human transthyretin; FIAPP, peptide with the sequence of residues 20 to 29 of the islet-associated polypeptide. (o-m), off-meridional reflection; (n-), the reflections do not index to the common cell edge dimension. There is evidence from other studies that this spacing arises from lipid contamination (Damas *et al.*, 1995).

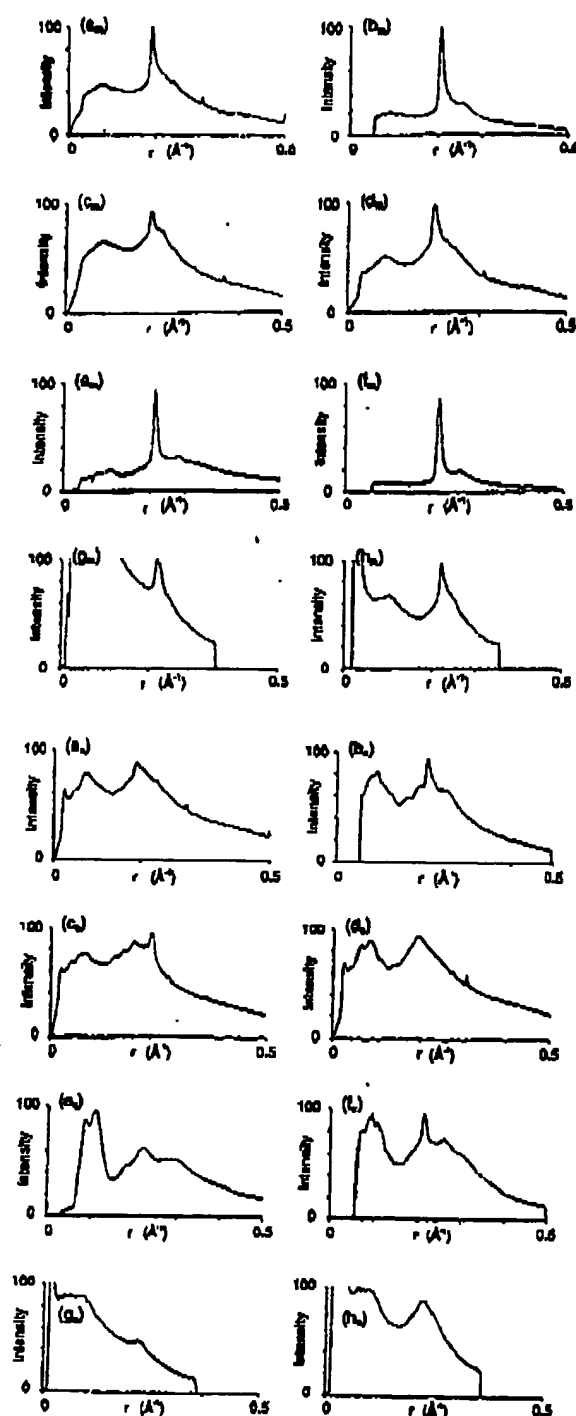


Figure 2. Comparison of the meridional and equatorial reflections. Meridional and equatorial profiles from samples of eight different amyloid fibrils, showing the close similarities in the meridional diffraction and the large differences in the distribution of the equatorial reflections between these diverse amyloid samples. The samples, illustrated in the same order as in Figure 1, are as follows; (a) ATTR2; (b) ATTR1; (c) AAPOAL; (d) AL; (e) FTIR; (f) FIAPP; (g) AA; (h) ALys (abbreviations as in legend to Figure 1). Meridional profiles are illustrated as parts (a<sub>m</sub>)

approximately 10 Å, as suggested earlier. It is known that the spacing in  $\beta$ -sheets is dependent on the side-chain composition of the  $\beta$ -sheets (Arnott *et al.*, 1967; Geddes *et al.*, 1968). A recent analysis of the X-ray diffraction patterns from prion rods and fibrils formed from peptides corresponding to fragments of the prion protein has shown that the  $\beta$ -sheet spacings vary in these samples because of differences in sequence (Nguyen *et al.*, 1995). The present results are also in agreement with those of Jarvis and co-workers, who have reported  $\beta$ -sheet spacings of 8 to 10 Å in synthetic fibrils prepared from peptides that correspond to single strands of the transthyretin molecule (Jarvis *et al.*, 1993). The slight variation in the equatorial reflections observed in the series of fibrils presented here therefore presumably reflects the differences in protein sequences in these diverse types of amyloid but falls within acceptable limits for amino acid compositions found in globular proteins.

The larger number of equatorial reflections revealed by the synchrotron X-ray source suggests the presence of protofilaments in amyloid fibrils. The short-range order involved in the packing of protofilaments, within or between the fibrils, can be described by a one-dimensional interference function dependent on the centre-to-centre separation (or diameter) of the protofilaments, and their arrangement in the fibrils (Burge, 1959, 1963). Electron microscopy studies of the sub-fibrillar structure of amyloid have revealed that different types of amyloid may show different numbers and arrangements of protofilaments in the fibrils (Shirahama & Cohen, 1967; Shirahama *et al.*, 1973; Cohen *et al.*, 1981). Fraser and co-workers have shown that the protofilaments formed by A $\beta$  peptides assemble into hollow rods or ribbons of various sizes under different conditions of pH (Fraser *et al.*, 1991) and, while A $\beta$ , amyloid A protein and immunoglobulin light chain amyloid fibrils are reported to be composed of five or six protofilaments around an electron lucent core (Cohen *et al.*, 1981; Kirschner *et al.*, 1987; Fraser *et al.*, 1991), transthyretin amyloid has been shown to be composed of four protofilaments in a square array (Serpell *et al.*, 1995). It may therefore be expected that the equatorial reflections produced by the amyloid fibrils of different types will reflect the variation in number and arrangement of protofilaments in their fibrils.

to ( $g_m$ ) of the Figure and equatorial profiles are parts (a<sub>e</sub>) to (g<sub>e</sub>). The profiles were extracted using an adapted version of PROFIDA (Lorenz & Holmes, 1993). The diffraction patterns were centred, rotated to align the meridional axis with the vertical axis of the screen, and corrected for beam polarisation. Profiles were averaged over both  $\Delta r$  and  $\Delta \theta$ , over the ranges  $0 < r < 0.5 \text{ Å}^{-1}$ ,  $\Delta r = 0.000782 \text{ Å}^{-1}$  and  $0 < \theta < 10^\circ$ ,  $\Delta \theta = 1^\circ$ . The profiles are plotted on the same arbitrary intensity scale for comparison.

Table 3. Equatorial reflections

| ATTR1 | ATTR2 | AL    | AApoAI | ALys  | AA    | FTTR  | FIAPP |
|-------|-------|-------|--------|-------|-------|-------|-------|
| 16.0  |       |       | 15.17  | 14.60 |       | 26.3  |       |
| 12.60 |       | 12.55 | 11.76  | 12.32 |       | 11.51 | 11.42 |
|       | 10.62 |       |        |       | 10.96 |       |       |
| 10.10 |       | 9.70  | 9.79   | 10.35 |       | 8.92  | 8.60  |
| 7.36  | 7.94  | 7.56  |        |       |       |       |       |
| 6.08  |       | 6.11  | 5.98   | 5.74  |       | 5.72  | 5.53  |
| 5.32  | 5.46  | 5.26  | 5.37   |       |       | 4.59  |       |
| 3.94  |       |       | 3.88   | 3.89  |       | 3.43  | 3.28  |

Spacing (in Å) of all equatorial reflections measured from diffraction patterns. Samples as in Table 2.

It is also possible that the diameters of the protofilaments (and therefore their centre-to-centre spacing) may vary because of the need to accommodate differently sized loops linking the  $\beta$ -structure core, and/or to allow for some variation in the lengths of the  $\beta$ -strands dependent on the nature of the precursor. These variations may account for the differences between the 25 to 35 Å diameter protofilaments seen in amyloid A protein and immunoglobulin light chain fibrils, and Alzheimer's amyloid and the 50 to 60 Å diameter protofilaments demonstrated in transthyretin amyloid (Fraser *et al.*, 1991; Cohen *et al.*, 1981; Serpell *et al.*, 1995). In view of these possible variations of structure, the observed equatorial spacings listed in Table 3 are difficult to interpret readily in more detail than is given above. Where there is a sufficient number of equatorial reflections and other information it is possible to analyze the substructure of the fibril in some detail, as for example, has been done for the transthyretin fibril (Blake & Serpell, 1996; Blake *et al.*, 1996). The number of observable equatorial reflections listed in Table 3 is insufficient to characterize all of the amyloid fibrils studied here but the similarity in the equatorial reflections displayed by the *ex vivo* fibrils on the one hand, and the synthetic peptide fibrils on the other, may reflect the fact that the protofilament packing in these two groups is related to the nature of their constituent polypeptides.

### A generic fibril structure

The degree of similarity we have observed in the diffraction patterns of these different amyloid samples is indicative of a common core molecular structure at least at the level of the protofilament. The X-ray pattern of one of these fibrils, the Val30Met transthyretin amyloid, has been analysed in detail to generate a novel molecular structure, which has been described (Blake & Serpell, 1996; Blake *et al.*, 1996), and it is reasonable to suppose that its basic structural elements are representative of the other amyloid fibrils examined here. In this molecular model the protofilaments that make up the observed fibrils are composed of a number of  $\beta$ -sheets (four in the case of transthyretin fibrils; but this number may be particular to transthyretin amyloid) running parallel to the axis of the protofi-

lament, with their component  $\beta$ -strands closely perpendicular to this axis. The regular orientation of the strands and sheets with respect to the fibril axis may account for the magnetic anisotropy observed in amyloid fibril samples, which allows samples of fibrils to be aligned in a magnetic field (Inouye *et al.*, 1993). The diamagnetic anisotropy of the planar peptide bond has the effect that  $\beta$ -sheets, in which the plane of the peptide bond is parallel to the sheet, have a tendency to orient parallel to an applied magnetic field (Worcester, 1978).

The meridional reflections from these diverse amyloids are all consistent with the model of the continuous  $\beta$ -sheet helix described in detail for the Val30Met amyloid fibril (Blake & Serpell, 1996). For all of the amyloids, the lowest-order reflection, at 4.8 Å, is the 24th order of the 115.5 Å repeat, suggesting that the amyloid core contains 24  $\beta$ -strands in each 115.5 Å-long repeating unit along the fibril axis (Figure 3). A twist of the  $\beta$ -sheet through 360° in 115.5 Å generates a relative twist of 15° between neighbouring  $\beta$ -strands if there are 24  $\beta$ -strands in the helical repeat. Most  $\beta$ -sheet structures in folded proteins are twisted rather than planar and have a right-handed twist of 0° to 30° between strands. The right-handed twisted conformation represents the lowest energy conformation of the  $\beta$ -sheet structure (Pauling & Corey, 1951; Chothia, 1973). This model of the amyloid protofilament core incorporates the most likely, lower energy, right-handed twisted  $\beta$ -sheets but the data do not differentiate between left and right-handed helices. In this model, the twisting of the  $\beta$ -sheets around a common helical axis, which is parallel to the axis of the protofilament, accounts for the repeating unit of approximately 115.5 Å that is observed in all the amyloid fibrils studied here. The model is therefore an elaboration of the classical cross- $\beta$  molecular structure, which permits the incorporation of the favourable twisted  $\beta$ -sheet structures (Pauling & Corey, 1951; Chothia, 1973). The helical structure of the protofilament enables the hydrogen bonding between the  $\beta$ -strands to be extended over the total length of the amyloid fibrils, thereby accounting for their characteristic rigidity and stability. The extended order in this dimension of the fibrils is responsible for the pseudo-crystalline sharpness of the meridional reflections.

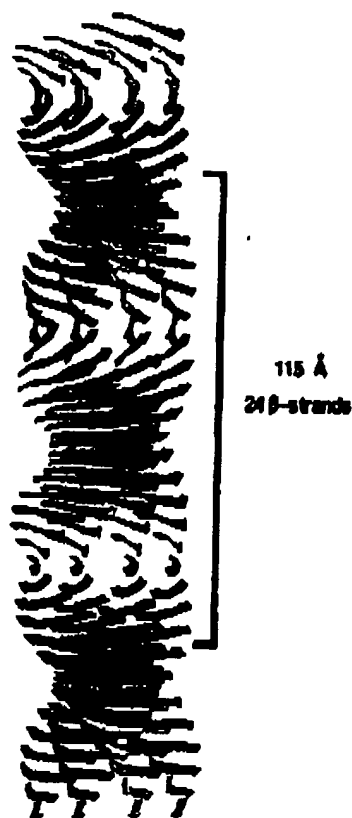


**Figure 3.** Model of the generic amyloid fibril structure. Molecular model of the common core protofilament structure of amyloid fibrils. A number of  $\beta$ -sheets (four illustrated here) make up the protofilament structure. These sheets run parallel to the axis of the protofilament, with their component  $\beta$ -strands perpendicular to the fibril axis. With normal twisting of the  $\beta$ -strands, the  $\beta$ -sheets twist around a common helical axis that coincides with the axis of the protofilament, giving a helical repeat of 115.5 Å containing 24  $\beta$ -strands (this repeat is indicated by the boxed region).

The present X-ray results support the view that this model represents the core molecular structure of all of the amyloid fibrils studied here, irrespective of the number or arrangement of protofilaments, and demonstrate the independence of the 115.5 Å helical repeat from the nature of precursor protein. The ability of this single structure to accommodate different length polypeptide chains may be understood in the following way. Very short peptide chains, say six to ten residues, are able to form a single  $\beta$ -strand, which can act as the basic unit to be repeated along the fibre axis. Longer polypeptides will be able to form a larger number of  $\beta$ -strands by folding their chains back and forth. In this way the cross- $\beta$  amyloid structure may be independent of the length of the polypeptide chains forming it. The features of the structure that may vary and be dependent on characteristics

of the precursor are mainly expressed in directions perpendicular to the fibre axis, where loops of varying length or other structures can be accommodated without affecting the core  $\beta$ -sheet structure. These variations would be expected to be reflected in variability of the spacings and intensities of the equatorial reflections. In contrast, the common  $\beta$ -sheet helical structure should result in a constant pattern for the spacings and intensities of meridional reflections. These characteristics are exactly what is observed in the diffraction patterns from different amyloid fibrils.

### Fibrillogenesis and a structural conversion

Table 1 lists the known or predicted structures of the amyloid fibril subunit precursors in their non-fibrillar form. The amyloidogenic proteins display a wide range of native folds, yet the present analysis has demonstrated that all amyloid fibrils have the same cross- $\beta$  molecular skeleton. Proteins such as the immunoglobulin light chain (Schormann *et al.*, 1995), transthyretin (Blake *et al.*, 1978; Terry *et al.*, 1993; Hamilton *et al.*, 1993; Sebastião *et al.*, 1996) and  $\beta_2$ -microglobulin (Becker & Reeke, 1985) have similar, mainly  $\beta$ -sheet native structures but, even so, must sustain significant structural changes when they are deposited in the cross- $\beta$  amyloid form (Blake & Serpell, 1996; Blake *et al.*, 1996), and it is known that the form of transthyretin that is amyloidogenic has a non-native conformation (Colon & Kelly, 1992; McCutchen *et al.*, 1993, 1995; Kelly, 1996). Proteins such as insulin (Adams *et al.*, 1969), cystatin C (Bode *et al.*, 1988), the amyloidogenic variants of lysozyme (Pepys *et al.*, 1993; Booth *et al.*, 1997), and the prion protein (Riek *et al.*, 1996), which have extensive native  $\alpha$ -helical structure, may undergo even larger conformational changes when they form amyloid fibrils.

Such a structural conversion has been demonstrated for the amyloidogenic variants of human lysozyme (Booth *et al.*, 1997), which show an increase in  $\beta$ -sheet content and a loss of  $\alpha$ -helical structure during fibril formation *in vitro*, and it is also associated with infectivity in the prion spongiform encephalopathies (Pan *et al.*, 1993; Gasset *et al.*, 1992, 1993; Harrison *et al.*, 1997). Studies of various peptides corresponding to regions of the Alzheimer's disease A $\beta$  peptide have also demonstrated that structural plasticity is related to fibril formation (Hilbich *et al.*, 1991; Barrow *et al.*, 1992; Talafous *et al.*, 1994; Sticht *et al.*, 1995; Soto *et al.*, 1995).

The present work demonstrates that, although the amyloidogenic proteins have very different precursor structures, they can all undergo a structural conversion, perhaps along a similar pathway, to a misfolded form that is the building block of the  $\beta$ -sheet helix protofilament. This mechanism of structural conversion and the generic structure of

the amyloid protofilament offer two distinct targets for therapeutic molecules: compounds that could interfere with the transition from precursor to  $\beta$ -structured fold and agents that might inhibit or reverse the packing of protofilaments into fibrils.

## Acknowledgements

We thank Drs G. A. Tennant, V. Bellotti and W. L. Hutchinson for preparing fibrils, and S. Lee for assistance with preparation of Figures. We thank Professor E. Lundgren and Dr O. Sangren, University of Umeå, Sweden, for providing variant transthyretin Val30Met fibrils extracted from vitreous humor. L.C.S. was supported by the Oxford Centre for Molecular Sciences, and P. E. F. by the Alzheimer's Society of Ontario and the Ontario Mental Health Foundation. This work was supported in part by MRC Programme grant (G7900510) to M.B.P. and MRC Project grants to M.B.P. and C.C.F.B. We dedicate this paper to the memory of the late Dr George Glenner, the champion of  $\beta$ -fibrillosis.

## References

- Adams, M. J., Blundell, T. L., Dodson, E. J., Dodson, G. G., Vijayan, M., Baker, E. N., Harding, M. M., Hodgkin, D. C., Rimmer, B. & Sheat, S. (1969). The structure of rhombohedral 2 zinc insulin crystals. *Nature*, 224, 491-495.
- Arnott, S., Dover, S. & Elliot, A. (1967). Structure of  $\beta$ -poly-L-alanine: refined atomic co-ordinates for an anti-parallel beta-plated sheet. *J. Mol. Biol.* 30, 201-208.
- Barrow, C. J., Yasuda, A., Kenny, P. T. M. & Zagorski, M. G. (1992). Solution conformations and aggregational properties of synthetic amyloid  $\beta$ -peptides of Alzheimer's disease. *J. Mol. Biol.* 225, 1075-1093.
- Becker, J. & Reeke, G. (1985). Three-dimensional structures  $\beta_2$ -microglobulin. *Proc. Natl Acad. Sci USA*, 82, 4225-4229.
- Blake, C. C. F. & Serpell, L. C. (1996). Synchrotron X-ray studies suggest that the core of the transthyretin amyloid fibril is a continuous  $\beta$ -sheet helix. *Structure*, 4, 989-998.
- Blake, C. C. F., Gelsow, M. J., Oatley, S. J., Rerat, B. & Rerat, C. (1978). Structure of prealbumin: secondary, tertiary and quaternary interactions determined by Fourier refinement at 1.8 Å. *J. Mol. Biol.* 121, 339-356.
- Blake, C. C. F., Serpell, L. C., Sunde, M. & Lundgren, E. (1996). A molecular model of the amyloid fibril. In *CIBA Symposium No. 199, The Nature and origin of Amyloid Fibrils*, pp. 6-21, John Wiley & Sons Ltd, Chichester, UK.
- Bode, W., Engl, R., Musil, D., Thiele, U., Huber, R., Karshikov, A., Brzin, J., Kos, J. & Turk, V. (1988). The 2.0 Å X-ray crystal structure of chicken egg white cystatin and its possible mode of interaction with cysteine proteinases. *EMBO J.* 7, 2593-2599.
- Bonar, L., Cohen, A. S. & Skinner, M. (1967). Characterization of the amyloid fibril as a cross- $\beta$  Protein. *Proc. Soc. Expt. Biol. Med.* 131, 1373-1375.
- Booth, D. R., Soutar, A. K., Hawkins, P. N., Reilly, M., Harding, A. & Pepys, M. B. (1994). Three new amyloidogenic transthyretin gene mutations: advantages of direct sequencing. In *Amyloid and Amyloidosis 1993* (Kisilevsky, R., Benson, M. D., Frangione, B., Gauldie, J. T., Muckle, J. & Youngs, I. D., eds), pp. 456-458, Parthenon Publishing, New York, Pearl River.
- Booth, D. R., Sunde, M., Bellotti, V., Robinson, C. V., Hutchinson, W. L., Fraser, P. E. et al. (1997). Instability, unfolding and fibrillogenesis in amyloidogenic lysozyme variants. *Nature*, 385, 787-793.
- Bradbury, E. M., Brown, L., Downie, A. R., Elliott, A., Fraser, R. D. B., Hanby, W. E. & Macdonald, T. R. R. (1960). The "cross-beta" structure in polypeptides of low molecular weight. *J. Mol. Biol.* 2, 276.
- Burge, R. E. (1959). X-ray scattering by bundles of cylinders. *Acta Crystallog.* 12, 285-289.
- Burge, R. E. (1963). Equatorial X-ray diffraction by fibrous proteins: short range order in collagen, feather keratin and f-actin. *J. Mol. Biol.* 7, 213-224.
- Burke, M. J. & Rougvie, M. A. (1972). Cross- $\beta$  protein structures I. Insulin fibrils. *Biochemistry*, 11, 2435-2439.
- Burtrick, L. D., Robinson, R. C. & Koepf, E. K. (1996). The structure of horse plasma gelolin to 2.5 Å. *Biophys. J.* 70, Pt. 2, pSUA12.
- Chothia, C. (1973). Conformations of twisted  $\beta$ -sheets in proteins. *J. Mol. Biol.* 75, 295-302.
- Cohen, A. S., Shirahama, T. & Skinner, M. (1981). Electron microscopy of amyloid. In *Electron Microscopy of Protein* (Harris, L., ed.), vol. 3, pp. 165-205, Academic Press, London.
- Colon, W. & Kelly, J. W. (1992). Partial denaturation of transthyretin is sufficient for amyloid fibril formation in vitro. *Biochemistry*, 31, 8654-8660.
- Come, J. H., Fraser, P. E. & Lansbury, P. T. (1993). A kinetic model for amyloid formation in the prion diseases: importance of seeding. *Proc. Natl Acad. Sci. USA*, 90, 5959-5963.
- Damas, A., Sebastião, M. P., Dorníngues, F. S., Costa, P. P. & Saraiva, M. J. (1995). Structural studies on FAP fibrils: removal of contaminants is essential for the interpretation of X-ray data. *Amyloid: Int. J. Exp. Clin. Invest.* 2, 173-1278.
- Eanes, E. D. & Glenner, G. G. (1968). X-ray diffraction studies on amyloid filaments. *J. Histochem. Cytochem.* 16, 673-677.
- Filshie, B. K., Fraser, R. D. B., MacRae, T. P. & Rogers, G. E. (1964). X-ray diffraction and electron microscope observations on soluble derivatives of keratin. *Biochem. J.* 92, 19-26.
- Fraser, P. E., Nguyen, J. T., Surewicz, W. K. & Kirschner, D. A. (1991). pH dependent structural transitions of Alzheimer's amyloid peptides. *Biophys. J.* 60, 1190-1201.
- Gasset, M., Baldwin, M. A., Lloyd, D. H., Gabriel, J.-M., Holtzman, D. M., Cohen, F. E., Fletterick, R. & Prusiner, S. B. (1992). Predicted  $\alpha$ -helical regions of the prion protein, when synthesized as peptides, form amyloid. *Proc. Natl Acad. Sci. USA*, 89, 10940-10944.
- Gasset, M., Baldwin, M., Fletterick, R. & Prusiner, S. (1993). Perturbation of secondary structure of the scrapie prion protein under conditions that alter infectivity. *Proc. Natl Acad. Sci. USA*, 90, 1-5.
- Geddes, A. J., Parker, K. D., Atkins, E. D. T. & Beighton, E. (1968). "Cross  $\beta$ " conformation in protein. *J. Mol. Biol.* 32, 343-358.

- Culchrest, P. & Bradshaw, J. (1993). Amyloid formation by salmon calcitonin. *Biochim. Biophys. Acta*, 111-114.
- Glenner, G. G. (1980a). Amyloid deposits and amyloidosis. The beta-fibrilloses (part one). *New Eng. J. Med.* 302, 1283-1292.
- Glenner, G. G. (1980b). Amyloid deposits and amyloidosis. The beta-fibrilloses (part two). *New Eng. J. Med.* 302, 1333-1343.
- Glenner, G. G. & Wong, C. W. (1984). Alzheimer's disease: initial report of the purification and characterization of a novel cerebrovascular amyloid protein. *Biochem. Biophys. Res. Commun.* 120, 885-890.
- Gorevic, P., Castano, E., Sarma, R. & Frangione, B. (1987). Ten to fourteen residue peptides of Alzheimer's disease protein are sufficient for amyloid fibril formation and its characteristic X-ray diffraction pattern. *Biochem. Biophys. Res. Commun.* 147, 854-862.
- Hamilton, J., Steirrauf, L., Braden, B., Liepnieks, J., Benson, M., Holmgren, G., Sandgren, O. & Steen, L. (1993). The X-ray crystal structure refinements of normal human transthyretin and the amyloidogenic Val-30-Met variant to 1.7 Å resolution. *J. Biol. Chem.* 268, 2416-2424.
- Harrison, P. M., Bamborough, P., Daggett, V., Prusiner, S. B. & Cohen, F. E. (1997). The prion folding problem. *Curr. Opin. Struct. Biol.* 7, 53-59.
- Hilbich, C., Kisters-Woike, B., Reed, J., Masters, C. & Beyreuther, K. (1991). Aggregation and secondary structure of synthetic amyloid  $\beta$ A4 peptides of Alzheimer's disease. *J. Mol. Biol.* 218, 149-163.
- Inouye, H., Fraser, P. E. & Kirschner, D. A. (1993). Structure of  $\beta$ -crystallite assemblies by Alzheimer  $\beta$ -amyloid protein analogues: analysis by X-ray diffraction. *Biophys. J.* 64, 502-519.
- Jarvis, J. A., Craik, D. J. & Wilce, M. C. J. (1993). X-ray diffraction studies of fibrils formed from peptide fragments of transthyretin. *Biochem. Biophys. Res. Commun.* 192, 991-998.
- Kelly, J. W. (1996). Alternative conformations of amyloidogenic proteins govern their behaviour. *Curr. Opin. Struct. Biol.* 6, 11-17.
- Kelly, J. W. (1997). Amyloid fibril formation and protein misassembly: a structural quest for insights into amyloid and prion diseases. *Structure*, 5, 595-600.
- Kirschner, D. A., Abraham, C. & Selkoe, D. A. (1986). X-ray diffraction from intraneuronal paired helical filaments and extra-neuronal amyloid fibres in Alzheimer's disease indicates cross  $\beta$  conformation. *Proc. Natl Acad. Sci. USA*, 83, 503-507.
- Kirschner, D. A., Inouye, H., Duffy, L., Sinclair, A., Lind, M. & Selkoe, D. A. (1987). Synthetic peptide homologous to  $\beta$ -protein from Alzheimer's disease forms amyloid-like fibrils *in vitro*. *Proc. Natl Acad. Sci. USA*, 84, 6953-6957.
- Lorenz, M. & Holmes, K. C. (1993). Computer processing and analysis of X-ray diffraction data. *J. Appl. Crystallog.* 26, 82-91.
- McCutchen, S., Colon, W. & Kelly, J. W. (1993). Transthyretin mutation Leu-55-Pro significantly alters tetramer stability and increases amyloidogenicity. *Biochemistry*, 32, 12119-12127.
- McCutchen, S. L., Lai, Z., Mirov, G. J., Kelly, J. W. & Colon, W. (1995). Comparison of lethal and non-lethal transthyretin variants and their relationship to amyloid disease. *Biochemistry*, 34, 13527-13536.
- Nelson, S., Lyon, M., Gallager, J., Johnson, E. & Pepys, M. B. (1991). Isolation and characterisation of the integral glycosaminoglycan constituents of human amyloid A and monoclonal light-chain amyloid fibrils. *Biochem. J.* 275, 67-74.
- Nguyen, J. T., Inouye, H., Baldwin, M. A., Fletterick, R., Cohen, F. E., Prusiner, S. B. & Kirschner, D. A. (1995). X-ray diffraction from scrapie prion rod and PrP peptides. *J. Mol. Biol.* 252, 412-422.
- Noles, R. T. & Atkinson, D. (1992). Conformational analysis of apolipoprotein A-I and E-3 based on primary sequence and circular dichroism. *Biophys. J.* 63, 1221-1239.
- Pan, K.-M., Baldwin, M. A., Nguyen, J. T., Gaseet, M., Serban, A., Groth, D., Mehlhorn, I., Huang, Z., Fletterick, R. J., Cohen, F. E. & Prusiner, S. B. (1993). Conversion of  $\alpha$ -helices into  $\beta$ -sheets features in the formation of the scrapie prion proteins. *Proc. Natl Acad. Sci. USA*, 90, 10962-10966.
- Pauling, L. & Corey, R. (1951). Configuration of polypeptide chains with favoured orientation around single bonds: two new pleated sheets. *Proc. Natl Acad. Sci. USA*, 37, 729-739.
- Pepys, M. B. (1996). Amyloidosis. In *The Oxford Textbook of Medicine* (Weatherall, D. J., Ledingham, J. G. G. & Warrell, D. A., eds), 3rd edit., vol. 2, pp. 1512-1524. Oxford University Press, Oxford.
- Pepys, M. B., Hawkins, P. N., Booth, D. R., Vigushin, D. M., Tennet, G. A., Soutar, A. K., Totty, N., Nguyen, O., Blake, C. C. F., Terry, C. J., Feast, T. G., Zalin, A. M. & Hsuan, J. J. (1993). Human lysozyme gene mutations cause hereditary systemic amyloidosis. *Nature*, 362, 553-557.
- Riek, R., Hornemann, S., Wider, G., Billster, M., Glockshuber, R. & Wüthrich, K. (1996). NMR structure of the mouse prion protein domain PrP(121-231). *Nature*, 382, 180-182.
- Schwarzman, N., Murrell, J. R., Liepnieks, J. & Benson, M. (1995). Tertiary structure of an amyloid immunoglobulin light chain protein: a proposed model for amyloid fibril formation. *Proc. Natl Acad. Sci. USA*, 92, 9490-9494.
- Sebastião, P., Dauter, Z., Saraiva, M. J. & Damas, A. M. (1996). Crystallization and preliminary X-ray diffraction studies of Leu55Pro variant transthyretin. *Acta Crystallog. sect. D*, 52, 566-568.
- Serpell, L. C., Sunde, M., Fraser, P. E., Luther, P. K., Morris, E., Sandgren, O., Lundgren, E. & Blake, C. C. F. (1995). The examination of the structure of the transthyretin amyloid fibril by image reconstruction from electron micrographs. *J. Mol. Biol.* 254, 113-118.
- Shirahama, T. & Cohen, A. S. (1967). High resolution electron microscopic analysis of the amyloid fibril. *J. Cell Biol.* 33, 679-706.
- Shirahama, T., Benson, M. D., Cohen, A. S. & Tanaka, A. (1973). Fibrillar assemblage of variable segments of immunoglobulin light chains: an electron microscopic study. *J. Immunol.* 110, 21-30.
- Soto, C., Castano, E., Frangione, B. & Inestrosa, N. (1995). The  $\alpha$ -helical to  $\beta$ -sheet transition in the amino-terminal fragment of the amyloid  $\beta$ -peptide modulates amyloid formation. *J. Biol. Chem.* 270, 3063-3067.
- Sticht, H. P., Bayer, P., Willbold, D., Damas, S., Hilbich, C., Beyreuther, K., Frank, R. & Rosch, P. (1995). Structure of amyloid A4(1-40)-peptide of Alzheimer's disease. *Eur. J. Biochem.* 223, 293-298.



- Soutar, A. K., Hawkins, P. N., Vigushin, D. M., Tennent, G. A., Booth, S., Hutton, T., Nguyen, O., Totty, N., Feast, T. G., Hsuan, J. J. & Pepys, M. B. (1992). Apolipoprotein A-1 mutation Arg-60 causes autosomal dominant amyloidosis. *Proc. Natl Acad. Sci. USA*, 89, 7389-7393.
- Tagliavini, F., Prelli, F., Verga, L., Giaccone, G., Jarma, R., Gorevic, P., Ghetti, B., Passerini, F., Ghibaudi, E., Forloni, G., Salmona, M., Bugiani, O. & Frangione, B. (1993). Synthetic peptides homologous to prion protein residues 106-147 form amyloid-like fibrils *in vitro*. *Proc. Natl Acad. Sci. USA*, 90, 9678-9682.
- Talafous, J., Marcinowski, K., Klopman, G. & Zagorski, M. (1994). Solution structure of residues 1-28 of the amyloid  $\beta$ -peptide. *Biochemistry*, 33, 7788-7796.
- Tan, S. Y., Pepys, M. B. & Hawkins, P. N. (1995). Treatment of amyloidosis. *Am. J. Kidney Dis.* 26, 267-285.
- Terry, C. J., Damas, A. M., Oliveira, P., Saraiva, M. J. M., Alves, A. L., Costa, P. P., Matias, P. M., Sakaki, Y. & Blake, C. C. F. (1993). Structure of Met30 variant of transthyretin and its amyloidogenic variations. *EMBO J.* 12, 735-741.
- Turnell, W., Sarra, R., Baum, J. O., Caspi, D., Baltz, M. L. & Pepys, M. B. (1986a). X-Ray scattering and diffraction by wet gels of AA amyloid fibrils. *Mol. Biol. Med.* 3, 409-424.
- Turnell, W., Sarra, R., Glover, I. D., Baum, J. O., Caspi, D., Baltz, M. L. & Pepys, M. B. (1986b). Secondary structure prediction of human SAA<sub>1</sub>, presumptive identification of calcium and lipid binding sites. *Mol. Biol. Med.* 3, 387-407.
- Worcester, D. L. (1978). Structural origins of diamagnetic anisotropy in proteins. *Proc. Natl Acad. Sci. USA*, 75, 5473-5477.

Edited by F. E. Cohen

(Received 8 May 1997; received in revised form 5 August 1997; accepted 5 August 1997)

biochemical society

# **TRANSACTIONS**

## **676th Meeting, Heriot-Watt University, Edinburgh**

Novartis Medal Lecture

**Antibodies: a Paradigm for the Evolution of Molecular Recognition  
colloquia**

**14-3-3 Proteins in Cell Regulation**

**Lessons from the Type II Family of G-Protein-Coupled Receptors:  
Their Ligands, Receptor Structure and Function**

**Mediation and Modulation of Antibody Function**

**Amyloidogenic Proteins Involved in Neurodegeneration and  
Therapeutic Implications**

**Tetrapyrroles: Their Life, Birth and Death**

## **Focused Meetings**

**Biometals 2002: Third International Biometals Symposium**

**High-Throughput Screening: The Way Ahead**

**Regulation of B-Lymphocytes in Health and Disease**

Univ. of Minn.  
Bio-Medical  
Library

# Amyloidogenic Proteins Involved in Neurodegeneration and Therapeutic Implications

Protein and Peptide Science Group Colloquium Organized and Edited by B. Austen (St George's Hospital Medical School, London) and G. B. Irvine (Medical Biology Centre, Queen's University Belfast) and Sponsored by Merck Sharpe and Dohme Ltd. and CIPHERGEN. 676th Meeting held at Heriot-Watt University, Edinburgh, 8-10 April 2002.

---

## Examining the structure of the mature amyloid fibril

O. S. Makin and L. C. Serpell<sup>1</sup>

Structural Medicine Unit, Cambridge Institute for Medical Research, Hills Road, Cambridge CB2 2XY, U.K.

---

### Abstract

The pathogenesis of the group of diseases known collectively as the amyloidoses is characterized by the deposition of insoluble amyloid fibrils. These are straight, unbranching structures about 70–120 Å (1 Å = 0.1 nm) in diameter and of indeterminate length formed by the self-assembly of a diverse group of normally soluble proteins. Knowledge of the structure of these fibrils is necessary for the understanding of their abnormal assembly and deposition, possibly leading to the rational design of therapeutic agents for their prevention or disaggregation. Structural elucidation is impeded by fibril insolubility and inability to crystallize, thus preventing the use of X-ray crystallography and solution NMR. CD, Fourier-transform infrared spectroscopy and light scattering have been used in the study of the mechanism of fibril formation. This review concentrates on the structural information about the final, mature fibril and in particular the complementary techniques of cryo-electron microscopy, solid-state NMR and X-ray fibre diffraction.

### Introduction

There are approx. 20 human diseases, including Alzheimer's, Parkinson's and the transmissible spongiform encephalopathies, that are charac-

terized by the deposition of amyloid fibrils [1]. The soluble precursor proteins from which the fibrils are assembled do not share primary sequences, function or native structure. However, amyloid fibrils formed from very different proteins appear to show considerable structural similarities [2]. Information about amyloid structure is essential in order to gain a greater understanding of fibrillogenesis and the associated conformational changes.

Specific chemical staining has been a key method by which amyloid has been identified. Indeed, amyloid means 'starch-like', due to its ability to be stained by iodine solution [3]. A characteristic apple-green birefringence pattern when stained with Congo Red dye and viewed under cross-polarized light is used to detect the presence of amyloid [4]. Amyloid fibrils may be identified by their morphology under the electron microscope, by a 'cross- $\beta$ ' X-ray diffraction pattern or the birefringence pattern observed after Congo Red binding. Initial work using electron microscopy by Cohen and others [5,6] showed that amyloid fibrils have a similar ultrastructure and morphology, being long, straight, unbranched assemblies approx. 100 Å wide and composed of two or more protofilaments, each 25–35 Å in diameter and arranged in a helical manner.

Information on structural changes accompanying fibril formation has been obtained by means of kinetic studies using CD, atomic-force microscopy and light scattering. Light scattering tracks changes in particle size, while CD pro-

---

Key words: diffraction, electron microscopy, NMR.

Abbreviation used: A $\beta$  peptide, amyloid- $\beta$  peptide.

<sup>1</sup>To whom correspondence should be addressed (e-mail ls279@cam.ac.uk).

vides information about changes to the protein conformation accompanying fibrillogenesis and the environment and orientation of aromatic side chains. Atomic-force microscopy provides high-resolution data on the mechanism and kinetics of assembly. These have demonstrated that fibrillogenesis is a process of nucleation and growth, with nucleation being the rate-limiting step.

Amyloid fibrils may be formed *in vitro* from synthetic peptides homologous to amyloid-forming proteins. Fibrils grown from synthetic peptides have the advantage of being more readily available and of greater purity than those extracted from tissue. Many researchers use truncated peptides which, while forming fibrils of morphological and chemical similarity to those formed by full-length peptides [7-9], have the advantages of forming fibrils that are straighter and more ordered than those formed from full-length peptides. In addition, the effect of the removal of certain residues on fibril growth and structure provides insights into the commonalities of amyloid [10,11].

This review considers three major ways by which the structure of amyloid might be elucidated; that is, cryo-electron microscopy, solid-state NMR and X-ray fibre diffraction.

### X-ray fibre diffraction

The main conclusion from X-ray diffractograms is that amyloid fibrils share a common 'cross- $\beta$ ' structure [12-15]. This is based on the observation that all the diffraction patterns show two major reflections. The first is a strong, sharp, meridional reflection at 4.7 Å, corresponding to the hydrogen-bonding distance between the  $\beta$ -strands that constitute a  $\beta$ -sheet. The second, slightly more diffuse reflection is on the equator around 10-11 Å that corresponds to the spacing between  $\beta$ -sheets. This reflection can vary depending on the side-chain composition of the amyloid protein or peptide.

In 1968, Geddes et al. [16] first described a model for a molecule exhibiting this type of diffraction pattern for the egg stalk of the lacwing *Chrysopa*. Here, the extended polypeptide chains fold back and forth to form a  $\beta$ -sheet ribbon 25 Å wide and indeterminately long, and the constituent  $\beta$ -strands run perpendicular to the fibre axis. These ribbons are flat, as described by Pauling and Corey [17], and stack face to face many times. Diffraction patterns from *ex vivo* transthyretin amyloid fibrils gave rise to a model in which

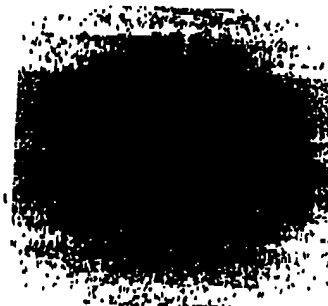
several  $\beta$ -sheets turn around a central axis [18]. Collection of fibre diffraction patterns from many other amyloid fibrils indicated that this model may constitute a generic model for the core structure of the amyloid protofilament [15].

Poorly aligned fibrils will only produce one-dimensional information, in the manner of powder diffractograms. *Ex vivo* samples can be aligned by means of a stretch frame, giving further two-dimensional information circularly averaged in reciprocal space about the fibre axis [19]. Synthetic samples can either be grown on a stretch frame, giving an improved fibre alignment, or grown in a strong magnetic field. Magnetically aligned truncated precursor peptides grow to produce structures that are capable of producing the highest-quality diffraction patterns [20]. In some cases these samples are no longer cylindrically symmetric, as the diffraction patterns down the fibre axis are not circularly symmetric, and may therefore be described as crystallites. Diffractograms of these crystallites, at multiple angles, provide additional information about the reciprocal space lattice [21].

Fibrils formed from fragments of the amyloid- $\beta$  peptide (A $\beta$  peptide) [20-25] and prion proteins [8] have yielded highly oriented diffraction patterns from which many structural models have been built (see [9] for review). The sharp reflection at 4.7 Å of the meridian of diffraction patterns from amyloid fibrils clearly shows that  $\beta$ -strands run perpendicular to the fibre axis, indicating that most proteins must undergo considerable conformational rearrangement upon conversion from soluble protein into insoluble

**Figure 1**  
X-ray fibre diffraction taken using a synchrotron radiation source from a stretch-frame-aligned sample of amyloid fibrils formed from A $\beta$ (11-25) peptide

Layer lines are observable with a spacing of 9.4 Å, corresponding to the repeat distance for an anti-parallel  $\beta$ -sheet. The strong sharp spacing on the meridian at 4.7 Å is clearly visible [25].



amyloid fibre. Diffraction patterns from A $\beta$ (11–25) also show highly oriented diffraction patterns with a layer-line spacing of 9.4 Å (Figure 1), revealing that these amyloid fibrils are made up of anti-parallel  $\beta$ -sheet structure [21].

### Solid-state NMR

Solid-state NMR provides high-resolution data about the distances between  $^{13}\text{C}$ -labels placed selectively in the precursor proteins. These data are accurate to approx. 0.2 Å for distances less than about 6 Å, although this precision is not maintained for larger distances. The result is that solid-state NMR is capable of accurately showing that the structure places the labels in such a way as to either be consistent or otherwise with the  $\beta$ -strands in a  $\beta$ -sheet being in register and parallel. Unfortunately, if the strands are out of register rather than being anti-parallel or if the sheet is composed of a mixture of parallel and anti-parallel strands, results may be produced that are misleading. This might explain the wide variation in reported results. Balbach et al. report [26] multiple-quantum NMR and rotational echo double-resonance results for A $\beta$ (16–22), which rule out a parallel  $\beta$ -sheet structure but support an anti-parallel structure; this is also the case for rotational resonance NMR on A $\beta$ (34–42) [27]. In the case of A $\beta$ (1–40), an in-register parallel  $\beta$ -sheet conformation has been reported using multiple quantum NMR [28] and likewise for A $\beta$ (10–35) by dipolar recoupling in a windowless sequence measurement [29]. It has been suggested that different-length fragments of A $\beta$  may arrange themselves in a parallel or anti-parallel  $\beta$ -sheet. A $\beta$ (11–25) forms fibrils that are clearly anti-parallel by X-ray diffraction measurements [21]. However, it remains unclear how a 40-residue peptide can fold into a fibre and maintain a parallel  $\beta$ -sheet arrangement. It is possible that the fibrils formed by full-length A $\beta$  consist of a mixture of parallel and anti-parallel  $\beta$ -sheets.

### Electron microscopy

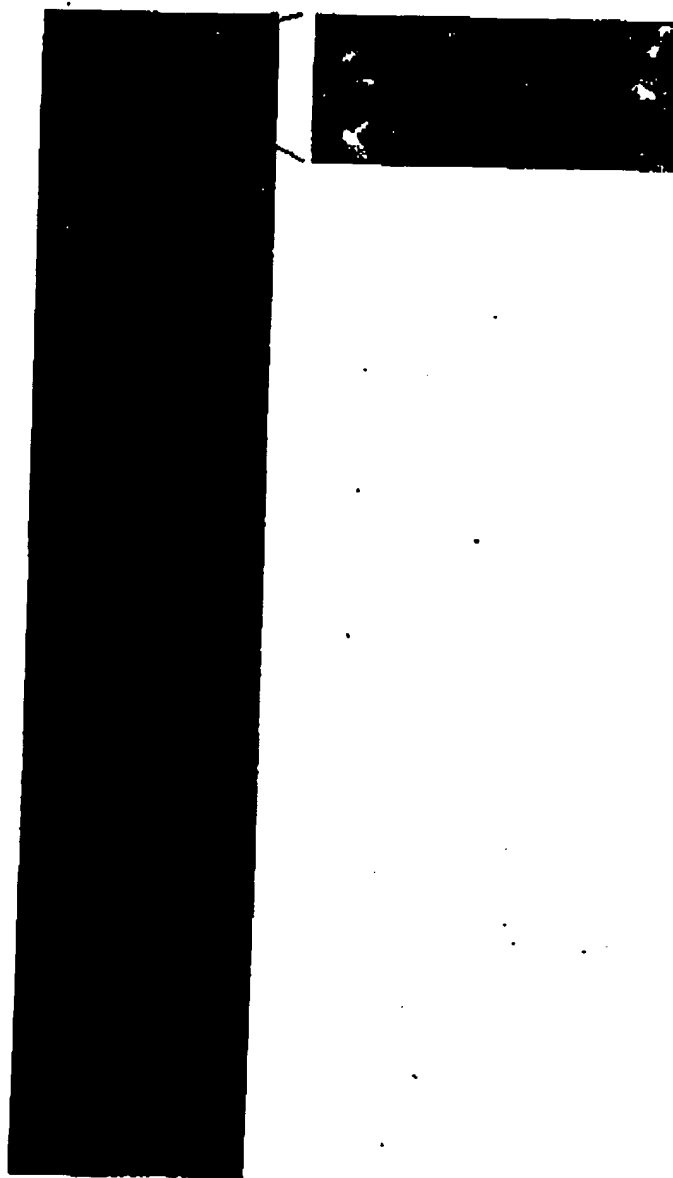
Electrons interact with matter in a far stronger manner than either X-rays or neutrons. This allows observation of single particles without requiring a crystalline sample or, as with X-ray fibre diffraction, the result being implicitly averaged. Unfortunately, this leads to substantial radiation damage at the levels of electron flux

required to obtain good contrast. Staining improves the contrast but results in the image being of the stain rather than the protein itself. Shadow imaging involves the angular deposition of heavy metal ions on the surface of the sample but the image is of the imprint of the fibrils in the metal layer, so the fibril position is clearer but internal structure is not observed. For cryo-electron microscopy, the sample is cooled to liquid nitrogen or helium temperature to reduce the magnitude of ionization damage and the protein is maintained in a hydrated state in ice. Low-dose electron microscopy is used to minimize the radiation damage to the sample.

The observed contrast-transfer-function-corrected electron-micrographic image is an approximation of the projection of the electron density of the specimen. Structural information can be extracted from the micrographs and proceeds via either three-dimensional reconstruction of the fibril electron-density function or direct visualization [30]. Fibrils may be helical, so under certain circumstances only a single micrograph is required for three-dimensional reconstruction [31]; however, this requires a single, straightened micrograph with sufficiently low noise to be of use. Averaging is not trivial since the fibrils often have appreciable curvature. One technique is to split the fibril into sections approx. one repeat long and then apply single-particle methods. This was used successfully to examine the protofilament composition of fibrils formed from an SH3 peptide [32]. This approach revealed that the fibrils are elliptical in cross-section and are composed of four protofilaments. Examination of apolipoprotein A1 fibrils and lysozyme fibrils also reveals structural information about varying protofilament arrangement within a single sample [33]. This method is possible when the fibrils show a well-defined twist in the images, indicating a long-range repeat. In the case of A $\beta$ (11–25), no long-range helical twist is evident [30]. However, high-resolution images from these well-ordered fibrils revealed striations running across the fibril image (Figure 2). Fourier-transform infrared spectroscopy revealed that these corresponded to a repeat distance of 4.7 Å, which is the hydrogen-bonding spacing of  $\beta$ -strands. This showed that we were directly visualizing the  $\beta$ -sheet structure within the fibrils! The fact that this was possible suggested several things. First, that the samples are quite resistant to radiation damage. Second, that for the structure to be visible as striation there must be more than one  $\beta$ -sheet and the  $\beta$ -sheets must be arranged

**Figure 2**  
Cryo-electron micrograph image of A $\beta$ (11-25) amyloid fibrils in vitreous ice [30]

Close examination reveals striations across the fibres with a spacing between them of 4.7 Å. The inset shows an averaged, enhanced image of the striations for clarity.



such that the  $\beta$ -strands are in direct register. Third, that the  $\beta$ -strands run perpendicular to the fibre axis.

### The future

Each of the techniques outlined herein provides particular data of utility to both the study of amyloid formed from specific peptides and the field of amyloid structure in general. They each have their own strengths and limitations, whether

it be spatial resolution, accuracy or specificity of information. The challenge we now face is the judicious collection of information in such a manner that the signal-to-noise ratio is improved, systematic errors accounted for and accuracy maintained. This alone may hold the key for the basis of an understanding of the structural commonalities and differences of amyloid.

We acknowledge the funding support of the Wellcome Trust and the Medical Research Council. We thank Bjarne Rasmussen for help at European Synchrotron Radiation Facility, Grenoble, France.

and the Laboratory of Molecular Biology for use of the cryo-electron microscopes.

## References

- 1 Kelly, J. W. (1996) *Curr. Opin. Struct. Biol.* 6, 11-17
- 2 Sunde, M. and Blake, C. (1998) *Q. Rev. Biophys.* 31, 1-39
- 3 Virchow, R. (1854) *Virchows Arch.* 6, 415-426
- 4 Puchtler, H., Sweet, F. and Levine, M. (1961) *J. Histochem. Cytochem.* 10, 355-364
- 5 Shirahama, T. and Cohen, A. S. (1967) *J. Cell Biol.* 33, 679-706
- 6 Cohen, A. S. and Calkins, E. (1959) *Nature (London)* 183, 1202-1203
- 7 Jarvis, J., Craik, D. and Wilke, M. (1993) *Biochem. Biophys. Res. Commun.* 192, 991-998
- 8 Nguyen, J. T., Inouye, H., Baldwin, M. A., Rietterick, R. J., Cohen, F. E., Prusiner, S. B. and Kirschner, D. A. (1995) *J. Mol. Biol.* 252, 412-422
- 9 Serpell, L. (2000) *Biochim. Biophys. Acta* 1502, 16-30
- 10 Halverson, K., Fraser, P. E., Kirschner, D. A. and Lansbury, Jr., P. T. (1990) *Biochemistry* 29, 2639-2644
- 11 Fraser, P. E., Nguyen, J. T., Inouye, H., Surewicz, W. K., Selkoe, D. J., Podlasky, M. B. and Kirschner, D. A. (1992) *Biochemistry* 31, 10716-10723
- 12 Bonar, L., Cohen, A. S. and Skinner, M. (1969) *Proc. Soc. Exp. Biol. Med.* 131, 1373-1375
- 13 Eanes, E. D. and Glenner, G. G. (1968) *J. Histochem. Cytochem.* 16, 673-677
- 14 Kirschner, D. A., Abraham, C. and Selkoe, D. (1986) *Proc. Natl. Acad. Sci. U.S.A.* 83, 503-507
- 15 Sunde, M., Serpell, L. C., Bartam, M., Fraser, P. E., Pepys, M. B. and Blake, C. C. (1997) *J. Mol. Biol.* 273, 729-739
- 16 Geddes, A. J., Parker, K. D., Atkins, E. D. T. and Beighton, E. (1968) *J. Mol. Biol.* 32, 342-358
- 17 Pauling, L. and Corey, R. (1951) *Proc. Natl. Acad. Sci. U.S.A.* 37, 729-739
- 18 Blake, C. C. F. and Serpell, L. (1996) *Structure* 4, 989-998
- 19 Damas, A. M., Sebastião, M. P., Domingues, F. S., Costa, P. P. and Saraiva, M. J. (1995) *Amyloid Int. J. Exp. Clin. Invest.* 2, 173-178
- 20 Inouye, H., Fraser, P. E. and Kirschner, D. E. (1993) *Biophys. J.* 64, 502-519
- 21 Serpell, L. C., Blake, C. C. F. and Fraser, P. E. (2000) *Biochemistry* 39, 13269-13275
- 22 Fraser, P. E., Nguyen, J. T., Chin, D. T. and Kirschner, D. A. (1992) *J. Neurochem.* 59, 1531-1540
- 23 Fraser, P. E., Duffy, L. K., O'Malley, M. B., Nguyen, J., Inouye, H. and Kirschner, D. A. (1991) *J. Neurosci. Res.* 28, 474-485
- 24 Fraser, P. E., Nguyen, J. T., Surewicz, W. K. and Kirschner, D. A. (1991) *Biophys. J.* 60, 1190-1201
- 25 Malinchuk, S. B., Inouye, H., Szumowski, K. E. and Kirschner, D. A. (1998) *Biophys. J.* 74, 537-545
- 26 Balbach, J. J., Shih, Y., Antzutkin, O. N., Leapman, R. D., Rizzo, N. W., Dyda, F., Reed, J. and Tycko, R. (2000) *Biochemistry* 39, 13748-13759
- 27 Lansbury, Jr., P. T., Costa, P. R., Griffiths, J. M., Simon, E. J., Auger, M., Halverson, K. J., Kocisko, D. A., Handsch, Z. S., Ashburn, T. T., Spencer, R. G. et al. (1995) *Nat. Struct. Biol.* 11, 990-998
- 28 Antzutkin, O. N., Balbach, J. J., Leapman, R. D., Rizzo, N. W., Reed, J. and Tycko, R. (2000) *Proc. Natl. Acad. Sci. U.S.A.* 97, 13045-13050
- 29 Benzinger, T. L. S., Gregory, D. M., Burkoth, T. S., Miller, Auer, H., Lynn, D. G., Botto, R. E. and Meredith, S. C. (2000) *Biochemistry* 39, 3491-3499
- 30 Serpell, L. C. and Smith, J. M. (2000) *J. Mol. Biol.* 299, 225-231
- 31 DeRosier, D. J. and Klug, A. (1968) *Nature (London)* 217, 130-131
- 32 Jiménez, J. L., Gujardo, J. I., Orlova, E., Zurdo, J., Dobson, C. M., Sunde, M. and Saibil, H. R. (1999) *EMBO J.* 18, 815-821
- 33 Jiménez, J. L., Tennent, G., Pepys, M. and Saibil, H. R. (2001) *J. Mol. Biol.* 311, 241-247

Received 6 March 2002

## Cholesterol and Alzheimer's disease

B. Wolozin<sup>1</sup>

Department of Pharmacology, Loyola University Medical Center, Bldg. 102, Rm. 3634, 2160 South First Avenue, Maywood, IL 60153, U.S.A.

## Abstract

Accumulation of a 40-42-amino acid peptide, termed amyloid- $\beta$  peptide (A $\beta$ ), is associated with Alzheimer's disease (AD), and identifying medicines that inhibit A $\beta$  could help patients with AD. Recent evidence suggests that a class of

medicines that lower cholesterol by blocking the enzyme 3-hydroxy-3-methylglutaryl-CoA reductase (HMG-CoA reductase), termed statins, can inhibit A $\beta$  production. Increasing evidence suggests that the enzymes that generate A $\beta$  function best in a high-cholesterol environment, which might explain why reducing cholesterol would inhibit A $\beta$  production. Studies using both neurons and peripheral cells show that reducing cellular cholesterol levels, by stripping off the cholesterol with methyl- $\beta$ -cyclodextrin or by treating the cells with HMG-CoA reductase inhibitors, decreases A $\beta$  production. Studies performed on

Key words: amyloid- $\beta$  peptide,  $\beta$ -secretase, statin.

Abbreviations used: AD, Alzheimer's disease; HMG-CoA reductase, 3-hydroxy-3-methylglutaryl-CoA reductase; A $\beta$ , amyloid- $\beta$  peptide.

<sup>1</sup>To whom correspondence should be addressed (e-mail bwolozin@lumc.edu).

# **Methods in Enzymology**

**Volume 309**

**AMYLOID, PRIONS, AND OTHER  
PROTEIN AGGREGATES**



## [34] X-Ray Fiber Diffraction of Amyloid Fibrils

By LOUISE C. SERPELL, PAUL E. FRASER, and MARGARET SUNDE

### Introduction

Amyloid is an ordered structure generated by the polymerization of amyloidogenic proteins. It is a high molecular weight, insoluble material and therefore the atomic structure cannot be investigated by conventional X-ray crystallography or nuclear magnetic resonance (NMR). However, information about its overall fibrillar structure can be obtained by X-ray fiber diffraction, particularly if high-resolution data can be collected.

The earliest reported use of this technique, investigating serum amyloid A and light chain amyloid, reported meridional reflections at 4.68 Å and equatorial reflections at 9.8 Å.<sup>1-3</sup> These diffraction patterns (Fig. 1) are consistent with fibrils composed of polypeptide chains extended in the so-called cross- $\beta$  conformation, a structure that had earlier been identified as a possible conformation for polypeptide chains on the grounds of model building by Pauling and Corey<sup>4</sup> and which was described for insect silk (*Crysope*) by Geddes and co-workers.<sup>5</sup> The meridional reflection indicates a regular structural repeat of 4.68 Å along the fibril axis, and the equatorial reflection indicates a structural spacing of 9.8 Å perpendicular to the fibril axis. A  $\beta$ -sheet structure (or more precisely a  $\beta$  ribbon), organized so that the sheet (or ribbon) axis is parallel to the fibril axis, with its constituent  $\beta$  strands perpendicular to the fibril axis, fulfills these spacing requirements (Fig. 2). The structural repeat of 4.68 Å along the fiber axis corresponds to the spacing of adjacent  $\beta$  strands and the 10- to 12-Å spacing perpendicular to the fiber axis corresponds to the face-to-face separation of the  $\beta$  sheets. This latter can only occur if the amyloid fibrils, or protofilaments, are composed of two or more  $\beta$  sheets. Subsequent analyses by X-ray diffraction on a variety of amyloids,<sup>6-11</sup> and also by solid-state NMR tech-

<sup>1</sup> E. D. Eanes and G. G. Glenner, *J. Histochem. Cytochem.* **16**, 673 (1968).

<sup>2</sup> L. Bonar, A. S. Cohen, and M. Skinner, *Proc. Soc. Exp. Biol. Med.* **131**, 1373 (1967).

<sup>3</sup> G. G. Glenner, E. D. Eanes, and D. L. Page, *J. Histochem. Cytochem.* **20**, 821 (1972).

<sup>4</sup> L. Pauling and R. Corey, *Proc. Natl. Acad. Sci. U.S.A.* **37**, 729 (1951).

<sup>5</sup> A. J. Geddes, K. D. Parker, E. D. T. Atkins, and E. A. J. Beighton, *J. Mol. Biol.* **32**, 343 (1968).

<sup>6</sup> M. J. Burke and M. A. Rougvie, *Biochemistry* **11**, 2435 (1972).

<sup>7</sup> D. A. Kirschner, C. Abraham, and D. A. Selkoe, *Proc. Natl. Acad. Sci. U.S.A.* **83**, 503 (1986).

<sup>8</sup> W. Turnell, R. Sarra, J. O. Baum, D. Caspi, M. L. Baltz, and M. B. Pepys, *Mol. Biol. Med.* **3**, 409 (1986).

<sup>9</sup> P. Gilchrist and J. Bradshaw, *Biochim. Biophys. Acta* **1182**, 111 (1993).

[34]

[34]

FIBER DIFFRACTION OF AMYLOID

521

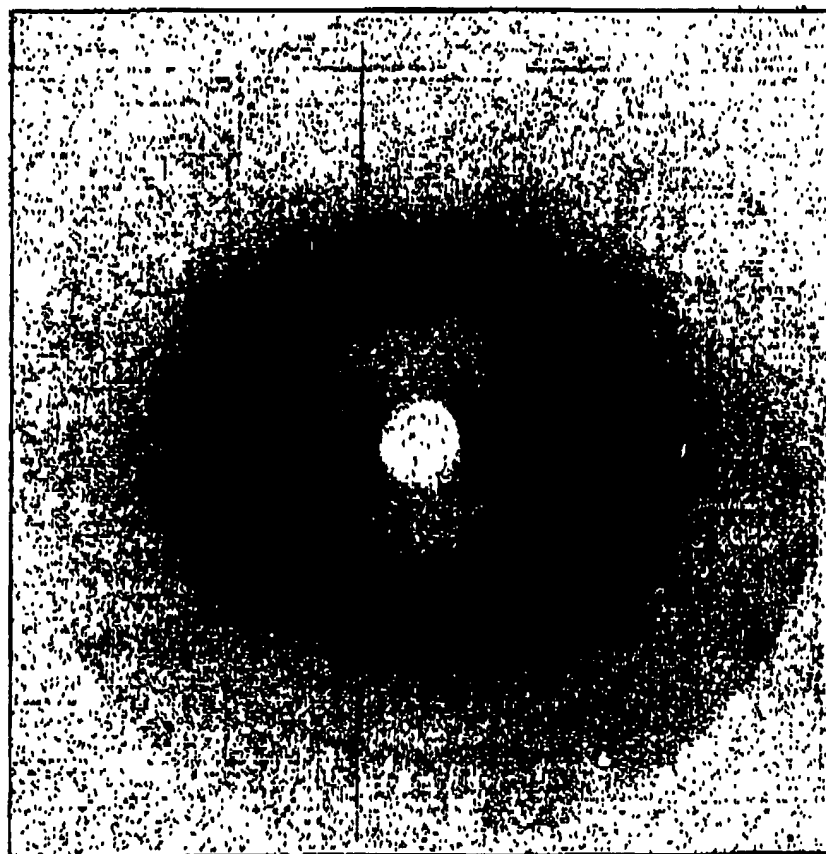


FIG. 1. Characteristic cross- $\beta$  X-ray fiber diffraction pattern. The fibril sample is composed of a 10 residue peptide with the sequence of the A strand of transthyretin, which forms amyloid fibrils spontaneously when dissolved in water. The fibrils were aligned in a magnetic field to improve alignment. The diffraction pattern shows the dominant reflections at 4.7–4.8 Å on the meridian and approximately 10 Å on the equator.

niques,<sup>12</sup> have confirmed that the protein chains in all amyloid fibrils have a predominantly cross- $\beta$  structure. Fiber diffraction data indicate that the  $\beta$  sheets in amyloid probably contain a mixture of parallel and antiparallel hydrogen-bonded  $\beta$  strands. The strong, sharp 4.7-Å reflection on the meridian indicates that the  $\beta$  strands must be perpendicular to the fiber axis. A purely antiparallel arrangement of strands would give rise to a smallest repeat spacing of 9.6 Å. The presence of only the intense 4.7-Å meridional

<sup>10</sup> J. T. Nguyen, H. Inouye, M. A. Baldwin, R. Fletterick, F. E. Cohen, S. B. Prusiner, and D. A. Kirschner, *J. Mol. Biol.* 252, 412 (1995).

<sup>11</sup> C. C. F. Blake and L. C. Serpell, *Structure* 4, 989 (1996).

<sup>12</sup> P. T. Lansbury, P. R. Costa, J. M. Griffiths, E. J. Simon, M. Anger, K. J. Halverson, D. A. Kocisko, Z. S. Hendsch, T. T. Ashburn, R. G. S. Spencer, B. Tidor, and R. G. Griffin, *Nature Struct. Biol.* 2, 990 (1995).

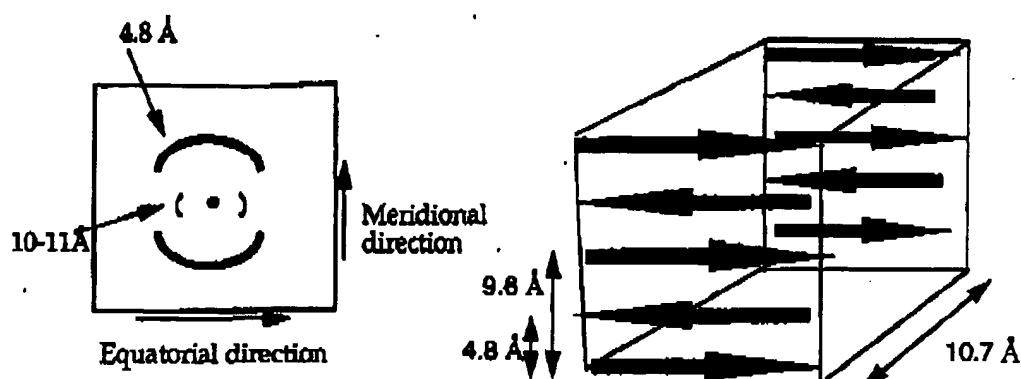


FIG. 2. Underlying structure that gives rise to the cross- $\beta$  reflections. On the left, a schematic representation of the characteristic 4.8-Å meridional and approximately 10-Å equatorial reflection, which are the two main features of the cross- $\beta$  pattern from amyloid. The diagrammatic representation of the  $\beta$ -sheet structure, shown on the right, indicates the molecular spacings that give rise to these reflections. The interstrand spacing in the direction of the fibril axis (4.8 Å) gives rise to the meridional reflection, and the intersheet spacing (10-11 Å) is perpendicular to this and produces the equatorial diffraction.

reflection could be due to a predominance of parallel  $\beta$  strands or to the fact that the  $2_1$  symmetry of an antiparallel  $\beta$  sheet gives rise to the systematic absence of this reflection.

Although evidence shows that a residual  $\alpha$ -helical structure is present in some amyloid fibrils,<sup>13,14</sup> fiber diffraction evidence does not support the idea that  $\alpha$  helices play a significant part in the ordered structure of the fibrils. If the fibrils contained a large amount of an ordered, repeating  $\alpha$ -helical structure, this would give rise to reflections at 5.4 and 1.5 Å, corresponding to the helical pitch and rise per residue, and these reflections are not observed in any of the amyloid fiber diffraction patterns that have been examined.

The reflections at approximately 4.7 Å on the meridian and 10 Å on the equator are seen in all amyloid fiber diffraction patterns and submit to the same interpretation, with some slight variation allowed in the precise spacings of the two reflections, to reflect the structural characteristics of different amyloids. For example, calcitonin fibrils grown *in vitro*<sup>9</sup> and insulin fibrils produced by heating and cooling the protein under acidic conditions both give fiber diffraction images exhibiting strong, sharp meridional reflections at 4.76 Å and more diffuse equatorial reflections at approximately 10 Å.<sup>6</sup> Purified amyloid cores isolated from senile plaques associated with

<sup>13</sup> J. D. Termine, E. D. Baner, D. Ein, and G. G. Glenner, *Biopolymers* 11, 1103 (1972).

<sup>14</sup> K.-M. Pan, M. A. Baldwin, J. T. Nguyen, M. Gasset, A. Serban, D. Groth, I. Melhorn, Z. Huang, R. J. Fletcher, F. E. Cohen, and S. B. Prusiner, *Proc. Natl. Acad. Sci. U.S.A.* 90, 10962 (1993).

Alzheimer's disease show reflections at 4.76 Å and approximately 10.6 Å<sup>7</sup> and prion rods exhibit a prominent interstrand spacing at 4.72 Å and an equatorial spacing of 8.82 Å.<sup>10</sup> High-resolution fiber diffraction studies of transthyretin amyloid have mainly been performed on fibrils composed of the Val30Met variant TTR.<sup>11,15,16</sup> Many studies of synthetic fibrils formed from peptides corresponding to fragments of the A $\beta$  peptide<sup>17-20</sup> and the prion protein<sup>10,21-23</sup> have been reported. These have used fiber diffraction to characterize the nature of fibrils formed from various fragments<sup>17-20,24-28</sup> and to determine the effect of pH, solution ions, and residue charge on fibril structure.<sup>19,26,28</sup> All of these patterns are consistent with a cross- $\beta$  structure, and the commonalities observed in the meridional diffraction patterns over the medium- and high-angle regions can only occur if all of these amyloid fibrils have well-defined and closely similar molecular structures. Fiber diffraction data indicate that different amyloid fibrils actually share a common molecular skeleton, the "protofilament" core structure, which is a continuous  $\beta$ -sheet helix.<sup>11,29</sup> A model of the core structure of the protofilament was constructed using the fiber diffraction pattern given by Val30Met transthyretin amyloid fibrils.<sup>11</sup> This model consists of four  $\beta$  sheets, hydrogen bonded in the direction of the fiber axis, with the  $\beta$  strands running perpendicular and the sheets twisting around a central

<sup>15</sup> C. Terry, A. M. Damas, P. Oliveira, M. J. M. Saraiva, I. L. Alves, P. P. Costa, P. M. Matias, Y. Sakaki, and C. C. F. Blake, *EMBO J.* 12, 735 (1993).

<sup>16</sup> A. Damas, M. P. Sebastião, F. S. Domingues, P. P. Costa, and M. J. Saraiva, *Amyloid Int. J. Exp. Clin. Invest.* 2, 173 (1995).

<sup>17</sup> D. A. Kirschner, H. Inouye, L. Duffy, A. Sinclair, M. Lind, and D. A. Selkoe, *Proc. Natl. Acad. Sci. U.S.A.* 84, 6953 (1987).

<sup>18</sup> P. Gorevic, E. Castano, R. Sarma, and B. Frangione, *Biochem. Biophys. Res. Commun.* 147, 854 (1987).

<sup>19</sup> P. E. Fraser, J. T. Nguyen, W. K. Surewicz, and D. A. Kirschner, *Biophys. J.* 60, 1190 (1991).

<sup>20</sup> H. Inouye, P. E. Fraser, and D. A. Kirschner, *Biophys. J.* 64, 502 (1993).

<sup>21</sup> J. H. Come, P. E. Fraser, and P. T. Lansbury, *Proc. Natl. Acad. Sci. U.S.A.* 90, 5959 (1993).

<sup>22</sup> F. Tagliavini, F. Prelli, L. Verga, G. Giaccone, R. Jarra, P. Gorevic, B. Ghetti, F. Passerini, E. Ghibaudi, G. Forloni, M. Salmona, O. Bugiani, and B. Frangione *Proc. Natl. Acad. Sci. U.S.A.* 90, 9678 (1993).

<sup>23</sup> H. Inouye and D. A. Kirschner *J. Mol. Biol.* 268, 375 (1997).

<sup>24</sup> K. Halverson, P. E. Fraser, D. A. Kirschner, and P. T. Lansbury, *Biochemistry* 29, 2639 (1990).

<sup>25</sup> C. B. Caputo, P. E. Fraser, I. E. Sobel, and D. A. Kirschner, *Arch. Biochem. Biophys.* 292, 199 (1992).

<sup>26</sup> P. E. Fraser, J. T. Nguyen, D. T. Chin, and D. A. Kirschner, *J. Neurochem.* 59, 1531 (1992).

<sup>27</sup> P. E. Fraser, J. T. Nguyen, H. Inouye, W. K. Surewicz, D. J. Selkoe, M. B. Podlisny, and D. A. Kirschner, *Biochemistry* 31, 10716 (1992b).

<sup>28</sup> P. E. Fraser, D. R. McLachlan, W. K. Surewicz, C. A. Mizzen, A. D. Snow, J. T. Nguyen, and D. A. Kirschner, *J. Mol. Biol.* 244, 64 (1994).

<sup>29</sup> M. Suode, L. C. Serpell, M. Bartlam, M. B. Pepys, P. E. Fraser, and C. C. F. Blake, *J. Mol. Biol.* 273, 729 (1997).

axis such there is a  $15^\circ$  twist between one strand and the adjacent one (see Ref. 11). This underlying cross- $\beta$  substructure appears to be the building block of all different amyloid fibrils.<sup>23</sup>

Several reports of fiber diffraction studies of *ex vivo* amyloid samples have noted the presence of lipid or other contaminants in samples that give rise to non-cross- $\beta$  reflections. These reflections are usually characterized as being of different appearance from the "amyloid" reflections (lipid-derived reflections are usually sharper than amyloid-derived reflections) and as being variable in intensity between one fiber sample and another. It is also possible to reduce the intensity of the foreign reflections by repeated washing of the amyloid fibrils.<sup>2,16</sup> Synthetic amyloid fibrils formed *in vitro* from pure protein components do not exhibit any anomalous or foreign reflections.<sup>30,31</sup> The presence of lipid in samples most commonly results in characteristic reflections at  $4.13^{2,16}$  and  $2.59 \text{ \AA}$ .<sup>11</sup> Fiber diffraction has also been used to study ligand and fibril interactions. Sulfate binding to Alzheimer A $\beta$  peptide-derived fibrils gives rise to an intense  $65\text{-\AA}$  meridional reflection that presumably arises from the periodic deposition of sulfate along the long axis of the fibrils.<sup>26</sup> This approach may give insight into the nature of binding of other ions and interacting molecules such as Congo red.

### Sample Preparation

#### *From ex Vivo Tissue Material*

Amyloid fibrils are usually isolated and purified according to the methods of Pras *et al.*<sup>32</sup> and Nelson *et al.*<sup>33</sup> Lipid can be removed using the method of Damas and colleagues,<sup>16</sup> and the salt concentration in fibril samples should be minimized.

#### *From Synthetic Peptides*

Peptides homologous to various regions of the A $\beta$  peptide,<sup>19,34,35</sup> islet-associated polypeptide IAPP,<sup>36-38</sup> transthyretin,<sup>30,39</sup> and other proteins have

<sup>30</sup> J. A. Jarvis, D. J. Craik, and M. C. J. Wilce, *Biochem. Biophys. Res. Commun.* **192**, 991 (1993).

<sup>31</sup> L. C. Serpell, D.Phil. Thesis, University of Oxford (1995).

<sup>32</sup> M. Pras, M. Schubert, D. Zucker-Franklin, A. Rimon, and E. Franklin, *J. Clin. Invest.* **47**, 924 (1968).

<sup>33</sup> S. Nelson, M. Lyon, J. Gallager, E. Johnson, and M. B. Pepys, *Biochem. J.* **275**, 67 (1991).

<sup>34</sup> C. Hilbich, B. Kisters-Woike, J. Reed, C. Masters, and K. Beyreuther, *J. Mol. Biol.* **218**, 149 (1991).

<sup>35</sup> A. Lomakin, D. S. Chung, G. B. Benedek, D. A. Kirschner, and D. B. Teplow, *Proc. Natl. Acad. Sci. U.S.A.* **93**, 1125 (1996).

<sup>36</sup> S. B. P. Charge, E. J. P. De Koning, and A. Clark, *Biochemistry* **34**, 14588 (1995).

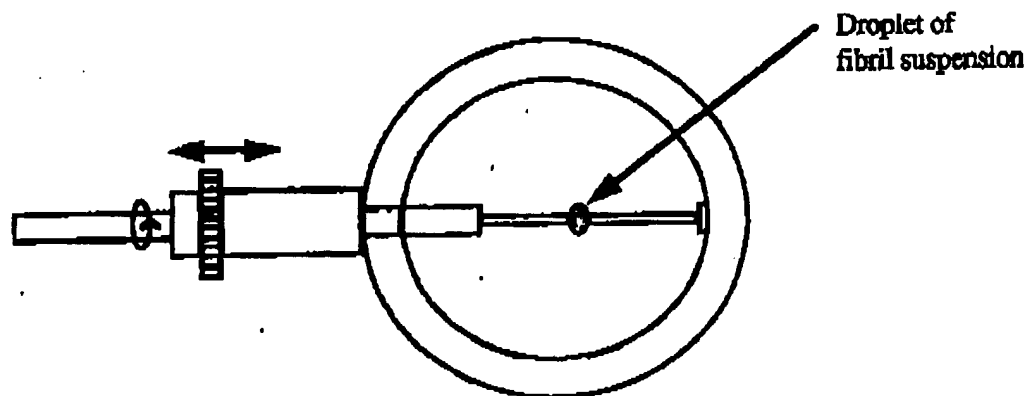


FIG. 3. Stretch frame apparatus used to prepare fibril samples. The droplet of fibril suspension is placed between the ends of two glass capillaries, one of which is attached to a screw. The capillaries can therefore be drawn apart slowly and in small increments to encourage gradual alignment of fibrils as the droplet dries.

been shown to form amyloid-like fibrils *in vitro*. The peptides are generally synthesized using conventional solid-phase synthesis methods and purified by reversed-phase high-performance liquid chromatography (HPLC). Depending on the nature of the amyloidogenic sequence, the peptides may be dissolved in water or in a range of organic solvents. The nature of the solvent can be manipulated to control the rate and extent of fibril formation. Reducing the rate of fibril formation, or imposing a need for slow concentration of the sample, may facilitate the alignment of fibrils, thereby improving the subsequent quality and information content of the diffraction pattern. The use of buffer solutions should be minimized, as salt crystals give strong diffraction spots that can overwhelm the amyloid fiber diffraction image.

#### Alignment of Fibrils

**Stretch Frame Method.** Glass capillary tubes of 1 mm diameter (Clark Electromedical Instruments, Reading, UK) are cut into lengths of 2–3 cm and prepared by dipping the tube ends into melted beeswax to form a plug in the mouth of the tube of about 1 mm in length. The capillaries are placed at opposite ends of the stretch frame (see Fig. 3) and secured with plasticine. A suspension of fibrils extracted from tissue or formed *in vitro* in a buffer of low salt concentration or in water is prepared at a concentration of 5–20 mg/ml. An aliquot (10–20  $\mu$ l) of the amyloid fibril suspension is placed

<sup>37</sup> T. T. Ashburn and P. T. Lansbury, *J. Am. Chem. Soc.* **115**, 11012 (1993).

<sup>38</sup> P. Westermark, U. Engstrom, K. Johnson, G. Westermark, and C. Betsholtz, *Proc. Natl. Acad. Sci. U.S.A.* **87** 5036 (1990).

<sup>39</sup> A. Gustavsson, U. Engstrom, and P. Westermark, *Biochim. Biophys. Acta* **175**, 3 (1991).

between the two capillaries. The wax serves to maintain the surface tension on the droplet. The droplet is allowed to dry at room temperature, and during drying the distance between the ends of the capillaries is increased slowly, by small increments, to stretch out the fibrils and encourage alignment.

*Magnetic Alignment of Synthetic Amyloid Fibrils.* Quartz or glass capillary tubes (0.7 or 1 mm diameter, W. Müller, D-1000 Berlin 27, Germany) are treated with Sigmacote (Sigma, St. Louis, MO) or any general siliconizing reagent. Initially, capillaries are washed with concentrated HCl, water, and methanol and allowed to dry (60°), rinsed thoroughly with undiluted siliconizing reagent, and dried in an oven at 80–100°.

A solution of amyloid forming peptide in distilled water (10–20 mg/ml) is drawn up into a siliconized glass capillary tube to give a length of solution of 2–4 mm. The capillary tube is sealed at one end using wax and placed into a 2-T magnet (Charles Supper Co.) so that the bottom of the fibril solution lies between the two poles of the magnet (see Fig. 4). The solution is allowed to dry gradually under ambient conditions of humidity and temperature. Under some solvent conditions, e.g., with hexafluoro-2-propanol present, the sample may be maintained in a humidity chamber to ensure that some hydration is retained. When it has dried to a disk the capillary tube is sealed with wax. The high degree of orientation introduced in these samples often gives rise to birefringence (Fig. 5).

#### Fiber Diffraction Data Collection

Fiber diffraction images from most amyloid fibril samples can be collected from any in-house source of X rays equipped with a suitable detector such as film or a MAR research image plate. However, the information content of X-ray diffraction images of amyloid fibrils is strongly dependent on relative fibril orientation, and the amount of diffracting material posi-

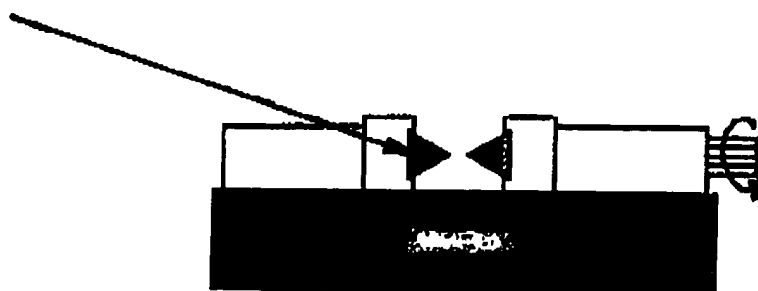


FIG. 4. Magnetic alignment of fibril samples. A 2-T magnet is used to align fibrils and synthetic peptides as they dry in the field. The poles of the magnet can be moved in and out to allow placement of the capillary tube. From Charles Supper Co., Inc.

[34]

[34]

## FIBER DIFFRACTION OF AMYLOID

333

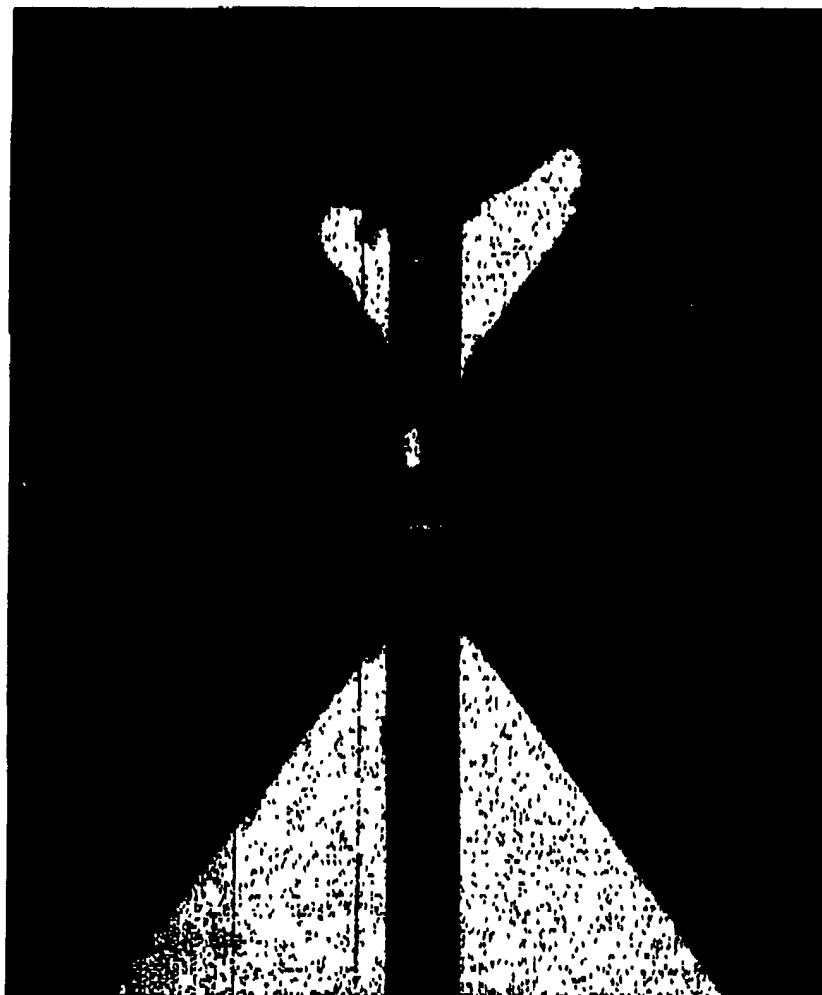
ion  
and  
sed  
agepil-  
ny)  
niz-  
ter,  
ted-20  
gth  
vax  
of  
4).  
id-  
ro-  
ber  
the  
cedol-  
tor  
ion  
ent  
ST-and  
out

FIG. 5. Birefringence observed in a sample of highly orientated fibrils. A high concentration solution of a synthetic peptide is placed in a siliconized glass capillary maintained in the presence of a magnetic field and it is slowly allowed to dry as the amyloid fibrils form. As the fibrils align, a strong birefringence is observed in the specimen under cross-polarized light.

tioned within the X-ray beam and fibril samples from *ex vivo* sources tend to be poorly aligned and may only exhibit the strong 4.7-Å reflection and diffuse 8- to 12-Å reflections with in-house sources. High-resolution data from these relatively poorly aligned samples will only be obtained from the high brilliance, coherent beam lines available at synchrotron sources such as Daresbury, United Kingdom (<http://www.dl.ac.uk>), the ESRF in Grenoble, France (<http://www.esrf.fr>), and APS/Biocat at Illinois Tech. Air scatter may also pose a problem with in-house sources of X rays, which are usually generated from Cu K $\alpha$  rotating anodes and have a wavelength of 1.5 Å. The use of X-ray beams with shorter wavelengths at synchrotrons removes this problem, which is particularly advantageous for the collection



of low-angle data. Alternatively, a helium chamber may be fitted between the specimen and the detector to remove air-scatter problems.

### Data Interpretation

Amyloid samples are usually exposed to the X-ray beam with the long axis of the fibrils more or less perpendicular to the direction of the beam. The X-ray reflections are then distinguished by their direction with reference to the fiber axis and their distance from the center of the pattern: meridional reflections are defined as those lying parallel to the fiber axis, whereas equatorial reflections are those positioned at right angles to the fiber axis. If the long axes of the individual fibrils within a bundle of fibrils, or the bundles themselves, deviate from the mean fiber axis, the corresponding reflections will be drawn out into arcs whose angular dispersion is related to the relative dispersion within the fibrillar bundles. In the most extreme unaligned case, where fibrils lie at all possible angles, the reflections are drawn out into complete rings, giving no indication as to whether they are meridional or equatorial. Although it is advantageous to obtain diffraction data from well-aligned samples, all that is required in the first instance is for the meridional and equatorial reflections to be separated, having arcs as opposed to rings. This should be possible for most amyloid fibril specimens.

Data can be viewed using programs such as IPDISP,<sup>40</sup> Mosfilm,<sup>41</sup> CCP13 program FIX,<sup>42</sup> Profida,<sup>43</sup> and others. For partially aligned diffraction patterns the first step is measurement of the reflections on the meridian and on the equator. The presence of reflections at approximately 4.7 and 10 Å that are characteristic of the cross- $\beta$  pattern is obviously essential. The presence of a 2.4-Å reflection on the meridian is common when the specimen diffracts well, as this is the harmonic of the 4.7- to 4.8-Å reflection. Measurement of other reflections on the meridian will allow indexing of these reflections to a unit cell, which is basically the smallest common factor of all of the reflections. In the case of TTR amyloid,<sup>11</sup> 115.5 Å was found to be the repeating unit. Following this we found that many other amyloid fibrils diffraction patterns show the same repeating unit.<sup>29</sup> Interpretation of equatorial reflections is more problematic and requires more in-depth study. When amyloid samples produce X-ray diffraction patterns with a

<sup>40</sup> CCP4-Collaborative Computational Project. Number 4. *Acta Cryst. D50*, 760 (1994). CCP4 <http://gserv.dl.ac.uk/CCP/CCP4>.

<sup>41</sup> Mosfilm, contact A. G. W. Leslie, MRC Laboratory of Molecular Biology, Cambridge, UK.

<sup>42</sup> CCP13 <http://wserv.dl.ac.uk/SRS/CCP13>.

<sup>43</sup> M. Lorenz and K. C. Holmes, *J. Appl. Crystallogr.* 26, 82 (1993).

[4]

[34]

FIBER DIFFRACTION OF AMYLOID

535

ch

ng

m.

er-

m:

is,

he

of

he

er-

he

he

to

to

in

be

ost

'13

at-

and

A

The

ec-

on.

of

tor

ind

oid

ion

pth

h a

CP4

UK.

range of well-defined equatorial reflections, it is possible to analyze the substructure of the fibrils further to gain insight into the arrangements of protofilaments. Burge<sup>44,45</sup> has shown that a short-range order in bundles of filaments gives rise to a series of "non-Bragg" reflections whose spacings are dependent on the center-to-center separation,  $a$ , of the filaments in the bundle. For filaments in contact, the value of  $a$  corresponds to the diameter of the filament. The center-to-center separation of fibrils may be influenced by sample preparation; dehydration of samples may distort the native protofilament packing observed in cross sections of embedded fibrils and give rise to different lateral organization of protofilaments. Use of the technique on the Val30Met transthyretin amyloid fibrils from familial amyloidotic polyneuropathy<sup>41</sup> gives a diameter of 64 Å for the protofilament as compared to approximately 60 Å from electron microscopy.<sup>46</sup>

When a highly aligned fiber diffraction specimen reveals a well-oriented pattern, the CCP13 program suite<sup>42</sup> can be applied for indexing, profile fitting, and integration of the diffraction spots. For example, magnetically aligned A $\beta$  peptides revealed extremely well-oriented fiber diffraction patterns with Bragg spacing along layer lines.<sup>20</sup> Inouye and Kirschner<sup>23</sup> have analyzed these patterns in detail, along with fiber diffraction patterns obtained from prion-related fibrils. They have identified so-called "beta ( $\beta$ ) crystallites," which constitute the protofilaments, have determined unit cells for these crystallites, and have studied the close packing of the protofilaments in the fibrils.<sup>23,47</sup> Given these very well-oriented patterns, it is possible to estimate particle size by measuring the breadth of reflections. This has been achieved for PrP synthetic fibers<sup>23</sup> from which a measurement of the width of an equatorial reflection at 9.04 Å of 0.02274 Å<sup>-1</sup> corresponds to a coherence length of 44 Å (see Refs. 23 and 29).

### Concluding Remarks

Use of fiber diffraction has shown similarities in the core structure of amyloid. Further improvements in the alignment of fibers, using magnetic fields, could lead to more detailed models of fibril protofilament. Information to be gained by use of this technique is limited by the rotational averaging that occurs and which has the effect that data can only be interpreted to the level of the ordered backbone structure. Details of side chain

<sup>44</sup> R. E. Burge, *Acta Crystallogr.* 12, 285 (1959).

<sup>45</sup> R. E. Burge, *J. Mol. Biol.* 7, 213 (1963).

<sup>46</sup> L. C. Serpell, M. Sunde, P. E. Fraser, P. K. Luther, E. Morris, O. Sandgren, E. Lundgren, and C. C. F. Blake, *J. Mol. Biol.* 254, 113 (1995).

<sup>47</sup> S. B. Malinchik, H. Inouye, K. E. Szumowski, and D. A. Kirschner, *Biophys. J.* 74, 537 (1998).

packing can only be obtained from specimens that exhibit the preferred orientation of fibrils, with ordered three-dimensional packing of the constituent molecules, and therefore give rise to single crystal-like diffraction patterns with Bragg reflections. These relatively ordered specimens are the exception and are unlikely in disease-state amyloid samples. However, the combination of molecular spacing data obtained from X-ray fiber diffraction patterns, with phase information from electron microscopic analysis, now promises to yield important insights into the structure of amyloid.

### Acknowledgments

The authors thank Colin Blake for essential involvement with the fiber diffraction studies of amyloid in Oxford. We are grateful to Colin Nave (SRS, Daresbury Laboratory), Trevor Greenhough (SRS, Daresbury Laboratory and Keele University), and Trevor Forsyth (Keele University) for advice on sample preparation and data collection; Karl Harlos (Oxford) and Bjarne Rasmussen (ESRF, Grenoble) for help with data collection; and Richard Denny (Daresbury Laboratory and Imperial College), John Squire (Imperial College), and Mark Bartlam (LMB, Oxford) for advice on data analysis. LCS acknowledges the Medical Research Council (UK) for support. PEF was supported by the Alzheimer's Society of Ontario and the Ontario Mental Health Foundation. MS was supported by the Medical Research Council (UK), the E.P.A. Cephalosporin Junior Research Fellowship from Lady Margaret Hall (Oxford), and The Oxford Centre for Molecular Sciences, which is funded by the BBSRC, EPSRC, and MRC.

## [35] Solid-State Nuclear Magnetic Resonance of Protein Deposits

By DAVID WEMMER

The central problem in applying physical methods to the study of protein deposits is the intermediate degree of order. The molecules aggregate into assemblies sufficiently large that the overall tumbling correlation time becomes very long, making normal "solution" nuclear magnetic resonance (NMR) line widths very large. However, the long-range order is not sufficient to give high-resolution diffraction data, although fiber diffraction data have been very useful in understanding the basic features of amyloid aggregates. Spectroscopic methods such as Fourier transform infrared spectroscopy (FTIR) can be used, but cannot generally give accurate structural information, especially on a site-resolved basis. One of the few methods that can still be applied, and can yield detailed local structural information,

FROM

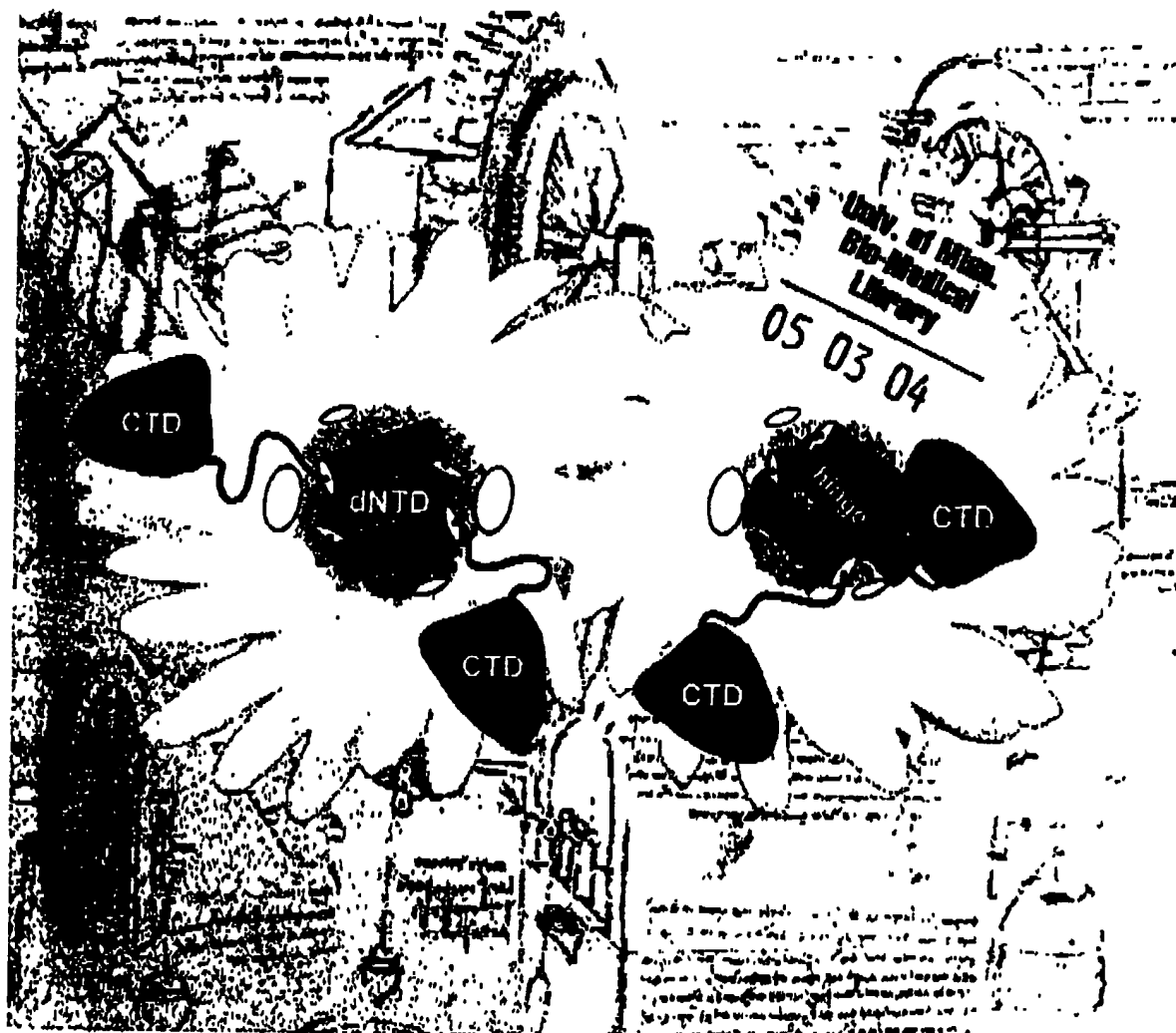
(FRI) 2 4 2005 13:34/ST. 13:03/NO. 5560118826 P 69

ISSN 0021-9258 (print)  
ISSN 1083-351x (electronic)  
JBC-HA3 279(17) 16895-18098 (2004)

The Online Version  
of This Issue Contains  
Supplemental Material

# The Journal of Biological Chemistry

APRIL 23, 2004 VOLUME 279 NUMBER 17



**ASBMB**

PUBLISHED BY THE AMERICAN SOCIETY FOR  
BIOCHEMISTRY AND MOLECULAR BIOLOGY

Founded by Christian A Herter and Sustained In Part by the Christian A Herter Memorial Fund

## Seeding Specificity in Amyloid Growth Induced by Heterologous Fibrils\*

NOTICE: THIS MATERIAL MAY BE PROTECTED  
BY COPYRIGHT LAW (TITLE 17 U.S. CODE)

Received for publication, October 14, 2003, and in revised form, January 28, 2004  
Published, JBC Papers in Press, January 29, 2004, DOI 10.1074/jbc.M311300200

Brian O'Nuallain†, Angela D. Williams†, Per Westermark§1, and Ronald Wetzel‡

From the †Graduate School of Medicine, University of Tennessee, Knoxville, Tennessee 37920,  
and ‡Department of Genetics and Pathology, Uppsala University, 751 85 Uppsala, Sweden

Over residues 15–35, which comprise the H-bonded core of the amyloid fibrils it forms, the Alzheimer's disease plaque peptide amyloid  $\beta$  (A $\beta$ ) possesses a very similar sequence to that of another short, amyloidogenic peptide, islet amyloid polypeptide (IAPP). Using elongation rates to quantify seeding efficiency, we inquired into the relationship between primary sequence similarity and seeding efficiency between A $\beta$ -(1–40) and amyloid fibrils produced from IAPP as well as other proteins. In both a solution phase and a microtiter plate elongation assay, IAPP fibrils are poor seeds for A $\beta$ -(1–40) elongation, exhibiting weight-normalized efficiencies of only 1–2% compared with A $\beta$ -(1–40) fibrils. Amyloid fibrils of peptides with sequences completely unrelated to A $\beta$  also exhibit poor to negligible seeding ability for A $\beta$  elongation. Fibrils from a number of point mutants of A $\beta$ -(1–40) exhibit intermediate seeding abilities for wild-type A $\beta$  elongation, with differing efficiencies depending on whether or not the mutation is in the amyloid core region. The results suggest that amyloid fibrils from different proteins exhibit structural differences that control seeding efficiencies. Preliminary results also suggest that identical sequences can grow into different conformations of amyloid fibrils as detected by seeding efficiencies. The results have a number of implications for amyloid structure and biology.

One of the major unanswered questions of amyloid fibril formation is the specificity with which primary sequences determine both amyloidogenicity and the details of amyloid structure. The observation that many globular proteins can be induced to generate amyloid<sup>1</sup> fibrils, albeit in some cases only under non-native conditions, has led to the notion that the amyloid folding motif is a kind of default structure in the protein folding pathway that many or all polypeptides can

engage when their normal folding pathways are compromised (1, 2). This seems a reasonable hypothesis, especially if the dominant driving force for amyloid formation is the formation of the backbone H-bonding network of these  $\beta$ -sheet-rich structures (3), since all polypeptides regardless of sequence share the polypeptide backbone. Amyloid stability, however, appears to be derived from a combination of forces, including but not limited to H-bonding, much in the manner of how globular proteins are stabilized (4). In addition, mutations associated with modest changes in side chain hydrophobicity, charge, etc., have been observed to have significant impact on fibril growth kinetics and stability (5–10). These considerations raise an interesting conundrum; if side chain packing contributes significantly to amyloid stability, how is it possible that so many proteins whose sequences evolved to fold into stable, globular structures (including many that contain little or no  $\beta$ -sheet structure in the native state) can be equally well accommodated into the  $\beta$ -sheet-rich amyloid folding motif? Does amyloid fibril formation follow the same or different folding rules compared with other collapsed states of polypeptide sequences?

One measure of packing specificity in the amyloid fibril is the efficiency with which fibrils composed of one protein sequence can act as seeds for the elongation of another amyloidogenic polypeptide. The ability of the folded structure at the growth point of the amyloid fibril to serve as a template for the recruitment of an incoming monomer can be likened to the abilities of domains and subdomains of globular proteins to pack together with high complementarity and specificity. Although such "cross-seeding" between two different amyloid proteins has been described (11–14), the data are often qualitative and/or difficult to assess quantitatively due to limitations in our understanding of the amyloid assembly mechanism. For example, it is well known that the addition of a fibril seed can eliminate or reduce the lag time in the spontaneous, nucleation-dependent generation of A $\beta$ <sup>2</sup> fibrils from rigorously disaggregated monomers (15, 16). However, it is not clear how to quantitatively interpret reductions in lag time or to compare one fibril to another with respect to their relative abilities as seeds to reduce lag times. Furthermore, some previous experimental explorations of seeding and cross-seeding may also have been compromised by the use of monomeric protein preparations that contained small but significant amounts of aggregate seeds.

Cross-seeding ability is not only of interest in terms of the structural aspects of amyloid fibril formation. Although the mechanisms by which amyloid fibril formation is initiated *in vivo* are still being worked out, it is very likely that, once these

\* The costs of publication of this article were defrayed in part by the payment of page charges. This article must therefore be hereby marked "advertisement" in accordance with 18 U.S.C. Section 1734 solely to indicate this fact.

† Supported by the Swedish Research Council and the Swedish Diabetes Association.

‡ Supported by NIA, National Institutes of Health Grant AG18416, the American Health Assistance Foundation, the Alzheimer's Association, the Lindsay Young Alzheimer's Disease Research Fund, and the Reuben Louise Cates Mount Research Endowment. To whom correspondence should be addressed: Graduate School of Medicine, University of Tennessee, 1924 Alcoa Highway, Knoxville TN 37920. Tel: 865-544-9158; Fax: 865-544-9235; E-mail: rwetzel@mc.utk.edu.

<sup>1</sup> Amyloid fibrils are classically defined as originating in tissue-associated deposits that yield bright green birefringence under the polarizing light microscope after Congo red staining. We refer here to *in vitro* generated fibrils as amyloid, cognizant that they may not resemble tissue-derived amyloid fibrils in all structural and functional respects (see "Discussion").

<sup>2</sup> The abbreviations used are: A $\beta$ , amyloid  $\beta$  protein; IAPP, islet amyloid polypeptide; ThT, thioflavin T; PBS, phosphate-buffered saline; PBSA, PBS plus sodium azide; WT, wild type; AD, Alzheimer's disease; HPLC, high performance liquid chromatography.

## Seeding Specificity in Amyloid Fibril Growth

17491

initial seeds are formed, fibrils grow *in vivo* through elongation by monomer additions (17). The ability of amyloid fibrils to be efficiently elongated *in vivo* has impact on a number of biological aspects of amyloid function. These include the questions of species and strain specificity in yeast (18, 19) and mammalian (20) prions, the feasibility of the recruitment-sequestration mechanism (21, 22), and the ability of short poly-Gln sequences to influence the nucleation of long poly-Gln repeats<sup>2</sup> in diseases such as Huntington's disease, the specificity of intracellular protein aggregation (24), and the better understanding of the mechanism of amyloid enhancement factor in the classic mouse amyloidosis model (25). Promiscuous cross-seeding among amyloid fibrils would suggest the possibility that one amyloid disease might influence another. For example, because the vast majority of type II diabetes patients have pancreatic amyloid deposits composed of islet amyloid polypeptide (26) and because IAPP and A $\beta$  share striking sequence similarity (see "Results"), it might be possible that cross-seeding of A $\beta$  amyloid formation by IAPP fibrils is the mechanism by which diabetics appear to exhibit an elevated risk for developing AD (27).

To test this latter hypothesis, we studied the abilities of A $\beta$  and IAPP fibrils to act as seeds for the elongation reactions of A $\beta$  and IAPP monomeric peptides. We used the pseudo-first order elongation kinetics in two separate assay modes as measures of relative seeding ability. To put these results into context we also surveyed a broad spectrum of amyloid fibrils as seeds for A $\beta$  elongation. The results show that in general seeding of fibril elongation is highly specific, being exquisitely sensitive to point mutations at certain positions in the amyloidogenic peptide. IAPP fibrils prove to be very poor seeds for A $\beta$ -(1-40) elongation, suggesting that heterologous seeding of amyloid formation probably does not influence AD risk in diabetics.

## EXPERIMENTAL PROCEDURES

**Materials**—Synthetic wild-type A $\beta$ -(1-40) and A $\beta$ -(1-42), the "Arctic" mutant (E22G), some proline mutants, and a Cys-1 analog of A $\beta$ -(1-40) were all obtained via custom syntheses from the Keck Biotechnology Center at Yale University. The 1-30 fragment of the immunoglobulin light chain Len and oxidized, full-length, C-terminal-amidated IAPP were also obtained from the Keck Center. A $\beta$ -(1-40) proline mutants F4P, R6P, and L17P were obtained from the Stanford University Protein and Nucleic Acids Biotechnology Facility. Recombinant human immunoglobulin  $\kappa$  light chain variable domain (JTO5) was a gift of Dr. Jonathan Wall (University of Tennessee Graduate School of Medicine), and A $\beta$ -(25-36) was a gift of Charles Murphy (University of Tennessee Graduate School of Medicine). Amyloid-like aggregates of synthetic Gln<sub>40</sub> and Gln<sub>47</sub> polyglutamine peptides (28) were obtained from Tina Richey (University of Tennessee Graduate School of Medicine). Amyloid fibrils of  $\beta$ 2-microglobulin were gifts of Susan Jones and Sheema Radford (University of Leeds). Fibrils of the yeast prion protein Ure2p (29) were gifts of Kimberley Taylor and Reed Wickner (National Institutes of Health). Bovine collagen and bovine serum albumin (essentially fatty acid free) were purchased from Sigma. N-terminal-biotinylated A $\beta$ -(1-40) was prepared by alkylating a Cys-1 analog of A $\beta$ -(1-40) (Keck Biotechnology Center custom synthesis) with PEO (polyethylene oxide)-iodoacetyl biotin (Pierce). All other chemicals were of analytical grade.

**General Methods**—The concentrations of disaggregated peptides were estimated from peak areas of the A<sub>215</sub> absorbance trace in analytical HPLC of aliquots of peptide solutions using standard curves generated from peptide standards calibrated by amino acid composition analysis, as described previously (30). Reverse phase HPLC was carried out on a ZORBAX SB-C3 column (Agilent Technologies) with a 3-61% (v/v) acetonitrile gradient in 0.05% aqueous trifluoroacetic acid (Pierce). ThT fluorescence measurements (31) of reaction samples were carried out by diluting aliquots of the reaction into PBS containing 10  $\mu$ M ThT. Thioflavin T fluorescence was then monitored by excitation at 460 nm and fluorescence emission at 482 nm. Unless otherwise indicated, all

quantitative experimental results shown are from measurements done in triplicate. Error bars in the figures represent S.D.

**Preparation of Soluble, Disaggregated Peptides, and Sonicated Fibril Seeds**—Wild-type and mutant A $\beta$  peptides were treated to remove aggregates as described (30, 32). Thus, synthetic lyophilized powder was exposed to sequential applications of trifluoroacetic acid and hexafluoroisopropanol and evaporated under an argon stream, trace volatile solvents were removed under high vacuum, and the peptide residue was dissolved in 3 mM NaOH followed immediately with the addition of a 10 $\times$  PBS buffer to generate 1 $\times$  PBS plus 0.05% sodium azide (PBFA). To remove any residual aggregates these solutions were centrifuged (51,500  $\times$  g, 17 h, 4  $^{\circ}$ C), and the upper [4] of the supernatant was carefully removed and analyzed for A $\beta$  concentration by HPLC as described above (generally about 60  $\mu$ M). Solutions were used immediately to conduct kinetic experiments (described below) or to make fibrils. Fibrils were made by spontaneous fibril assembly from disaggregated monomeric peptide as described previously (33). For some less stable proline mutants of A $\beta$ -(1-40), fibril formation reactions were conducted at higher concentrations of monomeric peptide (4). Fibril formation reactions were monitored by ThT fluorescence and by analysis of centrifugation supernatants by HPLC.

Human IAPP was solubilized and disaggregated using a 1:1 mixture of trifluoroacetic acid/hexafluoroisopropanol (34) as previously described (35). Disaggregated IAPP (about 30  $\mu$ M) was used immediately in elongation kinetics assays (described below) or to make fibrils as described previously (33). JTO5 fibrils were prepared as previously described (35). Preparation of reduced and alkylated ovalbumin (ovalbumin-RA) was described previously (33).

To improve seeding potency (11) and potentially normalize fibril size all aggregates were sonicated with a probe sonicator on ice for 2.5 min in 30-s bursts in PBFA containing 1 mM dithiothreitol (a precaution against oxidation; however, we have no evidence that oxidation occurs during sonication in the absence of dithiothreitol). The fact that the series of mutated A $\beta$  fibrils yields results consistent with what is known about A $\beta$  fibril structure (see "Results" and "Discussion") suggests that the sonication step does produce fibrils with very similar average molecular weights, which can therefore be assumed to have approximately the same number of growth sites per weight of fibril. Recent experimental titration of fibril growth sites further supports this assumption.<sup>4</sup> Initial IAPP aggregates from spontaneous aggregation experiments consist mainly of spheroidal aggregates and smaller amounts of amyloid fibrils and amorphous material (see "Results"). Except for collagen and reduced and alkylated ovalbumin, other aggregates prepared for use as seeds exhibited typical amyloid fibril structure in electron micrographs as well as typical ThT responses (data not shown).

**Solution Phase Aggregation Assays**—Aggregation kinetics studies were conducted using relatively high concentrations of peptide using modifications of the procedures described by Naki and Nakakuki (36) and Naki and Gejyo (37). A typical solution phase assay was carried out by incubating (unshaken) a solution of ~30  $\mu$ M concentrations of freshly disaggregated A $\beta$  or IAPP in PBFA in a water bath at 37  $^{\circ}$ C. For seeded reactions, solutions were preincubated to reach temperature, then seeded with 10–70  $\mu$ g/ml aggregate at time 0. Reactions were followed by removing aliquots of gently mixed suspensions and measuring ThT fluorescence. For each time point, an aliquot was removed from each of three independent samples and diluted into PBFA containing ThT. Because the ThT signal varies linearly with fibril mass for any given amyloid fibril, the signal can be used as a measure of the completeness of the fibril formation reaction and, when appropriately plotted, will yield values for the pseudo-first order rate constant (37).

**Solid Phase, Microtiter Plate-based Aggregation Assays**—Progress curves for polypeptide aggregation were also determined using a solid phase microtiter plate assay modified from previously described methods (38, 39). N-terminal-biotinylated A $\beta$ -(1-40) (see "General Methods" under "Experimental Procedures") was disaggregated, dissolved at a low micromolar concentration in PBS buffer, separated into aliquots, snap-frozen in liquid nitrogen, and stored at -80  $^{\circ}$ C. Sonicated fibrils or other aggregates were applied to the microplate wells by incubating 100  $\mu$ l/well of a 1  $\mu$ g/ml suspension of aggregate (i.e. 100 ng of aggregate/well) in PBFA for 18 h at 37  $^{\circ}$ C in activated high binding microtiter plates (BIA/BIA Plates, Costar, Atlanta, GA). The wells were then washed twice with PBFA containing 0.05% Tween 20 (Fisher) (assay buffer). This is the standard washing procedure carried out throughout this experiment. To ensure that aggregation rates are not significantly affected by variable efficiencies of aggregate adhesion to the plastic, we

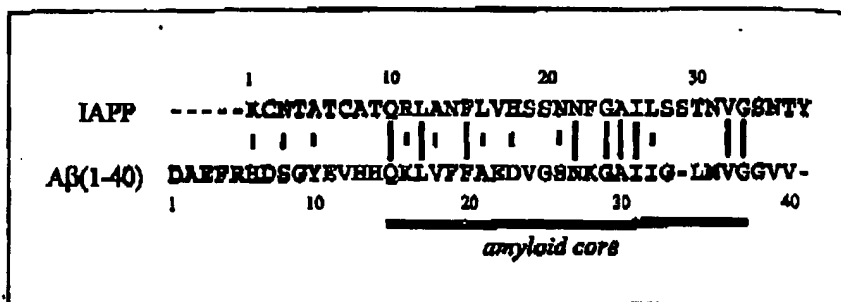
<sup>2</sup> A. M. Bhattacharyya and R. Wetzel, submitted for publication.

<sup>4</sup> S. Shivanian, B. O'Neill, and R. Wetzel, unpublished data.

17492

## Seeding Specificity in Amyloid Fibril Growth

**FIG. 1.** Sequence alignment of IAPP and A $\beta$ (1–40). The sequence alignment of IAPP and A $\beta$ (1–40) was carried out with the program ALIGN (58) available at [www.ch.embnet.org/software/LALIGN\\_form.html](http://www.ch.embnet.org/software/LALIGN_form.html). Lines indicate exact matches, and dashes indicate chemical similarity. The region of A $\beta$ (1–40) known to be involved in the H-bonded core (4, 28, 30, 44) is indicated below the alignment.



confirmed good immobilization by recovering unbound protein from the wells as part of the wash protocol and estimating the amount of non-absorbed protein using a protein assay (53). In all cases more than 95% of the aggregate remained on the plastic. Wells were blocked with 1% BSA in PBBSA (blocking buffer) for 1 h at 37 °C, then 100  $\mu$ l of assay buffer was added into each well, and the plate was sealed with an adhesive overlay.

For the assay, the microtiter plate was pre-equilibrated at 37 °C. The kinetics data were collected by determining individual time points in reverse temporal order. For each replicate series of each analysis on the plate, a 100- $\mu$ l aliquot of a 25 nM solution of biotinyl-A $\beta$  in assay buffer was added to a well by first removing the assay buffer in which the well was stored. This constitutes the longest time point of the kinetics run. The plate was resealed and returned to 37 °C incubation. At the appropriate time, the plate was again removed, and the storage buffer was removed from the wells designated for this time point and replaced with fresh aliquots of biotinyl-A $\beta$  solution. This process was repeated until the last incubation, constituting the earliest time point, was completed. After the last incremental incubation for the kinetics the plate was removed from 37 °C incubation and washed with assay buffer, 100  $\mu$ l was added per well of a 1:1000 dilution of a europium-streptavidin conjugate (PerkinElmer Life Sciences) in blocking buffer containing 0.05% Tween 20, and the plate was incubated at room temperature for 1 h. The plate was then washed 3 times, and europium was released from the microplate well surface using 100  $\mu$ l/well of chelation buffer (Enhancement Solution, PerkinElmer Life Sciences). After 10 min europium was measured by time-resolved fluorimetry (40) in a Victor<sup>2</sup> 1420 Multilabel Counter (PerkinElmer Life Sciences) using the programmed parameters for europium. Final of europium were determined from a standard curve and converted to final of biotin using the stated europium content of the commercial streptavidin reagent.

**Congo Red Staining and Birefringence of IAPP Aggregates**—Congo red staining of aggregates was carried out using a modified version (Sigma procedure H760) of the protocol of Puchler *et al.* (41). For each experiment 50  $\mu$ l of freshly prepared IAPP aggregates (about 0.2 mg/ml) was dried to a glass microscope slide overnight at 37 °C and then Congo red-stained. Birefringence was determined with an Olympus microscope (20 $\times$ ) equipped with a polarizing stage.

**Electron Micrographs**—Aggregates (0.1–0.4 mg/ml) were adsorbed onto carbon and Formvar-coated copper grids and then negatively stained with 0.5% uranyl acetate. Stained samples were examined and photographed in a Hitachi H-800.

## RESULTS

**Sequence Similarity between A $\beta$  and IAPP**—The A $\beta$  peptide is derived from the proteolytic processing of the cross-membrane region of the receptor-like, type I cross-membrane protein amyloid- $\beta$  protein precursor (42). IAPP, or amylin, is derived from the proteolytic processing of a propeptide and appears to play a role along with insulin in the regulation of glucose metabolism (43). Despite the absence of a larger sequence homology between their precursor proteins and no obvious relationship in known functions, the mature peptides A $\beta$  and IAPP have very similar sequences, as shown in Fig. 1. After introduction of a 1-residue gap in A $\beta$  to maximize the alignment, the 2 peptides overall share 25% sequence identity and 50% sequence similarity (Fig. 1). When the overlap region is confined to that portion of the A $\beta$  sequence, residues 15–37, known to be involved in the H-bonded core region of the amyloid fibril (4, 44), sequence identity jumps to 39%, and sequence

of the WT A $\beta$  sequence is compared with the sequence of the S20G (A $\beta$  position 25) single point mutant of IAPP, associated with both early onset diabetes (45) and enhanced amyloidogenicity (46, 47), the extents of identity and similarity climb further to 43 and 70%, respectively.

This striking similarity introduces the questions of whether these two highly amyloidogenic peptides use their shared sequences in similar ways to engage the amyloid folding motif and the extent to which they might thereby exhibit specificity in amyloid formation as measured by their sensitivities to heterologous seeding. The hypothesis that the shared sequence element is involved in the core structure of amyloid fibrils from both peptides is supported by the sharp reduction in amyloid growth observed when proline residues are substituted within this region in both A $\beta$  (4) and IAPP (48, 49). Given these facts it is not unreasonable to suppose that a growing A $\beta$  amyloid fibril might be able to relatively easily accommodate IAPP molecules into the fibril structure.

It should be stressed that, although the sequence similarities discussed above are in a structural sense undeniable, we infer no significance to this similarity outside of the context of amyloid formation. That is, it is highly unlikely that these sequences share a common precursor in evolution, and there is no reason to believe that their common sequence elements are associated with any similarity in the normal function of these polypeptides.

**Growth of IAPP and A $\beta$  Amyloid by Spontaneous, Nucleation-dependent Polymerisation and by Homologous Seeding**—The spontaneous, nucleation-dependent amyloid formation reaction by IAPP is complicated by the existence of two amyloid-related products. The first-formed product in the unseeded reaction consists of clusters of spheroidal bodies (Fig. 2A) that, despite their non-fibrillar morphologies, exhibit in our hands a number of other amyloid-like features. These include the ability to be labeled with the amyloid-selective (41, 60) dyes Congo red (Fig. 2, G and H) and thioflavin-T (see below). Their structural relationship to the classic amyloid fibril is also suggested by their response to sonication, which generates from these globular aggregates clusters of small fibrils (Fig. 2, B–D). When these initial globular aggregates are incubated in PBS at 37 °C for 2 weeks, they transform into short amyloid-like fibrils (Fig. 2, E–F). Although related phenomena have been reported previously (51), the exact relationship between the aggregates shown in Fig. 2A and previously described aggregates is not clear, as discussed below.

The kinetics of formation of these initial, globular aggregates from rigorously disaggregated IAPP exhibit a profile similar to that found for many amyloid fibrils, consisting of an initial lag phase followed by a rapid growth phase terminating at a plateau where fibrils and monomers exist at equilibrium (Fig. 3). Like amyloid fibrils, the growth of these globular aggregates can be conveniently monitored by their ability to bind to the dye thioflavin T and alter its fluorescence properties (Fig. 3). Unlike

## Seeding Specificity in Amyloid Fibril Growth

17493

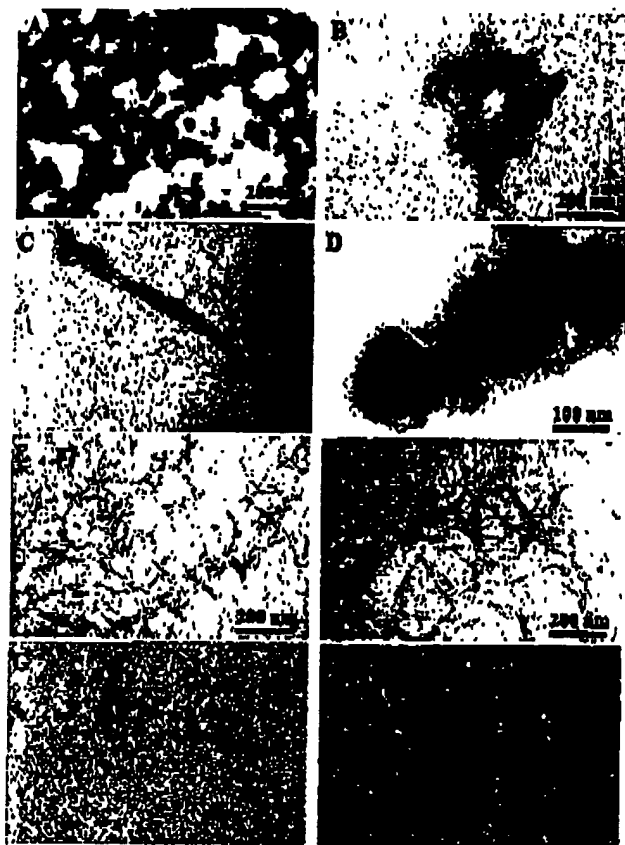


FIG. 2. Micrographs of IAPP aggregates. A-F, electron micrographs of IAPP aggregates from spontaneous growth of unseeded IAPP solutions. A, initial aggregate formed within 6 h. B-D, product of sonication of the initial aggregate. E and F, product of incubation of initial aggregate in PBS at 37 °C for 2 weeks. Where multiple images are shown for the same preparation (B-D), it reflects the range of image types represented among the grids; correspondingly, when only one image is shown for a preparation, only one image type was observed. C and E, polarized light microcopy of Congo red-stained IAPP aggregates. Fresh IAPP aggregates, stained and visualized as described under "Experimental Procedures," before (G) and after (H) sonication.

opment of these ThT-positive structures is very aggressive, so that even after a rigorous disaggregation protocol designed to eliminate all traces of seeds from the peptide (see "Experimental Procedures"), the lag phase is only 2 h. Other workers find essentially no lag phase on incubation of IAPP at neutral pH and describe an initial, amorphous product that appears to be somewhat different than the one described here in that it gives a relatively low ThT signal that has been attributed to small amounts of fibrils in the preparation (51); these differences may have to do with differences in disaggregation protocols and/or incubation buffers.

Interestingly, both globular and fibrillar IAPP aggregates are equally effective seeds for IAPP elongation, as judged by ThT kinetics, in that they eliminate the 2-h lag phase of the unseeded reaction when added at 8% by weight of total monomeric IAPP in the reaction (Fig. 3). As judged by the morphologies of the products of elongation, however, different IAPP seeds produce different results. The elongation of IAPP seeded with fibrillar IAPP aggregates (Fig. 2, E-F) produces what appears to be a homogenous fibrillar product (Fig. 4A). In contrast, the elongation of IAPP seeded by spheroidal IAPP aggregates (Fig. 2A) generates a mixture of aggregate types, including some fibrils. Interestingly, some grids in the EM of this aggregated product exhibit structures that give the appearance of amyloid fibrils growing out of the spheroidal an-

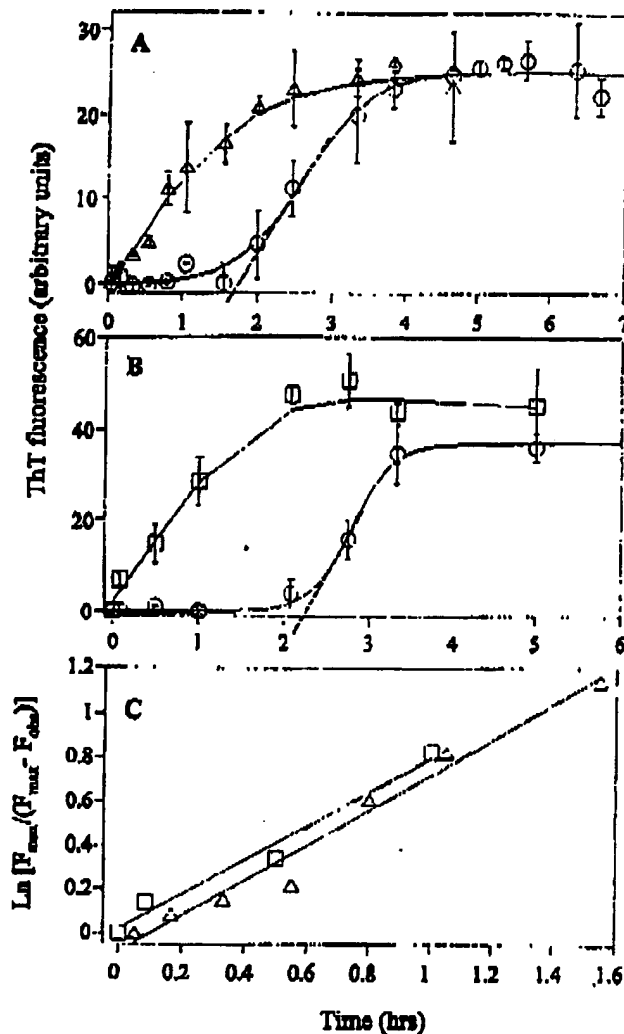


FIG. 3. IAPP aggregate growth with and without seeding. Disaggregated IAPP ( $\sim 30 \mu\text{M}$ ) was incubated without (○) or with (□ and Δ) sonicated aggregates (10  $\mu\text{g}/\text{ml}$ , or 8% by weight of monomer in solution). A, spheroidal IAPP aggregates as seeds (Δ); B, fibrillar IAPP aggregates as seeds (□); C, pseudo-first order kinetics plots of seeded elongation data from A and B.

gregate seeds (Fig. 4F), but further studies would be required to confirm this interpretation.

In contrast to IAPP, rigorously disaggregated A $\beta$ -(1-40) incubated at 50  $\mu\text{M}$  in PBS at 37 °C typically exhibit a lag phase of 3-7 days before aggregation begins (16). Seeding such reactions with preformed A $\beta$  amyloid fibrils reduces or eliminates this lag time in a dose-dependent manner (16). Fig. 5 shows that a solution of 30  $\mu\text{M}$  A $\beta$ -(1-40) under these conditions exhibits no indication by ThT fluorescence of fibril formation after 2 days of incubation. However, when an equivalent solution is seeded with 10  $\mu\text{g}/\text{ml}$  A $\beta$ -(1-40) fibrils ( $\sim 8\%$  by weight of the monomeric A $\beta$ -(1-40)), the reaction exhibits rapid fibril growth with no lag phase.

**Heterologous Seeding of A $\beta$  and IAPP Fibril Formation**—Because seeding effects on the length of the lag phase are qualitative, non-linear with dosage and cannot be easily modeled mathematically, we chose to compare homologous and heterologous seeding efficiencies where feasible by comparing the pseudo-first order rates of fibril elongation reactions seeded at levels sufficient to eliminate the lag phase. Such elongation reactions are conceptually simple, with rates dependent on the concentration of monomers, the concentration of growing ends of fibrils, and a second order rate constant characteristic of the



17494

## Seeding Specificity in Amyloid Fibril Growth

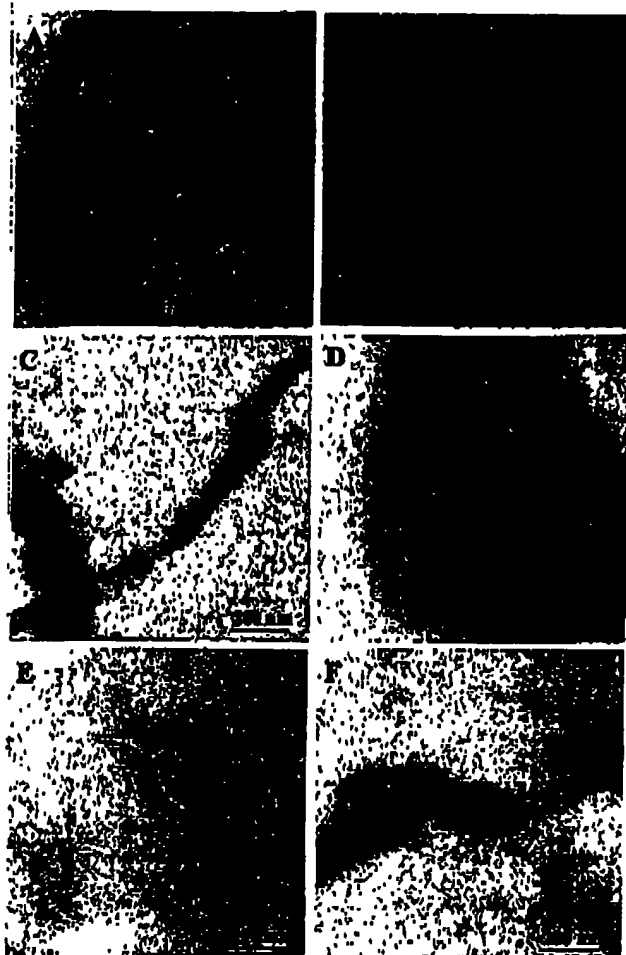


FIG. 4. Electron micrographs of the products of various seeding reactions as described under "Results." A, IAPP monomer seeded with IAPP amyloid fibrils. B and C, IAPP monomer seeded with A $\beta$ (1-40) fibrils. D, A $\beta$ (1-40) monomer seeded with A $\beta$ (1-40) fibrils. E, A $\beta$ (1-40) monomer seeded with IAPP amyloid fibrils. F, IAPP monomer seeded with spherical IAPP aggregates. Image selection is as described in legend to Fig. 2.

amyloidogenic peptide sequence and reaction conditions (37). If secondary nucleation events (53) are negligible under the typically heavily seeded, rapidly completed reactions, the concentration of fibril-growing ends does not change significantly during the course of the reaction, and the reaction appears to be pseudo-first order, with the unchanging concentration of fibril ends incorporated into the pseudo-first order rate constant.

To assess the relative seeding efficacies of various fibrils on IAPP elongation, we added equal weight concentrations (10  $\mu$ g/ml) of amyloid fibrils of IAPP (*i.e.* *bona fide* fibrils from an aged sample; see above), A $\beta$ (1-40), and A $\beta$ (1-42) to disaggregated monomeric IAPP. As can be seen in Fig. 6A, all three amyloid fibrils are equally effective at eliminating the normal 2-h lag phase of this reaction. Fig. 6B shows the pseudo-first order rate plot for the growth of amyloid fibrils as assessed by the increase in the thioflavin T signal, and Table I summarizes the rate constants derived from the kinetics analysis. Table I shows that A $\beta$ (1-40) and A $\beta$ (1-42) fibrils give essentially identical rate constants in seeding IAPP elongation. Fig. 6 and Table I also show that both A $\beta$  fibrils as well as the initial, globular IAPP aggregates are all quite similar to authentic IAPP fibrils in their abilities to seed IAPP elongation. These data might suggest that the strong sequence similarity be-

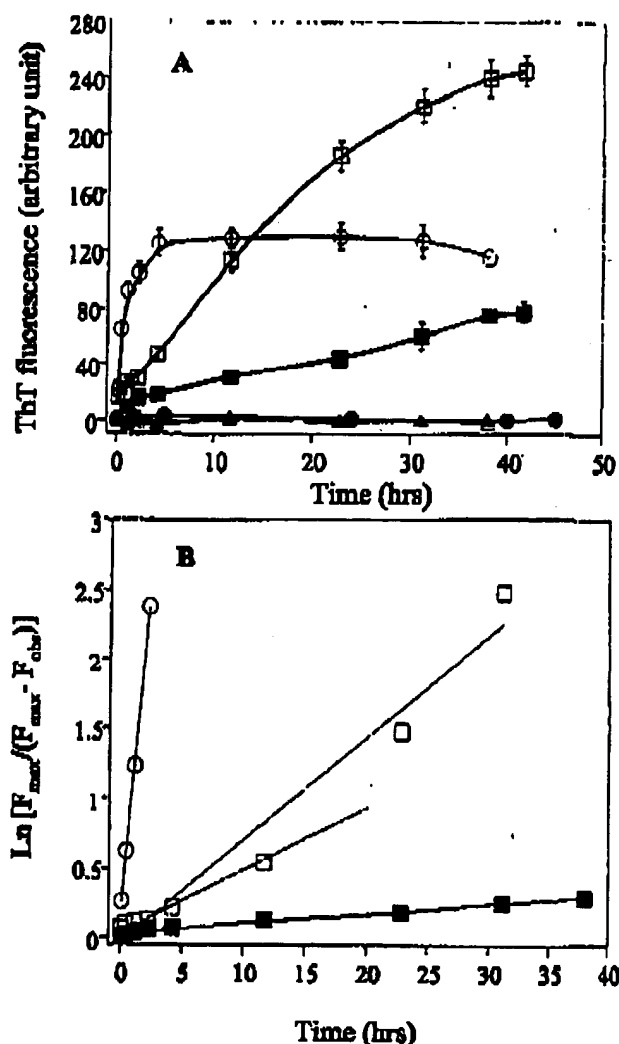


FIG. 5. A $\beta$ (1-40) fibril growth, plotted by thioflavin T signal (A) and by a first order kinetics treatment of the ThT data (B). Disaggregated A $\beta$ (1-40) (30  $\mu$ M) was incubated alone (○) or seeded with various sonicated aggregates: A $\beta$ (1-40) fibrils (10  $\mu$ g/ml, ○); initial, globular IAPP aggregates (△, 10  $\mu$ g/ml; ◇, 70  $\mu$ g/ml), or fibrillar IAPP aggregates (□, 10  $\mu$ g/ml; □, 80  $\mu$ g/ml). The dotted line in panel B shows the initial rate of the elongation reaction seeded with 50  $\mu$ g/ml IAPP fibrils. The slope of this line is 5.8 times the slope of the fit for the elongation reaction with 10  $\mu$ g/ml IAPP fibrils compared with the expected ratio of 5, based on the relative mass of IAPP fibril seeds.

hance, seeding properties. However, as will be seen below, such equipotent seeding efficiencies are unusual even for fibrils from peptides differing by only one amino acid and may, therefore, be a special case for IAPP aggregation.

Fig. 5 shows the abilities of various aggregates to seed elongation of A $\beta$ (1-40). In contrast to the potent ability of A $\beta$ (1-40) fibrils at 10  $\mu$ g/ml (7% by weight) to seed A $\beta$ (1-40) elongation, globular IAPP aggregates (Fig. 2A) are completely inert at stimulating A $\beta$ (1-40) elongation, even at a concentration of 70  $\mu$ g/ml (about 50% by weight of the solution phase A $\beta$ ). Although perhaps not surprising in isolation given the non-fibrillar morphology of the aggregate, this result was somewhat unexpected based on the potent ability of the same IAPP non-fibrillar aggregates to seed IAPP elongation (Fig. 3A). Fig. 5 also shows that IAPP amyloid fibrils (Fig. 2, E-F) are good seeds of A $\beta$ (1-40) elongation, albeit much less efficient than are A $\beta$  fibril seeds for IAPP elongation (Fig. 6). The pseudo-first order kinetics plots in Fig. 5B show that a concentration of

## Seeding Specificity in Amyloid Fibril Growth

1745

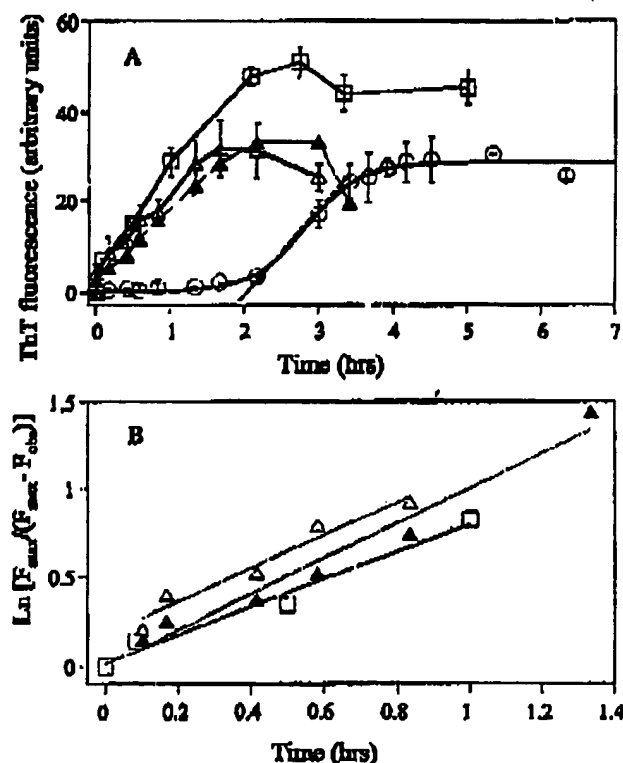


FIG. 6. Time course (A) and pseudo-first order kinetics plots (B) of IAPP fibril growth without (O) and with (A, Δ, and □) seeding. Disaggregated IAPP (30 μM) was seeded with sonicated amyloid fibrils of IAPP (□), Aβ(1-40) (Δ), or Aβ(1-42) (△).

TABLE I  
IAPP elongation rates for reactions seeded with various aggregates

| Aggregate as seed           | Rate constant <sup>a</sup> | Relative seeding efficiency |
|-----------------------------|----------------------------|-----------------------------|
|                             | $\text{h}^{-1}$            | %                           |
| IAPP fibrils <sup>b</sup>   | $0.904 \pm 0.05$           | 100                         |
| IAPP spheroids <sup>c</sup> | $0.968 \pm 0.08$           | 120                         |
| Wild-type Aβ(1-40)          | $0.940 \pm 0.18$           | 117                         |
| Wild-type Aβ(1-42)          | $1.01 \pm 0.06$            | 126                         |

<sup>a</sup> Values are from pseudo-first order fits of the data shown in Figs. 5 and 6.

<sup>b</sup> Aggregates from incubation of initial IAPP aggregates for 2 weeks at 37 °C, as described under "Results."

<sup>c</sup> Initial aggregates from spontaneous IAPP aggregation, as described under "Results."

efficient than the Aβ fibrils at supporting elongation; the ratio of these rates at identical weight concentrations of seeding fibrils gives a relative efficiency of IAPP seeds, compared with Aβ(1-40) seeds, of 2.2% (Table II). Although quite low, the Aβ elongation rate for IAPP seeding is clearly above the background when collagen, a fibrous protein exhibiting quite different secondary structure from amyloid fibrils, is used as a seed. As expected, Fig. 5B also shows that seeding efficiency increases as the mass of IAPP fibril seeds increases; although complicated by the non-linearity (see "Discussion") of the kinetics in the more heavily seeded experiment, the initial rates of these two reactions, which differ 5-fold in seed concentration, differ themselves by about 5-fold, as expected.

These solution phase-seeding experiments indicate a surprising lack of reciprocity in the cross-seeding reactions. Although Aβ(1-40) and both types of IAPP aggregates are essentially equally effective seeds for IAPP elongation, only Aβ(1-40) is an efficient seed for Aβ(1-40) elongation. IAPP fibrils exhibit 2.2% of the seeding efficacy of Aβ fibrils as a

no detectible seeding ability despite being excellent seeds for IAPP aggregation. This lack of reciprocity cannot be attributed to differences in the average molecular weights of the fibrils used as seeds, since the same fibril preparations were used in all experiments. The key to this lack of reciprocity may be related to the different degrees to which the structures of aggregation products resemble those of the aggregation seed (Figs. 2 and 4). The tendency of IAPP to form an unusual initial aggregation product complicates the interpretation of these results and suggests that the apparent lack of reciprocity in seeding may be a special case mechanistically linked to the diverse morphologies of IAPP aggregates.

Important subtleties of the elongation kinetics shown in Fig. 6 are (a) the modest upward curvature in the pseudo-first order plots for Aβ(1-40) elongation seeded by IAPP fibrils, where dramatic upward curvature might have been expected, and (b) the significantly higher ThT value at the plateau of the μg/ml IAPP-seeded reaction versus the Aβ-seeded reaction. These issues will be considered under "Discussion."

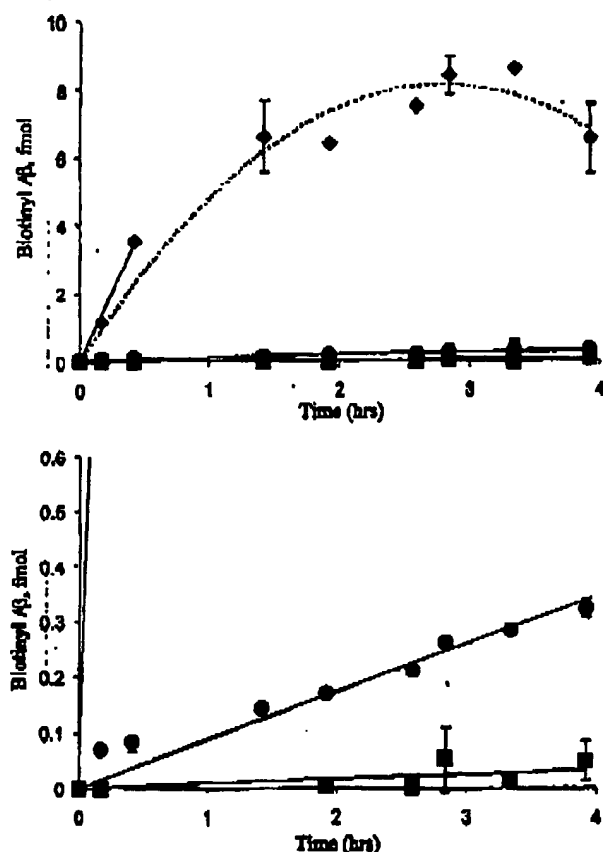
**Seeding Efficiencies Quantified in a Microtiter Plate Elongation Assay**—The solution phase, ThT-based assay described above is robust but relatively material-intensive. We explored the use of a microtiter plate elongation assay, adapted from previously described assays (88, 93), as a convenient alternative method for comparing seeding efficiency. In this assay small amount of fibrils immobilized non-covalently on the microtiter plate well serve as a seeding support for elongation of an N-terminal-biotinylated derivative of Aβ(1-40). The amount of biotin immobilized via Aβ elongation is quantified time-resolved fluorescence of europium ions introduced via complex with streptavidin; this assay approach has been well documented in application to polyglutamine aggregation (5). Fig. 7 shows the results of using this assay on immobilized Aβ(1-40) and IAPP fibrils. Panel A shows that although the homologous elongation reaction of Aβ(1-40) is quite efficient, the elongation of solution phase Aβ onto immobilized IAPP fibrils is almost negligible. Panel B shows an expanded view of the weak responders from Panel A. It can be seen that despite their low response, IAPP fibrils also give a linear response of final of IAPP immobilized per unit time. Remarkably, the relative seeding efficiency of IAPP fibrils, as determined by a comparison of the initial rates of elongation in the microplate assay, is very similar to their relative efficiency in the solution phase ThT assay (1.1% versus 2.2%, Table I). Similar good agreement was also obtained for other amyloid fibrils as well as a collagen control to assess the stimulatory ability of non-amyloid fibrous proteins when used as seeds as assayed by both methods (Table II). This good agreement supports the contention that both assays monitor the same fundamental process and suggests that the microplate assay can be used to routinely determine relative seeding efficiencies.

Encouraged by the excellent agreement between the widely different assay approaches, we used the more convenient microplate assay to assess the ability of a wider range of amyloid fibrils to serve as a seeding support for Aβ(1-40) elongation. First, we studied Aβ(1-40) elongation on a series of Aβ mutant fibrils, including amyloid from Aβ(25-35), Aβ(1-42), the E22G Arctic (54) mutant of Aβ(1-40), and a series of single point mutants of Aβ(1-40) substituted with proline. All the fibrils were sonicated before plating on microplate wells, and it was confirmed that >95% of the fibrils stuck to the wells. Table II includes the results of these elongation reactions compared with wild-type Aβ(1-40) fibrils. The results indicate that even single point mutants of an amyloidogenic peptide can produce fibrils that are measurably impaired in their ability

## Seeding Specificity in Amyloid Fibril Growth

TABLE II  
Seeded elongation of A $\beta$ (1-40) by solution phase and microplate assays

| Polymer as seed        | Solution phase assay       |                             | Microtiter plate assay |                             |
|------------------------|----------------------------|-----------------------------|------------------------|-----------------------------|
|                        | Rate constant <sup>a</sup> | Relative seeding efficiency | Rate <sup>b</sup>      | Relative seeding efficiency |
|                        | A <sup>-1</sup>            |                             | /mol h <sup>-1</sup>   |                             |
| A $\beta$ (1-40)       | 0.314 $\pm$ 0.05           | 100                         | 7.5 $\pm$ 1.1          | 100                         |
| A $\beta$ (1-40)(F4P)  | ND <sup>c</sup>            | ND                          | 10.9 $\pm$ 0.8         | 145.9                       |
| A $\beta$ (1-40)(R6P)  | ND                         | ND                          | 6.4 $\pm$ 0.17         | 85.8                        |
| A $\beta$ (1-40)(L17P) | ND                         | ND                          | 1.44 $\pm$ 0.05        | 19.2                        |
| A $\beta$ (1-40)(E22G) | 0.072 $\pm$ 0.01           | 22.9                        | 2.93 $\pm$ 0.08        | 39.1                        |
| A $\beta$ (1-40)(G33P) | ND                         | ND                          | 1.61 $\pm$ 0.1         | 21.5                        |
| A $\beta$ (1-40)(L34P) | ND                         | ND                          | 0.67 $\pm$ 0.04        | 8.9                         |
| A $\beta$ (1-42)       | 0.189 $\pm$ 0.02           | 60.3                        | 2.66 $\pm$ 0.31        | 35.6                        |
| A $\beta$ (25-35)      | 0.0087 $\pm$ 0.001         | 2.7                         | 0.488 $\pm$ 0.04       | 6.6                         |
| IAPP <sup>d</sup>      | 0.007 $\pm$ 0.001          | 2.2                         | 0.086 $\pm$ 0.01       | 1.1                         |
| Collagen               | 0                          | 0                           | 0.0075 $\pm$ 0.001     | 0.1                         |

<sup>a</sup> Pseudo-first order rate constant from data shown in Fig. 5 and similar data.<sup>b</sup> Initial rate constants from data shown in Fig. 7 or similar data.<sup>c</sup> ND, not determined.<sup>d</sup> IAPP fibrils from incubating spheroidal aggregates 2 weeks at 37 °C as described under "Results."FIG. 7. Elongation of protein polymers immobilized on microtiter plate wells by biotinylated A $\beta$ (1-40). Panel B is an expanded y-scale version of panel A. Immobilized proteins were A $\beta$ (1-40) amyloid fibrils ( $\bullet$ ), IAPP amyloid fibrils ( $\circ$ ), and collagen ( $\blacksquare$ ).

cant specificity to the fibril elongation reaction that is presumably controlled by the amyloid conformational preferences of the sequences (see "Discussion"). Amyloid fibrils composed of the A $\beta$ (25-35) fragment, a peptide that has been used in many studies as a surrogate for full-length A $\beta$ , are particularly poor at seeding A $\beta$ (1-40) elongation. This suggests a substantial difference between A $\beta$ (1-40) and A $\beta$ (25-35) fibril structure. The modest seeding ability of the E22G mutant for WT A $\beta$ (1-40) elongation is a dramatic demonstration that even a single point mutation in an amyloidogenic peptide can substantially change its seeding specificity and, hence, presumably its

The proline peptides listed in Table II are part of a series of proline mutants designed to probe the secondary structure of the A $\beta$  amyloid fibril (4). We selected a subset of these peptides to test their cross-seeding of the elongation of the WT peptide. The seeding abilities of these fibrils fall into two broad categories (Table II). Some mutant fibrils (F4P, R6P) exhibit similar seeding efficiency to that of WT fibrils. Others (L17P, G33P, L34P) give seeding efficiencies that are substantially lower than that of WT but are still significant compared with the seeding efficiency of most non-A $\beta$  fibrils (see below). Intriguingly, the pattern of the relative abilities of Pro mutant fibrils to seed WT A $\beta$ (1-40) elongation is consistent with our current knowledge of A $\beta$  fibril structure (see "Discussion").

We extended these studies to include amyloid fibrils from a number of proteins and peptides associated with amyloid diseases that exhibit no significant sequence similarity to the A $\beta$  peptide. As expected from the results with IAPP and the proline mutants of A $\beta$ , fibrils of these proteins are universally poor as seeds for elongation by A $\beta$ (1-40). Table III lists the rates of elongation in the standard microtiter plate assay and the rates relative to that for A $\beta$ (1-40) fibrils. It can be seen that all the relative rates are less than 10% that of WT A $\beta$ (1-40) fibrils, and some ( $\beta$ 2-microglobulin and LEN (1-30)) are so low as to be almost indistinguishable from the background rates seen for the non-amyloid protein aggregates collagen and denatured ovalbumin. In fact, with two exceptions, all of the fibrils tested exhibit seeding efficiencies of about 1% or less compared with that of A $\beta$ (1-40) fibrils. The exceptions are the amyloid-like aggregates grown from polyglutamine peptides (28) associated with Huntington's disease and other expanded CAG repeat diseases (55). The ability of these aggregates to do tolerably well as seeds for A $\beta$ (1-40) elongation contrasts with their lack of sequence homology with A $\beta$  and with the overall lack of complexity in the polyglutamine sequence. We can only surmise that the efficacy of these aggregates to seed A $\beta$  elongation stems from some coincidental similarity in the details of the folds that the A $\beta$  and polyglutamine peptides assume in forming their respective amyloid fibrils. If this hypothesis is correct, it would suggest that amino acid sequence effects on the specificity of cross-seeding reactions may be mediated by the way that side-chain packing within the fibril controls details of the folding of the polypeptide backbone (rather than by the way that side chains in the fibril directly interact with side chains in the in-coming monomer).

## DISCUSSION

The initial motivation for these studies was the confluence of

## Seeding Specificity in Amyloid Fibril Growth

174!

TABLE III  
Microplate seeding efficiencies for A $\beta$ -(1-40) elongation  
for various amyloid fibrils

| Aggregate/polymer used as seed  | Rate <sup>a</sup><br>/mM <sup>-1</sup> | Relative seeding efficiency |
|---------------------------------|--|-----------------------------|
| A $\beta$ -(1-40)               | 7.50 $\pm$ 1.1                         | 100                         |
| IAPP <sup>b</sup>               | 0.086 $\pm$ 0.01                       | 1.1                         |
| N light chain LEN-(1-30)        | 0.019 $\pm$ 0.001                      | 0.25                        |
| Polyglutamine Gln <sub>20</sub> | 0.44 $\pm$ 0.01                        | 5.9                         |
| Polyglutamine Gln <sub>30</sub> | 0.28 $\pm$ 0.01                        | 3.7                         |
| Ure2p                           | 0.069 $\pm$ 0.001                      | 0.92                        |
| N light chain JTO5              | 0.042 $\pm$ 0.008                      | 0.56                        |
| $\alpha$ 2 microglobulin        | 0.014 $\pm$ 0.001                      | 0.19                        |
| Collagen                        | 0.0075 $\pm$ 0.001                     | 0.1                         |
| Ovalbumin-RA                    | 0.009 $\pm$ 0.003                      | 0.12                        |

<sup>a</sup> Initial rates from elongation of biotinylated A $\beta$ -(1-40) on microplates coated with fibrils.

<sup>b</sup> Mature amyloid fibrils obtained by incubating initial spheroidal aggregates for 2 weeks at 37 °C.

and a reported relationship between type II diabetes (with its associated pancreatic deposition of IAPP amyloid) and disease risk in AD (27). However, despite the strong sequence similarity between these peptides, we find that IAPP amyloid is a very poor seed for A $\beta$ -(1-40) elongation *in vitro*. It is not clear, however, what level of efficiency in the heterologous seeding of A $\beta$  elongation by IAPP might be significant in terms of an elevated risk of A $\beta$  amyloid plaque formation and AD onset. Although, based on the results presented here, one expects that most cases of heterologous seeding between peptides of dissimilar sequence will be relatively inefficient, it is also true that almost all of the fibrils in the cross-seeding of A $\beta$  elongation in Table III exhibit finite seeding potentials that exceed the background levels of control proteins collagen and denatured albumin. Because the nature of seeded polymerization is that very small initial effects can have devastating consequences over time, it is difficult to gauge whether or not a particular, low cross-seeding efficiency might be potentially significant biologically; we believe that the work described here provides the theoretical framework and experimental tools to begin to address such questions. In any case, the apparent linkage between diabetes and AD may be related to other molecular interactions, such as the potential role for insulin-degrading enzyme in controlling A $\beta$  flux, steady state concentration, and therefore, aggregation (56).

Amyloid fibrils grown from purified peptides and proteins *in vitro* are remarkably similar, in both electron micrographs and x-ray fiber diffraction, to amyloid fibrils extracted from human tissue (57). At the same time, it is well known that amyloid fibrils in tissue contain a number of other molecules besides the major constituent protein. Despite the similar appearance of fibrils grown in the absence of these other molecules, it is possible that amyloid fibrils in tissue are functionally distinct from fibrils grown *in vitro* from the pure, major constituent protein. This is relevant to the work described here, since we attempt to draw biological conclusions from studies of such artificial fibrils. We think it is justified to do this, since amyloid deposits in authentic disease tissue from both Alzheimer's disease (38) and Huntington's disease brains<sup>5</sup> are capable of carrying out elongation reactions *in vitro* when provided with appropriate monomeric building blocks. At the same time, amyloid fibrils grown *in vitro* may not be identical in structure and/or function to naturally derived amyloid in some other respects.

The surprising potency of A $\beta$  fibrils as seeds for IAPP aggre-

gation is interesting from two points of view. First, we found other cases in the survey reported here in which an aggregate of a peptide of less than 98% sequence identity was essentially equipotent with WT fibrils for seeding amyloid growth by V monomer. Second, the strong seeding by A $\beta$  fibrils represent case of non-reciprocity in heterologous seeding (although the significance of this observation is uncertain given the plethora of aggregation products observed in IAPP aggregation and extremely aggressive nature of even the unseeded reaction. Perhaps IAPP is a special case in that, as a very aggressive amyloid forming peptide, it requires a less structurally homologous fibril to initiate polymerization and has a number of avenues available through which it can form amyloid-like products.

Our studies on cross-seeding within the family of A $\beta$  peptides show the sensitivity of seeding efficiency to small sequence changes and suggest a number of biological points. Those amyloid fibrils compared by the microtiter plate as listed in Table II, the A $\beta$  fibril with the poorest ability to seed A $\beta$ -(1-40) elongation is A $\beta$ -(25-35). It seems very unlikely that this short peptide, which contains within its 11 amino acids only 5 residues likely to exist in H-bonded  $\beta$ -sheet in the fibril and which lacks another major segment involved in  $\beta$ -sheet formation (4), could be capable of making fibrils that share significant structural or shape relationship to 1-40 fibrils (in side of a generic amyloid fold). In fact, the relative seeding efficiency of these fibrils is about 5% that of WT A $\beta$ -(1-fibrils (Table II), about the same efficiency as the better seed fibrils from non-homologous peptides listed in Table III. In contrast, fibrils of biologically relevant A $\beta$  analogs A $\beta$ -(1-59) and A $\beta$ -(1-40) E22G (54) exhibit seeding efficiencies in 20-40% range compared with WT A $\beta$ -(1-40). The former is significant since elevated levels of the 1-42 peptide thought to be more relevant to AD disease risk than high levels of the 1-40 peptide (59). The latter is significant since peptide, associated with the Arctic familial mutation responsible for early onset AD (54), exhibits similar or even greater specificity with respect to WT A $\beta$ -(1-40) in protofibril and fibril formation occurring spontaneously *in vitro* from 1:1 mixture of these peptides (60).

The studies reported here on the abilities of amyloid fibrils from various point mutants of A $\beta$  strongly suggest that seeding specificity has less to do with primary sequence similarity and more to do with shape, i.e. the details of the conformation of the amyloid fibril, and in particular of the network of H-bond donors and acceptors at the fibril growing end. Apparent fibrils from single point mutants of A $\beta$  can differ from WT in this required shape almost as much as fibrils from unrelated peptides. The proline replacement analogs of A $\beta$ -(1-40) studied here were shown elsewhere (4) to fall into two classes, (a) F4P and R6P mutants, which form fibrils with WT-like stabilities and hydrogen exchange properties, and (b) the I G33P, and L34P mutants, which form fibrils only with reduced stabilities and which exhibit measurably different hydrogen exchange protection associated with small but significant structural perturbations in their amyloid fibrils. The results in Table II mirror these classes, with F4P and mutant fibrils exhibiting seeding abilities in the range of A $\beta$ -(1-40) fibrils, while the L17P, G33P, and L34P mutants exhibit significantly lower seeding efficiencies. In particular, L34P fibrils exhibit a relative seeding efficiency less than 10%, in the same range as a polyglutamine fibril (Table II). Thus, point mutants can make fibrils that are strong or weak seeds for WT A $\beta$  elongation, depending on how much the structure of the mutant fibrils deviates from the structure of WT fibrils.

<sup>5</sup> Osmund, A. P., Berthelot, V., and Wetzel, R. (2002) Program 293.8, 3002 Abstract Viewer/Itinerary Planner, Society for Neuroscience, Washington, D. C.

This astounding sensitivity of fibril seeding efficiency to single point mutations suggests that polypeptide chains do not sacrifice their exquisite capabilities for folding specificity when they undergo alternative assembly into amyloid fibrils. In fact, it would appear possible that even protein mutants that fold into very similar structures in the native state may well be capable of folding into functionally distinct and discriminatory amyloid fibrils.

This plasticity in amyloid structure is also suggested by our interpretation of some of the details of the IAPP fibril-seeded A $\beta$  elongation reaction (Fig. 5). From much experience using the ThT assay to monitor amyloid growth, we know that the signal strength at the reaction end point is quite reproducible for any given amyloid growth reaction.<sup>6</sup> We also know that the ThT signal, normalized for constant fibril weight, can differ for the amyloid fibrils of different point mutants of A $\beta$  over a 6-fold range.<sup>5</sup> The 2-fold difference between the ThT signals in Fig. 5 for the two A $\beta$  elongation reactions that have reached equilibrium (○, □) suggest that the structures of these A $\beta$  fibrils are substantially different, presumably influenced by the nature of the seed. The other unexpected aspect of Fig. 5 is the persistence of the low elongation rate for A $\beta$  elongation seeded by IAPP fibrils. In an elongation of monomer A seeded by fibril B, one might have expected that, as more and more monomer A incorporates onto the growing ends of fibril B, the fibril ends will eventually take on the character of A fibrils in all respects, including their intrinsic homologous seeding rate. Thus, in cross-seeded reactions one might have expected to see a non-linear pseudo-first order kinetics curve, with a slow start followed by a surge to a new, much faster rate identical to that of the homologically seeded reaction. In fact, there is a small amount of upward curvature in the plot in Fig. 5B for A $\beta$  elongation seeded by 50  $\mu$ g/ml IAPP fibrils; however, the corresponding slope for A $\beta$  elongation seeded by 50  $\mu$ g/ml A $\beta$  fibrils would be 5 times the slope shown for the A $\beta$ -seeded A $\beta$  elongation in Fig. 5. Clearly the cross-seeded reaction, by the time it reaches completion, has not achieved anything close to this projected rate. This suggests that over the entire cross-seeded elongation reaction, the elongation rate changes little from the initial rate, which was initially established by the unique conformation of the IAPP fibrils (at the same time, the slight but significant upward curvature (never observed in homologically seeded reactions) may be consistent with a trend toward such a conformational switch as the heterologously seeded fibrils continue to grow). Thus, both the ThT amplitude and the elongation kinetics suggest that A $\beta$  fibrils propagated from an IAPP seed are conformationally different from A $\beta$  fibrils grown from A $\beta$  seeds.

If confirmed by further experiments, these results from IAPP fibril seeding of A $\beta$ -(1-40) elongation suggest that a single peptide sequence is capable of forming multiple amyloid conformations depending on the seeding fibril and perhaps other variables. Such behavior would be consistent with the recently described ability of certain yeast prion proteins to make amyloid fibrils that exhibit different seeding capabilities depending on the details of how the seeding fibrils are generated (18, 61) and, more broadly, could provide the underlying structural basis for species barriers and strain phenomena in prion infectivity (18-20, 61).

The studies described here reveal unanticipated subtleties in the conformations of amyloid fibrils as measured by their cross-seeding efficiencies. Although the wide ability of unrelated polypeptides to grow into amyloid fibrils might suggest that the forces driving amyloid formation are not very discriminating,

our data suggest that amyloid exhibits the same degree of structural specificity as found for the folding of evolved, globular protein structures. We believe that further studies of the kind described here will reveal much about the structures and biological properties of amyloid fibrils.

**Acknowledgments**—We acknowledge Reed Wickner and Kimberly Taylor for the Ure2p fibrils, Susan Jones and Sheena Radford for the  $\beta$ 2-microglobulin fibrils, Jonathan Wall for amyloid fibrils of JTO5 and Len-(1-30), Charles Murphy for the A $\beta$ -(35-38) peptide, and Tina Richey for the amyloid-like aggregates of polyglutamine peptides. We are grateful to Craig Wooliver for advice on the Congo red staining procedure.

**Note Added in Proof**—An article (Janson, J., Laedke, T., Parisi, J. E., O'Brien, P., Petersen, R. C., and Butler, P. C. (2004) *Diabetes* 53, 474-481) recently appeared showing that, while patients with Alzheimer's disease do not appear to be statistically at risk of developing diabetes, patients with type II diabetes do have an increased risk of developing Alzheimer's disease. It is interesting, and possibly relevant, that these epidemiological trends appear to be recapitulated by the cross-seeding effects reported here, in which IAPP fibrils are inefficient at seeding A $\beta$  elongation, while A $\beta$  fibrils are very efficient at seeding IAPP elongation. The A $\beta$  peptide is produced throughout the body, and it is conceivable that small amounts of A $\beta$  fibrils might be produced outside the brain, especially in patients with elevated fibril levels in the brain.

#### REFERENCES

- Fandrich, M., Fletcher, M. A., and Dobson, C. M. (2001) *Nature* 410, 166-168
- Dobson, C. M. (2001) *Biochem. Soc. Symp.* 269, 1-36
- Fandrich, M., and Dobson, C. M. (2002) *EMBO J.* 21, 6482-6490
- Williams, A., Portelius, E., Kheterpal, I., Guo, J., Cook, R., Xu, Y., and Wetzel, R. (2004) *J. Mol. Biol.* 335, 833-843
- Hilbich, C., Kisters-Wolke, B., Reed, J., Masters, C. L., and Beyreuther, K. (1992) *J. Mol. Biol.* 224, 469-473
- Wood, S. J., Wetzel, R., Martin, J. D., and Hurlb, M. R. (1998) *Biochem. J.* 334, 734-750
- Eder, W. P., Scimone, E. R., Ghilardi, J. R., Lu, Y. A., Felix, A. M., Vinters, H. V., Mantyh, P. W., Lee, J. P., and Maggio, J. E. (1996) *Biochemistry* 35, 13914-13921
- Muramoto, A., Irie, K., Murakami, K., Ohgushi, H., Shindo, M., Nagao, M., Shimizu, T., and Shirasawa, T. (2002) *Biochem. Biophys. Res. Commun.* 294, 306-311
- Murakami, K., Irie, K., Muramoto, A., Ohgushi, H., Shindo, M., Nagao, M., Shimizu, T., and Shirasawa, T. (2003) *Biochem. Biophys. Res. Commun.* 294, 5-10
- Chiti, F., Stefani, M., Taddei, N., Ramponi, G., and Dobson, C. M. (2003) *Nature* 424, 806-808
- Jarrett, J. T., and Lansbury, P. T., Jr. (1992) *Biochemistry* 31, 12345-12352
- Hsu, H., Weisberg, P. H., and Lansbury, P. T., Jr. (1996) *Chem. Biol.* 3, 149-169
- Hasegawa, K., Yamaguchi, I., Omata, S., Gejyo, F., and Nalid, H. (1999) *Biochemistry* 38, 15514-15521
- Martinez-Rocha, L. A., Zurdo, J., Spencer, A., Noppa, W., Banerjee, V., Archer, D. B., Janiak, M., and Dobson, C. M. (2000) *J. Struct. Biol.* 130, 339-351
- Evans, K. C., Burger, E. P., Cho, C.-G., Weisberg, K. H., and Lansbury, P. T., Jr. (1996) *Proc. Natl. Acad. Sci. U. S. A.* 93, 763-767
- Wood, S. J., Chan, W., and Wetzel, R. (1996) *Biochemistry* 35, 12623-12633
- Eder, W. P., Scimone, E. R., Ghilardi, J. R., Vinters, H. V., Lee, J. P., Mantyh, P. W., and Maggio, J. E. (1996) *Biochemistry* 35, 743-757
- Chiza, P., and Weissman, J. S. (2001) *Nature* 410, 223-227
- DePace, A. H., and Weissman, J. S. (2002) *Nat. Struct. Biol.* 9, 989-998
- Haseguchi, M., Priola, S. A., Chakry, J., and Caughey, B. (2000) *Proc. Natl. Acad. Sci. U. S. A.* 97, 5836-5841
- McCampbell, A., and Fischback, K. H. (2001) *Nat. Med.* 7, 528-530
- Chen, S., Bartholier, V., Yang, W., and Wetzel, R. (2003) *J. Mol. Biol.* 311, 173-182
- Pekker, A. T., Ishii, Y., Balbach, J. J., Antzutkin, O. N., Leapman, R. D., Delaglio, F., and Tycko, R. (2002) *Proc. Natl. Acad. Sci. U. S. A.* 99, 16742-16747
- Rajan, R. S., Illing, M. E., Bence, N. F., and Kopito, R. R. (2001) *Proc. Natl. Acad. Sci. U. S. A.* 98, 13060-13065
- Lundmark, K., Westmark, O. T., Nystrom, S., Murphy, C. L., Salomon, A., and Westermark, P. (2003) *Proc. Natl. Acad. Sci. U. S. A.* 99, 6979-6984
- Westmark, P., and Wilander, E. (1978) *Diabetologia* 15, 417-421
- Oik, A., Stolt, R. F., van Harskamp, F., Pole, H. A., Hoffman, A., and Breteler, M. M. (1999) *Neurology* 53, 1937-1942
- Chen, S., Bartholier, V., Hamilton, J. B., O'Neill, B., and Wetzel, R. (2002) *Biochemistry* 41, 7391-7399
- Taylor, K. L., Cheng, N., Williams, R. W., Steven, A. C., and Wickner, R. B. (1999) *Science* 285, 1330-1334
- Kheterpal, I., Williams, A., Murphy, C., Blodges, B., and Wetzel, R. (2001) *Biochemistry* 40, 11757-11767
- Levy, H. (1999) *Methods Enzymol.* 209, 274-284
- Kheterpal, I., Zhou, S., Cook, R. D., and Wetzel, R. B. (2000) *Proc. Natl. Acad. Sci. U. S. A.* 97, 13597-13601
- O'Neill, B., and Wetzel, R. (2002) *Proc. Natl. Acad. Sci. U. S. A.* 99, 1444-1449

<sup>6</sup> A. D. Williams, unpublished information.

## Seeding Specificity in Amyloid Fibril Growth

174

34. Chen, S., and Wetzel, R. (2001) *Protein Sci.* 10, 887-891
35. Wall, J., Schall, M., Murphy, C., Hrnica, R., Stevens, P. J., and Solomon, A. (1999) *Biochemistry* 38, 14101-14108
36. Naldi, H., and Nakakuki, K. (1996) *Lab. Invest.* 74, 374-383
37. Naldi, H., and Oefro, P. (1999) *Methods Enzymol.* 308, 305-318
38. Kaler, W. P., Simson, E. R., Ghilardi, J. R., Felix, A. M., Lu, Y. A., Vinters, H. V., Mantyh, P. W., and Maggio, J. E. (1997) *Nat. Biotechnol.* 15, 258-263
39. Berthelot, V., and Wetzel, R. (2003) in *Methods in Molecular Biology* (Potter, N. T., ed) pp. 295-303, Humana Press Inc., Totowa, NJ
40. Diamantidis, E. P. (1983) *Clin. Biochem.* 11, 129-150
41. Puchtler, H., Sweat, F., and Lovina, M. (1963) *J. Histochem. Cytochem.* 10, 355-364
42. Selkoe, D. J. (1994) *Annu. Rev. Neurosci.* 17, 489-517
43. Cobre-Medina, S., Mulder, H., Palmy, M., Westermark, G., Torzell, J., Westermark, P., Sundler, F., Ahren, B., and Betsholtz, C. (1998) *Biochem. Biophys. Res. Commun.* 250, 371-377
44. Torok, M., Milton, S., Kaye, R., Wu, P., McIntire, T., Glabe, C. G., and Lansbury, R. (2002) *J. Biol. Chem.* 277, 40810-40815
45. Sakagashira, S., Sanku, T., Hanabusa, T., Shimomura, H., Obagi, S., Kumagaya, K. Y., Nakajima, K., and Nanjo, K. (1996) *Diabetes* 45, 1379-1381
46. Sakagashira, S., Hiddinga, H. J., Tetsuchi, K., Sanku, T., Hanabusa, T., Nanjo, K., and Eberhardt, N. L. (2000) *Am. J. Pathol.* 157, 2101-2108
47. Ma, Z., Westermark, G. T., Sakagashira, S., Sanku, T., Gustavsson, A., Sakamoto, H., Engstrom, U., Nanjo, K., and Westermark, P. (2001) *Amy* 2, 242-248
48. Westermark, P., Engstrom, U., Johnson, K. H., Westermark, G. T., and Scholtz, C. (1990) *Proc. Natl. Acad. Sci. U. S. A.* 87, 5038-5040
49. Moriarty, D. P., and Raleigh, D. P. (1999) *Biochemistry* 38, 1811-1818
50. LeVine, H., III (1995) *Amyloid* 2, 1-6
51. Higham, C. E., Jaikaran, E. T., Fraser, P. E., Cross, M., and Clark, A. (2001) *FEBS Lett.* 470, 55-60
52. Ferrone, F. (1999) *Methods Enzymol.* 308, 256-274
53. Berthelot, V., Hamilton, J. R., Chen, S., and Wetzel, R. (2001) *Anal. Biochem.* 295, 227-236
54. Nilberth, C., Westlund-Danielsson, A., Eckman, C. B., Condros, M., Axelman, K., Forsell, C., Stenb, C., Luchman, J., Teplow, D. B., Yuan, S. G., Naslund, J., and Lennfelt, L. (2001) *Nat. Neurosci.* 4, 887-893
55. Cummings, C. J., and Zoghbi, H. Y. (2000) *Hum. Mol. Genet.* 9, 909-919
56. Galasko, D. (2003) *Neurology* 60, 1886-1887
57. Sunde, M., and Blake, C. (1997) *Adv. Protein Chem.* 50, 123-159
58. Huang, X., and Miller, W. (1991) *Adv. Appl. Mathem.* 12, 327-367
59. Selkoe, D. J. (1994) *Nature* 369, (Suppl. 6738), A23-A31
60. Khoshdel, L., Lashmel, H. A., Hartley, D. M., Wala, T., Lansbury, P. T., Jr., Wetzel, R. (2003) *Biochemistry* 42, 14092-14098
61. Chien, P., DePace, A. B., Collins, S. R., and Walsman, J. S. (2003) *Nature* 424-431

# New clothes for amyloid enhancing factor (AEF): silk as AEF

Robert Kisilevsky<sup>1</sup>, Laura Lemieux<sup>1</sup>, Lee Boudreau<sup>1</sup>, Yang Dun-Sheng<sup>2</sup> and Paul Fraser<sup>2</sup>

1. Department of Pathology, Queen's University, and The Syl and Molly Apps Research Center, Kingston General Hospital, Kingston, Ontario Canada K7L 3N6
2. Department of Medical Biophysics, University of Toronto and The Center for Research in Neurodegenerative Diseases, Toronto, Ontario, Canada M5S 1A8

**KEY WORDS:** AEF, silk, AA amyloid, amyloid enhancing factor, prions

**ABBREVIATIONS:** AEF = amyloid enhancing factor; NAEF = native AEF; SAEF = modified silk AEF; BME =  $\beta$ -mercaptoethanol; DDW = distilled deionized water; IAPP = islet amyloid polypeptide; SDS = sodium dodecylsulfate

## Abstract

Amyloid enhancing factor (AEF) is an activity that appears naturally during the course of persistent inflammation and precedes, by 24–48 h, AA amyloid deposition in appropriate murine models. AEF is defined by its biological properties, namely, when administered intravenously or intraperitoneally to a mouse, it primes the recipient for the rapid induction of AA amyloid when they are given an inflammatory stimulus. Available evidence indicates that AEF is protein in nature, but a specific molecular species (if a singular species exists) has not been identified. Past work (Ganowiak et al., *Biochem. Biophys. Res. Commun.* 199:306–312, 1994) has shown that AEF activity may be imparted to two different proteins (IAPP and  $\beta$ -protein) provided each is organized in the form of an amyloid fibril. Since a characteristic property of proteins in amyloid fibrils is their  $\beta$ -sheet organization, one possibility is that AEF activity, in part, depends on such organization, and other proteins with such properties may also have AEF activity. To investigate this possibility, silk, a protein which contains substantial  $\beta$ -sheet content, was denatured in LiSCN and allowed to renature slowly under reducing conditions to form a gel. The denatured silk preparation was then sonicated thoroughly to permit intravenous injection and assessed for AEF activity. The modified silk, presented as small fibrils in a  $\beta$ -sheet conformation as assessed by electron

microscopy and circular dichroism, respectively. This silk at 0–50  $\mu$ g/animal was administered intravenously as "AEF" followed immediately by subcutaneous AgNO<sub>3</sub> as the inflammatory stimulus. Six days later the spleens were examined for the presence of AA amyloid and following Congo red staining, the amount of amyloid quantified by image analysis. Modified silk without an inflammatory stimulus, and non-sonicated modified silk, failed to induce AA amyloid. Sonicated modified silk followed by AgNO<sub>3</sub> induced large quantities of splenic AA amyloid in a dose dependent fashion. Modified silk in quantities as small as 1–5  $\mu$ g/animal can function as AEF. The AEF properties of the modified silk were stable at 4°C for at least 4 weeks (the longest period tested). This procedure may provide a means of standardizing AEF preparations.

## Introduction

Amyloid enhancing factor (AEF) has been called "an enigma wrapped in a mystery"<sup>1</sup>. It has been the subject of investigation by many groups for almost 35 years. Since the initial description of cell or tissue extracts from amyloidotic animals that have the property of being able to enhance or accelerate susceptibility to amyloidogenesis in recipients<sup>2–4</sup>, data have been accumulated without satisfactorily explaining what structural ele-

Correspondence: Dr. Robert Kisilevsky, Department of Pathology, Queen's University, Kingston, Ontario Canada K7L 3N6  
Tel: 613-545-6411 Fax: 613-545-2907

Submitted: July 7, 1998

Revision Accepted: December 11, 1998

ments are necessary for AEF activity, nor how AEF exerts its effect.

AEF is defined in the biological context of *in vivo* inflammation-associated (AA) amyloidogenesis, as a factor which when injected intravenously substantially reduces the murine splenic AA amyloid induction time usually required by inflammatory stimuli. The subject was reviewed in considerable detail several years ago<sup>5</sup>. Among the conclusions reached at that time were that AEF is protein in nature, its activity is dependent on its conformation, different proteins with common secondary, tertiary, or quaternary organization may all have AEF activity, and AEF may be acting as a nidus, or scaffold, for amyloid fibrillogenesis. The data supporting these conclusions have been adequately cited in the above review but may be briefly reiterated. Proteases, but neither lipases nor nucleases (RNAase or DNAase) destroy AEF activity<sup>6</sup>. Denaturation of AEF preparations with heat, guanidine, or urea destroys AEF activity<sup>6</sup>. Naturally occurring amyloid fibrils composed of different amyloid proteins possess AEF activity, suggesting that a common structure rather than composition is responsible for AEF activity<sup>7-10</sup>. Pure amyloid peptides lack AEF activity until they organize themselves into amyloid fibrils<sup>11,12</sup>. And, the kinetics of amyloid formation *in vivo* in the presence and absence of AEF is identical, save for the absence of a lag period during induction when AEF is injected intravenously<sup>13</sup>, and follows the pattern seen in *in vitro* amyloid fibrillogenesis "seeded" processes<sup>14-18</sup>.

Work attempting to elucidate AEF's critical properties, and its mode of action, would be greatly facilitated by a procedure to prepare an "AEF" from relatively pure inexpensive materials. The findings that pure amyloid peptides possess AEF activity when organized into fibrils<sup>11,12</sup>, and the  $\beta$ -sheet protein configurational characteristics of amyloid fibrils suggested that silk might fulfill the necessary requirements. Silk, in addition to being a material of immense commercial value for fabric production, is a fiber with many of the structural features of amyloid<sup>19-22</sup>, and is the epitome of a protein which contains substantial  $\beta$ -sheet content<sup>21,22</sup>. Raw silk is inexpensive, and when rid of its non-protein components consists primarily of two classes of polypeptides, one in the  $M_r$  range of 200-300K and the other in the range of 25-50K<sup>20,22</sup>. However, raw silk is clearly not in an injectable form.

A series of experiments were therefore undertaken to modify raw silk in an attempt to obtain an inexpensive, compositionally defined, and readily prepared "AEF" which, if successful, could be used to answer questions about native AEF's critical properties and its mode of action.

## Methods

### Materials

The following common chemicals (reagent grade) were purchased from Sigma, (St. Louis MO): Sodium dodecyl sulfate (SDS), Tris(hydroxymethyl)-aminomethane (TRIS),  $\beta$ -mercaptoethanol (BME), and Congo red (97% pure) lot # 085H4386. LiSCN was purchased from Aldrich Chemical Co. (Milwaukee, WI). Raw silk (from *Bombyx mori*) was purchased from a local crafts shop.

### Animals

All animals were CD1 female mice (Charles Rivers, Montreal, Quebec) 8-10 weeks of age and weighing 25-30 g which had access to laboratory chow (Purina 5015) and water ad libitum.

### Preparation of silk

The raw silk was boiled extensively (2 h) in 2%  $\text{Na}_2\text{CO}_3$ , to remove non-protein components, rinsed in copious amounts of distilled deionized water (DDW), then ethanol, and dried at 60°C<sup>19</sup>. The appearance of the dried washed silk was ivory white, and composed of matted, short strands. Ten mg of the treated silk were dissolved in 700  $\mu\text{l}$  of 65% aqueous LiSCN prepared from a freshly opened bottle (or one stored under nitrogen)<sup>19</sup>. After 20 min the solution was brought to 1%  $\beta$ -mercaptoethanol. Following an additional 20 min the solution was dialysed overnight against DDW allowing the silk to renature in the form of a loose gel. The solution was brought to 10 ml with DDW, and solid NaCl to bring the salt concentration to 0.9% (0.15 M), and 1mg/ml silk, following which it was heated at 37°C for 1h to complete the renaturation process and then thoroughly sonicated. The sonication was performed with the sample on ice for brief pulses of 1-2 sec for a total period of 20 sec using a Vibracell (Sonics and Materials Inc., Danbury, CN) with the variable amplitude set at 60 on the dial.

### AEF preparation

AEF was prepared as water washed AA amyloid fibrils, from amyloid laden spleens as described previously<sup>4,23</sup>, and stored at -20 °C at a concentration of 1mg protein/ml.

### Electrophoresis

Following the boiling of raw silk in  $\text{Na}_2\text{CO}_3$  and its washing in DDW and ethanol, 10 mg was dissolved in 65% LiSCN in electrophoresis sample buffer lacking SDS (Tris-HCl, 60 mM pH 6.8, 5% BME, and urea 8 M). The LiSCN was then removed by dialysis against the same sample buffer, following which SDS was added to 2%. The samples were then subjected to electrophoresis as described by



Laemmli *et al.*<sup>24</sup>, using a 7% polyacrylamide gel, and stained with silver by the method of Oakley *et al.*<sup>25</sup>.

#### Electron microscopy

Samples were prepared by applying droplets of the silk solution (at 1 mg/ml or 200 µg/ml) to pioloform carbon-coated grids which were then blotted to remove excess water and air-dried. The fibrils were then negatively stained with 1% phosphotungstic acid (w/v) and visualized on a Hitachi H-7000 electron microscope operated at 75 kV.

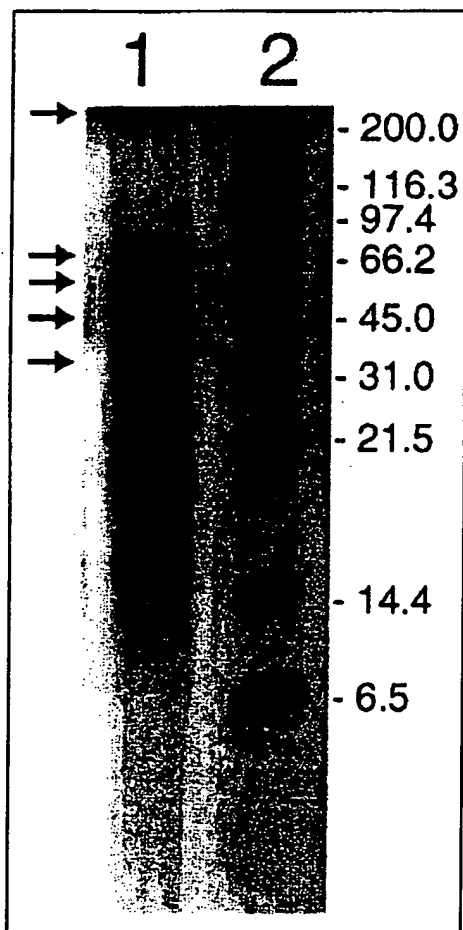


**FIGURE 1.** Electrophoresis of LiSCN/ $\beta$ -mercaptoethanol denatured raw silk prior to its renaturation and sonication (Lane 1). Arrows indicate the presence of protein bands at molecular weights greater than 200K, and in the range of 14-66K. Molecular weight markers are indicated in Lane 2, and in descending order are, myosin 200K,  $\beta$ -galactosidase 116.25K, phosphorylase b 97.4K, serum albumin 66.2K, ovalbumin 45K, carbonic anhydrase 31K, trypsin inhibitor 21.5K, lysozyme 14.4K and aprotinin 6.5K.

Calibration of the electron microscope was done with paracrystalline tropomyosin.

#### Circular dichroism

A stock solution of extracted and dialysed silk preparation was examined by circular dichroism to determine the protein secondary structure. Aliquots were run either directly as concentrated solutions at 1 mg/ml or were diluted in 10 mM phosphate buffer, pH 7 to a final concentration of 500 µg/ml. Spectra were collected on a Jasco 720 spectropolarimeter from 250-190 nm with a path length of 0.1mm and a scan time of 20 nm/min (bandwidth 1.0 nm, step-resolution 0.1nm).

#### Amyloid induction

Amyloid was induced as described previously<sup>6</sup>, by intravenously injecting either native AEF or modified silk in varying doses, 0 - 250 µg protein/animal, (3 animals at each dose), followed by 0.5 ml 2% AgNO<sub>3</sub> injected subcutaneously in the back to produce a small sterile abscess. The animals were killed after 6 days by CO<sub>2</sub> narcosis and their spleens fixed in ethanol:acetic acid as described previously<sup>26</sup>. Routine procedures were used to prepare sections for histology which were stained with Congo red<sup>27</sup>.

#### Amyloid quantitation

Congo red stained spleen sections were assessed by image analysis for the quantity of amyloid as described previously<sup>28</sup>. Briefly, 3 standard spleen sections, containing a range of AA amyloid quantities (3%-30% of splenic area), were used to calibrate the image analyser with a set of constant reference points. The crossed polars were angled at 90 degrees to give maximum darkness in areas devoid of amyloid. The same tissue sections on the same glass slides were always used for this purpose, and can therefore be used as a reference to prepare other standards, if necessary. The image analysis program, M5 version, is from MCID Imaging Research Inc., Brock University, St. Catharines, Ontario, Canada. The upper and lower limits for the intensity, hue, and saturation are set at 1 and 0.09, 170.16 and 53.44, and 1 and 0, respectively. Minor adjustments in these settings are performed on each occasion that the apparatus is calibrated to ensure that the standards provide a constant reading on each occasion that the apparatus is used. A TV camera (Hitachi 3CCD color camera) is mounted on the microscope, which provides a 100 X image, and the image is transported to a Pentium type computer with a Matrox digitizing board. Following calibration multiple fields (n=6) were examined in each section to be quantified and the quantity of amyloid in each mouse spleen was expressed as the percent of splenic area occupied by amyloid.

## Results

### *Characteristics of modified silk*

A fractionation of proteins in the protein composition of washed silk is shown in Figure 1. Following treatment with  $\text{Na}_2\text{CO}_3$ , water, and ethanol, silk consists predominantly of two groups of protein components, one with bands in the  $M_r$  range of 14-66K (Figure 1, arrows), and the other greater than 200K, as demonstrated previously<sup>20,22</sup>. Following renaturation and sonication the silk consists of small twisting fibrils approximately 7-8 nm in diameter and of variable length as shown by electron microscopy (Figure 2).

### *Circular dichroism*

Circular dichroism spectroscopy of modified silk preparations at different concentrations displayed a classical  $\beta$ -sheet conformation as demonstrated by the intense minima at approximately 218 nm (Figure 3).

### *Activities of native AEF and silk "AEF"*

Comparisons of the effects of native AEF (NAEF) and modified silk (SAEF) are shown in Figures 4-6. Figures 4 and 5 illustrate that both NAEF and SAEF, at a variety of doses, possess AEF biological activity. The silk preparation at low doses, on a protein basis, is more effective than the native material. Quantities of SAEF as low as 0.05 - 0.75  $\mu\text{g}/\text{mouse}$  were effective in priming the recipient animals for splenic, perifollicular AA amyloid deposition upon

the administration of an inflammatory stimulus. Though the effectiveness, or specific activity, of the SAEF appeared to be higher than NAEF (Figure 6) the anatomic distribution of AA amyloid was the same (i.e. the perifollicular area) with all preparations of AEF used. Radiolabelled native AEF when injected intravenously does localize to the splenic perifollicular areas<sup>6</sup>. The Congo red staining for amyloid in the perifollicular areas of the spleen with each AEF preparation was not due to the injected fibrils which localized to these same areas. This is illustrated by the observation that neither NAEF nor SAEF when administered without a subsequent inflammatory stimulus showed any perifollicular Congo red staining for amyloid (data not shown). SAEF which has not been sonicated is not effective, probably because the unsonicated silk gel particles are too large to pass through the lung capillary network. Active SAEF preparations stored at 4°C for periods as long as 4 weeks retained their potency. It is possible that the preparation remains active indefinitely given the stable nature of silk fibres, but, this was not directly tested.

A dose response curve illustrating the effect of different amounts of SAEF and NAEF is shown in Figure 6. As with past dose response curves with cellular AEF<sup>29</sup>, KCl solubilized AEF<sup>30</sup>, and glycerol solubilized AEF<sup>6</sup>, the effect of SAEF increases rapidly at low doses and begins to plateau at higher doses. However, in contrast to native material, quantities of SAEF in the range of 250  $\mu\text{g}/\text{mouse}$  induced less amyloid than that in the range of 12-50  $\mu\text{g}/\text{mouse}$  (see Discussion).

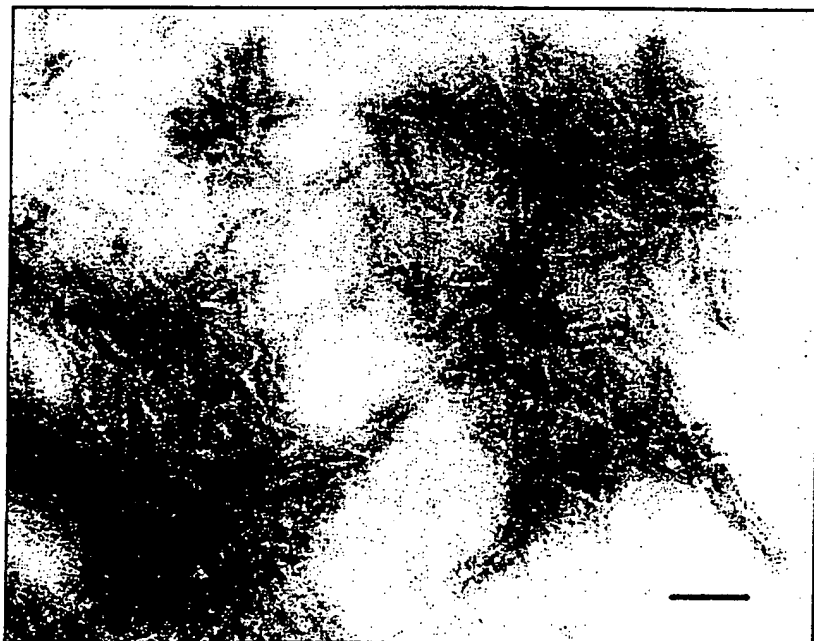


**FIGURE 2.** Negative stain transmission electron microscopy of modified silk following its gelation and sonication. Note that the silk consists of amyloid-like fibrils, unbranched and maintaining a uniform diameter of approximately 7-8 nm. Although individual fibrils were easily distinguished, they were also present in various states of aggregation ranging from larger clusters to small aggregated bundles. Magnification X 140,000, scale bar = 75 nm.

## Discussion

The ability to accelerate the induction of murine AA amyloid using biologically derived materials was discovered over 30 years ago<sup>2,4</sup>. The nature of the active material (which for the present purposes we will call AEF) and how it accomplishes its effects mechanistically have been the subject of numerous studies, none of which have yet provided conclusive and satisfactory answers. Past work has clearly shown that the active constituent(s) is protein by nature<sup>6</sup>, is common to diverse forms of amyloid<sup>7-10</sup>, and has its activity destroyed by denaturing techniques and is therefore probably dependent on its conformation<sup>6</sup>. The observation that different forms of amyloid could provide active AEF preparations indicated that AEF was not a specific amyloid peptide, although it did not rule out that one of the common constituents of amyloid deposits was the active molecule. This latter possibility was deemed to be much less likely when it was shown that pure amyloid peptides (IAPP, transthyretin, and the A $\beta$ -protein) acquired AEF activity after they formed fibrils, but not before<sup>11,12</sup>. This observation provided further support for the concept that AEF activity depended on protein conformation. Given that both naturally occurring, as well as test-tube prepared, amyloid fibrils possess AEF activity, and that one of the defin-

ing characteristics of such fibrils is their  $\beta$ -sheet protein organization, a distinct possibility is that AEF activity is at least partly dependent on this protein configuration which serves as a template for further amyloid formation. The process is quite analogous to that proposed for prions<sup>31</sup>.

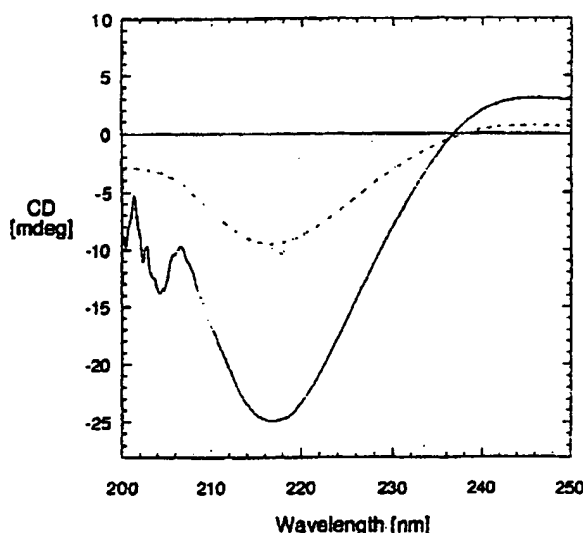
The process of preparing native AEF is tedious, time consuming, and expensive. Sufficient numbers of mice must be primed to produce adequate quantities of splenic amyloid (1-2 weeks) following which the spleens are collected and extracted either with 4M glycerol<sup>6</sup>, or AA amyloid fibrils (as AEF) are prepared with standard saline and distilled water washing procedures, which requires an additional week<sup>4,23</sup>. The product, though effective, is a mixture of components normally found in amyloid<sup>6</sup>. Trying to identify which constituent is the active moiety (if it is only one) requires denaturation techniques<sup>6</sup>, which by their very nature destroy AEF's biological activity. The use of synthetic peptides provides the necessary purity of material, but expense (several hundred US dollars for tens of mg) precludes their use on a routine basis. In contrast, many grams of raw silk may be purchased for \$25-50 US and following its washing with Na<sub>2</sub>CO<sub>3</sub>, distilled deionized water, and ethanol provides sufficient material, to be modified as AEF in 2 days, for a lifetime of work.

It was with these points in mind that we considered silk as a potential starting material to prepare a candidate AEF for future study. Raw silk is inexpensive, plentiful, and techniques for the removal of its non-protein components have been developed<sup>19</sup>, and yield pure protein isolates<sup>20,22</sup>. Furthermore, until amyloid was characterized, silk was the prime example of a protein with  $\beta$ -pleated sheet structure<sup>21</sup>, and is similar in other respects to amyloid in that it is fibrillar (Figure 2) and may exhibit red/green birefringence in polarized light when stained with Congo red (data not shown). However, in its native state, silk is a non-injectable material.

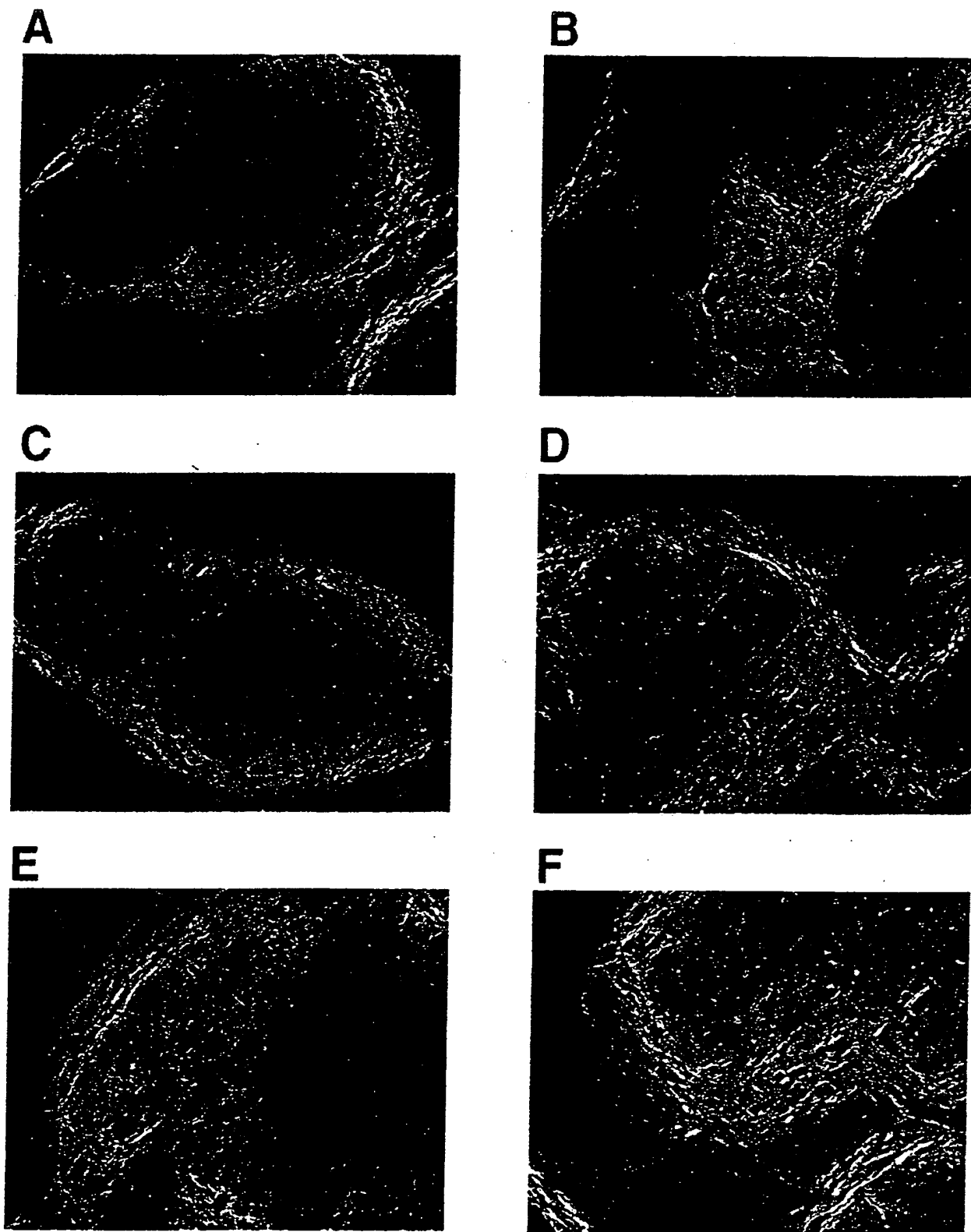
Our raw silk, which was washed free of non-protein material and dried 10 years ago, has remained stable at room temperature since then and has been used in the present AEF studies for the last 3 years. The procedure we developed provides injectable active material in two days, and is stable for at least a month at 4°C (the longest period examined). Furthermore, the modified silk is among the most potent forms of AEF we have encountered, having substantial activity in quantities less than 1  $\mu$ g/mouse.

Though modified silk appears to have advantages over native AEF, and fibrils composed of synthetic amyloid peptides, there are several problems with SAEF, discovered through trial and error, which need to be resolved and understood, and there are many questions concerning the structure of silk vis-a-vis its AEF properties which need to be addressed.

Doses of SAEF in the range of 200-250  $\mu$ g/mouse and higher are less effective than lower doses. These higher doses

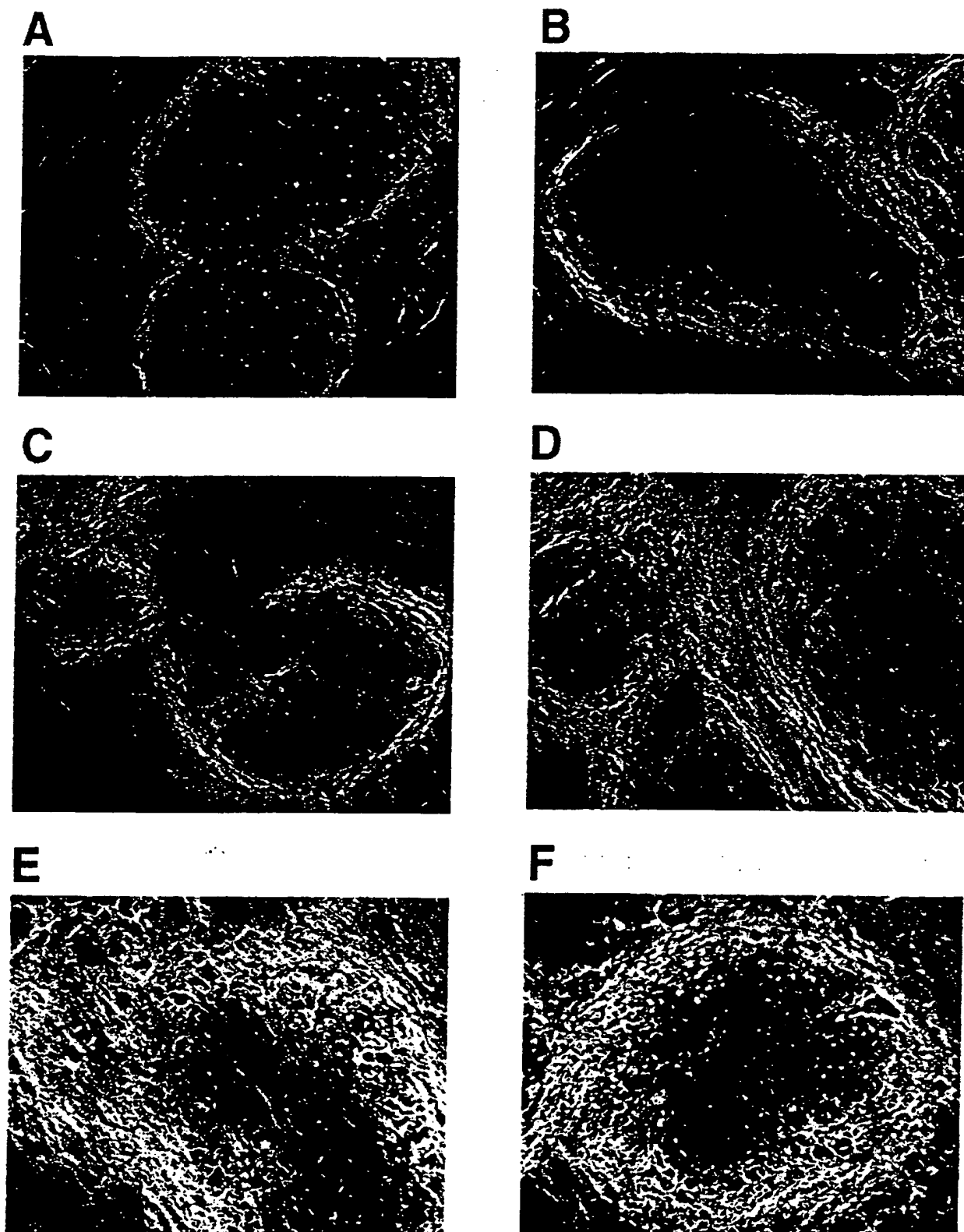


**FIGURE 3.** Circular dichroism spectroscopy of modified silk preparations at different concentrations. The preparation examined at 1mg/ml (solid line) displayed a classical  $\beta$ -sheet conformation as demonstrated by the intense minimum at approximately 218 nm. Further dilution of the sample to 0.5 mg/ml did not appear to affect the folded state of the dialysed silk as a similar but attenuated signal was observed (dotted line).



**FIGURE 4.** AA amyloid induced after 6 days by varying doses of modified silk, as AEF, and AgNO<sub>3</sub>, as the inflammatory

stimulus. Panels A - F, SAEF administered at 0.05, 0.2, 0.75, 3.0, 12.5, and 50 µg/mouse respectively.

*Kisilevsky et al.*

**FIGURE 5.** AA amyloid induced after 6 days by varying doses of native AEF and AgNO<sub>3</sub> as the inflammatory stimulus.

Panels A-F represent doses of 5, 10, 25, 50, 100 and 200 µg/mouse respectively.

reduced the amount of splenic amyloid by 20-25% so that AA amyloid occupied only 10-15% of splenic area at these doses. In contrast increasing doses of NAEF continued to increase the splenic area occupied by AA amyloid and reached a plateau (25% of splenic area) at doses in the range of 200-250  $\mu\text{g}/\text{animal}$ . The explanation for this phenomenon (greater potency of SAEF at low doses but lower potency at higher doses) is not immediately apparent. It may relate to SAEF being a particulate which following injection is cleared from the circulation by the reticuloendothelial system (RES)<sup>6</sup>. Excess quantities of SAEF may induce a blockade of the RES, the site where serum amyloid A (the AA precursor) is converted to AA amyloid. Such a blockade may interfere with amyloid formation.

The second problem relates to the nature of the lithium salt, LiSCN, that is necessary to dissolve raw silk. This salt is very hygroscopic and apparently sensitive to air. Bottles of LiSCN opened for any length of time provide a lithium preparation that is cloudier than material from a freshly opened bottle, and though it is capable of dissolving raw silk, it leads to a silk gel preparation that lacks AEF activity. This finding may be a problem from one perspective, but may yet provide an interesting opportunity from a different perspective. Since the same starting material may be manipulated to provide both active and inactive preparations, a comparison of the physical and chemical properties of these two preparations may provide the correlations necessary to understand the basis for AEF activity.

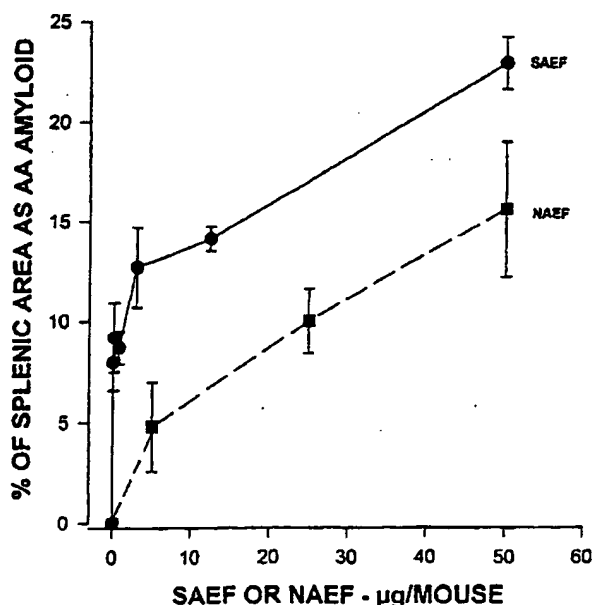


FIGURE 6. Percent splenic area occupied by amyloid as a function of different doses of SAEF or NAEF. For SAEF and NAEF, values are the mean  $\pm$  SEM of three animals and five animals respectively, per time point.

Among several techniques which we have used to try to dissolve silk, only the LiSCN was effective. Non-effective denaturants included, 8 M urea, 6 M guanidine - HCl, 6 M guanidine SCN, and 65% LiCl. Furthermore, we have not as yet attempted to denature non-carbonate treated silk for its AEF activity and therefore do not know if carbonate stripping of non-protein components is necessary to elicit silk's AEF potential.

Given that we have examined only one source of silk, that of *Bombyx mori*, there are several questions concerning silk structure that need to be addressed regarding its AEF properties. It is not at present clear if *B. mori* is the only silk source which may provide an active SAEF or whether sources from other species may prove to be (or not) as effective. Neither is it clear whether specific intersheet spacing of the silk protein, which may differ in different forms of silk, is responsible for the SAEF activity. Answers to such questions await future work.

## Acknowledgments

This work was supported by research funds provided by the Medical Research Council of Canada, grant MT-3153 (RK), The Alzheimer Association of Ontario (PF), the Ontario Mental Health Foundation (PF), and Neurochem Inc., (RK and PF).

## References

- 1 Cathcart ES (1995). AEF: an enigma wrapped in a mystery. *Amyloid Int J Exp Clin Invest* 2, 126-127
- 2 Werdelin O and Ranlov P (1966). Amyloidosis in mice produced by transplantation of spleen cells from casein-treated mice. *Acta Pathol Microbiol Scand* 68, 1-18
- 3 Hardt F (1971). Transfer amyloidosis. *Am J Pathol* 65, 411-424
- 4 Hardt F and Ranlov P (1976). Transfer amyloidosis. *Int Rev Exp Pathol* 16, 273-334
- 5 Kisilevsky R, Gruys E and Shirahama T (1995). Does amyloid enhancing factor (AEF) exist? Is AEF a single biological entity? *Amyloid Int J Exp Clin Invest* 2, 128-133
- 6 Axelrad MA, Kisilevsky R, Willmer J, Chen SJ and Skinner M (1982). Further characterization of amyloid enhancing factor. *Lab Invest* 47, 139-146
- 7 Niewold THA, Hol PR, van Andel ACJ, Lutz ETG and Gruys E (1987). Enhancement of amyloid induction by amyloid fibril fragments in hamster. *Lab Invest* 56, 544-549
- 8 Baltz ML, Caspi D, Hind CRK, Feinstein A, and Pepys MB (1986). Isolation and characterization of amyloid enhancing factor (AEF). In Glenner GG, Osseman EF, Benditt EP, Calkins E, Cohen AS, and Zucker-Franklin D (eds.) *Amyloidosis*, pp. 115-121. (New York, New York: Plenum Press)

- 9 Ali-Khan Z, Qurtion R, Robitaille Y, Alizadeh-Khiavi K and Du T (1988). Evidence for increased amyloid enhancing factor activity in Alzheimer brain extract. *Acta Neuropathol* 77, 82-90
- 10 Varga J, Flinn MS, Shirahama T, Rodgers, OG, and Cohen AS (1986). The induction of accelerated murine amyloid with human splenic extracts. Probable role of amyloid enhancing factor. *Virchows Arch.B Cell Pathol.* 51, 177-185
- 11 Ganowiak K, Hultman P, Engstrom U, Gustavsson A and Westermark P (1994). Fibrils from synthetic amyloid-related peptides enhance development of experimental AA- amyloidosis in mice. *Biochem Biophys Res Commun* 199, 306-312
- 12 Johan K, Westermark G, Engstrom U, Gustavsson A, Hultman P, and Westermark P (1998). Acceleration of amyloid protein A amyloidosis by amyloid-like synthetic fibrils. *Proc Natl Acad Sci* 95, 2558-2563.
- 13 Kisilevsky R and Boudreau L (1983). The kinetics of amyloid deposition: I. The effect of amyloid enhancing factor and splenectomy. *Lab Invest* 48, 53-59
- 14 Jarrett JT and Lansbury PT (1993). Seeding one-dimensional crystallization of amyloid - A pathogenic mechanism in Alzheimer's disease and scrapie. *Cell* 73, 1055-1058
- 15 Jarrett JT, Berger EP and Lansbury PT (1993). The carboxy terminus of the  $\beta$ -amyloid protein is critical for the seeding of amyloid formation -implications for the pathogenesis of Alzheimer's disease. *Biochemistry* 32, 4693-4697
- 16 Jarrett JT and Lansbury PT (1992). Amyloid fibril formation requires a chemically discriminating nucleation event - studies of an amyloidogenic sequence from the bacterial protein OsmB. *Biochemistry* 31, 12345-12352
- 17 Come JH, Fraser PE and Lansbury PT (1993). A kinetic model for amyloid formation in the prion diseases - importance of seeding. *Proc Natl Acad Sci USA* 90, 5959-5963
- 18 Harper JD and Lansbury PT (1997). Models of amyloid seeding in Alzheimer's disease and scrapie: Mechanistic truths and physiological consequences of the time-dependent solubility of amyloid proteins. *Annu Rev Biochem* 66, 385-407
- 19 Pandit MW, Sagar AJ and Rao MSN (1972). Studies on silk fibroin. I. Molecular weight, sedimentation coefficient, viscosity and optical rotation of silk fibroin from carbonate-extracted silk fiber. *Arch Biochem Biophys* 149, 259-268
- 20 Fournier A (1979). Quantitative data on the Bombyx mori silkworm: a review. *Biochimie* 61, 283-320
- 21 Marsh RE, Corey RB and Pauling L (1955). An investigation of the structure of silk fibroin. *Biochim Biophys Acta* 16, 1-34
- 22 Creighton TE (1993). Conformational Properties of Polypeptide Chains. In Creighton TE (ed.) *Proteins: Structures and Molecular Properties*, pp. 193. (New York: W.H.Freeman and Co.)
- 23 Niewold TA, Gruys E, Kisilevsky R and Shirahama TS (1991). Fibril amyloid enhancing factor (FAEF)-accelerated amyloidosis in the hamster is not dependent on serine esterase activity and mononuclear phagocytosis. *Scand J Immunol* 34, 101-107
- 24 Laemmli UK (1970). Cleavage of structural proteins during the assembly of the head of bacteriophage T4. *Nature* 227, 680-684
- 25 Oakley BR, Kirsch DR, and Morris NR (1980). A simplified ultrasensitive silver stain for detecting proteins in polyacrylamide gels. *Anal Biochem* 105, 361-363.
- 26 Lyon AW, Narindrasorasak S, Young ID, Anastassiades T, Couchman JR, McCarthy K and Kisilevsky R (1991). Co-deposition of basement membrane components during the induction of murine splenic AA amyloid. *Lab Invest* 64, 785-790
- 27 Puchtler H, Sweat F and Levine M (1962). On the binding of Congo red by amyloid. *J Histochem Cytochem* 10, 355-364
- 28 Kisilevsky R, Lemieux LJ, Fraser PE, Kong XQ, Hultin PG and Szarek WA (1995). Arresting amyloidosis *in vivo* using small-molecule anionic sulphonates or sulphates: Implications for Alzheimer's disease. *Nature Med* 1, 143-148
- 29 Axelrad MA, Kisilevsky R and Beswetherick S (1975). Acceleration of amyloidosis by syngeneic spleen cells from normal donors. *Am J Pathol* 78, 277-284
- 30 Axelrad, M.A. and Kisilevsky, R. (1980). Biological Characterizations of Amyloid Enhancing Factor. In Glenner, G.G., Costa, P.P. and de Freitas, F. (eds.) *Amyloid and Amyloidosis*, pp. 527-533. (Amsterdam: Excerpta Medica)
- 31 Lansbury PT (1997). Yeast prions: Inheritance by seeded protein polymerization? *Curr Biol* 7, R617-R619

**This Page is Inserted by IFW Indexing and Scanning  
Operations and is not part of the Official Record**

## **BEST AVAILABLE IMAGES**

Defective images within this document are accurate representations of the original documents submitted by the applicant.

Defects in the images include but are not limited to the items checked:

- ☐ **BLACK BORDERS**
- ☐ **IMAGE CUT OFF AT TOP, BOTTOM OR SIDES**
- ☐ **FADED TEXT OR DRAWING**
- ☐ **BLURRED OR ILLEGIBLE TEXT OR DRAWING**
- ☐ **SKEWED/SLANTED IMAGES**
- ☐ **COLOR OR BLACK AND WHITE PHOTOGRAPHS**
- ☐ **GRAY SCALE DOCUMENTS**
- ☒ **LINES OR MARKS ON ORIGINAL DOCUMENT**
- ☐ **REFERENCE(S) OR EXHIBIT(S) SUBMITTED ARE POOR QUALITY**
- ☐ **OTHER:** \_\_\_\_\_

**IMAGES ARE BEST AVAILABLE COPY.**

**As rescanning these documents will not correct the image problems checked, please do not report these problems to the IFW Image Problem Mailbox.**